Materials Forming, Machining and Tribology

Kapil Gupta *Editor*

Materials Forming, Machining and Post Processing

Springer

Materials Forming, Machining and Tribology

Series Editor

J. Paulo Davim, Department of Mechanical Engineering, University of Aveiro, Aveiro, Portugal

This series fosters information exchange and discussion on all aspects of materials forming, machining and tribology. This series focuses on materials forming and machining processes, namely, metal casting, rolling, forging, extrusion, drawing, sheet metal forming, microforming, hydroforming, thermoforming, incremental forming, joining, powder metallurgy and ceramics processing, shaping processes for plastics/composites, traditional machining (turning, drilling, miling, broaching, etc.), non-traditional machining (EDM, ECM, USM, LAM, etc.), grinding and others abrasive processes, hard part machining, high speed machining, high efficiency machining, micro and nanomachining, among others. The formability and machinability of all materials will be considered, including metals, polymers, ceramics, composites, biomaterials, nanomaterials, special materials, etc. The series covers the full range of tribological aspects such as surface integrity, friction and wear, lubrication and multiscale tribology including biomedical systems and manufacturing processes. It also covers modelling and optimization techniques applied in materials forming, machining and tribology. Contributions to this book series are welcome on all subjects of "green" materials forming, machining and tribology. To submit a proposal or request further information, please contact Dr. Mayra Castro, Publishing Editor Applied Sciences, via mayra.castro@springer.com or Professor J. Paulo Davim, Book Series Editor, via pdavim@ua.pt

More information about this series at http://www.springer.com/series/11181

Kapil Gupta
Editor

Materials Forming, Machining and Post Processing

Springer

Editor
Kapil Gupta
Department of Mechanical and Industrial
Engineering Technology
University of Johannesburg
Doornfontein, Johannesburg, South Africa

ISSN 2195-0911 ISSN 2195-092X (electronic)
Materials Forming, Machining and Tribology
ISBN 978-3-030-18853-5 ISBN 978-3-030-18854-2 (eBook)
https://doi.org/10.1007/978-3-030-18854-2

This Springer imprint is published by the registered company Springer Nature Switzerland AG
The registered company address is: Gewerbestrasse 11, 6330 Cham, Switzerland

Preface

Materials forming, machining and post-processing techniques are fundamental manufacturing techniques that are required individually or simultaneously to manufacture near-net-shape engineered parts. Their working principles, process mechanisms, salient features and latest developments are of prime importance. Modelling and optimization of the aforementioned techniques to improve quality, productivity and sustainability are also a major requirement. This book provides insights into some of the important forming, machining and post-processing techniques being used commercially.

There are a total of 11 chapters in this book. Chapter "Fundamentals in Sheet and Tube Forming: Material Characterization, Conventional and Novel Processes and Involved Mechanics" sheds light on fundamentals and advances in sheet metal and tube forming processes. Analysis and optimization of the metal injection moulding process for near-net-shape manufacturing of engineered parts are discussed in Chapter "Analysis and Optimization of Metal Injection Moulding Process". With the help of a case study, the feasibility and suitability of friction stir welding for 3D printed thermoplastic parts is discussed in Chapter "On Friction-Stir Welding of 3D Printed Thermoplastics". Chapter "4D Printing" provides insights into the latest technology 4D printing. Comprehensive information on non-conventional micro-machining processes is given in Chapter "Non-conventional Micro-machining Processes". Formation of a desirable surface integrity on super-alloys by wire spark erosion machining is discussed in Chapter "RETRACTED CHAPTER: Investigation on Spark Erosion Machining Induced Surface Integrity of Super-Alloys". Environmentally friendly lubricants and lubrication/cooling techniques are comprehensively discussed in Chapter "Role of Eco-Friendly Cutting Fluids and Cooling Techniques in Machining". Chapter "Titanium Machining Using Indigenously Developed Sustainable Cryogenic Machining Facility" also reports on green machining of titanium alloys where an indigenously developed cryogenic machining setup has been used for experimental research. Laser-based advanced post-processing and surface treatment techniques are detailed in Chapter "Advanced Laser Based Surface Treatment Techniques to Improve the Quality of the Products". Chapter "LASER Cladding—A Post Processing Technique for Coating, Repair and

Re-manufacturing" reports in detail the fundamentals of laser cladding technique. An experimental study on the effects of the laser beam and electron beam welding on different material grades is reported in Chapter "Electrochemical Behaviour and Surface Studies on Austenitic Stainless Steel and Nickel-based Superalloy Dissimilar Weld Joints".

I sincerely acknowledge Springer for this opportunity and their professional support. Finally, I would like to thank all the chapter contributors for their availability and valuable contributions.

Johannesburg, South Africa Kapil Gupta
June 2019

Contents

Fundamentals in Sheet and Tube Forming: Material Characterization, Conventional and Novel Processes and Involved Mechanics

Chetan P. Nikhare

Abstract This chapter introduces the ways to characterize the materials for both sheet and tube materials. This mostly includes the tensile test for sheet metal, and tensile and ring test for tube metal. This also includes in providing the direction of inputting the material data in finite element simulations. The chapter further discusses the conventional method to form sheet and tube metal to the desired shape. Further, it will walk through the formability of metal and then introduce the novel techniques such as hydroforming, rubber forming, electric forming, incremental forming, roll forming, tailor welded blanks, and some high speed forming such as electromagnetic and explosive forming. In addition, conventional and rotational flaring, Reuleaux forming were discussed for tube forming. Further, some of the common challenges were discussed.

Keywords Material characterization · Sheet forming · Tube forming · Novel forming · Mechanics

List of Symbols

β	Strain ratio
ε	True strain
ε_t	Strain in thickness direction
ε_w	Strain in width direction
ε_1	Strain in direction 1
ε_2	Strain in direction 2
σ	True stress
c	Clearance between punch and die wall
d_0	Initial hole diameter

C. P. Nikhare (✉)
Mechanical Engineering Department, The Behrend College Advanced Manufacturing and Innovation Center, The Pennsylvania State University, Room 233, 5350 Technology Drive, Erie, PA, USA
e-mail: cpn10@psu.edu

K. Gupta (ed.), *Materials Forming, Machining and Post Processing*, Materials Forming, Machining and Tribology, https://doi.org/10.1007/978-3-030-18854-2_1

d_f	Final hole diameter
D_0	Initial blank diameter
D_p	Punch diameter
e	Engineering strain
F_{max}	Maximum punch force
HER	Hole expansion ratio
K	Strength coefficient
L	Length of sheet metal
LDR	Limiting Drawing Ratio
n	Strain hardening exponent
R	Plastic anisotropy
R_{avg}	Normal (average) anisotropy
ΔR	Planar anisotropy
R_0	Plastic anisotropy in rolling direction
R_{45}	Plastic anisotropy in 45° to rolling direction
R_{90}	Plastic anisotropy in 90° to rolling direction
R_{11}	Stress ratio in rolling direction
R_{12}	Stress ratio in 45° to rolling direction
R_{22}	Stress ratio in 90° to rolling direction
R_d	Die radius
S	Engineering stress
T	Sheet metal thickness
UTS	Ultimate tensile strength of a material

Within the metal forming industry, sheet metal forming claims a huge share for the number of products. Sheet metal manufacturing is not only one of the most preferred manufacturing processes in automotive and aerospace industries, but also in household industries and others. Sheet metal products offer various advantages such as easy to produce, inexpensive, safe, high quality, produce lighter parts, and variety of shapes over casting and forging. Products from sheet metal manufacturing processes can be found easily which are surrounded to us. They are kitchen wares, kitchen drain systems, plumbing pipes, sheet metal safety doors, computer cabinets, electronic gadgets shell, study tables, file cabinets, and jewelry. Automotive and aerospace components are body-in-white components, a driving shaft, assembled camshaft, exhaust systems, engine cooling system, radiator frame, safety requirements, engine bearer, integral member, cross member, frame structure parts, and axle elements. These products provide many capabilities as well as flexibility. The common materials used in this process are low to high strength steels, advanced steels, 1XXX to 7XXX series aluminum alloys, magnesium alloys, copper, and titanium.

This chapter provides the route for understanding the mechanical properties of a material for sheet metal forming operations and how to characterize the material for better understanding and applying them for designing the better efficient products. Further, the chapter discusses sheet metal forming tests and how to characterize

the material geared towards this forming processes. Then the chapter includes various conventional and novel techniques for this forming processes. The chapter also details on tube forming processes and further detail the mechanics involved in these processes. Finally, it describes some of the challenges in this area.

1 Materials Characterization of Sheet and Tube Material

Traditionally the material was characterized using a tensile test. For this, a sample should be prepared as per the ASTM standard. There are two types of sample for tensile test: a flat specimen and a cylindrical specimen. Depending on the usage of a material for deformation the specific specimen needs to be selected for characterization. In this chapter, we will be limiting our discussion on a flat specimen, which is used in sheet metal characterization.

1.1 Tensile Test for Sheet Metal

Figure 1 shows the tensile sample based on ASTM E8 standard [1]. Table 1 provides all the dimension in both metric and English units. For most metallic materials this specimen is used for characterization. Some hard to machine or deform materials may change the dimension based on the machining accuracy and material machinability. Once the sample is prepared the test can be performed. Two raw data i.e., force to pull the specimen and displacement to elongate the specimen would be required to plot the stress-strain curve. The load cell in the tensile test machine would provide the force data based on the calibration of the load cell. The displacement can be measured through various ways: (a) actuator linear voltage displacement transducer (LVDT), (b) extensometer (contact), (c) laser (non-contact) extensometer, and (d) digital image correlation (DIC). The LVDT provides the displacement data in terms of voltage or directly in displacement unit based on how the machine is set up for output channel. The LVDT will always be inaccurate as it provides the specimen displacement plus the machine compliance. This can be corrected by pulling a comparably thick or hard specimen, so the machine would reach to a maximum load cell capability without any plastic deformation in a specimen. Further, for each force value of a targeted specimen, the displacement of a thick or hard specimen for the same force value needs to be deducted from the targeted specimen displacement to calculate the only displacement of a targeted specimen. To avoid this hassle, more accurate readings can be achieved by using extensometers. The extensometer needs to be installed on the gage area of the specimen. This extensometer contacts the specimen and thus also called as contact extensometer. As soon as the machine put enough force above yielding, the extensometer needs to be removed manually to prevent damage. There are two ways the extensometer can be damaged: when the extensometer extended above its limit, and/or due to shock at fracture. In both cases,

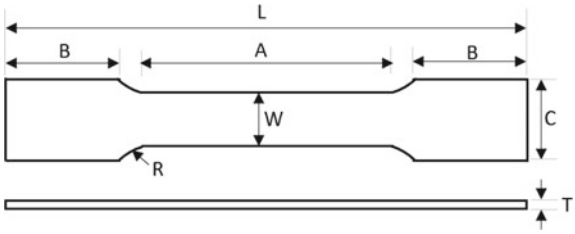

Fig. 1 Tensile sample as per ASTM standard [1]

Table 1 Tensile sample dimension as per ASTM standard [1]

	Dimension mm (inch)
A—Gage length	50 (2)
B—Grip length	12.5 (0.5)
C—Grip width	20 (0.75)
L—Specimen length	200 (8)
R—Fillet radius	12.5 (0.5)
T—Specimen rhickness	Material thickness
W—Gage width	12.5 (0.5)

Fig. 2 Tensile sample with a speckled pattern in the gage area

the extensometer voids the calibration and cannot be used to achieve accuracy for the next specimen. To capture the complete displacement data from the extensometer the laser extensometer can be used. The laser extensometer tracks the two point on the gage length during the test to calculate the displacement. Figure 2 shows the utilization of a laser extensometer to capture displacement. To acquire the complete strain field on the sample, DIC can be utilized. DIC needs the speckled pattern as shown in Fig. 3 to identify the displacement of each point with respect to all other points during the test. A single camera provides the in-plane strain field, however, 2 cameras can provide the out of plane strain field too.

It is well known that sheet metal is produced through the rolling process by decreasing the thickness of the sheet. Due to which the sheet metal grain is elongated in a rolling direction and thus the direction of a specimen needs to be known before testing. Due to the difference in grain elongated direction, the material can behave differently when pulled in various direction. That's why a good understanding on anisotropic properties of a material is required. A material can be called anisotropy if the mechanical properties of a material are different in different direction (shown in Fig. 4). Due to this, the metal which is stamped with same punch force can provide earing (wavy shape on edge) in the part as shown in Fig. 5. Two values can provide the anisotropy of a material called as planar and normal (average) anisotropy. For this, the plastic anisotropy "*R*" of a material can be calculated from the specimen

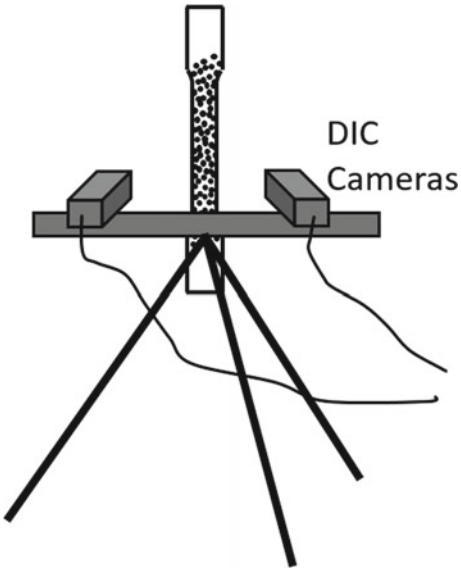

Fig. 3 Digital image correlation camera setup for strain mapping

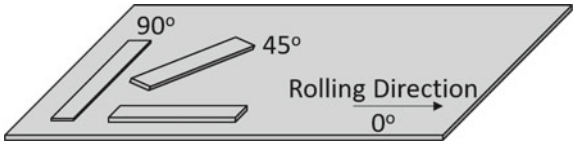

Fig. 4 Illustration of specimen orientation for sheet metal forming characterization

which is tested in tension at a particular strain value. Plastic anisotropy "*R*" is the ratio of strain in the width to strain in the thickness direction of a specimen tested in tension. Note that *R* value needs to be calculated for specimen tested at same strain value. Mathematically, *R* value can be determined from Eq. 1.

$$R = \frac{\varepsilon_w}{\varepsilon_t} \tag{1}$$

Thus, normal (average) and planar anisotropy can be determined from Eqs. 2 and 3.

$$R_{avg} = \frac{R_0 + 2R_{45} + R_{90}}{4} \tag{2}$$

$$\Delta R = \frac{R_0 - 2R_{45} + R_{90}}{2} \tag{3}$$

Three case can be made from planar anisotropy value [2]:

Case 1: If $\Delta R = 0$, then the material is isotropic and no earing will occur
Case 2: If $\Delta R =$ negative, then the earing will occur in 45° direction

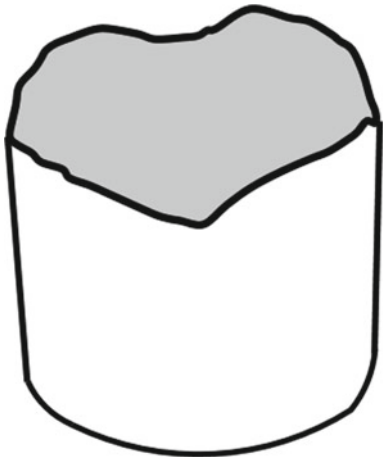

Fig. 5 Deep drawn cup with earing

Case 3: If $\Delta R =$ positive, then the earing will occur in 0° and 90° direction

The drawability of a material can be enhanced by having a higher R_{avg} value [3]. It was mentioned that the limiting drawing ratio (LDR) can be closely determined by using Eq. 4. [3]

$$\text{LDR} = 0.6\ R_{\text{avg}} + 1.8 \tag{4}$$

1.2 Tensile Test for Tube Metal

Two types of tube metal can be found (a) welded tube, and (b) seamless tube. A welded tube is manufactured by continuously rolling the sheet metal followed by welding at the open edge. Seamless tubes are formed by heating the billet and then inserting the mandrel through the center of the billet to form the hollow tube. During both processes, a good amount of straining occurs at the circumferential direction and thus the behavior of the material in tube longitudinal direction is different than in circumferential direction. To characterize the tube material, the specimens can be made in a longitudinal direction (Fig. 6). The smaller the gage width, the smaller the curvature and thus more accurate property can be measured. The circumferential tube material can be characterized in two ways. First, cut circular rings and then open to make the flat tensile specimens. However, through this method, circumferential stresses would be unable to generate and thus data might be inaccurate. A second method is the ring test method. In this method, a circular section is cut with a tensile geometry as shown in Fig. 7 and then tested by applying a circumferential stress through a semi-circular die by pulling them apart.

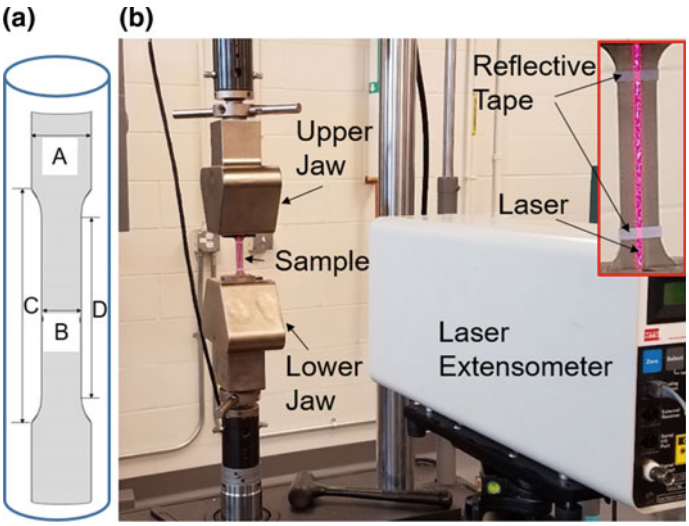

Fig. 6 Tube tensile specimen with test setup with laser extensometer (permission to reprint from ASME) [4]

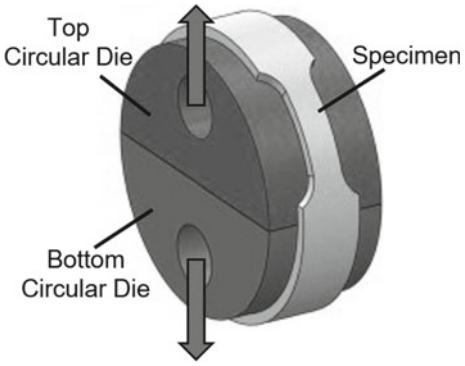

Fig. 7 Ring test for tube sample characterization (Permission to reprint from ELSEVIER) [5]

1.3 Material Input in Finite Element Method

To reduce the expenditure on trialing the manufacturing process on a workshop, a computer-based simulation is commonly used in industries. A computer-based simulation works on the principle of mathematical iteration and Finite Element Method (FEM). After experimental material characterization, the tensile test data needs to convert to a true stress-strain curve for FEM. The true stress and true strain can be calculated by using Eqs. 5 and 6. Further plot the true stress-strain curve and then using the power law (Eq. 7) provide the best fit to the curve.

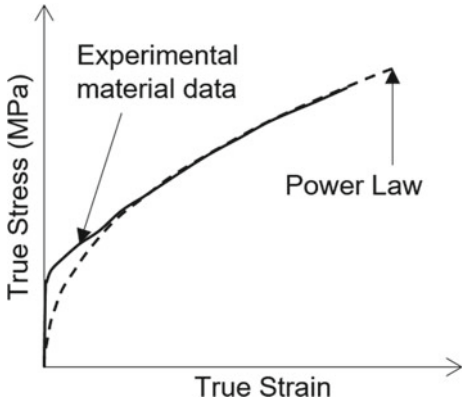

Fig. 8 Best fit power law for material stress strain data

$$\sigma = S(1 + e) \tag{5}$$

$$\varepsilon = LN(1 + e) \tag{6}$$

$$\sigma = K\varepsilon^n \tag{7}$$

If the power law provides the exact fit then in the material mechanical property section provide K and n value. If the power law doesn't provide the exact fit, then use the tabular format to provide the data as mentioned in Fig. 8.

If the material is anisotropic, then provide the rolling direction stress-strain curve and in the plastic anisotropic tab provide the plastic anisotropic strain or stress values depending on the software need, feed the R values instead of 1. 1 means isotropic material properties. Abaqus simulation software needs stress ratio and can be calculated by these Eqs. 8–10 [6].

$$R_{11} = \sqrt{\frac{R_{90}(R_0 + 1)}{R_0(R_{90} + 1)}} \tag{8}$$

$$R_{22} = \sqrt{\frac{R_{90}(R_0 + 1)}{(R_0 + R_{90})}} \tag{9}$$

$$R_{12} = \sqrt{\frac{3(R_0 + 1)R_{90}}{(2R_{45} + 1)(R_0 + R_{90})}} \tag{10}$$

2 Sheet Forming Processes

Let's now focus on sheet metal manufacturing. Sheet metal forming is one of the major manufacturing processes where the sheet metal is processed to achieve the

desired part. Sheet metal forming is a big umbrella under which these manufacturing processes come which are listed below. Out of these only, few will be discussed in this chapter.

Shearing	Redrawing	Hemming
Punching	Stamping	Seaming
Blanking	Tailor Welded Blanks	Bulging
Parting	Hydroforming	Embossing
Lancing	Hydraulic pulse forming	Hot Forming
Slitting	Rubber forming	Explosive Forming
Perforating	Sheet metal spinning	Electromagnetic forming
Dimpling	Incremental forming	Peen Forming
Beading	Wire drawing	Laser Beam Forming
Bending (90°, air bend and V bend, roll bend)	Pipe drawing	Microforming
	Flanging	Electrohydraulic Forming
Channel Forming	Coining	Origami Forming
Dome test/Cup test/Limiting dome height test	Ironing	Magneticpulse forming
	Tube reduction/expansion	Superplastic forming
Deep drawing	Tube Flaring	
	Roll forming	

After material characterization, it is important to find the sheet metal characteristics. Sheet metal characteristics provide the knowledge of a sheet metal which can provide an indication of its performance during the sheet metal operation. These include formability, forming limit, hole expansion for edge stretchability, and bendability in which the process does a less influence in performance.

2.1 Dome Test

This test is also called as cup test, Erichsen test, or limiting dome height test (ASTM E2218) [7]. In this test, the sheet metal is clamped between the die and the blankholder. The die and the blankholder consist of a lock bead in which the sheet metal is been locked and the only area available for stretching is the inside disc material from the lock bead. A hard hemispherical punch is used to stretch the material. The punch pushes the sheet metal towards the die to provide a dome shape (see Fig. 9). To measure the strain achieved by the metal, circles can be electrochemically etched on the sheet metal surface. However, this technique only provides the strain measurement at any paused frame. DIC can be used by speckling the sheet surface with white paint and black dots to capture the evolution of strain during the stretching process. During the process, the force keeps ramping with respect to the displacement as shown in Fig. 10. When the material cannot sustain any more force the necking occurs and force starts to drop. The displacement at fracture "*d*" provides the indication of a formability of a material. The machine needs to stop at this point to analyze the formability. This test provides the maximum strain the material can

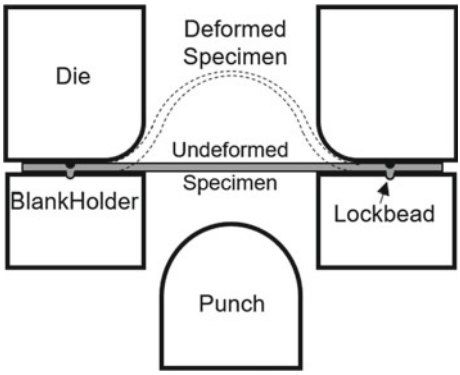

Fig. 9 Schematic illustration of dome test

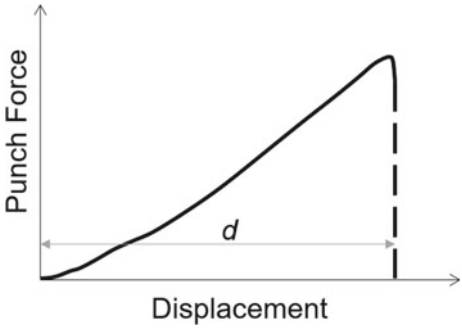

Fig. 10 Force displacement curve during dome test

take before it fails and that is called the limiting strain for that particular strain path. In this test, a full circular sheet can provide an equi-biaxial strain path, if the process is frictionless. A close to frictionless process can be achieved by applying multiple layers of polyethylene and oil between punch and sheet surface.

2.2 Forming Limit Diagram

To understand the formability of a sheet material in various deformation modes, Forming Limit Diagram (FLD) is essential. FLD is a plot between a major and minor strain of a critical location in a particular strain path or deformation mode. This concept was initially introduced by Keeler and Backhofen [8]. Further, this became an important approach to identify the forming limits of a sheet metal. In this diagram, the limiting strain at each deformation modes are joined and an envelope is created which is called as Forming Limit Curve (FLC). Below this curve, the metal deformation is safe and above this curve the metal necks and fails. It was observed that this envelope is sensitive to these variables planar and normal anisotropy value "*R*-values", strain hardening exponent "*n*-value", temperature, strain rate "ε/sec-value",

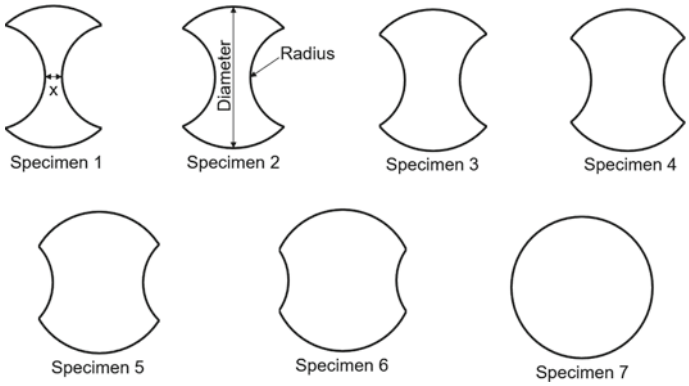

Fig. 11 Sample shapes for forming limit curve testing (Permission to reprint from ASME) [9]

size of grain at start of deformation, prestrain, path dependence, tool geometry, in and out of plane forming, coefficient of friction between sheet metal and tool which changes the strain path, and blank holding force [9]. To achieve a critical strain point to draw the FLC envelope, various sample dimensions are needed to experiment in dome test as shown in Fig. 11. Figure 11 shows samples from uniaxial to equi-biaxial strain path. The disk diameter and cut radius for specimens are 101.6 and 38.1 mm. The x dimension from specimen 1 to 6 are 12.7, 25.4, 38.1, 50.8, 63.5, and 76.2 mm [9]. Only 7 samples are shown to get a good curve, however more or fewer samples can be used based on the availability and accuracy. For each strain path, multiple samples need to be tested as statistically the material variability comes in the account and may not neck at the same location or at the same punch depth. The strains at the neck can be achieved by either circle grids or by DIC. Sometimes it is also important to measure the safe point near the crack, where the neck would not be visible. When drawing the FLC all fail points should be above the curve and neck points on the curve. While drawing this curve it may be possible that some of the neck and safe points are in the fail region but none of the fail points should be in the safe region. This method will provide the FLC of a particular sheet metal. The FLC is shown in Fig. 12. Industry uses 5% marginal curve to design tools for stamping. Figure 12 also shows the curve generated from recently developed biaxial test concept. Let's get an information on the biaxial test.

2.3 Biaxial Test

Traditionally, sheet metals were dominantly characterized by uniaxial tension test and dome height test. However, these tests do not provide an extensive non-contact material data in all deformation mode. Thus recently a new test machine is devised called as a biaxial test which can test the material from uniaxial to equi-biaxial

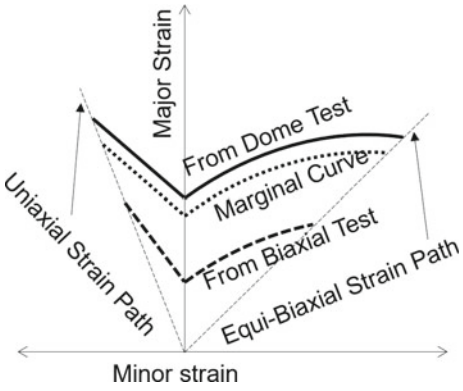

Fig. 12 Forming limit curve for done and biaxial test

strain path. In this test, the samples region which is considered for data acquisition does not touch any tool unlike in dome test. The specimen looks like a cruciform as shown in Fig. 13. The specimen consists of 4 perpendicular arms and a small indented region from both sides at the center. The whole idea of this thinner center region is to provide a uniform strain region is all test where the data can be acquired. Various cruciform geometries are investigated and can be found in these literature [10–16]. Depending on the capability the specimen can be utilized, with a note that a uniform strain region should appear at the center region. The specimen can be used as a uniaxial sample if it is mounted only on one axis of the machine and second axis is not in consideration. Figure 14 shows the biaxial machine with a mounted specimen and with DIC set-up. If the specimen is mounted on both axis and one of the axes is allowed to provide compression displacement then near to negative plane strain condition can be analyzed. If one of the axes is not allowed to move then the condition will be a plane strain. If one of the axes is providing a positive displacement then near to positive plane strain can be achieved, and if both axes are providing a same positive displacement then equi-biaxial strain condition can be achieved. The advantage of this machine is that only one dimension specimen can be used to cover all strain paths and the specimen is not in contact with the tool. Due to which a pure material FLC can be achieved and thus the forming limits are lower than the dome test. In dome test, the punch pushes the sheet metal for deformation. Due to which, normal compressive stress through the thickness generated which suppresses the void and delays the failure. This effect is called as pressurization effect [9].

2.4 Limiting Drawing Ratio Test (Deep Drawing Test)

The deep drawing process is one of the important manufacturing processes within the sheet metal forming. In this process, the sheet metal which is

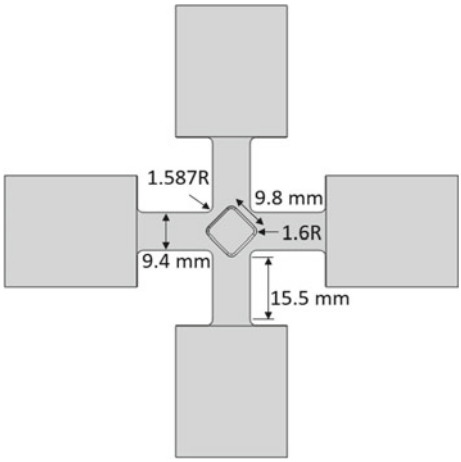

Fig. 13 Cruciform specimen for test on biaxial machine (Permission to reprint from ASME) [9]

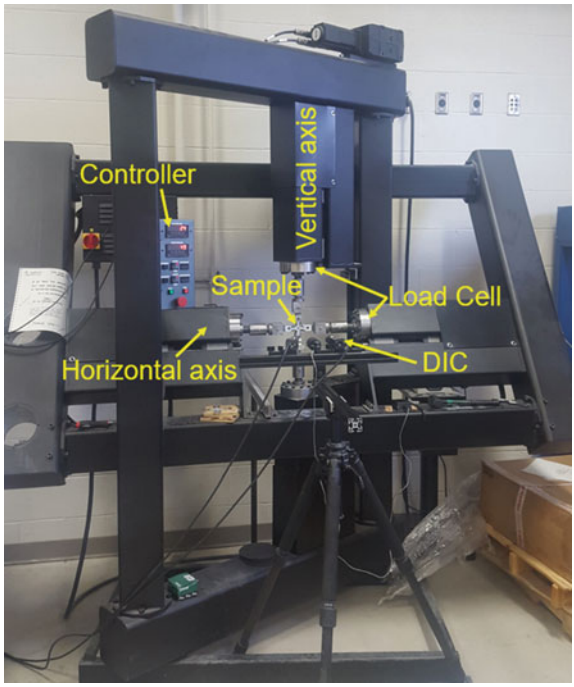

Fig. 14 Penn State Behrend Biaxial machine (Permission to reprint from ASME) [9]

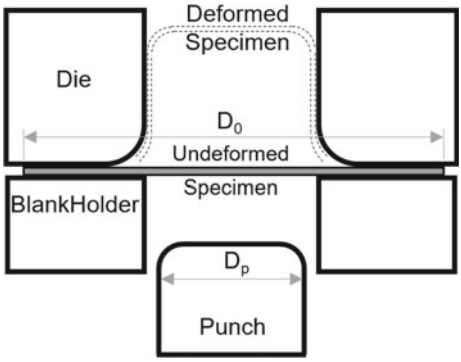

Fig. 15 Schematic illustration of deep drawing process

placed between the die and the blankholder is allowed to slide to achieve the deeper parts (Fig. 15). As the sheet metal is allowed to slide or draw between the die and blankholder this process is called deep drawing process. Most of the circular or square shape deep parts are manufactured by this process. Examples are pots, pans, metal cups, kitchen sinks, auto parts, fuel and oil tanks, beverage and food cans, containers. This process is widely used due to its simplicity of forming common simple parts. However, more complex parts can also be drawn through this process. The manufacturing challenges increase as the complexity of the part increases. Most of the challenges are a failure due to excessive thinning or wrinkling. Wrinkling can be avoided by using draw beads in proper places. Draw beads are similar as lock beads, however, they allow the metal to draw-into avoid wrinkling in the parts. Excessive thinning can be avoided by adjusting the blankholding force.

For simple circular parts, the number of variable influences the material drawing are: punch diameter, die radius, blank diameter, the clearance between punch and die wall (this should be slightly higher than the blank thickness), blank thickness, blankholder force, friction between all sliding surfaces, and sheet metal mechanical properties. Due to multiple mechanisms involved in this process, a simple approximate equation of maximum punch force is given in Eq. 11 [3] (Fig. 16).

$$F_{max} = \pi D_p T (UTS)\left[\left(\frac{D_0}{D_p}\right) - 0.7\right] \tag{11}$$

Deep drawing process is only possible if

$$D_0 > D_p + 2c + 2R_d \tag{12}$$

A trend is drawn based on Eq. 8 considering the lowest $D_0/D_p = 1.2$, $D_p = 50$ mm, $T = 2$ mm and $UTS = 400$ MPa, which provides the straight line. If closely observe this equation, it shows that the force was calculated by multiplying the area (perimeter of circle multiply by the thickness of sheet metal) by the tensile stress of a metal. The deep drawn process is meant to provide the part without failure, it

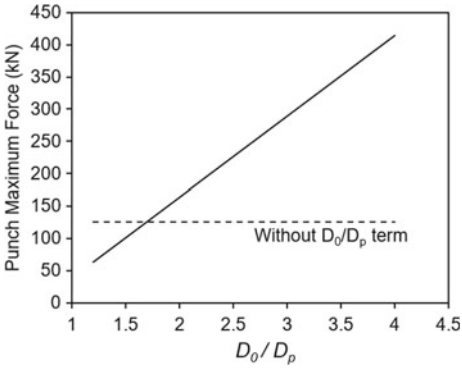

Fig. 16 Maximum force required during circular deep drawing process

means that the part may not reach the tensile stress. Thus, this equation provides the upper bound value for maximum punch force which would need during circular cup drawing. If D_0/D_p term was not considered then the force would be constant. Thus the D_0/D_p term is important, however, for smaller ratio, the force would be less but with a higher ratio, the cup would tear and reach the tensile stress. Thus the term D_0/D_p is significant in the deep drawing process. This term is then used to evaluate the property of sheet metal in the deep drawing process.

As this process provides the pure drawing of a sheet metal through a circular channel, a drawability of the metal can be evaluated. Thus this process is utilized to characterize the sheet metal drawing property. This property is also called as deep drawability and is named as limiting drawing ratio (LDR). LDR is the ratio of circular sheet metal undeformed diameter to the punch diameter and is given in Eq. 13.

$$LDR = \frac{D_0}{D_p} \tag{13}$$

To experimentally evaluate the deep drawn process, the sheet metals should be sheared with different diameter and then tested in the Erichsen cup drawn set-up (Fig. 15 with punch diameter of 50 mm, die hole diameter as 55.12 mm, and die radius of 20.11 mm). The smaller sheet diameter should be used first and then draw by considering all parameters same. If the cup tear at die or punch radius then smaller sheet diameter is needed. But if the cup is completely drawn then use the next higher diameter and continue this process till the cup tears. Once you identify the sheet diameter where the cup tears during the drawing process, the LDR can be calculated by dividing the one lower diameter by the punch diameter (Eq. 13).

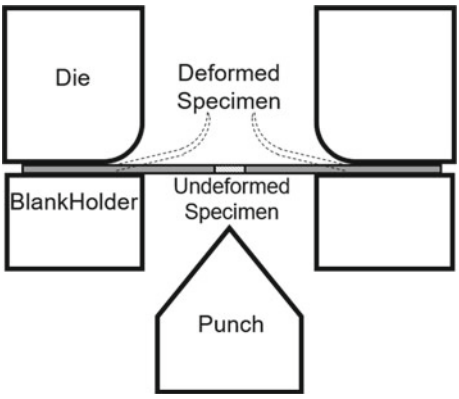

Fig. 17 Schematic illustration of hole expansion test

2.5 Hole Expansion Test

Hole expansion is also one of the material property which provides an indication on the edge of the sheet metal stretching in a circumferential direction and initiation of a crack. A traditional uniaxial test provides the stress-strain curve of a material in one direction but fails to predict the development of strains in radial and circumferential direction. This test provides an opportunity to experience the evolution of strains in radial and circumferential directions. For this, a hole can be made on the sheet metal. This sheet metal is placed between the die and blankholder (Fig. 17). Enough application of force can be applied on sheet metal by a blankholder so the sheet metal should not slide during hole expansion process. Then the conical punch (hemispherical and cylindrical punches were also listed in use) displaces to expand the hole. During this process, the sheet metal edge first expands a little then bends and then starts flaring. The process continues until the neck initiates. The deformed hole diameter is measured and hole expansion ratio is calculated by using Eq. 14.

$$HER = \frac{d_f - d_o}{d_o} * 100\% \tag{14}$$

A different mechanics observed when expanding the hole using a cylindrical and hemispherical punch. In cylindrical punch deformation, the hole only expands to a bigger circle unless the material is having anisotropic behavior. With a hemispherical punch, the circle expands but also bends to take the spherical shape. Figure 18 provides the deformed sample for steel and aluminum. Using the hemispherical punch it was proposed that a single specimen can be experimented to create an FLC [17]. When the specimen neck at the hole edge during the process, the punch can still displace to further crack the specimen. Then along the crack, the strain evolution can be measured and plotted to create an FLC (Fig. 19). This will provide the points from uniaxial to near positive plane strain.

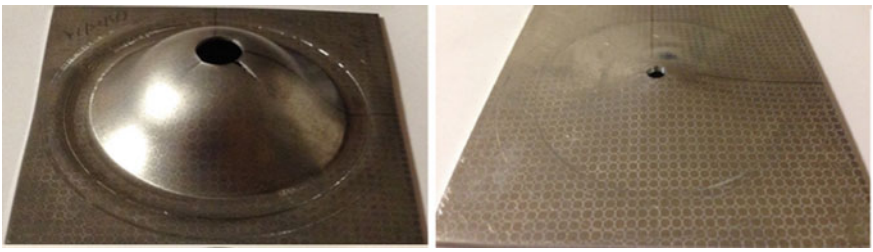

Fig. 18 Mild steel (left) and 5083 Aluminum alloy (right) after hole expansion with hemispherical punch (Permission to reprint from IDDRG) [17]

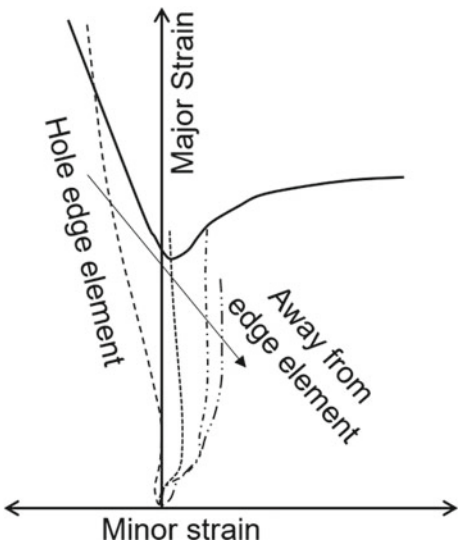

Fig. 19 Strain path in hole expansion test

With the recent development of new biaxial test machine as explained in Sect. 2.3, the cruciform can be made with a hole at the center as shown in Fig. 20. The specimen will then be tested in different strain path i.e., from uniaxial to equi-biaxial strain path. With this test, the hole will be purely expanded and no bending or flaring would occur.

The manufacturing process which was used to create the hole in the sheet metal influences the hole expansion ratio. The manufacturing process to create hole are punching, drilling, milling, electric discharge machine, water jet machine and so on. The conclusion is that rougher the surface more stress concentrations would be included and the edge would crack faster. The hole expansion test became more popular when many of the advanced high strength steels (AHSS) showed the tendency of edge cracking during the deformation [18–21]. These AHSS can easily initiate the cracks due to variation in strain levels at their multi-phase microstructure locations.

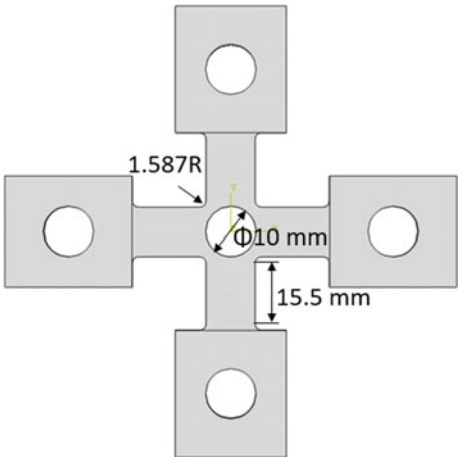

Fig. 20 Cruciform specimen for hole expansion test on Biaxial machine

It was noted that the parameters like material ductility, microstructure, hole edge quality and hole diameter influence the hole expansion capability.

3 Sheet Forming Processes—Conventional Techniques

Let's explore some of the commonly found sheet metal forming processes. These are the ones, which generally used in every sheet metal company.

3.1 Shearing

A starting point of sheet metal forming is to shear or cut the sheet metal from a large sheet coil to the desired dimension, which is considered, as a blank. Now the shearing can be a straight shear or a particularly closed shape shear. For straight shearing operation, a straight tool called the shear blade can be used as shown in Fig. 21. This figure shows the side view. To reduce the shearing force the operation can be performed like a scissor cutting a paper. That is cutting the metal incrementally. For closed loop shear (for example to make a circular hole or circular blank), a close dimension shear tool will be required.

An approximate relation is provided to determine the maximum punch force in shearing operation is given in Eq. 15.

$$F_{max} = 0.7TL(UTS) \tag{15}$$

This force is determined by multiplying the area of the shear and the approximate shear strength of a material. Theoretically using maximum shear stress theory or distortion energy theory, the shear strength should be in between 0.5 to 0.577 of tensile strength.

Depending on the shearing shape, the operations named as:

- Punching: The sheet metal without the sheared piece (left image in Fig. 22). Here the sheared piece is a scrap.
- Blanking: The sheared piece (right image in Fig. 22). Here the sheet metal without the sheared piece is a scrap.
- Perforating: shearing number of holes in a sheet metal, similar to a 3 hole punch in a paper.
- Parting: Making 2 or more pieces from the large sheet.
- Notching: Shearing a shape from the edge, so as to create a notch in the edge.
- Lancing: Creating a tab in the metal without removing any material.
- Slitting: Shearing a piece of sheet metal to create the tab without removing any material.

3.2 Bending

Bending is one of a very commonly used operation to provide a quick 2-dimensional shape. Most of these operations include only a bend, however, some studies are

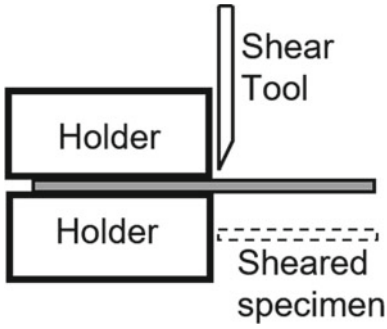

Fig. 21 Schematic illustration of shearing operation

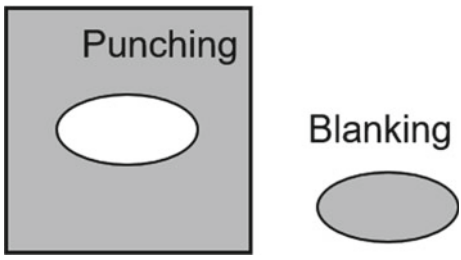

Fig. 22 Punching and blanking in a shearing operation

conducted for the application with a stretch bend or bending under tension. In a normal bend operation the neutral line would stay mostly at the center of the thickness. A typical bending operation is shown in Fig. 23. The outer layer of thickness would be in tension and inner layer will be in compression. Note that, do not bend a material so the crack would initiate at the tension surface. For this, a criterion is to bend the metal with a minimum bend radius of three times the thickness of the metal [3].

3.3 Stamping

Stamping is the general name for the sheet metal forming. This is not related to a particular process or mechanics. At any time there might be multiple mechanics may be involved in deep drawing, stretching, bending at various locations. For example, the part which is stamped in the below Fig. 24, multiple deformation modes may have experienced like stretching at the top surface, bending tension and bending compression at the edges. More detailed 3D image can be seen in [22]. Based on which design is been stamped, the die and punch were modeled on the Computer Aided Design (CAD). Further, the tool geometries are imported to the Computer Aided Engineering (CAE) software. Based on the material which is going to be stamped all related mechanical properties like a true stress-strain curve, anisotropy values, and forming limit curve were fed to software. Then a stamping simulation was performed. Based on the detail observation on the simulated stamped part critical locations could be identified and tool design can be modified to form the safe part. Once the part is passed, the die and punch production can be done through Computer Aided Manufacturing (CAM) and then the tool tryout can be performed on the shop floor. Once the trial is successful the production of the part can be started.

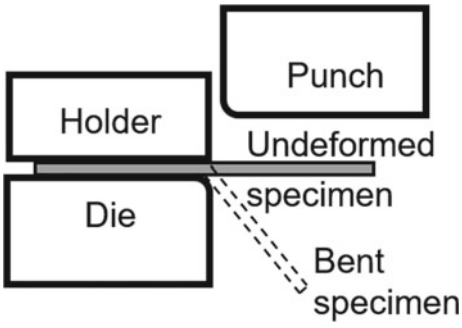

Fig. 23 Schematic illustration of bending operation

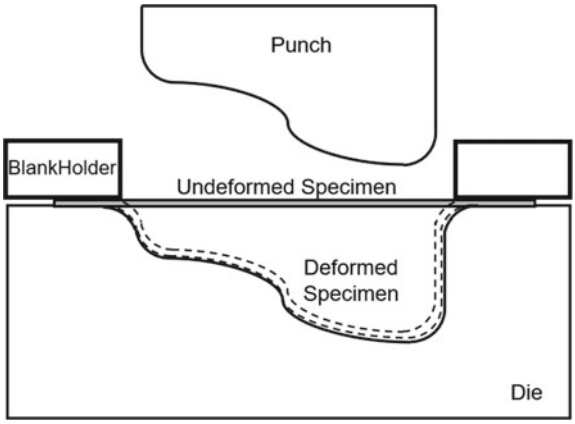

Fig. 24 Schematic illustration of stamping process

4 Sheet Forming Processes—Novel Techniques

After getting enough details on the conventional forming, let us look at some of the novel forming processes, which provides better formability and lighter parts. Due to stringent environmental regulation, the stronger and lighter parts are needed. It should also note that nearly about 70% of the parts are sheet metal in the automobile thus crashworthiness should not be compromised. Vehicle fuel efficiency can be achieved by using lower density material or improving the processes so the lower gage metals can be used. In both cases, the implementations are having many challenges. Steel which is a denser material are in abundance, but processing for higher strength and lower thickness gets expensive. On the other hand, the lower density material does not exhibit similar ductility as steel. These novel process techniques are needed which would use these materials and result in better formability for the same desired part with higher efficiency.

4.1 Hydroforming

The manufacturing process where fluid pressure is applied to ductile metallic blank to form the desired component shape is called Hydroforming. There are two types of hydroforming processes viz. sheet metal hydroforming and tube hydroforming. If the blanks used are sheet metal, the process is called sheet metal hydroforming and if tubular section blanks are used, then it is called as tube hydroforming. In either of these processes, a hydroforming tool (punch or die), a hydraulic press, and a fluid-pressure intensification system are required. Sheet and tube hydroforming processes are shown in Figs. 25 and 26.

Hydroforming technology is currently applied in many areas of manufacturing of sheet metal components in order to achieve lightweight construction of industrial

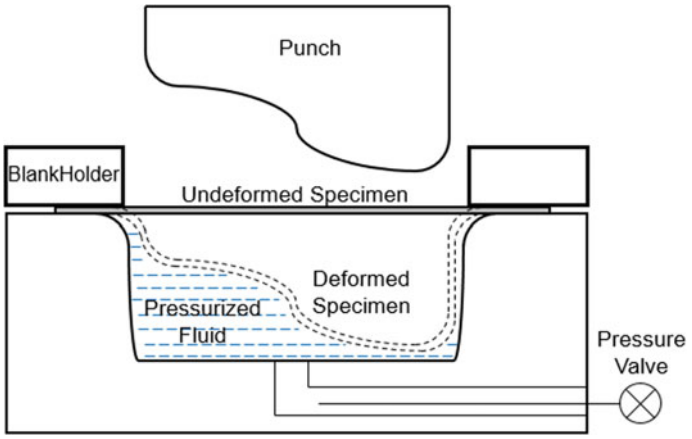

Fig. 25 Schematic illustration of sheet hydroforming process

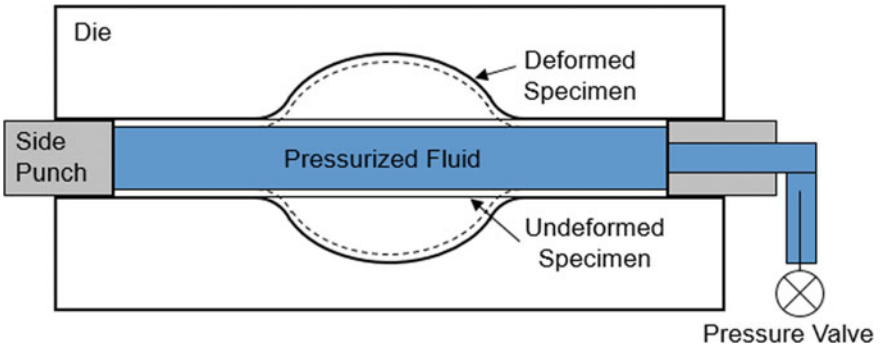

Fig. 26 Schematic illustration of tube hydroforming process

parts. Many kinds of parts of the automotive vehicle such as body shell, driving shaft, assembled camshaft, exhaust systems, engine cooling system, radiator frame, safety requirements, engine bearer, integral member, cross member, frame structure parts, axle elements, and others such as plumbing fixtures, and oven door handles are manufactured by hydroforming process. In hydroforming, additional preforming operations, such as bending, can be considered for adjusting the cross-sections of the part. Most parts formed in the tube hydroforming process have a tubular shape. Because many sheet metal components such as parts of vehicles and electrical devices should be formed successfully using high strength steel, aluminum and titanium blanks that are generally known to have low formability, the hydroforming has become an important process. Generally, this process produces higher and more uniform strain distribution over the entire sheet surface.

Using sheet metal hydroforming, a greater depth of draw (up to 1.5 times) is possible compared to conventional draw-die operations. Due to the application of

sealing, the sheet hydroformed part has less thinning than the sheet stamped part and the limiting draw ratio (LDR) can be remarkably improved. Other advantages of the process include improved surface finish, lower spring-back, shorter tool development time and lower tooling costs. However, due to longer cycle times, sheet metal hydroforming is more suited for low volume production. Larger panels generally require very large hydraulic presses which can mean high capital expenditure. Also, leakage issue increases the sealing cost.

Tube hydroforming has achieved its position in the vehicle industry as a desirable manufacturing process due to its ability to produce complex structures at different sections of the part in one stroke. Tube hydroforming is also known as profile or extrusion hydroforming. The tube is expanded to the desired shape with the assistance of fluid pressure and axial punch feed. It has been observed that 40% of maximum thickening occurs around the edge of the tube. Other advantages of the process includes part consolidation, weight reduction through more efficient section design and tailoring of the wall thickness, improved structural strength and stiffness, lower tooling cost due to fewer parts, fewer secondary operations (no welding of section required and hole may be punched during hydroforming), tight dimensional tolerances and low springback, and reduced scrap. Depending on the product to be produced, the tubular blanks can be made from aluminum extrusions, copper pipes or individually fabricated parallel or tapered sections of sheet metal. Tube hydroforming can be split into three process related classes: a high pressure (fluid pressure from 83 to 414 MPa), multi-pressure (fluid pressure from 69 to 173 MPa), and low pressure (fluid pressure less than 83 MPa). In high pressure, the material is been stretched to it forming limit, whereas in multi-pressure the tube is preformed and then stretched to get the desired shape. However, in low pressure the tube is just shaped to the desired dimension without stretching the material.

4.2 Rubber Forming

One of the main disadvantages we learn from hydroforming process is high-pressure fluid leakage. To overcome this challenge a more flexible material for example rubber or polyurethane can be used instead of oil or water. The rubber is filled in the steel container which can be used as a die as shown in Fig. 27. Then a similar experimental set-up can be utilized as in hydroforming. The sheet metal is placed over the die and held by the blankholder. The punch descends and deforms the sheet metal with the rubber pressure from the die side. The rubber conforms to the shape of sheet metal uniformly and provides pressure to form the part. The disadvantage of this process is that it limits the deeper parts and also the rubber could only produce low pressure near about 10 MPa. This process is more suitable for custom parts such as aircraft sheet metal parts. Due to a low cost of tooling the experimental setup gets inexpensive.

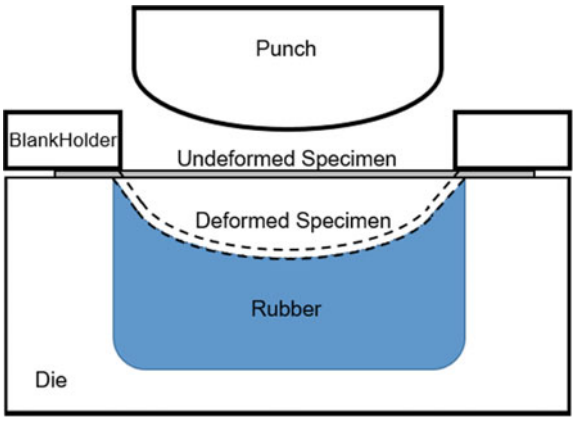

Fig. 27 Schematic illustration of rubber forming

4.3 Tailor Welded Blanks

Tailor welded blank (TWB) is also one of the technique for weight savings. In TWB two or more sheets are welded together in a single sheet for stamping as shown in Fig. 28. Sheets of different gauges, material properties, strength, coating types etc. can be welded together to produce a single blank. Tailoring of these sheets is done according to the requirements of the product leading to component optimization. This process is mostly done to reduce the cost, and mass and increase the structural integrity. Stamping can be performed through conventional or novel techniques.

The TWB technology offers various cost and performance advantages and therefore has been encouragingly adopted by the automotive industry. Though applications of tailored blanks in areas other than automotive industry have been conceived, a number of manufacturing difficulties need to be overcome before the process can be transferred to these applications. There are also certain limitations associated with

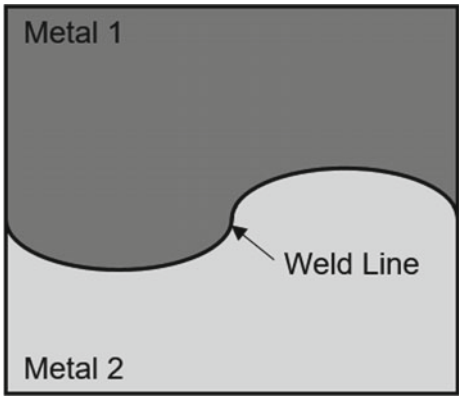

Fig. 28 Tailor welded blanks

tailored blanks, due to which their applications have been limited to some specific areas only even in the automotive industry. For more advances to be done in the TWB technology, these limitations have to be studied and minimized.

Following are the advantages and disadvantages of TWB's

Advantages:

- Improves material utilization
- Improves product quality
- Lower tolerances
- Stiffer parts
- Compact design flexibility
- Fewer parts
- Less design and development time
- Reduce manufacturing costs
- Better usage of metal properties.

Disadvantages:

- Reduce formability as compared to ordinary sheet
- Better welding techniques make process expensive
- Increase in process time (sheet metal cutting, then joining and coiling)
- Challenges in surface finish
- Multiple blank holder and force required due to different sheet properties and thickness
- Movement of a weld line.

4.4 Roll Forming

Roll forming is the sheet metal forming processes where various two-dimensional shapes are generated by rolling the metal sheet. In this process, the flat sheet enters the rolling line. The progressive rollers provide the shape to the sheet metal progressively so when the sheet metal leaves the rolling line it does have a shape of last rolling station (Fig. 29). More detailed image can be referred from [23]. As the shape achieved by the sheet metal is of the last rolling station a two dimension shape with a longer length is generated. These products will have the deformation mode of plane strain. At each station, the roller dies slightly changes its shape towards final shape. The main roller dies can be above and below the sheet metal while the secondary dies try to bend the sheet metal to conform the shape. Due to sliding motion at each station, the friction would be higher and thus lubrication would be necessary to reduce the wear of roller dies. The higher production rate depends on the lubrication, the thickness of a material, material properties, bend radius and number of roll stations.

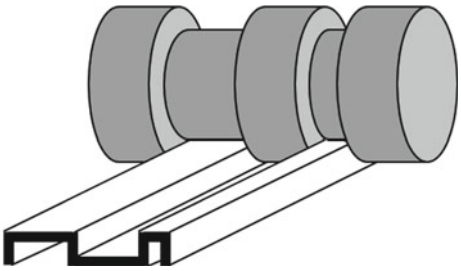

Fig. 29 Schematic illustration of roll forming

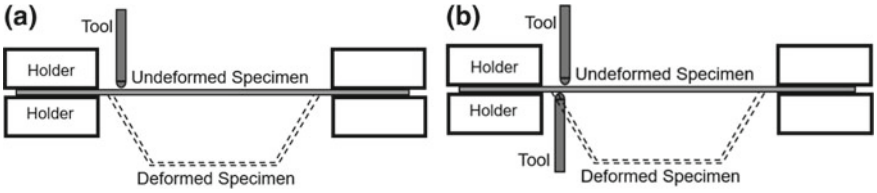

Fig. 30 Schematic illustration of **a** single point incremental forming, and **b** double point incremental forming

4.5 Incremental Forming

Incremental Forming (IF) is the die-less and highly capable process to form the deeper part compared to conventional sheet metal forming which uses die, punch and holder. Two types of incremental forming are more common (a) single point incremental forming (SPIF) as shown in Fig. 30a, b) double point incremental forming (DPIF) in Fig. 30b. In SPIF the single point tool is used to form the part. The part profile program is imported to the CNC or robotic arm. In this case, either the tool or the frame holding the sheet material is movable. At any time a single point tool touches the sheet metal at one point and forces that point to deform plastically. In the next step the tool touches and deforms the next sheet metal point and thus the process continues. Therefore the process is named as incremental forming. As the process is very flexible, other advantages it accompanied are low hardware cost, enhanced formability, less time-to-market delivery, and can achieve a variety of complicated shapes, eliminating the complicated die design.

4.6 Electric Assisted Forming

In electric assisted forming, an electric current is applied to the metal either through the metal dies or directly through metal. Due to passing of electric current through the metal and depending on the metal resistivity, and current density, the metal gets

warm or hot. Due to this heating, the metal gets soften and can be stamped easily and can increase ductility and results in higher formability of sheet metal. This process can be used in normal stamping, incremental forming or precision forming. The mechanics during this process is when the electrons flow through the metal it hits the grain boundaries which then resist the passage and thus energy dissipates as heat. Due to this heat, the dislocation will be annihilated and the material would flow easily when the force is applied.

4.7 Explosive Forming

Explosive forming comes under the category of high energy rate forming (HERF). In this process, the explosive is used as a source of energy to form the material. As the rate of forming is very high the material should be ductile at higher strain rate condition. The process consists of an assembly of sheet metal clamp on the die and the die cavity is been vacuumed as shown in Fig. 31. The assembly is then submerged in the water tank which is placed under the ground. The explosive is mounted at a particular height so a set amount of energy is transferred to sheet metal for forming. The water tank is then closed to reduce the waste of energy. The charge is then detonated and shock wave travels and transfers the huge amount of energy to the metal which then formed as per the die shape. This process is mostly utilized to form the metal with higher thickness as much as 25 mm. The setup time is longer for this process and thus the quantity produced is low, but larger and thicker parts can be formed.

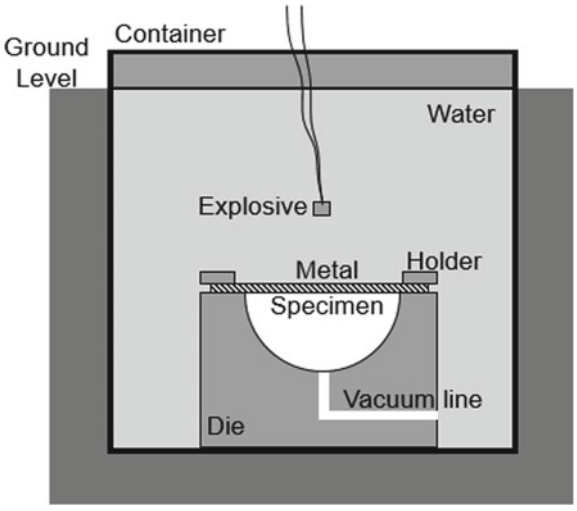

Fig. 31 Schematic illustration of explosive forming

4.8 Electro Hydraulic Forming

Electro hydraulic forming is similar to explosive forming. In this process instead of explosive, an electric current is discharged through a wire which vaporizes and dissipates the shock wave to deform the part (Fig. 32). This forming process also comes under the category of HERF. The process is similar as explained above in the explosive forming. An assembly of die and holder clamping the sheet metal is submerged in the water in the tank. Two electrodes with a thin wire are submerged in the water and position at a stand-off distance from the specimen depending on the energy required to deform the metal. The container is then sealed so minimal of the energy gets wasted and most use during the process. Both electrodes are connected to a power supply and a capacitor bank. The capacitor bank is stored with electrical energy. Just before starting the process the vacuum is created in the die cavity and then the electric current is discharged from the capacitor bank to the electrodes. Due to sudden charge release, the thin wire combust suddenly and created a shock wave. The shock wave travels through the water and transmits the energy to the specimen which then deforms the metal to a die cavity. After every process, the thin wire needs to be replaced. This process produces a lower magnitude energy as compared to explosive forming and thus a smaller and thinner metal can be formed. Thus, this process is not required to be under the ground level. This process is also considered for the low production rate.

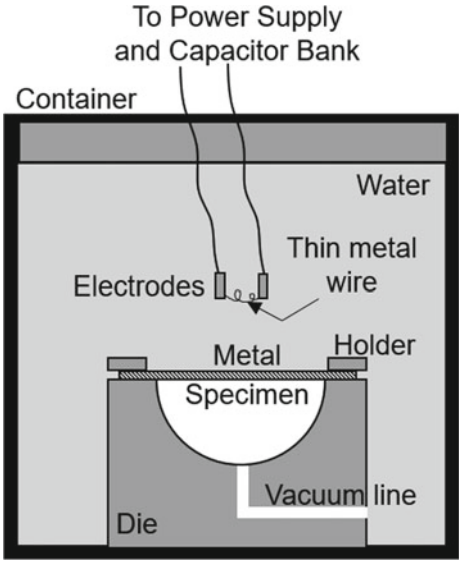

Fig. 32 Schematic illustration of electro hydraulic forming

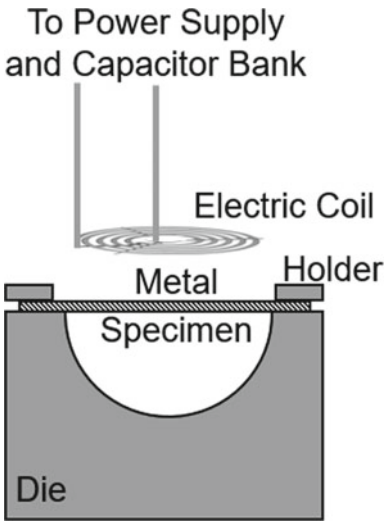

Fig. 33 Schematic illustration of electromagnetic forming

4.9 Electromagnetic Forming

Electromagnetic forming is the one more process which comes under HERF. In this process, the deformation of sheet metal occurs due to magnetic force (Fig. 33). The process is again similar to explosive forming. In this process, an electric coil is used to produce the magnetic field. The assembly of sheet metal in the die and holder set is placed at a standoff distance from the electric coil. The electric coil leads are connected to the power supply and a capacitor bank. Electric energy is stored in the capacitor bank. Once the set-up is ready a huge amount of energy is released through the electric coil which then generates the magnetic field. This magnetic field gets restricted by the nearby conductive material which then creates the eddy current within the metal. This eddy current produces its own magnetic field and repels the original magnetic field which creates the force and a deformable metal gets shaped. In this case is the specimen. This method can also be applied in the tube, the coil should be placed inside the tube and tube outer surface is placed in the die. During the process, the tube gets bulge and deform to a die shape. Due to the amount of energy this process produces, it can be used for low volume and thinner parts.

5 Tube Forming Processes

In sheet metal forming we mostly discussed forming of a sheet metal, which is shaped like a flat long piece with negligible thickness. However if the sheet metal is rolled and joined at their longitudinal edges, a tube metal is formed as shown in Fig. 34. These tubular parts are used for various applications such as exhaust tubes, heat exchangers,

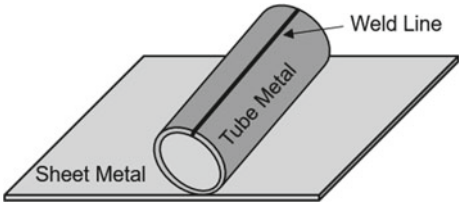

Fig. 34 Tube from sheet metal

support frames, engine cooling system, radiator frame, safety requirements, engine bearer, integral member, cross member, plumbing fixtures, and oven door handles. Tubes, as manufactured, cannot be used for all purposes and thus forming of tubes is needed get the desired shape. One of the tube forming process, tube hydroforming, is already discussed in the hydroforming section. In this section, some more tube forming processes will be discussed.

5.1 Tube Flaring

Tube flaring is one of the tube end forming process. In this process, the tube is placed in the die for support and a conical punch engages the end of the tube and progresses along the axis of the tube for flaring the shape as shown in Fig. 35. In this process, the tube end edge expands to the desired flare shape. The tool is not necessarily a conical shape and can be of any shape from square to cone to elliptical, depending on the end shape required. Various factors can influence the process such as the tube length. As the tube length increases, the chances of buckling the tube is higher. This also depends on the tool angle, if the tool angle is higher the tube will prone to buckling. Friction increases the flaring force and thus lubrication is required during the process. Other than flaring this process can be used to either expand or reduce the tube. For this process, the punch would be inserted in the tube to flare the end to the require shape and then continue this process till the whole tube is of the same shape. Similarly dies can be used to insert the tube into a reduce die section where the reduction can be performed for the whole tube.

5.2 Rotational Flaring

The rotational tube flaring is similar to conventional flaring with only addition is that when the punch descends to flare the tube, the tool is also rotating at its descend direction axis. It should be noted that the tube should be held tightly in the fixture so as to avoid the rotation of the tube. During this process, the shear stress acts on the tube wall which provides the higher formability for tubes and can be expanded more.

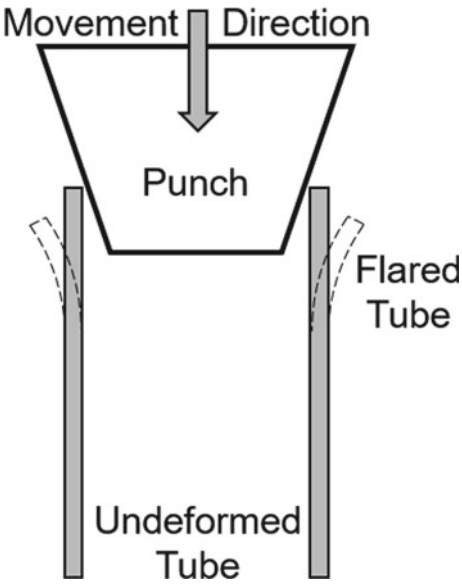

Fig. 35 Schematic illustration of conventional tube flaring

The typical force-displacement curve for conventional and rotational tube flaring is shown in Fig. 36.

5.3 Tube Hydroforging

Tube hydroforging is the combination of tube hydroforming and forging process. In this process, the tube is placed in the die and then the tube is preformed into an approximate die shape by hydroforming. The hydroforming can be high or low pressure. Once the part is approximately shaped, then the part of the die moves to compress the tube without any fluid inside to give the final shape. This process is in

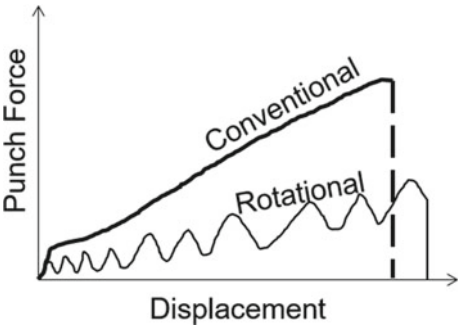

Fig. 36 Force displacement comparison between conventional and rotational tube flaring

a way efficient as compared to only hydroforming as it is hard to punch the material by an axial punch and often bursting or wrinkling occurred. In this process, the hydroforming can be performed until the metal limiting thinning and then a forging operation can be performed to provide the final shape. In forging process the metal is not stretched and thus bursting or fracture would not be a question.

5.4 Reuleaux Forming

It is always believed that when something is rotating it will always create a circle. But with Reuleaux forming various shapes are possible. The Reuleaux system [24] provides a rotary motion in the z-axis (vertical) and planar motion on x- and y-axes. One way to accommodate this is to use a kinematically programmed computer numerical control (CNC) machine. Figure 37 shows the experimental setup for Reuleaux tube forming on a HAAS milling machine. The creation of a Reuleaux triangle tool for forming a square tube is shown in Fig. 38. If a square tube of side "a" is required to form through Reuleaux tool, then create the equilateral triangle for side "a". Then create circles of radius "a" by considering vertex of triangle as a center. Similarly, draw two more circles of same radius "a" with center as other two remaining vertexes of the triangle. Trim all lines and arcs except arcs adjacent to lines of the triangle. This creates the Reuleaux triangle. Create the center point (let's say point P) (center point of the equilateral triangle). The punch rotates at center point "P" on an axis perpendicular to the page. To create a square cup, the tool moves such that when the tool is rotating counterclockwise, the point P translates clockwise. Figure 39 provides a series of steps which would create 1/3rd of the square profile while P covered one full translation cycle. That is, for each tool rotation around the axis at P, the point P makes three completions of the translating profile to create the square cup. The locus along which the point "P" travels is not a circle but rather a path that consists of four elliptical arcs (Fig. 40). The equations for generation of a profile are given in Fig. 40.

This process is similar to rotational flaring which only difference is that it uses triangular tool and kinematics to create the final square tube. In this process, again shear mechanics in involved and thus can produce a shape with uniformly distributed thickness.

6 Mechanics in Sheet Metal Forming

In this section, various mechanics in sheet metal forming will be discussed. Assume a circle is etched on a sheet metal and then the sheet metal is pulled to deform to a particular shape. The etched circle will also deform and it will take a shape as per the applied force in the different direction. The final shape will provide an indication that how that region of sheet metal gone through a deformation mechanics.

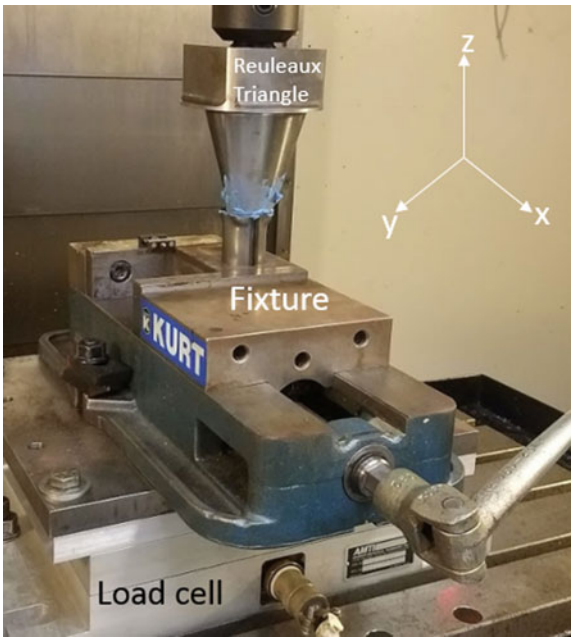

Fig. 37 Experimental setup for Reuleaux forming (Permission to reprint from IDDRG) [25]

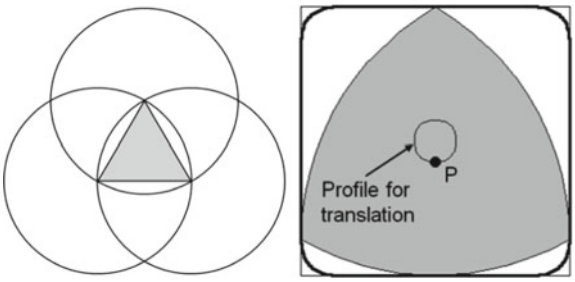

Fig. 38 Reuleaux tool generation

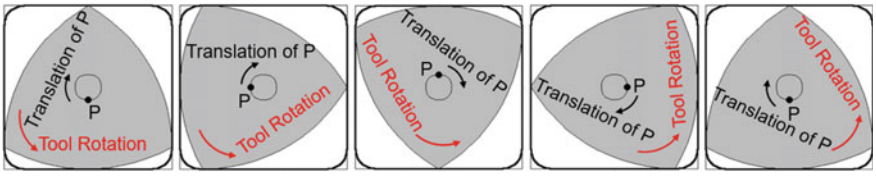

Fig. 39 One cycle of Reuleaux tool rotation to create square shape

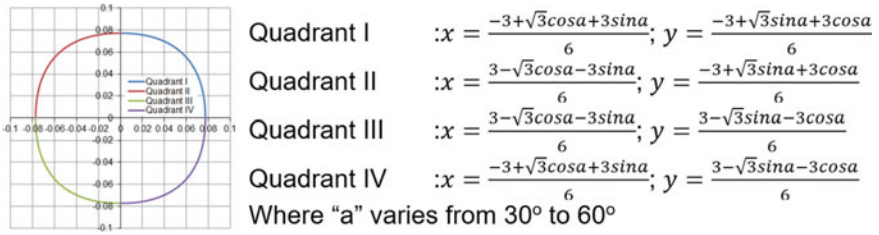

Fig. 40 Profile of point "P" and equation of 4 quadrants profile

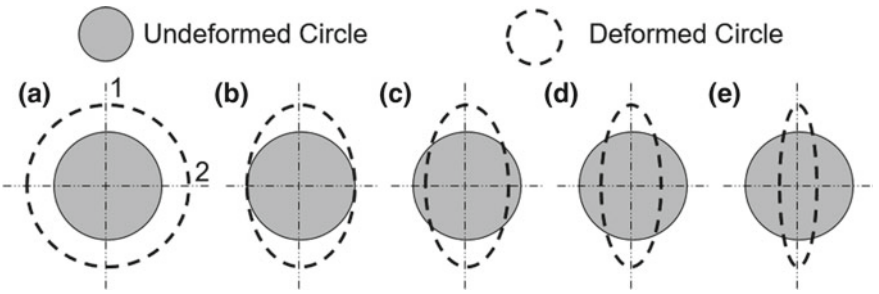

Fig. 41 Circle deformation in **a** equi-biaxial, **b** plane strain, **c** uniaxial tension, **d** pure shear, and **e** uniaxial compression deformation modes

6.1 Equibiaxial Tension

In this mechanics, the circle enlarges to a bigger circle. This means that the circle was pulled from all direction with equal force. This deformation mode is called as equi-biaxial tension or balanced biaxial stretching (Fig. 41a). After measuring the strain in a dominant direction (direction 1 in Fig. 41a) and perpendicular to a dominant direction (direction 2 in Fig. 41a) on the plane of the sheet, the major and minor strain can be calculated and thus the strain ratio (Eq. 16) can be evaluated. In equi-biaxial tension the strain ratio, β is 1, as both major and minor strain are equal and positive.

$$\beta = \frac{\varepsilon_2}{\varepsilon_1} \tag{16}$$

6.2 Plane Strain

In plane strain mechanics the sheet metal is pulled in such a way that direction 2 size does not change while direction 1 is elongated to become an ellipse (Fig. 41b). In this case, the force applied was higher in direction 1 and compared to direction 2, and direction 2 force was enough to keep the initial circle dimension same. As the

direction 2 size does not change, the strain in this direction is zero and thus the strain ratio, β is 0.

6.3 Uniaxial Tension

In uniaxial strain mechanics, the material is only pulled in one direction like a tensile test. Due to which the size of the circle in direction 2 is compressed (Fig. 41c). Thus the strain in the direction 2 is negative. It was also observed that the strain in direction 1 is twice than the strain in direction 2 and thus the strain ratio, β is $-1/2$.

6.4 Pure Shear

In pure shear, the force is applied to the sheet metal in such a way that the tension in the direction 1 and compression in direction 2 (Fig. 41d). Due to this, the material is compressed in direction 2. It was observed that strains are equal in both direction but opposite in nature and thus the strain ratio, β is -1.

6.5 Uniaxial Compression

The uniaxial compression is similar to uniaxial tension, however, in this case, a compression force was applied in direction 2 only. Due to this kind of force in the direction 1 started to elongate (Fig. 41e). It was found that the direction 2 strain was twice than the direction 1 with opposite sign. Thus the strain ratio, β is -2.

6.6 Through Thickness Pressure

In all above five mechanics, it was assumed that the third direction strain is negligible and thus it was not taken into consideration. However, in some case, the sheet metal thickness (direction 3) was compressed in such a way that the normal stresses/pressure generated in thickness direction influences the deformation and thus it is important to take in account. Due to normal stresses in the thickness direction, it was found that the formability of metal increases. The reason behind this increase in formability was that during compression of sheet metal through-thickness direction, the voids were suppressed and delayed the failure.

6.7 Through Thickness Shear

This is similar to the above case with a difference of shear stress generates through the thickness direction. This mechanics was observed in single point incremental forming, rotational and Reuleaux forming. Due to shear stress in the thickness direction, the principal stresses are angled in different than the plane of the sheet direction and thus the FLC needs to be drawn with the third axis of thickness strain. These shear stresses provide the increase in formability of metal.

7 Common Challenges in Sheet Metal Forming

It is more than a century when a sheet metal process saw its existence and has been seen a huge advancement till then. From hand-held tool forming to a robotic operation on the shop floor, the technology has emerged a lot. As discussed above a large number of processes and a wide variety of application of those parts have a huge impact on development. However, there are still some challenges due to implementations of newer regulations and material developments. Some of them are discussed here.

7.1 Springback

Springback is the unwanted shape which results after releasing the forming load from the formed metal. This is also called as elastic recovery. When the metal is deformed, the metal follows its stress-strain curve for that particular deformation in which it is forming. Metal first follow the elastic region of stress-strain curve and then yields and then do some plastic deformation to permanently deform the metal. If the load is released at this point, then metal would like to recover elastically as shown in Fig. 42. This change in shape is called springback (Fig. 43). This phenomenon is very common in conventional metals and proper solutions were applied for example die compensation, rotational rollers in die or punch radius, passing electric current to eliminate the springback. It was always assumed that the elasticity of a material remains constant. However advanced materials such as AHSS behaves differently for springback. The elastic recovery of AHSS is depended on how much strain is accumulated during deformation, and based on that strain the elastic recovery would be different.

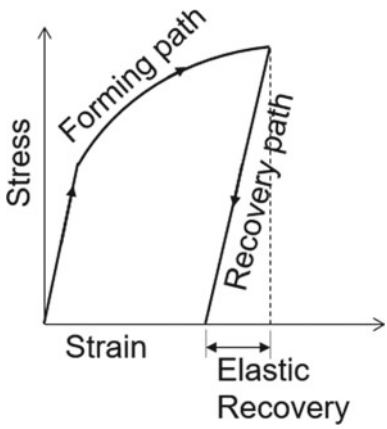

Fig. 42 Elastic recovery on stress-strain curve

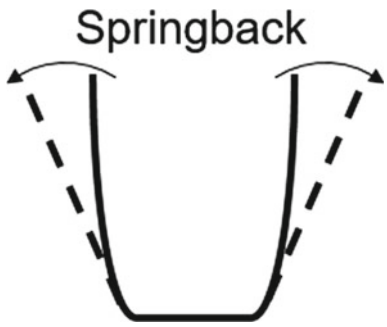

Fig. 43 Channel springback

7.2 Buckling and Wrinkling

When the metal cannot sustain any more force in compression, buckling or wrinkling occurs. Buckling and wrinkling terms are used interchangeably in sheet forming, whereas in tube forming buckling is a common term. The parameter influences the buckling or wrinkling is the excessive force in compression, material strength, the thickness of a material, and the length of the material between applications of force. Length is the dominant factor for buckling. Wrinkling in sheet metal forming occurs due to insufficient blankholding force. When the metal draws in the die the circumferential stresses acts on the wall of the metal and due to insufficient blankholding force the material wrinkles.

7.3 Fracture

Fracture is defined as the separation of metal in two or more pieces. Materials used in sheet metal are supposed to be ductile as they required shaping and stretching

of workpieces. However, depending on the deformation mode the metal can go in sudden fracture without any sign of necking. For this reason, an FLC needs to be experimentally plotted for a particular material. Based on the part shape and metal used the die and punch should be properly designed so none of the strains go beyond the FLC in any of the deformation modes. Most of the conventional materials used in sheet metals provide the ductile behavior and predicts closely to FLC. However, most advanced material such as AHSS needs more attention as they developed with the purpose of weight saving with higher load-bearing capacity. These steels are multi-phase microstructure and interaction of hard and soft phase during deformation would be critical and may lead to early failure.

References

1. Standard, ASTM E8 (2004) Standard test methods for tension testing of metallic materials. Annual book of ASTM standards, 3, pp 57–72
2. Lajarin SF, Nikhare CP, Marcondes PVP (2018) Dependence of plastic strain and microstructure on elastic modulus reduction inadvanced high strength steels. J Braz Soc Mech Sci Eng 40:87
3. Kalpakjian S, Schmid SR (2014) Manufacturing engineering and technology. Pearson, Upper Saddle River, p 913
4. Pier BF, Nikhare CP (2018) Outer diameter to thickness ratio effect on tube flaring behavior. In: Proceedings of the ASME 2018 international manufacturing science and engineering conference
5. Dick CP, Korkolis YP (2014) Mechanics and full-field deformation study of the ring hoop tension test. Int J Solids Struct 51(18):3042–3057
6. Documentation, A. and Manual, U., 2010. Version 6.10. Dassault Systemes
7. Standard, ASTM E2218-02 (2008) Standard test method for determining forming limit curves. Annual book of ASTMStandards, vol 03.01. ASTM International, West Conshohocken, PA
8. Keeler SP, Backofen WA (1963) Plastic instability and fracture in sheets stretched over rigid punches. Asm Trans Q 56(1):25–48
9. Nikhare CP (2018) Experimental and numerical investigation of forming limit differences in biaxial and dome test. J Manuf Sci Eng 140(8):081005
10. Makinde A, Thibodeau L, Neale KW (1992) Development of an apparatus for biaxial testing using cruciform specimens. Exp Mech 32(2):138–144
11. Ohtake Y, Rokugawa S, Masumoto H (1999) Geometry det0ermination of cruciform-type specimen and biaxial tensile test of C/C composites. In: Key engineering materials, vol 164. Trans Tech Publications, pp 151–154
12. Welsh JS, Adams DF (2002) An experimental investigation of the biaxial strength of IM6/3501-6 carbon/epoxy cross-ply laminates using cruciform specimens. Compos A Appl Sci Manuf 33(6):829–839
13. Merklein M, Biasutti M (2013) Development of a biaxial tensile machine for characterization of sheet metals. J Mater Process Technol 213(6):939–946
14. Hanabusa Y, Takizawa H, Kuwabara T (2013) Numerical verification of a biaxial tensile test method using a cruciform specimen. J Mater Process Technol 213(6):961–970
15. Usui H, Iizuka T (2014) Investigation of the shape of a cruciform biaxial tensile specimen intended for a combination of plane strain tensile states. In: Key engineering materials, vol 622. Trans Tech Publications, pp 308–313
16. Leotoing L, Guines D, Zidane I, Ragneau E (2013) Cruciform shape benefits for experimental and numerical evaluation of sheet metal formability. J Mater Process Technol 213(6):856–863

17. Lester S, Nikhare C (2014) Investigation of strain development and hole expansion ratio in mild steel and AA 5083. In: International Deep Drawing Research Group 2014 conference, pp 210–215
18. Hyun DI, Oak SM, Kang SS, Moon YH (2002) Estimation of hole flangeability for high strength steel plates. J Mater Process Technol 130–131:9–13
19. Uthaisangsuk V, Prahl U, Bleck W (2009) Stretch-flangeability characterisation of multiphase steel using a microstructure based failure modelling. Comput Mater Sci 45:617–623
20. Ko YK, Lee JS, Huh H, Kim HK, Park SH (2007) Prediction of fracture in hub-hole expanding process using a new ductile fracture criterion. J Mater Process Technol 187–188:358–362
21. Wiedenmann R, Sartkulvanich P, Altan T (2009) Finite element analysis on the effect of sheared edge quality in blanking upon hole expansion of advanced high strength steel. In: International Deep Drawing Research Group conference, Golden, Colorado, pp 559–570
22. http://resources.jorum.ac.uk/xmlui/bitstream/handle/123456789/997/Items/T173_2_section32.html
23. https://www.manufacturingguide.com/en/roll-forming
24. Reuleaux F (1963) The kinematics of machinery. Dover Publications, New York
25. Horstman R, Nikhare CP (2018) An investigation on square tube forming using a Reuleaux triangle. In: International Deep Drawing Research Group 2018 conference

Analysis and Optimization of Metal Injection Moulding Process

C. Veeresh Nayak, G. C. Manjunath Patel, M. R. Ramesh, Vijay Desai and Sudip Kumar Samanta

Abstract Near net shape metal injection moulding (MIM) process is employed to manufacture the complex shaped metal parts and can readily be used without the requirement of secondary processes. Appropriate control at various stages (i.e. feedstock preparation, injection moulding, binding, debinding, and sintering) of the MIM process is essential to obtain pore-free structure that yield good compact in MIM parts. In MIM process, the outputs (such as, surface roughness, micro-hardness, and ultimate tensile strength) of injection molded parts is influenced majorly by injection speed, feedstock flow velocity, injection temperature and mold temperature. The present work is focused to study and analyse the effect of influencing variables of nickel based (Cr_3C_2-NiCr + NiCrSiB) metal injection moulded parts using statistical Taguchi method. Taguchi method is employed to conduct actual experiments and Pareto analysis of variance is conducted to analyze and estimate the significant contribution of input variables on different outputs. Taguchi and Pareto ANOVA methods determine the different set of optimal levels for each output, separately. Determining single optimal level for all the outputs is often difficult due to the conflicting requirements (maximize: MH, UST; minimize: SR) in injection moulded parts. Therefore, Principal component analysis (PCA) is applied to determine the relative importance (weight fraction) for individual outputs. Grey relational analysis (GRA) is applied to convert the multiple objective functions with different set of weight fractions determined using PCA to single objective function through suitable mathematical formulation. The grey relation grading has been determined and single optimal levels for satisfying the conflicting requirements are solved in the present work. The hybrid Taguchi-GRA-PCA method determined optimal solutions are tested with practical

C. Veeresh Nayak · M. R. Ramesh · V. Desai
Department of Mechanical Engineering, National Institute of Technology Karnataka, Surathkal 575025, India

G. C. Manjunath Patel (✉)
Department of Mechanical Engineering, PES Institute of Technology and Management, Shivamogga 577204, Karnataka, India
e-mail: manju09mpm05@gmail.com

S. K. Samanta
Near Net-Shape Manufacturing Group, CSIR-Central Mechanical Engineering Research Institute, Durgapur 713209, India

K. Gupta (ed.), *Materials Forming, Machining and Post Processing*, Materials Forming, Machining and Tribology, https://doi.org/10.1007/978-3-030-18854-2_2

experiments and resulted in better metal injection mould properties. The result could help any novice user to gain best properties in metal injection moulded parts.

Keywords Metal injection moulding · Density · Hardness · Ultimate tensile strength · PCA · Taguchi · Optimization

1 Introduction

Metal injection moulding (MIM) process is proved as an economical route to fabricate large quantity of micro components of complex geometry [1]. The process was developed and commercialized early in 1970–80s. The MIM process is of similar construction and working principle to that of plastic injection molding and powder metallurgy processes. MIM process is cost effective and near net shape manufacturing process, as the parts are directly used in services without the requirement of secondary manufacturing processes [2]. The process is now commercialized to manufacture parts used in industrial, commercial, medical, aerospace and automobile applications [3].

In recent past, the micro-injection moulding process had drawn significant attention for researchers/investigators across the globe, towards the enhancement of surface and mechanical properties. Theoretical, numerical and classical engineering experimental methods are established during that period. Theoretical, numerical and classical engineered experimental methods are the major class of research works happened when the process developed. The numerical tool has been developed to improve the mould design that enhance the injection simulation [4]. Merz et al. [5] investigated different binder system on the properties of metal powder injection moulded parts. Thermal elimination, supercritical carbon dioxide and catalytic debindering processes are the commonly used methods in recent literature [2, 6]. The mean size of the metal powders greatly influences on the properties of injection moulded parts [2, 7]. The appropriate choice of ratio of powder to binder and mixing methods decides the success or failure of metal injection moulded parts [7, 8]. The powder and binder mixing and associated homogeneous filling of feedstock into the mould is dependent on the viscous flow of the mixture into the mould [9, 10]. Sintering process in metal injection moulding is of paramount importance to gain better dense parts [11]. Injection parameters (i.e. injection pressure, injection velocity) are also of paramount importance on the final outcome of the products. Research efforts are also done by altering mould and melt temperature for enhanced mechanical and microstructure properties of injection moulded parts [12]. The friction and wear behaviour of metallic parts are influenced significantly by the surface property [13]. The wear behaviour of injection moulded parts depends primarily on the surface property than the bulk property [13]. Aggarwal et al. [7], showed short filling time requires higher injection pressure, whereas it affects the die life. Whereas, long filling time could result in incomplete fill of mould cavity. The optimum filling time is dependent on the temperature gradient exist between the mould and melt

temperature [7]. Numerical and simulation methods use many assumptions and are difficult to meet in actual industrial practice. Although classical or traditional experiment methods provide good insight of individual factor effects, but it requires many experimental trials.

Statistical methods study many factors by varying simultaneously between their respective operating levels by conducting minimum experimental trials. Statistical Taguchi method is applied to minimize the shrinkage in the green part by optimizing the moulding parameters namely, holding time, injection speed, holding pressure, cooling time and injection temperature [14, 15]. Taguchi method is applied to optimize the heating rate and sintering parameters (i.e. temperature, time and atmosphere) on the density of metal injection moulded parts [11]. Yaralagadda [16] used artificial neural networks to study the impact of cavity thickness, flow length, mould and melt temperature on injection time of MIM parts. From the above research work, it was observed that injection speed, injection temperature, flow velocity, sintering temperature, and mould temperature influence critically the metal injection moulded parts. Therefore, significant scope for researchers to explore their individual effects and optimize for the desired properties of metal injection moulded parts.

Optimization of metal injection moulded parts is of industrial relevance, as improper choice of metal injection moulded parameters results in defects (shrinkage, porosity, distortion and so on) that attain desired strength in the parts. Classical or traditional experiment methods results in local solutions (say, low strength and hardness) and could not produce satisfactory results when the individual parameter is studied with wide operating range after keeping the rest of parameters at fixed values. Conventional methods practiced currently in metal injection moulding industries is considered as a tedious task for manufacturers due to complex and non-linear (that is, high values of melt and low mould temperature and vice versa, results in the approximately same impact on the strength and properties of a part). Further, the conflicting (that is, minimum surface roughness, and maximum strength and hardness) requirements in the metal injection moulded parts requires systematic methods for conducting optimization. In recent past, grey relational analysis (GRA) is used as a powerful tool for process analysis and optimizing the complex inter-relationships among multiple outputs. GRA was applied to optimize the conflicting outputs that determine the set of input variables [17–19]. Principal component analysis (PCA) is applied to estimate the weight fractions associated to different output functions, this could enable industry personnel to know and apply the relative importance during the optimization task [17]. Single optimization method might not be effective to locate the best set of design variables, when applied to optimize any process. Taguchi method integrated with GRA and PCA proved as useful tool to improve the performance of plastic injection moulding process [20, 21]. Therefore, a significant scope to study, analyse and optimize the parameters of a metal injection moulding process using hybrid Taguchi, PCA and GRA methods exist.

2 Manufacturing Process

The MIM working principle is explained in Fig. 1. The required quantity of metal powder with desired size and thermoplastics (i.e. binder) are thoroughly mixed by utilizing the kneaders to obtain the feedstock. The thermoplastic behaves as the intermediate processing aid and later removed from the part or component after injection moulding. The binder system plays a vital role to carry the metal powder homogeneously for powder compaction to obtain desired shape and size. The feedstock is heated to make the metal powder get soften that allow ease of flow and injected to the mould cavity using injection moulding machine. The obtained injection moulded part is referred as green part, which is subsequently exposed to solution (i.e. chemical) debinding. In chemical debinding, only one part of the binder system is excluded to obtain an opening the micro-channels in the component that facilitate ease of extraction of remaining binder in the subsequent thermal debinding stage. Further, the sintering process is carried out initially for compaction and finally for forming a solid mass of materials by the application of heat without melting.

2.1 Powders Particle Size and Shape for MIM

Cr_3C_2-NiCr and NiCrSiB composites are composed of carbide particles reinforcing a metallic matrix, combining the properties of high hardness and toughness of metals. Cr_3C_2-NiCr and NiCrSiB feedstock powders are "agglomerated and sintered under hot isostatic pressure". The composites can be used for higher temperature applications in light of the excellent corrosion and oxidation resistance of the nickel chromium alloy and reasonable wear resistance of the chromium carbides at temperatures up to 900 °C. The chemical composition of NiCrSiB is as follows, Cr—7.5%, Fe—2.5%, B—1.6%, Si—3.5% and remaining is Ni.

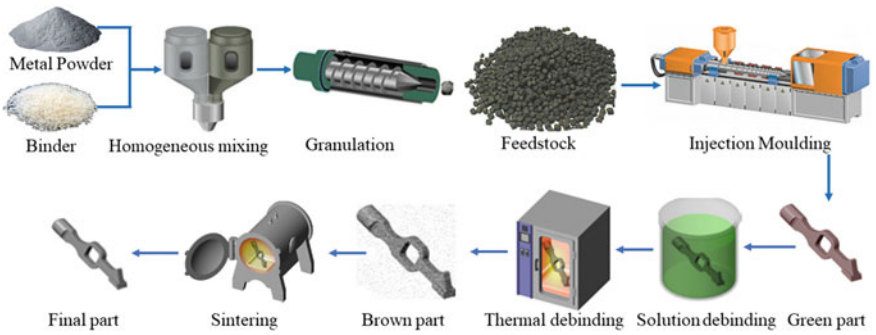

Fig. 1 Schematic diagram representing the steps in powder injection moulding process

These composites exhibit high hardness and different wear behaviours. Carbide based composite are widely used in abrasive and oxidising environments for various applications. In addition to these features, the coefficient of thermal expansion of Cr_3C_2 (10.3×10^{-6} °C^{-1}) is nearly similar to that of iron (11.4×10^{-6} °C^{-1}) and nickel (12.8×10^{-6} °C^{-1}) that constitute the base of most high temperature alloys. This minimizes stress generation through thermal expansion mismatch during thermal cycles. The chemical composition of Cr_3C_2-NiCr is as follows, Ni—30%, C—9.5%, and remaining is Cr.

In MIM process, the morphology of metal powders is of paramount importance as it influence largely on the properties (i.e. density, strength and surface characteristics) of MIM parts. Recent literature [22] reported the irregular shape of powder particles exhibit better shape retention in the moulded parts during removal of binder. Further, the packing coordination of metal powders for compaction and the part density is also affected by an irregular particle size and shape. Due to lack of sintering stability the coarse powders are generally not preferred. The best powder particle size varies in the ranges of 15 and 45 μm.

The metal powder characterization with respect to particle size and shape is of great importance for successful processing and finally the processed component subjected to critical loading during the practical usage. The component poses highest strength when the particles are densely packed without the voids, can be used during critical loading applications [23]. Increase in particle size and its distribution width improve the compaction strength [24]. The irregular size and shape of powder particle increases the compaction strength due to interparticle friction among metal powders, and after removal of binder in debinding stage the packing density decreases due to created voids [8, 24]. Further, viscosity increases during moulding and lowering the final density of the part after performing sintering. It is also noted that, the packing density improves with the spherical shape of powder particles and lowers the viscosity in feedstock during injection moulding. This could result in good compact green strength and density and improves density after sintering compared to irregular shape and size of metal powders. Previous literature [25] showed the optimal shape of the metal powders must be between spherical and irregular. Figures 2 and 3 showed the size and shape of metal powders (i.e. NiCrSiB and Cr_3C_2-NiCr) and its distribution. The details of powder particle analysed through scanning electron microscope is presented in Table 1 (refer Fig. 3).

3 Materials and Methodology for MIM Process

The steps involved in metal injection moulding process is discussed as follows,

Step 1: Preparation of feedstock

The primary raw materials such as metal powders and thermoplastic binder are used for MIM process. The binder serves as an intermediate processing aid and later removed from the part using solution and thermal debinding process after debinding.

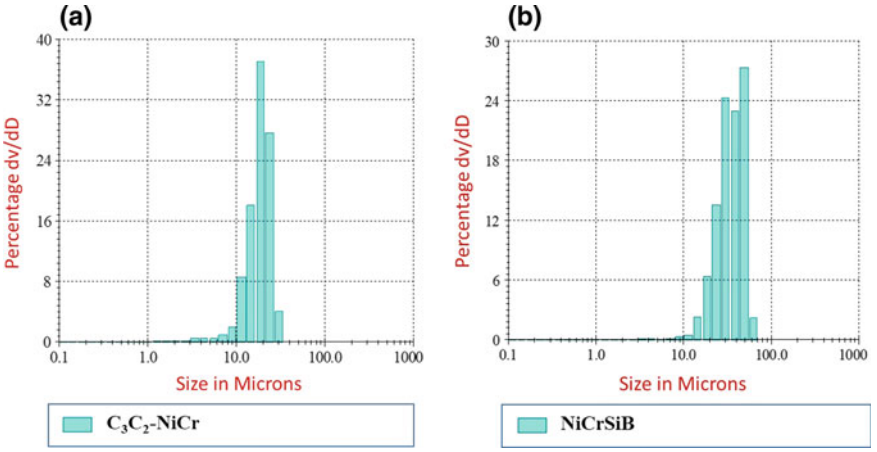

Fig. 2 Shows the metal particle distribution graph **a** NiCrSiB **b** Cr_3C_2-NiCr

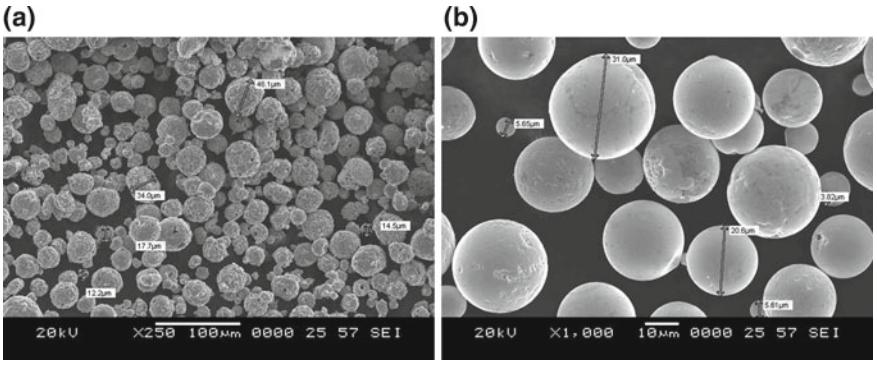

Fig. 3 SEM photograph metal powders **a** Cr_3C_2-NiCr powder **b** NiCrSiB powder

Table 1 Characteristics of metal powders (Cr_3C_2-NiCr + NiCrSiB)

Individuals	Details
Identification	Cr_3C_2-NiCr + NiCrSiB
Powder source	Spraymet Surface Technologies Pvt. Ltd.
Tap density, g/cm^3	4.96
True pycnometer density, g/cm^3	8.03
Powder size	D10 = 0.59 μm D50 = 1.45 μm D90 = 7.05 μm D97 = 16.90 μm

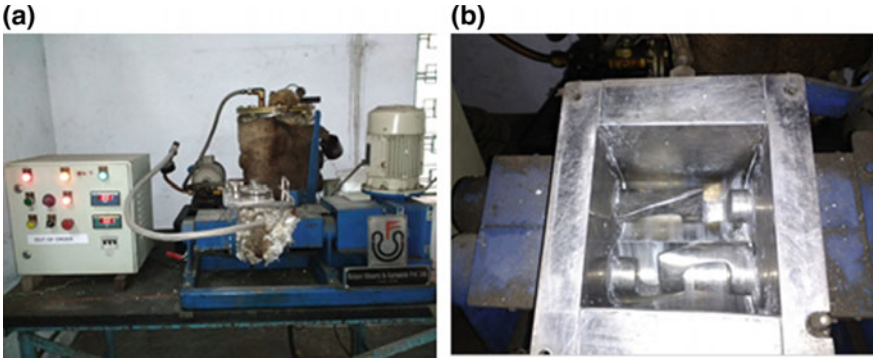

Fig. 4 Sigma blade mixer: **a** sigma blade mixer with temperature unit **b** mixing chamber

The blended powder and binder is mixed homogeneously is worked to plasticised state at an elevated temperature utilising kneader or shell roll extruder. The blended powder mix must be free from agglomeration and porosity, any deficiency in mixing stage will continue for subsequent stages. Further, too little binder might not be sufficient to coat all the metal powder and initiates voids in the mixture, which results in high viscosity feedstock and difficult to mould. Contrary, excess binder offer low moulded strength and inhomogeneous part which result in dimensional problems. Further, use of excess binder will slow down the debinding process and may cause part slump when the particle settles or migrate during debinding [26]. In subsequent stages namely sintering there will be major changes in the dimensions of the part. The feedstock is prepared using Sigma Z blade mixer and the mixing chamber is shown in Fig. 4.

To study the rheological properties, the viscosity of a feedstock has been measured using a rotational rheometer (Make: MCR501 Anton Paar, Austria) shown in Fig. 5. The rheological characteristics were studied at four different temperatures in the ranges of 150–180 °C with the step interval of 2 °C in the rotational rheometer.

In rotational rheometer, the two factors to be considered during viscosity measurement such as, small gap (approximately 50 μm) must be maintained between the two parallel plates to eliminate the initial secondary flows, and to establish good control over shear rate that minimize viscous heating [27]. In MIM process, uniform filling into the mould is dependent on the steady flow, which in turn dependent on the feedstock rheological property (i.e. viscosity).

Figure 6 shows the results of pilot experiments that were conducted to know the viscosity and its shear sensitivity at different temperatures. The increase in shear rate was observed with decrease in viscosity [28]. Further, the viscosity of the medium size powder particle is comparatively higher than the fine powder particles. This might be due to the fact that the fine powder particles are augmented to smaller interstitial spaces compared to coarse size powder, thus increase inter particle friction. Further, the fine powder particle pose large surface contact area when bombarded with

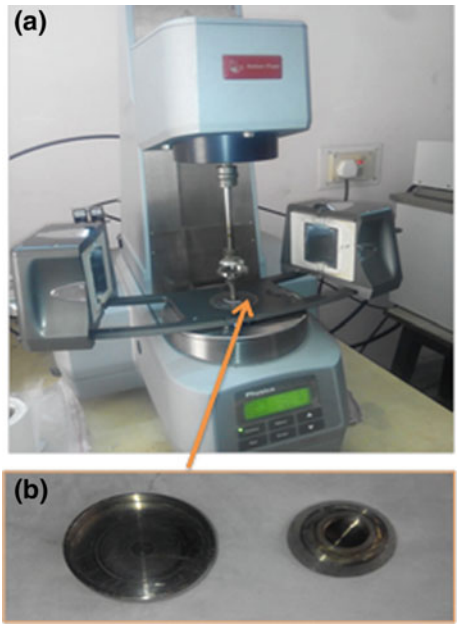

Fig. 5 Rotational rheometer with **a** open chamber **b** plate

neighbouring particles [29]. Important to note that a sudden change in the viscosity in moulded parts results in cracking and distortion [30].

Step 2: Injection Moulding

The injection moulding process is complex and non-linear as the properties are influenced by many variables. The appropriate choice of injection moulding variables has showed significant impact to manufacture the defect free part. The schematic view of metal injection moulding machine is shown in Fig. 7. In MIM process, initially the mould is open, while the screw (i.e. ram) is positioned at the extreme left position. When the feedstock is heated to desired temperature, the mould closes and the screw pushed the feedstock to fill the mould cavity. To compensate for shrinkage (if any) the feedstock is forced to the mould during the cooling stage and the back pressure is maintained in the feedstock till the gate freezes. After the part ensures completely solidified the back pressure is removed and the part is ejected from the mould halves. The solidified ejected part in metal injection moulding part is referred as green part (refer Fig. 8). The MIM green parts are similar to forming of plastic parts in injection moulding process. Important to note that, wide variety of part geometries can be produced similar to plastic parts in metal injection moulding process [31].

Prior to practical experiments, the mould tool is designed by utilizing modelling software (Pro/Engineer Wildfire 5.0). The obtained model using Pro/E tool is converted to Initial Graphics Exchange Specification (IGES) for machining in computer numerical control equipment.

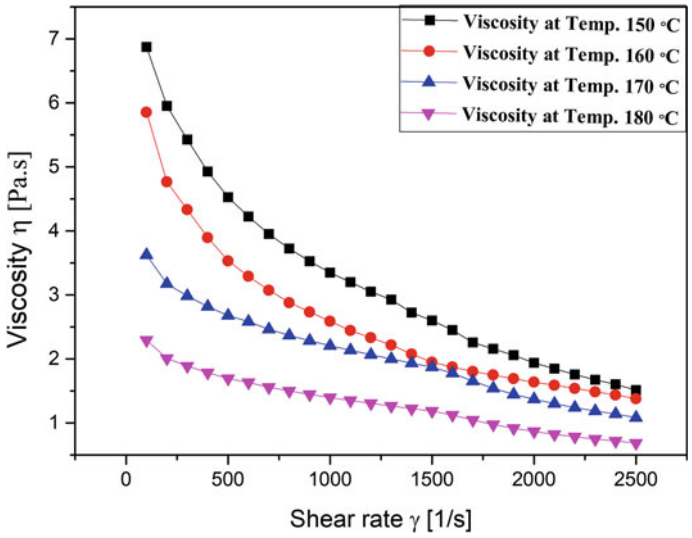

Fig. 6 The relation between viscosity of Cr_3C_2-NiCr + NiCrSiB feedstock and shear rate

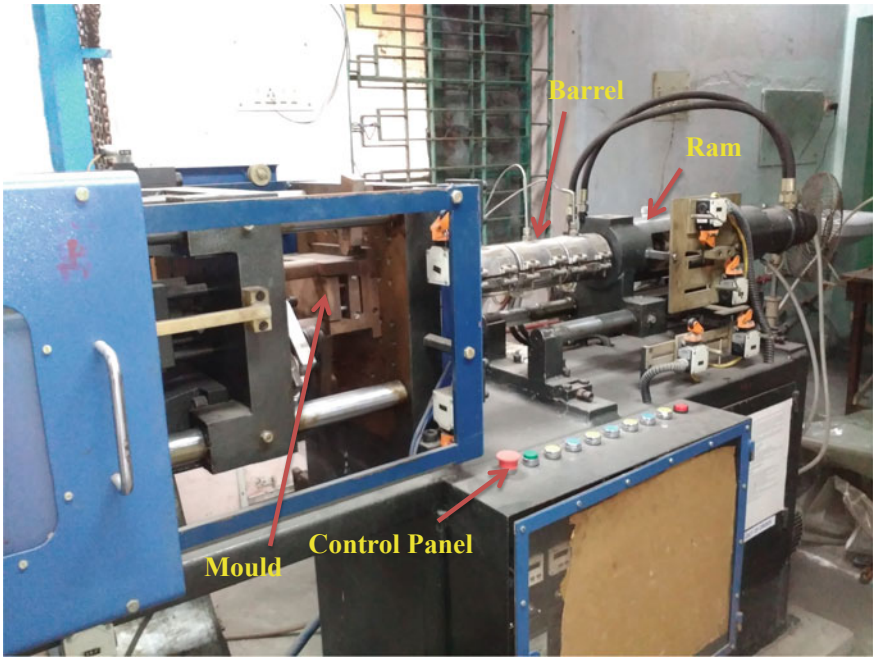

Fig. 7 Injection mould used for fabrication

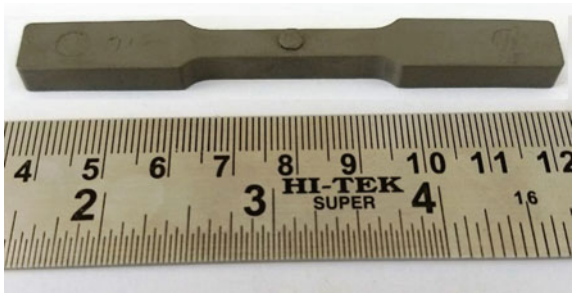

Fig. 8 Defect-free MIM "green" part

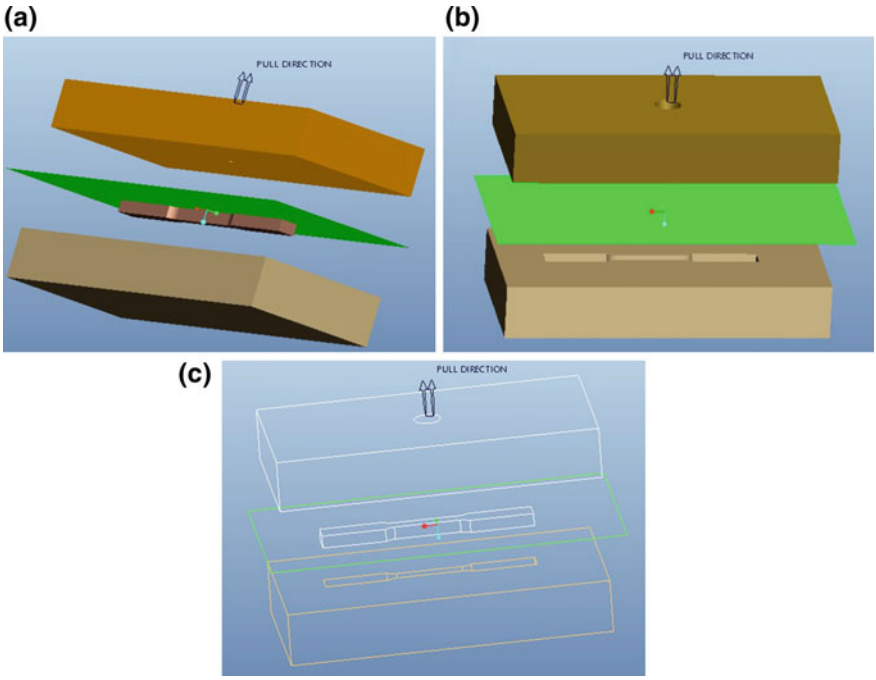

Fig. 9 Injection mould inserts with **a** reference part & parting surface **b** cavity **c** wireframe model of core cavity

The injection pressure was recorded by utilizing pressure sensor which could operate in the range of 10–100 bar (Make: GEMS-UK, Model: 1200BGC4001A3UA), installed in the hydraulic line will help to push the feedstock with the help of injection screw inside the barrel. A 40 mm diameter standard screw and barrel assembly is employed in the injection moulding machine. The present work uses the multiple injection speed to inject the feedstock into the mould. The present work attempt to study the properties with different injection speed, which is varied from 10 to 40% (i.e. 13.8–55.2 cc/s) to that of maximum injection speed (i.e. 138 cc/s) (Fig. 9).

Table 2 The details of binder and their corresponding properties

Binder (B)	Nature	Binder name	Melt temperature, °C	Density, g/cm^3
B 1	Primary	PolyethyleneGlycol-600 (PEG 600)	64.38	1.29
B 2		Paraffin wax (PW)		0.92
B 3	Secondary	Low-density polyethylene (LDPE)	180	0.91
B 4	Surfactant	Stearic acid (SA)	70.1	0.94

Step 3: Binder for MIM

In MIM, the primary usage of a binder is to facilitate ease of metal flow and establish better powder particle compaction in the mould cavity. Further, binder is designed to serve as a multi-component system. The binder (say thermoplastic) also acts as a backbone component, which retains the mould shape without altering the dimensions for the subsequent stages. Later, the second component (i.e. wax) is applied to enhance the mixture flowability. In subsequent stages the wax is extracted during debinding which create the pores in part. These pores facilitate the gaseous products of the remaining polymer to diffuse out of the structure, without creating the internal vapor pressure that might have resulted in the part failure. Furthermore, removing approximately the 50% of binder quantity could substantially decrease the carbon pick-up while performing thermal debinding process. Finally, the surfactant is added as an additive to limit the contact angle by lowering the surface energy at the binder-powder interface. The binder details used for the experiments are presented in Table 2.

Step 4: Debinding

Thermal debinding of the injection moulded part has been conducted by utilizing the electric resistance furnace shown in Fig. 10. Prior to thermal debinding, the solvent debinding has been done by dipping the specimen in n-hexane (C_6H_{14}) solution and heating the solution below its melting point of paraffin wax, where majority of the PEG-66, PW and SA were removed by dissolving in n-hexane (C_6H_{14}). Solvent debinding have been carried out in a drying oven maintained at different temperatures and time. After solvent debinding the specimens are dried for 2 h at 40 °C in a drying oven (DASS and Co-Howrah). In the thermal debinding process, the remaining binders (if any) such as PEG-600, PW, SA and LDPE from the moulded specimen was removed with the help of tube type furnace (Make: DASS and Co-Howrah, Model No.: EN120 QT). Important to note that the thermal debinding has been carried out at different holding time and temperatures in a hydrogen atmosphere, where the heating step rate was 1 °C/min. The present work uses a multi-component binder (such as PEG-600, PW, SA and LDPE) and must be removed in different processing steps. Noteworthy that, at least one binder component must be of 30% and more, in the binder-mix, and that major proportion of the binder needs to be

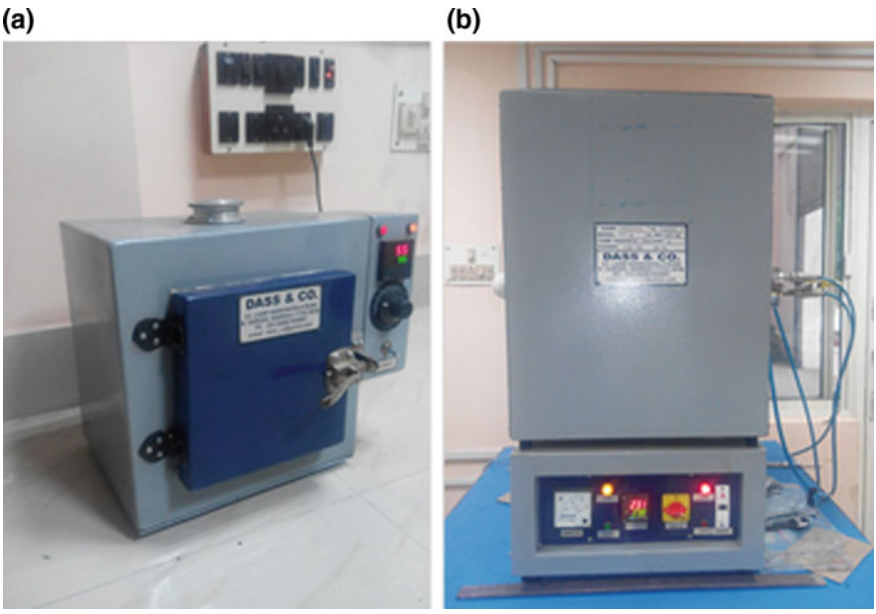

Fig. 10 Debinding furnaces **a** drying oven **b** thermal debinding furnace

removed first in the debinding process to evade the insulated compact of pores [32]. At higher temperature the percentage of PEG 600, PW and SA dissolve in n-hexane, this might be due to fact that increased solubility and diffusivity could result in major percentage of weight loss. Furthermore, with time progresses the available time to dissolve the PEG 600, PW and SA in n-hexane and weight loss increases.

The experimental observation depicts that the solvent debinding above 50 °C, resulted in the formation of a crack in the compacted part (refer Fig. 11). The obtained results are due to the thermal expansion and contraction. The insoluble binder stayed for longer duration in n-hexane solution resulted in swelling and expansion [33, 34]. The solvent debinding was conducted at higher working temperatures, which results in less compact and found drastic decrease in temperature. The sudden drop in temperature causes contraction. The parts exposed to sudden contraction and expansion, induce internal stresses in the compact and finally initiate crack. The experiments also performed by maintaining the solvent debinding above 50 °C, which results in part sagging as a result of softening of the binder component PEG 600, PW and SA. The crack and part (i.e. compact) sagging occurs above 50 °C, through pilot experiment the optimum solvent debinding compact temperature has been kept fixed to 48 °C. The optimized solvent debinding compact temperature (i.e. 48 °C) resulted in better compact, with no crack or distortion observed in the specimen. The binder present in the green part (refer Fig. 12a) and removal after subsequent debinding process is clearly seen in Fig. 12b, c, wherein the binder surrounds the powder particles. After subsequent stages of thermal and solvent debinding, the removal of

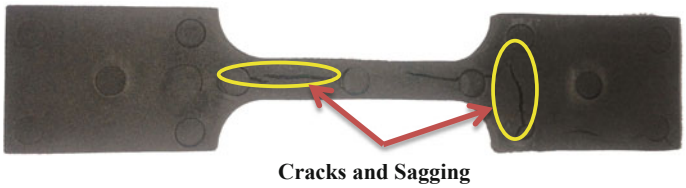

Fig. 11 Shows the cracks and sagging on compact after debinding

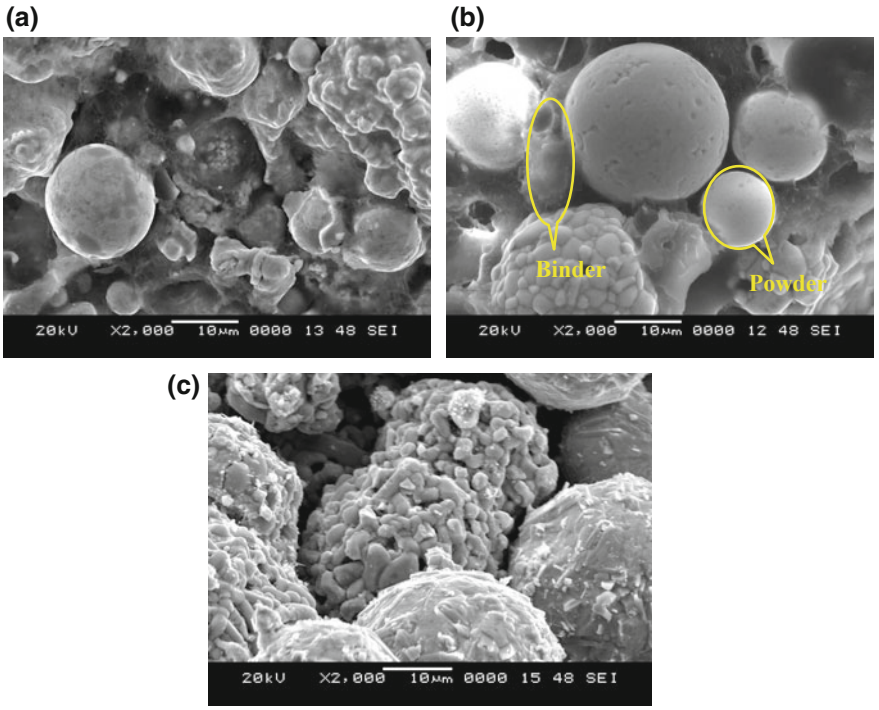

Fig. 12 Shows SEM Micrograph of a specimen **a** green part **b** solvent debinding **c** thermal debinding

major (i.e. the binder LPDE and remaining PW and SA which have not been removed in solvent debinding) constituents of the binder adhered on the powder particle can be seen in Fig. 12c.

Step 5: Sintering process

Sintering process is conducted initially for compaction and finally for forming a solid mass of materials by the application of heat without melting. The obtained part (i.e. brown part) after subsequent debinding stages is placed in a furnace, where the temperature and the atmosphere are precisely controlled. The brown part is heated approximately to 85% of materials melting temperature, which burn off the secondary

Fig. 13 Comparison of **a** green and **b** sintered part

polymer binding material. At high working temperatures, the metal powder particles tend to fuse and eliminate the faults or pores volume occupied formerly by the binder in the part [35]. The particles are bound together by atomic motion, that could reduce the high surface energy which is associated with an un-sintered powder [36]. In sintering process, the pore volume formerly occupied by the binder is removed that exhibit substantial shrinkage in the part. The shrinkage (linear up to 15–20%) occurs after the sintering process can be observed clearly in Fig. 13. If required the sintered metal injection moulded part is further processed by utilizing conventional metal working processes namely heat treatment or surface treatment in the same way as the cast or wrought parts.

In the present work, the thermal debound tensile compact (i.e. specimen) has been sintered. As the rule of thumb, as temperature tends to increase, density also increases but beyond the formation of the liquid phase, and the part shape starts distorting [37]. The sintering process has been carried out at a controlled temperature of 1200 °C, and a pure hydrogen atmosphere, to resist the effect of oxidation. The sintering cycle is continued by varying or raising the temperature from 1 to 5 °C/min, and also maintaining the soaking time allowed to remove the remaining binder in the compact and to stabilize the furnace temperature. Initially, constant (i.e. 2 °C/min) heating rate is maintained till the temperature attain 1000 °C, followed by a soaking time of 80, 80 and 30 min for the temperature of 250, 400 and 1000 °C respectively. In subsequent stages, the heating rate approximately 1 °C/min is maintained for densification of tensile specimen till the temperature attain 1200 °C and for cooling cycle, a 5 °C/min was adopted till it reaches to 200 °C, later the furnace cooling has been done (Fig. 14).

The microstructure of Cr_3C_2-NiCr + NiCrSiB powder particles are bound together and isolated pores are separated from the grain boundary in the sintered specimen is shown in Fig. 15.

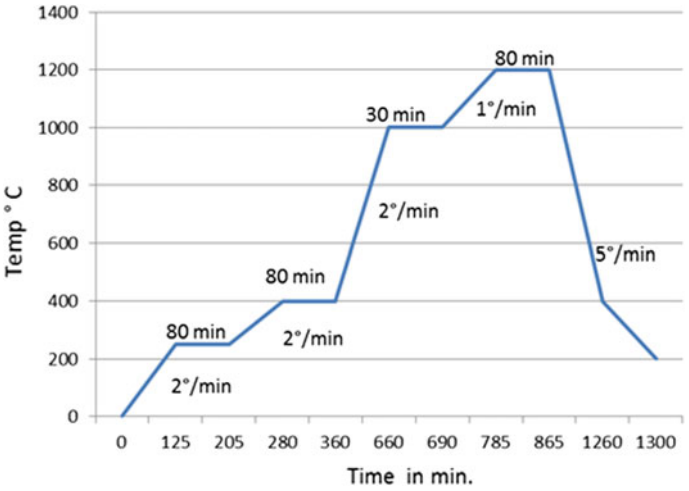

Fig. 14 Sintering cycle conducted at different temperature intervals

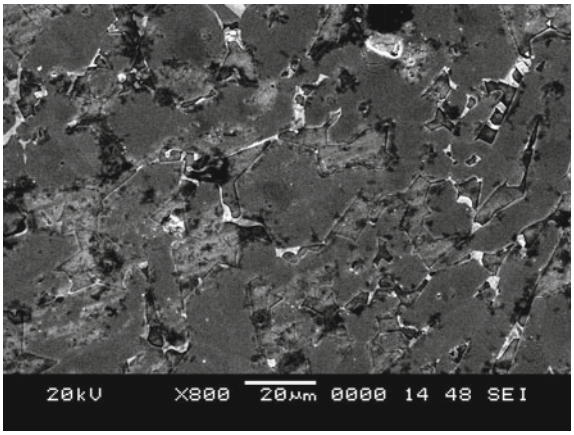

Fig. 15 SEM photograph of a sintered specimen

The density of a sintered component was measured using Archimedes immersion method. Mechanical strength, surface and microstructure characteristics are dependent primarily on the density of the injection moulded parts. The density of the sintered part (Cr_3C_2-NiCr + NiCrSiB) exhibits 8.03 g/cc. The sintered density decreases at 1200 °C, might be due to the excessive liquid phase introduced in the powder matrix. However, the presence of liquid phase in solids could improve the density, whereas too much excess liquid could reduce the sintered density, due to coarse micro-structure. During the liquid phase sintering phenomenon, the melting of particle begins which results in a solid-liquid mixture due to thermal cycle [38]. The Vickers microhardness measurements are tested on the cross-sectional area of

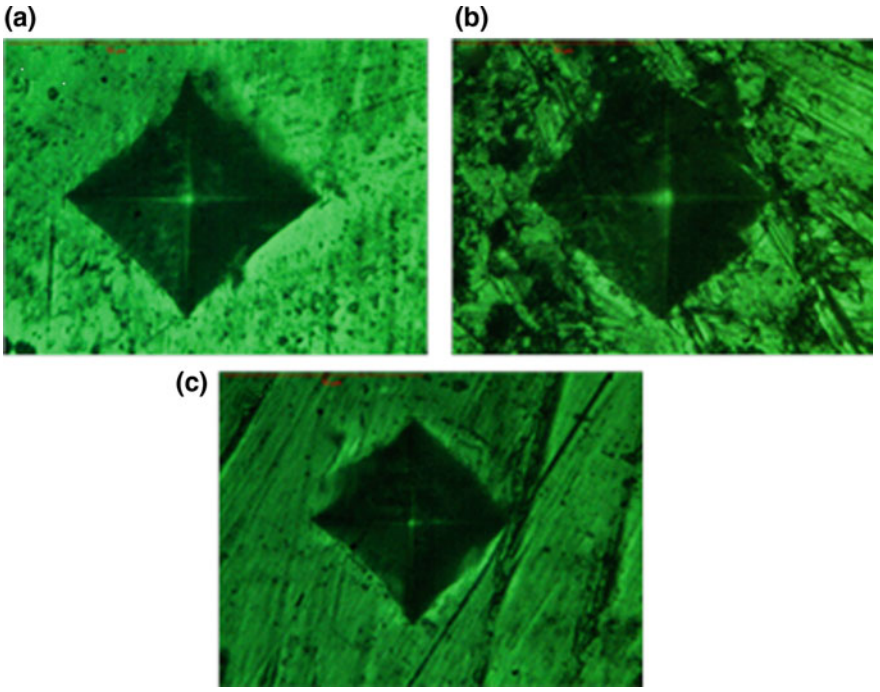

Fig. 16 Microhardness indentation on Cr_3C_2-NiCr + NiCrSiB

Table 3 Linear shrinkage of the MIM part

Material	Length (shrinkage %)	Width (shrinkage %)	Thickness (shrinkage %)
Cr_3C_2-NiCr + NiCrSiB	14.98–15.63	16.22–17.56	15.43–16.73

the tensile test specimen at the core region as shown in Fig. 16. Prior to measurement, the surface area of the specimen was polished to nullify the effect of dirt, debris and discontinuities (if any). The resulted microhardness on the sintered part is 710 Hv. The highest hardness was obtained on the sintered specimen subjected to a temperature of 1200 °C.

After sintering process, the density improves by eliminating the pores and shrinkage which might present in the specimen. The shrinkage of the part after sintering process was measured in three different directions (i.e. length, width and thickness) and the obtained results are presented in Table 3. In general phenomenon, the shrinkage should be approximately equal in all directions. However, Table 3 show there is a variation of shrinkage occurs and this might be attributed to the segregation of powder and binder phase in the specimen during injection stage.

4 Results and Discussion

The metal injection moulding parameters are selected generally in industrial practice, with the available experts, costly simulation and trial run practical experiments. These methods do not provide economical manufacturing route, as a result of a time consuming, poor utilization of equipment, and defective products. Taguchi method suggests limited experiments based on an available orthogonal array, analyse and determine the optimal input parameters for the output (response) variable. MIM process is a multi-input and multi-output system, Taguchi method determines a set of different combination of independent variables for each output variable. For example, optimum parameter condition for minimizing the surface roughness of the injection moulded parts might not be same as maximizing the microhardness and tensile strength. Taguchi method may not produce the feasible solution for the conflicting requirement of minimum surface roughness and maximum strength and hardness. Grey relational analysis is applied to choose single operating conditions for the conflicting multiple output characteristics by converting to the single output function. Multiple outputs might have many optimal solutions and select the best solution is dependent on the users or investigator preference assigned to each output solution. Assigning highest importance to surface roughness might result in poor hardness and strength and vice versa, due to the complex and multivariate metal injection moulding system. Therefore, PCA is applied to locate the importance (i.e. weight fraction) for each output quality characteristics. The combined Taguchi-Grey and PCA method attempt to convert multiple conflicting output quality characteristics (i.e. SR, MH, and UTS) to single output objective function for solving optimization of MIM process.

4.1 Statistical Taguchi Method

Dr. Genichi Taguchi developed Taguchi method, is an effective tool for study and analyse the parameter through suitable design to obtain a high quality injection moulded parts. Taguchi method uses an orthogonal array (set of well-balanced planned limited experimental runs) to know the complete insight of parameter between there corresponding operating levels. Four control factors (feedstock flow velocity, mould temperature, injection speed and injection temperature) are studied for determining the optimal parameter setting of a process. The operating condition of input variables used for experimentation and process optimization is presented in Table 4. The standard S/N ratio for any output quality characteristics will fall in any of the following, nominal-the-best, lower-the-better and higher-the-better. Smaller-the-better quality characteristics is used to determine the optimal set of parameters for the response, surface roughness (refer Eq. 1). Contrary, larger-the-better quality characteristics are used for the response, micro-hardness and ultimate tensile strength

Table 4 Injection moulding parameters and operating levels

Input variables or process parameters	Unit	Symbol	Level 1	Level 2	Level 3	Level 4
Injection speed (max. capacity 138 cc/s), IS	%	A	10	20	30	40
Feedstock flow velocity, FV	m/s	B	2	4	6	8
Injection temperature, IT	°C	C	150	160	170	180
Mould temperature, MT	°C	D	30	40	50	60

(refer Eq. 2), respectively. S/N ratio computation corresponds to the responses are defined as follows,

$$S/N\ \text{ratio}_{SR} = -10\log\left[\frac{1}{n}\sum_{i=1}^{n} y_i^2\right] \tag{1}$$

$$S/N\ \text{ratio}_{MH\ \text{and}\ \text{UTS}} = -10\log\left[\frac{1}{n}\sum_{i=1}^{n}\frac{1}{y_i^2}\right] \tag{2}$$

The term, n represents the number of replications or experiments, i refer to the experiment number and y_i depicts the response value for ith experiment. The L_{16} orthogonal array experiments are conducted for modelling and process optimization is shown in Table 5. The average values of the outputs (i.e. MH, UTS and SR) correspond to a different combination of experimental input conditions is presented in Table 5.

4.1.1 Pareto Analysis of Variance

Pareto analysis of variance employs pareto principle for data analysis and process optimization [39]. Pareto ANOVA do not require higher computational time for data analysis of the parametric design. The analysis does not demand separate ANOVA table and thereby do not use Fisher's test. The Pareto ANOVA method is more suitable for engineers and industry personnel, as they do not require highest computational knowledge and skills. The computation of pareto analysis of variance is done for the obtained S/N ratio values of MH, SR, and UTS.

Response: Micro-hardness

Table 6 show the summary results of pareto analysis of variance for the response, micro-hardness. The sample example for the computation of Pareto ANOVA for factor A is discussed as follows,

Table 5 L_{16} orthogonal array experiments for MIM process

Exp. no.	Input parameters (coded)				Input parameters (un-coded)				Average values of outputs			Average S/N ratio values of outputs		
	IS, %	FV, m/s	IT, °C	MT, °C	IS, %	FV, m/s	IT, °C	MT, °C	MH	UTS, MPa	SR, μm	MH	UTS, MPa	SR, μm
L_1	1	1	1	1	10	2	150	30	510	562	1.78	54.15	54.99	−5.01
L_2	1	2	2	2	10	4	160	40	520	572	1.69	54.32	55.15	−4.56
L_3	1	3	3	3	10	6	170	50	535	578	1.56	54.57	55.24	−3.86
L_4	1	4	4	4	10	8	180	60	520	566	1.60	54.32	55.06	−4.08
L_5	2	1	2	3	20	2	160	50	562	590	1.31	54.99	55.42	−2.35
L_6	2	2	1	4	20	4	150	60	574	596	1.28	55.18	55.50	−2.14
L_7	2	3	4	1	20	6	180	30	560	586	1.36	54.96	55.36	−2.67
L_8	2	4	3	2	20	8	170	40	548	575	1.25	54.78	55.19	−1.94
L_9	3	1	3	4	30	2	170	60	572	589	1.06	55.15	55.40	−0.51
L_{10}	3	2	4	3	30	4	180	50	588	598	0.86	55.39	55.53	1.31
L_{11}	3	3	1	2	30	6	150	40	592	610	1.03	55.45	55.71	−0.26
L_{12}	3	4	2	1	30	8	160	30	590	606	0.96	55.42	55.65	0.35
L_{13}	4	1	4	2	40	2	180	40	592	595	1.02	55.45	55.49	−0.17
L_{14}	4	2	3	1	40	4	170	30	598	606	0.84	55.53	55.65	1.51
L_{15}	4	3	2	4	40	6	160	60	590	592	0.78	55.42	55.45	2.16
L_{16}	4	4	1	3	40	8	150	50	586	590	0.92	55.36	55.42	0.72

Table 6 Pareto ANOVA for the response, MH and UTS

Outputs		Micro-hardness					Ultimate tensile strength				
Process parameters	Levels	A	B	C	D	Total	A	B	C	D	Total
Sum at factor levels	1	217.36	219.74	220.14	220.06	880.44	220.44	221.3	221.62	221.65	886.2
	2	219.91	220.42	220.15	220.00		221.47	221.83	221.67	221.54	
	3	221.41	220.40	220.03	220.31		222.29	221.76	221.48	221.61	
	4	221.76	219.88	220.12	220.07		222.01	221.32	221.44	221.41	
Sum of squares of differences		48.06	1.48	0.036	0.2248	49.808	7.991	0.9515	0.1451	0.1331	9.220
Percent contribution ratio		96.504	2.97	0.072	0.454		86.663	10.319	1.574	1.444	
Cumulative contribution ratio		96.504	99.474	99.546	100		86.663	96.982	98.556	100	
Optimum levels		A_4	B_2	C_2	D_3		A_3	B_2	C_2	D_1	

$$\text{Sum at factor A level 1 } (A_1) = 54.15 + 54.32 + 54.57 + 54.32 = 217.36$$
$$\text{Sum at factor A level 2 } (A_2) = 54.99 + 54.18 + 54.96 + 54.78 = 219.91$$
$$\text{Sum at factor A level 3 } (A_3) = 55.15 + 55.39 + 55.45 + 55.42 = 221.41$$
$$\text{Sum at factor A level 4 } (A_4) = 55.45 + 55.53 + 55.42 + 55.36 = 221.76$$

Sum of squares of differences, S_A

$$= (A_1 - A_2)^2 + (A_1 - A_3)^2 + (A_1 - A_4)^2 + (A_2 - A_3)^2 + (A_2 - A_4)^2 + (A_3 - A_4)^2$$
$$= (217.36 - 219.91)^2 + (217.36 - 221.41)^2 + (217.36 - 221.76)^2 + (219.91 - 221.41)^2 + (219.91 - 221.76)^2 + (221.41 - 221.76)^2$$
$$= 48.06$$

$$\text{Total sum of squares, } S_T = S_A + S_B + S_C + S_D = 48.06 + 1.48 + 0.036 + 0.2248 = 49.808$$

$$\text{Individual factor contribution}(\%) = (S_A/S_T) \times 100 = (48.06/49.808) \times 100 = 96.504$$

Table 6 show the summary of Pareto ANOVA results for the response, MH. Important to note that, injection speed contribute more than 96.5% on micro-hardness, followed by feedstock velocity, mould temperature and injection temperature at 2.97, 0.454 and 0.072%, respectively. The summation of the outputs corresponds to the factor and their respective levels are determined and choice of optimum levels was decided based on the pareto principle. The optimal levels correspond to highest value of summation of S/N ratio for each factor is determined. The optimal injection moulding condition determined using pareto analysis of variance is $A_4B_2C_2D_3$. Higher injection speed is required to completely fill the mould cavity, without causing any defects. Low values of injection speed could always have resulted in incomplete mould fill and causes flow lines on the injection moulded part [40, 41]. Injection temperature is directly proportional to rheological property (i.e. feedstock viscosity). Low injection temperature implies a low feedstock viscosity, which often find difficult for the flow of feedstock into mould cavity. Whereas, with higher feedstock velocity and injection temperature cause severe problems with feedstock separation. Higher mould temperature is essential to keep the feedstock viscosity and ensures complete fill of micro-pores in the injection moulded parts. Noteworthy that, the optimum levels ($A_4B_2C_2D_3$) determined for the factors is not among the set of L_{16} experimental conditions. This might occur due to multi-factor nature of 16 experiments conducted out of $4^4 = 256$ total possible sets.

Response: Ultimate Tensile Strength

Pareto ANOVA is conducted to check the performance and contribution of each factor on the response, ultimate tensile strength (refer Table 6). The results showed the injection speed contributes at about 86.67%, followed by the feedstock flow velocity at 10.32%, injection temperature at 1.57% and mould temperature at 1.44%. The optimal choice of factor levels corresponds to maximum S/N ratio (from four levels) is found to be $A_3B_2C_2D_1$. The combination of low values of mould and injection temperature results in low temperature gradient leads to low cycle time and thereby improved the compaction strength. The Pareto ANOVA determined optimum levels are not among the combination of L_{16} orthogonal array experiments.

Response: Surface Roughness

The summary results of Pareto ANOVA presented in Table 7, shows that the injection speed contributes 94.24% to surface roughness followed by feedstock flow velocity, mould temperature and injection temperature at about 3.26, 1.51 and 0.99%, respectively. The optimal parameter levels that minimize the surface roughness values is found to be $A_4B_2C_2D_3$. Higher injection speed and mould temperature is essential to keep the feedstock viscosity low that help to keep the feedstock in close contact with the die surface walls, which results in close replica die surface finish. The suggested optimal parameters are not studied in the L_{16} orthogonal array of experiments.

The Pareto ANOVA was conducted to study and analyse the data for all the responses, MH, UTS and SR. Important to note that, injection speed contribute highest compared to rest of the parameters (i.e. feedstock flow velocity, injection temperature and mould temperature) for all outputs (i.e. micro-hardness, ultimate tensile strength and surface roughness). Injection speed has significant control over the most likely defects such as, flash, sticking of material in the cavity, voids due to trapped gases, burn marks, weld lines and flow mark. Further, die life is also affected by the injection speed. Thereby, injection speed is considered as the highest contributing

Table 7 Pareto ANOVA for the response, SR

Factors	Levels	A	B	C	D	Total
Sum at factor levels	1	−17.51	−8.04	−6.69	−5.82	−21.5
	2	−9.10	−3.88	−4.40	−6.93	
	3	0.89	−4.63	−4.80	−4.18	
	4	4.22	−4.95	−5.61	−4.57	
Sum of squares of differences		1169.8	40.29	12.27	18.77	1241.1
Percent contribution ratio		94.24	3.25	0.9881	1.512	
Cumulative contribution ratio		94.24	97.49	98.48	100	
Optimum levels		A_4	B_2	C_2	D_3	

factor which has major impact on MH, SR and UTS. Higher injection speed is almost essential to compensate for rapid cool of the molten feedstock, which includes the metal granules poses better thermal conductivity with a goal to completely fill mould cavity. Thereby, feedstock flow velocity is of secondary importance. However, the injection temperature is also sensitive to materials temperature which has an impact on the viscosity of the melt. Mould temperature also had significant impact on the final injection moulded parts, as the residual stresses and mould temperature are highly inter-related [42].

4.2 Grey Relational Analysis (GRA) and Principal Component Analysis (PCA)

GRA is employed to solve the complex and multivariate injection moulded system, wherein the relationships between the parameters are unknown or incomplete or uncertain. In the present work, there is a problem associated to the selection of appropriate processing conditions for the conflicting requirements (i.e. *maximize:* UTS and MH; and *minimize:* SR) in the injection moulding process. In such cases, GRA is applied to convert multiple conflicting objective functions to single objective function for maximization. The following steps are employed for conversion of multi-response problem to single response function (i.e. grey relational grading),

1. The S/N ratio values of experimental output data are normalized between the range of zero and one
2. Compute the grey relational coefficient from the pre-processed experimental data
3. Calculate the equivalent grey relational coefficients
4. Estimate the output weights utilizing principal component analysis (PCA)
5. Determine overall grey relational grading (GRG).

Step 1: Normalization of experimental data (S/N ratios)

Data pre-processing (i.e. normalization) is conducted to convert the original output raw data (i.e. S/N ratios) of the design matrix in the range between 0 and 1. Deng [43] reported the normalized value equal to 1 indicates the better (i.e. desired) performance. The data computation to conduct normalization for a matrix of m experiments and n output characteristics is done using the below (Eq. 3).

$$x_i^*(k) = \frac{x_i^0(k) - \min x_i^0(k)}{\max x_i^0(k) - \min x_i^0(k)}, \text{ (normalization range between 0 and 1)} \quad (3)$$

$x_i^*(k)$ is sequence after data pre-processing, $x_i^0(k)$ is the actual or original sequence of S/N ratio, i = 1, 2, 3,…, m, and $k = 1, 2,\ldots,$ n, with m = 16 and n = 3. max $x_i^0(k)$ is the largest value of $x_i^0(k)$ and min$x_i^0(k)$ is the lowest value of $x_i^0(k)$. The S/N ratio values of MH, UTS, and SR are set to be the reference sequence $x_0^0(k)$, k = 1–3 and

Table 8 Data pre-processing of S/N ratio of L_{16} orthogonal array experiments

Exp. no.		Average S/N ratio values of outputs			Data pre-processing for S/N ratios		
		MH	UTS, MPa	SR, μm	MH	UTS	SR
Reference sequence, $x_0^0(k)$					1.000	1.000	1.000
Comparability sequence, $x_i^*(k)$							
L_1	1	54.15	54.99	−5.01	0.000	0.000	0.000
L_2	2	54.32	55.15	−4.56	0.122	0.219	0.063
L_3	3	54.57	55.24	−3.86	0.301	0.345	0.16
L_4	4	54.32	55.06	−4.08	0.122	0.092	0.129
L_5	5	54.99	55.42	−2.35	0.61	0.593	0.372
L_6	6	55.18	55.50	−2.14	0.743	0.715	0.400
L_7	7	54.96	55.36	−2.67	0.588	0.511	0.326
L_8	8	54.78	55.19	−1.94	0.451	0.282	0.428
L_9	9	55.15	55.40	−0.51	0.721	0.573	0.628
L_{10}	10	55.39	55.53	1.31	0.894	0.756	0.882
L_{11}	11	55.45	55.71	−0.26	0.937	1.000	0.663
L_{12}	12	55.42	55.65	0.35	0.915	0.916	0.748
L_{13}	13	55.45	55.49	−0.17	0.937	0.695	0.675
L_{14}	14	55.53	55.65	1.51	1.000	0.916	0.910
L_{15}	15	55.42	55.45	2.16	0.915	0.634	1.000
L_{16}	16	55.36	55.42	0.72	0.873	0.593	0.800

the comparability sequences i = 1, 2, 3,…, 16, k = 1–3. The data pre-processed S/N ratio values correspond to MH, UTS, and SR is presented in Table 8.

Step 2: Compute the deviation sequence, i.e. $\Delta 0_i(k)$

The term $\Delta 0_i(k)$ represent the deviation sequence, which is the absolute difference between the reference and comparable sequence value after conducting normalization. The deviation sequence values are determined using Eq. 4.

$$\begin{aligned} \Delta 0_i(k) &= \left|x_0^*(k) - x_i^*(k)\right| \\ \Delta_{\max} &= \text{max.max. } \Delta 0_i(k) \\ \Delta_{\min} &= \text{min.min. } \Delta 0_i(k) \end{aligned} \tag{4}$$

The results of computation of deviation sequences $\Delta 0_i(k)$, was presented in Table 9,

$$\Delta 0_1(1) = \left|x_0^*(1) - x_1^*(1)\right| = |1.000 - 0.000| = 1.000$$
$$\Delta 0_1(2) = \left|x_0^*(2) - x_1^*(2)\right| = |1.000 - 0.000| = 1.000$$

Table 9 Deviation sequence of L_{16} orthogonal array experiments

Deviation sequence		MH, Δ_{01}	UTS, Δ_{02}	SR, Δ_{03}
L_1	1	1.000	1.000	1.000
L_2	2	0.878	0.781	0.937
L_3	3	0.699	0.655	0.840
L_4	4	0.878	0.908	0.871
L_5	5	0.390	0.407	0.628
L_6	6	0.257	0.285	0.600
L_7	7	0.412	0.489	0.674
L_8	8	0.549	0.718	0.572
L_9	9	0.279	0.427	0.372
L_{10}	10	0.106	0.244	0.118
L_{11}	11	0.063	0.000	0.337
L_{12}	12	0.085	0.084	0.252
L_{13}	13	0.063	0.305	0.325
L_{14}	14	0.000	0.084	0.090
L_{15}	15	0.085	0.366	0.000
L_{16}	16	0.127	0.407	0.200

$$\Delta 0_1(3) = \left|x_0^*(3) - x_1^*(3)\right| = |1.000 - 0.000| = 1.000$$

Thereby, $\Delta 0_1 = (1.000, 1.000, 1.000)$; $\Delta 0_2 = (0.878, 0.781, 0.937)$ and $\Delta_{\max}$ and $\Delta_{\min}$ are the maximum and minimum value of $\Delta 0_i$. The sample computation was conducted for i = 1–16, and the determined values of all $\Delta 0_i$ for i = 1–16 are presented in Table 9. The values correspond to $\Delta_{\max}(k)$ and $\Delta_{\min}(k)$ are found as follows,

$\Delta_{\max} = \Delta_{01}(1) = \Delta_{01}(2) = \Delta_{01}(3) = 1.000$ and $\Delta_{\min} = \Delta_{14}(1) = \Delta_{11}(2) = \Delta_{15}(3) = 0.000$

Step 3: Computation of grey relational coefficient (GRC)

After data pre-processing and deviation sequence, GRC is determined to know the relationship exists between the optimum (i.e. ideal or best) and the actual normalized S/N ratio. The computation of GRC (refer Eq. 5), $\xi_{(k)}(k)$ is done as follows,

$$\xi_{i\,(k)}(k) = \frac{\Delta_{\min} + \psi\Delta_{\min}}{\Delta_{0i}(k) + \psi\Delta_{\max}}, \quad 0 \prec \xi\left[x_0^*(k),\ x_i^*(k)\right] \leq 1 \tag{5}$$

The term ψ is the distinguished coefficient whose value vary in the range between zero and unity. Smaller the distinguished coefficient value, larger will be the distinguished ability. The present work set the $\psi = 0.5$. The computation of the grey relational coefficient $\xi_1(k)$ is done as follows,

Table 10 Grey-relational coefficient correspond to outputs of MIM process

Exp. no	Grey relation coefficient, ξ		
	MH	UTS	SR
L_1	0.333	0.333	0.333
L_2	0.363	0.390	0.348
L_3	0.417	0.433	0.373
L_4	0.363	0.355	0.365
L_5	0.562	0.551	0.443
L_6	0.660	0.637	0.454
L_7	0.548	0.506	0.426
L_8	0.477	0.411	0.467
L_9	0.642	0.539	0.574
L_{10}	0.825	0.672	0.809
L_{11}	0.888	1.000	0.597
L_{12}	0.855	0.856	0.665
L_{13}	0.888	0.621	0.606
L_{14}	1.000	0.856	0.848
L_{15}	0.855	0.577	1.000
L_{16}	0.797	0.551	0.714

$$\xi_1(1) = \frac{0.000 + (0.5)(1.000)}{1.000 + (0.5)(1.000)} = 0.333$$
$$\xi_1(2) = \frac{0.000 + (0.5)(1.000)}{1.000 + (0.5)(1.000)} = 0.333$$
$$\xi_1(3) = \frac{0.000 + (0.5)(1.000)}{1.000 + (0.5)(1.000)} = 0.333$$

Thereby, the GRC $\xi_1(k) = (0.333, 0.333, 0.333)$, where $k = 1$–3, similar procedure employed for the remaining L_{16} orthogonal array to obtain the GRC (refer Table 10).

Step 4: Determination of grey relational grading (GRG)

After performing computation of GRC, the GRG, γ_i is estimated based on the average sum of all the multiple output characteristics of grey relational coefficients is defined as follows,

$$\gamma_i = \frac{1}{n} \sum_{k=1}^{n} \xi_i(k) \tag{6}$$

In injection moulding process, the impact of each input factor on the output system might not be same always, thereby Eq. 6 can be modified accordingly as follows,

$$\gamma_i = \frac{1}{n} \sum_{k=1}^{n} w_k \xi_i(k) \tag{7}$$

The term w_k refers to the weight of the output function, the appropriate choice of weights reflects significantly the quality of injection moulded parts. Thereby, the weights are decided for each output function using the principal component analysis (PCA). PCA method starts with the multi-response array with m experiments and n performance characteristics. The methodology employed to determine weights for each quality characteristics is described as below [21].

Step 1: The general form of multiple output quality characteristic matrix is defined as follows,

$$x_i(j),\ i = 1, 2, \ldots, m,\ \ j = 1, 2, \ldots, n$$

$$x_i = \begin{bmatrix} x_1(1) & x_1(2) & x_1(3) & \cdots\cdots & x_1(n) \\ x_2(1) & x_2(2) & x_2(3) & \cdots\cdots & x_2(n) \\ \vdots & \vdots & \vdots & \vdots\ \vdots\ \vdots & \\ x_m(1) & x_m(2) & x_m(3) & \cdots\cdots & x_m(n) \end{bmatrix}$$

For the present work, the term x is the grey relational coefficient and the value of m and n is found to be 16 and 3, respectively.

Step 2: Compute the correlation coefficient array

The computation of correlation coefficient array is done as shown below,

$$R_{jl} = \left(\frac{Cov(x_i(j), x_i(l))}{\sigma_{(x_i)}(j) \times \sigma_{(x_i)}(l)} \right)$$
$$= \left(\frac{Covariance\ sequences\ of\ x_i(j)\ and\ x_i(l)}{Standard\ deviation\ of\ x_i(j) \times Standard\ deviation\ of\ x_i(l)} \right)$$

Step 3: Estimate the eigen values and eigen vectors

The correlational coefficient array was used to determine the eigen values and eigen vectors.

$$(R - \lambda_k I_m) V_{ik} = 0 \tag{8}$$

The term λ_k represents the eigen values $\sum_{k=1}^{n} \lambda_k = n,\ k = 1, 2, \ldots,$ n; $V_{ik} = [a_{k1} a_{k2} \ldots a_{kn}]^T$—depicts the eigen vector corresponds to the eigen value λ_k.

Table 11 Eigen values and percent contribution for principal components

Principal component	Eigen value	Explained variation (%)
First	2.5368	84.56
Second	0.4184	13.94
Third	0.0448	01.50

Table 12 The eigenvectors for principal components

Quality characteristics	Eigen vector		
	First principal component	Second principal component	Third principal component
Micro hardness	0.619	0.000	0.785
Ultimate tensile strength	0.555	0.707	−0.438
Surface roughness	0.555	−0.707	−0.437

Step 4: Calculate the principal components

The formulation of uncorrelated principal components is as follows,

$$Y_{mk} = \sum_{i=1}^{n} x_m(i) \times V_{ik}$$

where, Y_{m1} and Y_{m2} are the first principal and second principal components and so on.

The essential array for the multiple performance characteristics representing the GRC of individual performance characteristics is presented in Table 10. The GRC data are used to estimate the correlation coefficient matrix that help to know the eigen values according to Eq. 8, is presented in Table 11. The eigen vector associated to individual eigen value is shown in Table 12. The square of each eigen values represent the explained variation of associated performance characteristic to the principal component. The variance contribution of first principal components representing the three quality characteristics is found equal to 84.56% (refer Table 11). Interesting to note that, the percent contribution (i.e. weights) of MH, UTS and SR are found equal to 0.3840, 0.3080 and 0.3080 (refer Table 13), respectively.

The values of grey relational grading are computed with the help of each GRC and their corresponding weights is conducted as follows,

$$\lambda_1 = (0.333 \times 0.3840) + (0.333 \times 0.3080) + (0.333 \times 0.3080) = 0.334$$

Table 13 The relative importance (weight fraction) of individual quality characteristics

Quality characteristics	Contribution
Micro hardness	0.3840
Ultimate tensile strength	0.3080
Surface roughness	0.3080

Similar methodology was employed to compute the GRG for the comparability sequence $i = 1$–16 and the determined values are presented in Table 14. The calculated grey relational grading is used to obtain the optimum injection moulding parameters for quality parts.

Pareto ANOVA is conducted on the single grey relational grading to know the optimal levels of injection moulding parameters and their corresponding percent contributions. The results showed the injection speed is treated as the most dominant factor compared to feedstock velocity considering all the responses. However, the effect of mould and injection temperature does not find much contribution considering all the responses. The injection speed, feedstock flow velocity, injection temperature and mould temperature set at optimum levels 4, 2, 2, and 1, respectively i.e. $A_4B_2C_2D_1$ combination resulted as an ideal condition after considering all the multiple performance characteristics (refer Table 15). Higher values of injection speed are essential to ensure the feedstock to completely fill the mould cavity. As injection speed increases the time required to fill the feedstock decrease, and thereby low values of mould and injection temperature is sufficient to attain better compact. Thus, capable to produces better quality injection moulded part. It is worth mentioning that the optimal parameter combination was not found among the 16 sets of different combination of experiments conducted. This might occur due to multi factor nature of Taguchi experimental design (i.e. $3^4 = 81$).

4.3 Summary Results of Optimization

Taguchi method determined different combination of moulding parameters (i.e. injection speed, feedstock flow velocity, injection temperature and mould temperature) for MH, UTS and SR. Thus, Taguchi method alone limit to contribute single parametric combination for all outputs (i.e. MH, UTS, and SR), which are in conflict with one another. The decision regarding uncertainty is solved utilizing combination of GRA and PCA. GRA helps to convert the conflicting multiple objective functions to single objective function. Determining the solutions for conflicting objective functions is considered as a tedious task, as the solutions are dependent on the desired (i.e. importance assigned for each output function) performance by the investigator. The weight fractions for different output functions are decided based on statistical analysis of experimental data utilizing PCA. All the outputs (i.e. 38.40% for MH, 30.80% for UTS and 30.80% for SR) had shown significant impact according to

Table 14 Grey relational grading for multiple performance characteristics

Exp. no.	Input parameters (coded)				Input parameters (un-coded)				Output	
	IS, %	FV, m/s	IT, °C	MT, °C	IS, %	FV, m/s	IT, °C	MT, °C	PCA-GRG	S/N for PCA-GRG
1	1	1	1	1	10	2	150	30	0.3336	−9.54
2	1	2	2	2	10	4	160	40	0.3667	−8.71
3	1	3	3	3	10	6	170	50	0.4084	−7.78
4	1	4	4	4	10	8	180	60	0.3612	−8.85
5	2	1	2	3	20	2	160	50	0.5220	−5.65
6	2	2	1	4	20	4	150	60	0.5895	−4.59
7	2	3	4	1	20	6	180	30	0.4975	−6.06
8	2	4	3	2	20	8	170	40	0.4536	−6.87
9	3	1	3	4	30	2	170	60	0.5893	−4.59
10	3	2	4	3	30	4	180	50	0.7729	−2.24
11	3	3	1	2	30	6	150	40	0.8329	−1.59
12	3	4	2	1	30	8	160	30	0.7968	−1.97
13	4	1	4	2	40	2	180	40	0.7189	−2.87
14	4	2	3	1	40	4	170	30	0.9088	−0.83
15	4	3	2	4	40	6	160	60	0.8140	−1.79
16	4	4	1	3	40	8	150	50	0.6957	−3.15

Table 15 Pareto ANOVA for grey relational grading (GRG)

	GRG (multiple quality characteristics)					
Input factors	Levels	A	B	C	D	Total
Sum at factor levels	1	−34.87	−22.64	−18.87	−18.40	−77.07
	2	−23.17	−16.37	−18.12	−20.04	
	3	−10.39	−17.22	−20.07	−18.81	
	4	−08.64	−20.84	−20.01	−19.82	
Sum of squares of differences		1801.685	105.7371	10.6803	7.4555	1925.56
Percent contribution ratio		93.57	5.49	0.555	0.387	
Cumulative contribution ratio		93.57	99.06	99.61	100	
Optimum levels		A_4	B_2	C_2	D_1	

Table 16 Summary results of single and multiple objective optimization for MIM process

Optimization	Method	Output	Optimal input condition	Experimental output		
				MH	UTS	SR
Single response optimization	Taguchi	MH	$A_4B_2C_2D_3$	610	596	0.88
		UTS	$A_3B_2C_2D_1$	598	616	0.92
		SR	$A_4B_2C_2D_3$	596	592	0.75
Multi-response optimization	GRA and PCA		$A_4B_2C_2D_1$	608	602	0.83

the principal component analysis. The composite value of combination of weights and the output functions are used to calculate the grey relational grading. Pareto ANOVA determined the optimal combination for all combination of output characteristics. Summary results for both the individual and combined response optimized conditions are presented in Table 16.

The suggested optimal injection moulding conditions determined by Taguchi method resulted in individual improvement in MH, UTS and SR (refer Table 16). Further, Taguchi, GRA and PCA determined optimal conditions resulted in high values of MH, and UTS, while minimizing the SR (refer Table 16). Confirmation experiments are conducted for the optimized conditions determined for single response by Taguchi method and for multiple responses by Taguchi-based GRA and PCA. Taguchi method determined optimal parametric conditions resulted in better performance in MH, UTS and SR, respectively. Taguchi-based GRA and PCA determined optimized conditions resulted in better properties.

5 Conclusions

In the present work, the input parameters (injection speed, mould temperature, injection temperature and feedstock flow velocity) on the surface quality and mechanical strength of nickel based (Cr_3C_2-NiCr + NiCrSiB) metal injection moulded parts are studied. Taguchi method is employed for conducting minimum experiments, Pareto ANOVA for determining optimal levels and estimate percent contribution, PCA for estimating weight fractions for individual output, and GRA for mathematical formulation of multiple objective functions to single objective function for conducting the optimization. The following conclusions are drawn for the present work,

1. Taguchi method minimizes the experiments required to determine the optimal levels for an output. Pareto ANOVA suggests injection speed is the most significant factor for SR, MH, and UTS. Feedstock flow velocity is of secondary importance towards all outputs. Injection speed set at higher level showed better properties, as higher speed is attributed to ensure completely fill the feedstock in the mould cavity, without causing defects (pores). $A_4B_2C_2D_3$ for MH, $A_3B_2C_2D_1$ for UTS, and $A_4B_2C_2D_3$ for SR are treated as optimal conditions to attain best properties in injection moulded parts.
2. Multiple conflicting outputs (maximize: MH, and UTS, and minimize: SR) have many optimal solutions depending on output importance and choice of single solution is a tedious task. Thereby, PCA is employed to know the weight fraction (i.e. importance) for each output. The weight fractions for MH, UTS and SR are found equal to 0.3840, 0.3080 and 0.3080). Important to note that, MH is treated as highest importance compared to SR, and UTS from the experimental data and statistical analysis.
3. GRA is applied to solve multi-objective optimization for MIM process. The hybrid Taguchi-GRA-PCA recommended the optimal levels for MIM process, when the MH, UTS and SR are simultaneously considered for optimization. The best properties (i.e. MH, UTS and SR) for MIM is obtained for injection speed (55.2 cc/s, level 4), feedstock flow velocity (4 m/s, level 2), injection temperature (160 °C, level 2) and mould temperature (30 °C, level 1). The selected feedstock powder loading formulations exhibited pseudo plastic flow behaviours, which is found to be best suited for MIM processes. Pareto ANOVA applied for GRG is tested for MIM parameters, the injection speed resulted in highest contribution, followed by feedstock flow velocity towards the multiple-performance characteristics. Note that, injection temperature and mould temperature showed the negligible impact on multiple outputs.
4. The present work limits the risk of obtaining the defective component, which normally occur with the currently employed try-error experiment method. Further, the results are very useful to MIM industries to obtain the desired moulding properties.

References

1. Piotter V, Gietzelt T, Merz L (2003) Micro powder-injection moulding of metals and ceramics. Sadhana 28(1–2):299–306
2. Abolhasani H, Muhamad N (2010) A new starch-based binder for metal injection molding. J Mater Process Technol 210:961–968
3. Hamidi MFFA, Harun WSW, Samykano M, Ghani SAC, Ghazalli Z, Ahmad F, Sulong AB (2017) A review of biocompatible metal injection moulding process parameters for biomedical applications. Mater Sci Eng, C 78:1263–1276
4. Barrière T, Gelin JC, Liu B (2002) Improving mould design and injection parameters in metal injection moulding by accurate 3D finite element simulation. J Mater Process Technol 125:518–524
5. Merz L, Rath S, Piotter V, Ruprecht R, Ritzhaupt-Kleissl J, Hausselt J (2001) Feedstock development for micro powder injection moulding. Microsyst Technol 8(2–3):129–132
6. Enneti RK, Shivashankar TS, Park SJ, German RM, Atre SV (2012) Master debinding curves for solvent extraction of binders in powder injection molding. Powder Technol 228:14–17
7. Aggarwal G, Park SJ, Smid I (2006) Development of niobium powder injection molding: Part I. Feedstock and injection molding. Int J Refract Metals Hard Mater 24(3):253–262
8. Li Y, Li L, Khalil KA (2007) Effect of powder loading on metal injection molding stainless steels. J Mater Process Technol 183(2–3):432–439
9. Bigg DM (1998) Rheological analysis as a tool to predict quality in powder injection molding. In: Processing annual technical conference-ANTEC, conference proceedings, vol 1, pp 997–1000. Soc Plast Eng, 1998
10. Zhang T, Jiang Z, Wu J, Chen Z (1990) Influence of rheological behavior of ceramic mixes on injection molding of ceramic compacts. J Am Ceram Soc 73(7):2171–2175
11. Ji CH, Loh NH, Khor KA, Tor SB (2001) Sintering study of 316L stainless steel metal injection molding parts using Taguchi method: final density. Mater Sci Eng, A 311(1–2):74–82
12. Apichartpattanasiri S, Hay JN, Kukureka SN (2001) A study of the tribological behaviour of polyamide 66 with varying injection-moulding parameters. Wear 251:1557–1566
13. Kameo K, Nishiyabu K, Friedrich K, Tanaka S, Tanimoto T (2006) Sliding wear behavior of stainless steel parts made by metal injection molding (MIM). Wear 260:674–686
14. Kamaruddin S, Khan ZA, Foong SH (2010) Application of Taguchi method in the optimization of injection moulding parameters for manufacturing products from plastic blend. Int J Eng Technol 2(6):574–580
15. Berginc B, Kampus Z, Sustarsic B (2006) The use of the Taguchi approach to determine the influence of injection-moulding parameters on the properties of green parts. J Achiev Mater Manuf Eng 15(1–2):63–70
16. Yarlagadda PK (2002) Development of an integrated neural network system for prediction of process parameters in metal injection moulding. J Mater Process Technol 130:315–320
17. Lu HS, Chang CK, Hwang NC, Chung CT (2009) Grey relational analysis coupled with principal component analysis for optimization design of the cutting parameters in high-speed end milling. J Mater Process Technol 209(8):3808–3817
18. Tsao CC (2009) Grey-Taguchi method to optimize the milling parameters of aluminum alloy. The Int J Adv Manuf Technol 40(1–2):41–48
19. Patel GCM, Krishna P, Parappagoudar MB (2014) Optimization of squeeze cast process parameters using Taguchi and grey relational analysis. Proc Technol 14:157–164
20. Siddiquee AN, Khan ZA, Mallick Z (2010) Grey relational analysis coupled with principal component analysis for optimisation design of the process parameters in in-feed centreless cylindrical grinding. The Int J Adv Manuf Technol 46(9–12):983–992
21. Fung CP, Kang PC (2005) Multi-response optimization in friction properties of PBT composites using Taguchi method and principle component analysis. J Mater Process Technol 170(3):602–610
22. Bhero S (2014) Metal injection moulding as a possible processing route for porous prostheses. Int J Res Chem, Metall Civil Eng 1(1):50–53

23. Poh L, Della C, Ying S, Goh C, Li Y (2018) Powder distribution on powder injection moulding of ceramic green compacts using thermogravimetric analysis and differential scanning calorimetry. Powder Technol 328:256–263
24. Rajabi J, Muhamad N, Sulong AB (2012) Effect of nano-sized powders on powder injection molding: a review. Microsyst Technol 18(12):1941–1946
25. Chua MIH, Sulong AB, Abdullah MF, Muhamad N (2013) Optimization of injection molding and solvent debinding parameters of stainless steel powder (SS316L) based feedstock for metal injection molding. Sains Malaysiana 42(12):1743–1750
26. Benson JM, Richter W, Chikwanda HC (2011) Rheological assessment of titanium MIM feedstocks. J South Afr Inst Min Metall 111(3):133–136
27. Li SL, Huang BY, Li YM, Liang SQ, Li DX, Fan JL, Jiang F (2003) Effects of sintering atmosphere on the microstructure and mechanical property of sintered 316L stainless steel. J Cent South Univ Tecnol 10(1):1–6
28. Li Y, Huang B, Qu X (1999) Viscosity and melt rheology of metal injection moulding feedstocks. Powder Metall 42(1):86–90
29. Gülsoy HÖ, German RM (2008) Production of micro-porous austenitic stainless steel by powder injection molding. Scr Mater 58:295–298
30. Mohamad NN, Muhamad N, Jamaludin KR, Ahmad S, Ibrahim MHI (2009) Flow behaviour to determine the defects of green part in metal injection molding. Int J Mech Mater Eng 4(1):70–75
31. Ott EA, Peretti MW (2012) Metal injection molding of alloy 718 for aerospace applications. JOM 64(2):252–256
32. Suri P, Atre SV, German RM, de Souza JP (2003) Effect of mixing on the rheology and particle characteristics of tungsten-based powder injection molding feedstock. Mater Sci Eng, A 356(1–2):337–344
33. Hwang J, Choi S, Hong S, Kim N (2013) Determination of the flow stress and thermal properties of ceramic powder feedstock in ceramic injection molding. J Mech Sci Technol 27(6):1815–1824
34. Guoxin H, Lixiang Z, Yunliang F, Yanhong L (2008) Fabrication of high porous NiTi shape memory alloy by metal injection molding. J Mater Process Technol 206(1–3):395–399
35. Lee J, Seok H, Lee H (2003) Effect of the gate geometry and the injection speed on the flow behaviors of a semi-solid A356 Al Alloy. Met Mater Int 9(4):351–357
36. Atre SV, Park SJ, Zauner R, German RM (2007) Process simulation of powder injection moulding: identification of significant parameters during mould filling phase. Powder Metall 50:76–85
37. Liu X, Li Y, YUE J, Luo F (2008) Deformation behavior and strength evolution of MIM compacts during thermal debinding. Trans Nonferrous Met Soc China 18:278–284
38. Jamaludin KR, Muhamad N, Rahman A, Nizam M, Amin M, Yulis S, Hafiez N (2009) Moulding parameter optimisation for the best sintered density. In: Proceedings of the world congress on engineering 1: 1–3 July, London, UK
39. Park S (1996) Robust design and analysis for quality engineering. Boom Koninklijke Uitgevers
40. Kryachek VM (2004) Injection molding (review). Poroshkovaya Metallurgiya (Powder Metallurgy) 7:12–27
41. Maeda YH, Nomura Sugiama D (1996) Optimization of green compact forming conditions in metal injection moulding. J Jap Inst Met 60(11):1108–1111
42. Siegmann A, Buchman A, Kenic S (1987) Residual stresses in injection-molded amorphous polymers. Polym Eng Sci 27(14):1069–1078
43. Deng J (1989) Introduction to grey system theory. The J Grey Syst 1(1):1–24

On Friction-Stir Welding of 3D Printed Thermoplastics

Sunpreet Singh, Chander Prakash and Munish K. Gupta

Abstract The use of thermoplastic materials, specifically in automotive industry, is increasing exponentially due to their numerous overpowering quality characteristics in comparison of metals and alloys. Three-dimensional (3D) printing technologies are established as one of the best methods for fabricating customized, complex, durable and mechanically strong structures. However, such parts often required to be assembled when subjected to industrial applications, automotive sector for instance. The service life of the joints made with adhesives, glues and mechanical fasteners is greatly depending on working conditions, for e.g.: moisture. Recently, researchers have highlighted the utility of friction stir welding (FSW) of thermoplastics for a wide range of conventionally made thermoplastics structures and very less information is available on FSW of three-dimensional (3D) prints. This chapter outlines the recent research trends in FSW and a specified case study focusing optimization of tensile strength of the specimens, made with 3D printing, by friction stir welding (FSW). Further, as-welded and fractured specimens were analyzed through scanning electron microscopy to identify the joint quality and reasons of failure. It has been found that the chips formation of thermoplastic fibers while welding was the most critical issue, opening new research areas for forthcoming 3D printing and FSW practices.

Keywords 3D printing · Friction stir welding · Optimization · Process parameters · Thermoplastics · Tensile strength

1 Introduction

The word "welding" demonstrates the permanent joining of similar/dissimilar materials with the help of heat and/or force or both. This joining technology allows the manufacture of very complex geometries which otherwise are impossible to fabricate

S. Singh (✉) · C. Prakash
School of Mechanical Engineering, LPU, Phagwara, India
e-mail: snprt.singh@gmail.com

M. K. Gupta
Mechanical Engineering, NIT, Hamirpur, India

K. Gupta (ed.), *Materials Forming, Machining and Post Processing*, Materials Forming, Machining and Tribology, https://doi.org/10.1007/978-3-030-18854-2_3

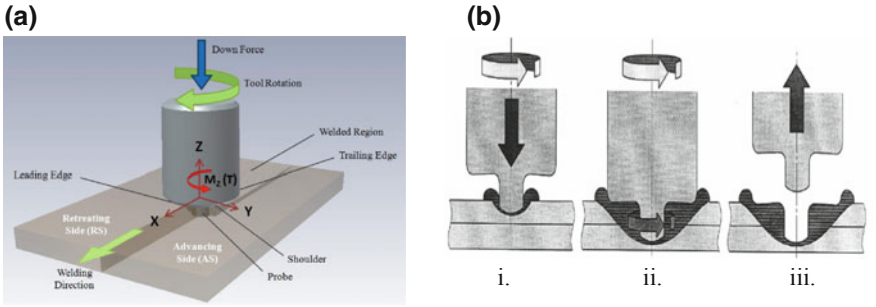

Fig. 1 Schematic of FSW for **a** seam joint [9] and **b** lap joints [10]

as a single piece [1]. Friction stir welding, abbreviated as FSW, is one of the latest and widely practiced solid state welding processes patented by Cambridge University (UK) in late 19th century [2]. Welding of alloys of aluminium (Al), magnesium (Mg), copper (Cu), stainless steel (SS), stainless steels, etc., which face problems with conventional welding methods are now possible FSW [1]. FSW process was specifically invented for welding Al alloys but with the passage of time, inventions have been achieved to weld Cu, Mg, SS, titanium (Ti) and thermoplastics [3–6]. This process has attracted the attentions of many manufacturing industries dealing with assembly of automobiles and aerospace products. The invention of FSW process has also overcome the limitations of traditional fusion welding techniques as heat effected zone can be partially or completely eliminated owing to zero melting principle. Simultaneously, many of the existing the environmental and safety issues, associated with conventional welding methods, can be avoided through FSW [7].

The working of FSW has changed over the past decades as now more robust and flexible CNC controlled system results in better control of the process variables, inbuilt heating arrangement and utilization of different weld-able materials. Generally, the success of this process greatly relies on the development of heat during to frictional force at the tool tip and counter workpiece interfaces [8]. In case of FSW of seam joints, the cylindrical tool forces the parts to weld by pushing it, while rotation, to pierce into the joint and moving along the predefined weld line (refer Fig. 1a). Consumable as well as non-consumable tools could be used as per the requirements. A shoulder piece is connected at the top of rotating tool to avoid spattering of material from the butting surface and also guarantee the required pin penetration [9]. Whereas in case of FSW of lap joints, the rotating tool penetrates the work-materials (plunging-i), allowed to maintain its position (holding-ii) until uniform heat waves propagate and allow atomic diffusion and finally retrieved back (withdrawing-iii) (refer Fig. 1b) [10].

There exist three phases in FSW and all these can be designated as a function of time period for which tool and workpiece are made in contact with each other. During first phase or “Plunge Period”, the tool is rotated and moved in vertical downward direction and penetrated inside the workpiece to a defined thickness. The tool remains

in this position, during the "Dwell Period", until the preliminary softening and plastic deformation of the material take place. Then, welding action can be started in the withdrawing phase by moving the tool or workpiece, relative to one another across the weld line [9, 11]. In order to achieve metallurgical bonding, the materials must be exposed to sufficient temperature and pressure for required span of time. Therefore, the intermetallic compound thin layer is generally formed along the interface [12].

The obtained quality characteristics of FSWed parts are greatly influenced by the process variables of the setup such as: probe geometry/features, tool rotation/feed rate, plunge depth, tilt angle, sideways tilt angle, shoulder geometry/features, forces, etc. Moreover, the advancing-retreating mechanism of this joining process also needs to be understood in-depth, as it influences heating, plasticizing and shoulder pressure [13, 14]. Majority of the reported research is focusing on the weld-ability of various materials (alloys, thermoplastics and thereby combinations), tool design, and optimization of the aforementioned variables in response of mechanical/metallurgical characteristics. The Sect. 1 of this chapter highlights the recent advances in FSW, whereas Sect. 2 represents a case study focusing optimization of tensile strength of FSWed 3D printed parts. Section 3 ends this chapter by outlining the possible future trends in the light of performed case study.

2 Research Advances in FSW

Welding made of different material combinations has been attracting gradual significance in engineering requests since of their technical and commercial aids [15–17]. It has been seen that Al in combinations of other common engineering materials has increased its pace in-terms of industrial utility, especially in transportation and electric power industries. One of such example is of Al/Cu based bimetallic dissimilar joints which are of great importance in electrical connections, since this can lessen materials expenses and heaviness during prolonging the service lifecycle [18–20]. In Fig. 2a, the rotating collar started blending against the highest point of tests at the point demonstrated as "contact" and around 10 s past the weld was permitted to initiate. It is obvious that after begin of welding process; an expansion in temperature can be seen.

In Fig. 2b [21], no noteworthy increment in temperature is observed during the initial period. In fact, an ascent in temperature is not seen until the point when the pivoting pin initially approached the thermocouple from a distance of 50 mm. The stirred zone of air welded samples demonstrated exceptionally complex intervened stream shapes, in which re-solidified Mg and Al composites were swirled together and fragile intermetallic phases Al3Mg2 and Al12Mg17 and Al2Mg3 were formed. The stirred zone of submerged welded sample demonstrated a much smoother interface and less intermixing. Their temperature distributions, during processing, were recorded for both submerged and open conditions; and thereby compared, refer Fig. 3 [23].

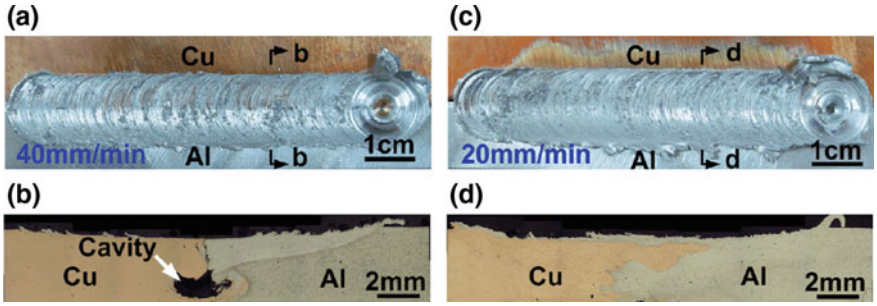

Fig. 2 Cross sections of friction stir welded joints at different traverse speeds 40 mm/min (**a** and **b**) and 20 mm/min (**c** and **d**) [21]

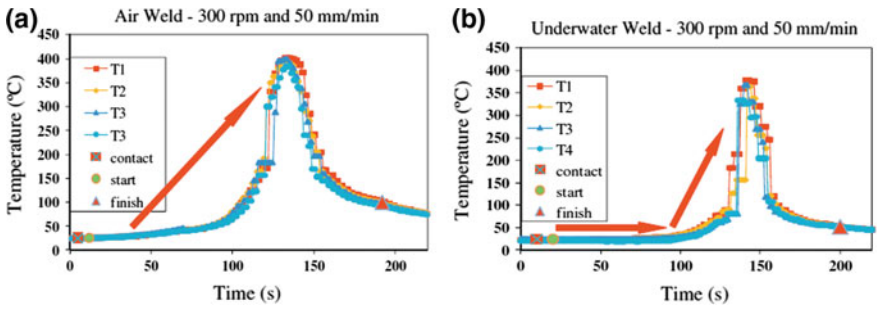

Fig. 3 Temperature profiles for **a** the room temperature weld initiated at 25 °C, and **b** underwater weld, at a rotation speed of 300 rpm and travel speed of 50 mm/min [23]

Sun et al. examined the spot welded Al-6061 alloy and mild steel plate with a thickness of 1 mm, which contained two stages during the whole welding process. The welds obtained were having smooth surface without keyholes and no intermetallic compound layer, refer Fig. 4, was formed along joint boundary [24].

Recently, FSW has been applied to join similar and dissimilar thermoplastic materials [25–27]. Bilici and Yukler have performed number of experiments to study, optimize and evaluate the mechanical properties of resulting parts. In one of their studies [26], FSW (spot welding) parameters were studied in response of static strength of high density polyethylene sheets. In lap-shear tests, two crack modes were observed, for example, cross nugget failure and pull nugget failure. It has been found that tool plunge depth, rotational speed and dwell time were important to withstand the failure modes. Gao et al. showed that the addition of carbon nanotubes reduced the defects (such as: pores and crack) and increased the tensile strength and elongation; however hardness of the joint was sacrificed [28]. Azarsa and Mostafapour used response surface technique (RSM) to inquire about at the optimum process parameters for the improvement of bending strength of FSWed high thickness polyethylene parts. It has also been found that burning and degradation of HDPE (see Fig. 5a) can happen at an excessively high rotational speed and may lead to tunnel imperfection (across the

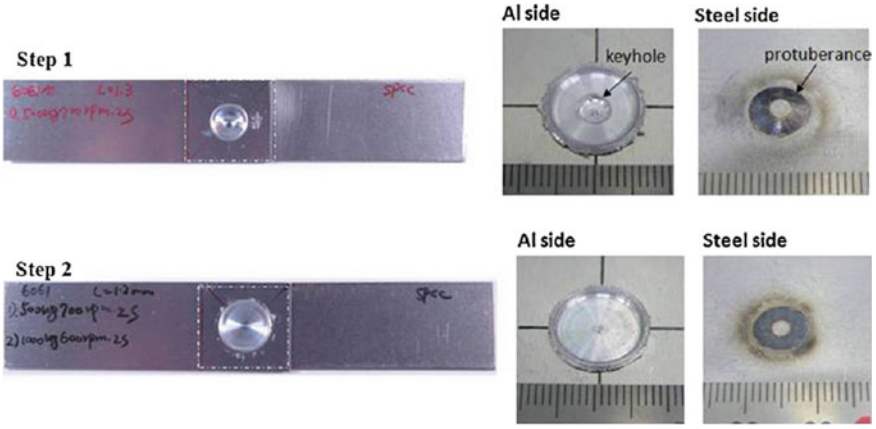

Fig. 4 Spot welded specimens [24]

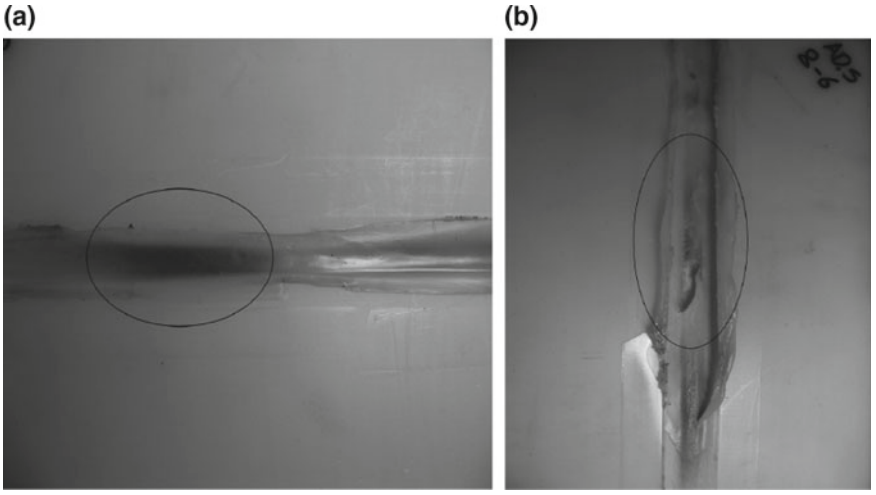

Fig. 5 Burning and degradation of thermoplastic at higher temperature (**a**) and external voids (**b**) [29]

weld line), particularly in case of low shoe temperature. Similarly, high transverse speed of tool (>100 mm/min) can increase the deformations in weld line as well as outside voids (see Fig. 5b) [29].

Ratanathavorn proposed a test study to achieve understanding on the impacts of welding parameters on the nature of hybrid joints in term of the greatest tensile shear strength. A range of thermoplastics and thermoplastics with filaments (counting: polypropylene, polyamide-12, polyethylene terephthalate, fiber-fortified polyethylene terephthalate and fiber-strengthened polyamide) were joined to Al composite sheets by FSW. Some of the important findings are as [30]:

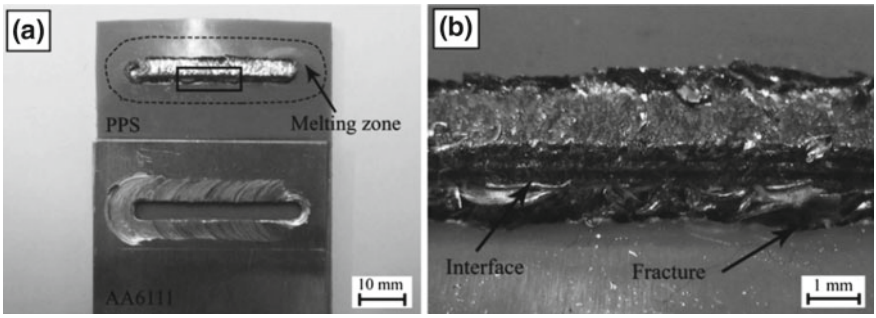

Fig. 6 Macrograph of fractured specimens on Al and PPS side because of melting and re-solidification of PPS outside of stirred zone (**a**) and micrograph of fractured surface at aluminium stir zone (**b**) [40]

- Defects produced, such as: holes and localities with very larger and no chips, within the weld line can be easily recognized through non-destructive testing methods.
- The most critical process parameters were pin geometry and thread, translation speed and rotation direction.
- Tool rotational course controls the direction of material flow inside the weld hole.
- Utilizing clockwise rotational course isn't ideal because of lost material through a work-piece surface.
- A direct material blending is more attractive because of its low void development and additionally great material course in the weld hole.

Table 1 summarizes the key findings of various research attempts made for welding dissimilar materials combinations.

For meeting with the challenges being faced by the manufacturing companies dealing with hybrid assemblies of metals and thermoplastics, FSW is one of the best choices nowadays [36–39]. Ratanathavorn and Melander created overlap joints of Al (AA-6111) with a high temperature and chemical inert thermoplastic (PPS) using FSW. The tool was utilized to produce metallic chips in place of plasticising the Al plate as in the traditional FSW process. Thermoplastic was liquefied and fused with the chipped zone to form a joint as seen in Fig. 6 [40].

3 FSW and 3D Printing

Not much work has been reported on the applications or benefits of 3D printing technology in FSW. Friction welding for 3D printing products was licensed in 2004 [41]. The first report on friction stir process as a manufacturing method to 3D printed components was distributed via Airbus in 2006 [42]. Airbus and Boeing highlighted that the innovation is fit for tending to two of the predefined challenges, (i) accomplishing high throughput and (ii) less material wastage [42, 43]. Sharma et al. developed

Table 1 Summary of major finding in FSW of dissimilar materials

S. no.	Material combination	Major findings	Ref.
1	Al and Cu	• Composite like phase formed in weld nugget resulted into distinct rise in hardness along with excellent metallurgical bonding for quality tensile and bending strength	[21]
2	Al and Steel	• The influences of tool speed, rotation speed and tool offset; and were correlated with welding forces applied on the FSW tool as well as temperature distributions • It has been found that the highest tensile strength achieved was about 15% of lesser than that of Al alloy. Further at higher welding speed, the high temperature duration, interlayer thickness and material strain rate were reduced	[22]
3	Al and Mg	• The intermetallic compounds behaved insignificantly in regards of the mechanical properties	[23]
4	Al and Steel-304	• The transverse tensile strength of around 93% of the Al-6061 base metal was obtained with hybrid FSW, higher than the tensile strength of FSW welds • This was because of the precipitates prompted softening of the mix zone brought about around 50% reduction of hardness in stirred zone than Al base metal	[17]
5	Acrylonitrile-Butadiene-Styrene (ABS) sheets	• It has been discovered that high axial force promoted the squeeze of the molten polymeric material, preventing introduction of air into the weld and helps cooling of the weld without shrinkage and voids development. It additionally enhanced rigidity and strain of welds • Axial force adds to material blending and avoid the development of cavities in the withdrawing side of mix zone	[31, 32]
6	ABS sheets	• The tensile strength of the joined sheets has been altogether influenced by the hot shoe temperature	[33]
7	Polycarbonate sheets	• FSW successfully joined polycarbonate sheets, of 3 mm thickness, and built up a prototypal setup to screen the calculation of forces and tool temperature	[34]
8	Polyethylene sheets	• Tool rotations played critical role and contributed 73.85% in the tensile strength of FSWed polycarbonate sheets	[35]

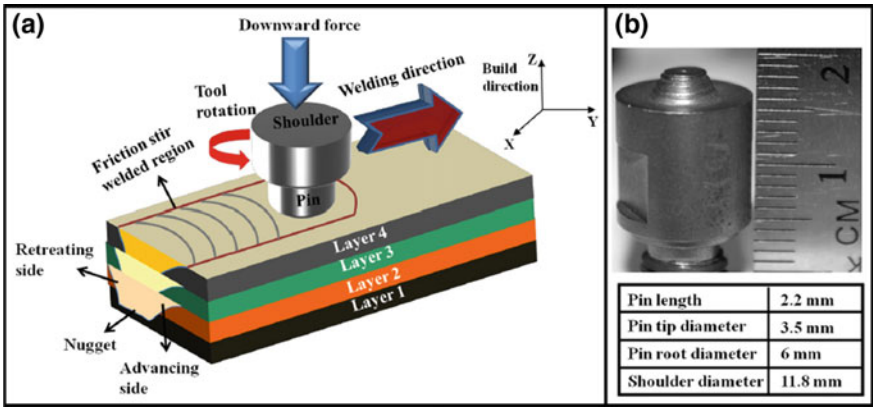

Fig. 7 Schematic illustration of the FS3DP process (**a**) and dimensions of the tool (**b**) [46]

functionally graded material through FS3DP process [44]. FSW turns the tide and brings about a radical change in the situation of block joining additive manufacturing of monolithic stiffened airframe panels [45].

Palanivel et al. utilized a multi-layered stack containing four sheets and a fabricate height of 5.6 mm was produced by consecutively building and CNC machining of the welded layers, allude Fig. 7. Friction stir-3D printing (FS3DP) was performed by using a right handed stepped tool pin made of tool steel [46].

3.1 Tool Design

The welding parameters and tool geometry strongly affect the quality of stirred zone and weld strength [47, 48]. There are two main parts, i.e. shoulder and pin [49], around which material deformed [50]. Different shapes of shoulder and pin are shown in Fig. 8a, b. Pin diameters [51], pin angle [52], thread orientation [53], length [54] and profile [55] are important in FSW. The shoulder generates heat during the welding process, forges material, prevents expulsion and assists material movement [56]. Pirizadeh et al. designed a novel tool with two shoulders, refer Fig. 9. Tensile strength has been improved by controlling the levels of input variables. An increase in the rotational speed decreased the tensile strength, whereas both low and high levels of translational speeds led to low heat generation and poor mixing. Use of convex pin was also found to be superior as compared to simple pin [57].

Eslami et al. produced welds with a newly designed tool (see Fig. 10) to improve the welds surface quality and strength significantly. Number of experiments were performed at selected parametric setting, and resulted into poor precision. This means there is still need of much effort to control the processing of welding materials [58].

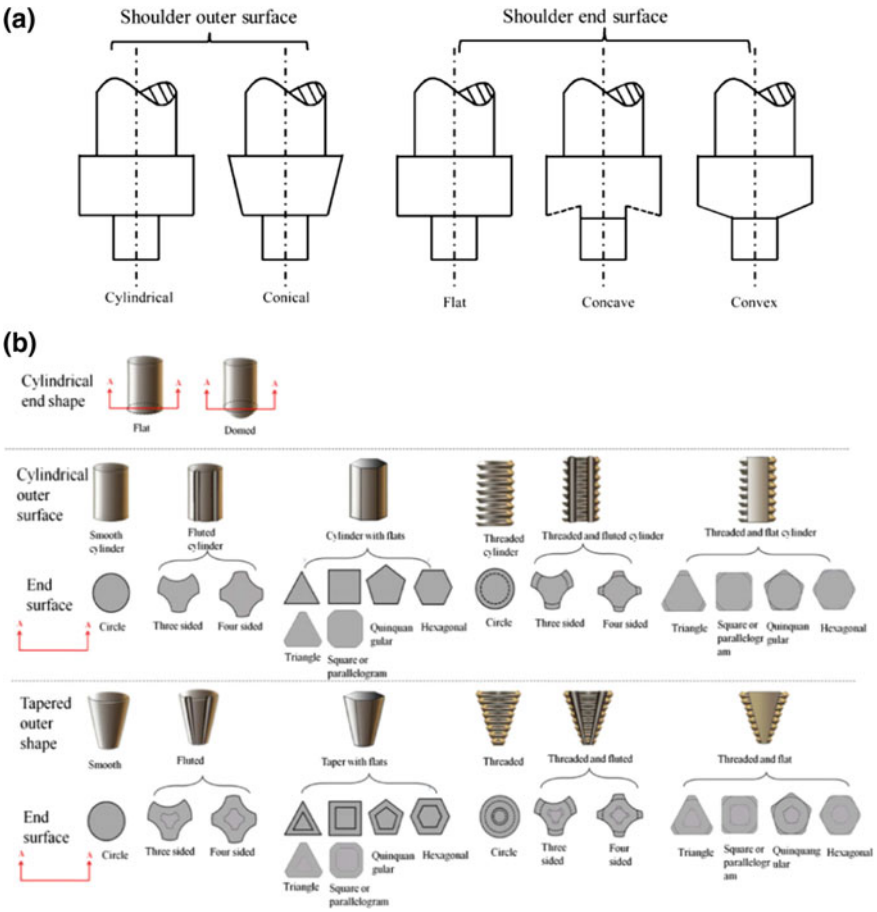

Fig. 8 Different shapes of shoulder (**a**) and pin (**b**) [56]

Sadeghian and Givi studied the effect of parameters including: geometry of the tools such as pin profile, diameters ratio and welding speeds such as rotational and linear. Optimized results produced with central composite design highlighted the optimal conditions as 2°—tilt angle, 900 rpm—rotational speed, conical tool, diameters ratio—20/6 and linear speed—25 mm/min [59].

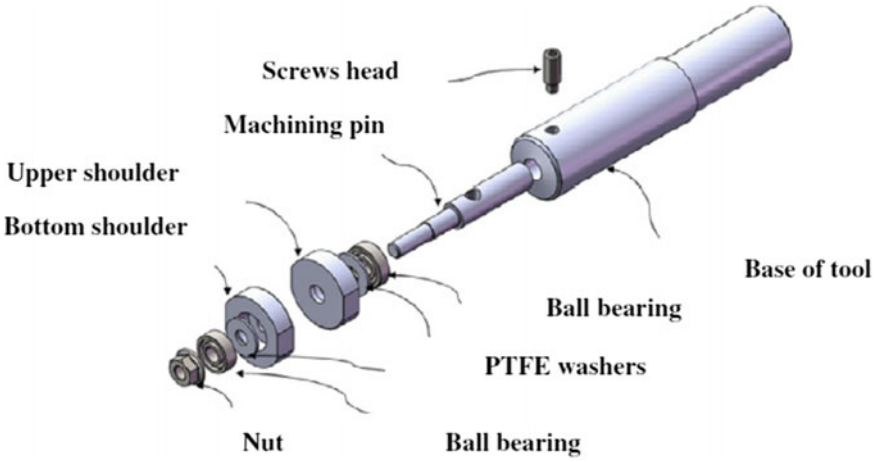

Fig. 9 Schematic of newly designed tool [57]

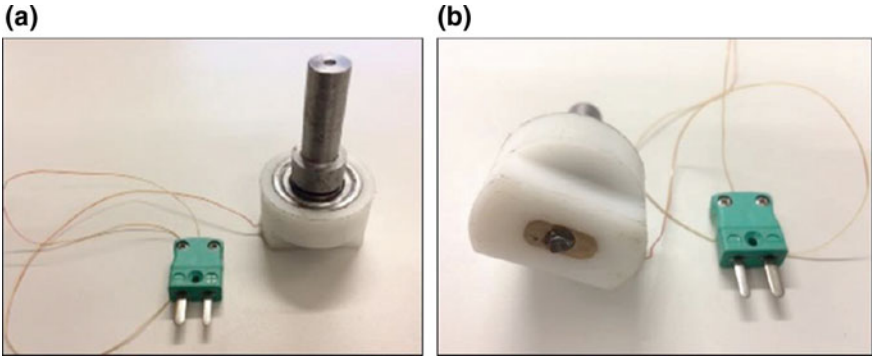

Fig. 10 Stationary shoulder and rotating probe developed: **a** isometric view and **b** bottom view [58]

3.2 Friction Stir Welding of 3D Printed Acrylonitrile Butadiene Styrene: Case Study

In the present case study, FSW of 3D printed acrylonitrile butadiene styrene specimens has been carried out by using CNC—Vertical Milling Machine. An open source 3D printer (fused deposition modelling) has been used to print ready to weld specimens. The half-length of the tensile test specimens (recommended by ASTM-638; type IV) was printed at judiciously selected process parameters (such as: 100% density, 0.254 layer thickness and 0° build angle). Friction welding was performed in the mid-way with an in-house developed cylindrical tool tip of 10 mm length and 5 mm diameter, refer Fig. 11. Wooden shoulder and bearing was used to maintain the back-up plate in stationary condition while processing. The back-up plate helped to

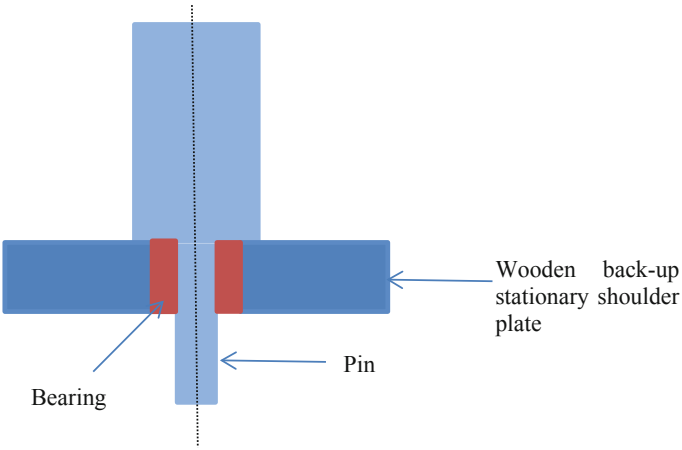

Fig. 11 Schematic view of friction tool used for welding

Table 2 Control log of experimentation

S. no.	Tool rotational speed (rpm)	Tool feed rate (mm/min)	Depth of penetration (mm)	Tensile strength (MPa)	S/N ratio (dB)
1	900	5	1.5	34.77	30.8241
2	900	7	2	36.07	31.1429
3	900	9	2.5	39.22	31.8702
4	1000	5	2	39.99	32.0390
5	1000	7	2.5	41.60	32.3819
6	1000	9	1.5	40.25	32.0953
7	1100	5	2.5	42.32	32.5309
8	1100	7	1.5	42.38	32.5432
9	1100	9	2	44.67	33.0003

avoid spattering of the heated polymer from the weld line. The design was finalized on the basis of success achieved from pilot runs.

Welding has been carried out by using three process variables of friction stir welding as per L9 orthogonal array. Here in this case study, tool rotational speed, feed rate of the tool and depth of penetration have been used at three different parametric levels. Table 2 shows the control log of experimentation according to Taguchi's design of experimentation technique. Taguchi L9 orthogonal array has been used and each experiment was repeated three times (a total of 27 experiments) in order to minimize the experimental error. Figure 12 shows cross-sectional macrograph of the FSWed specimen.

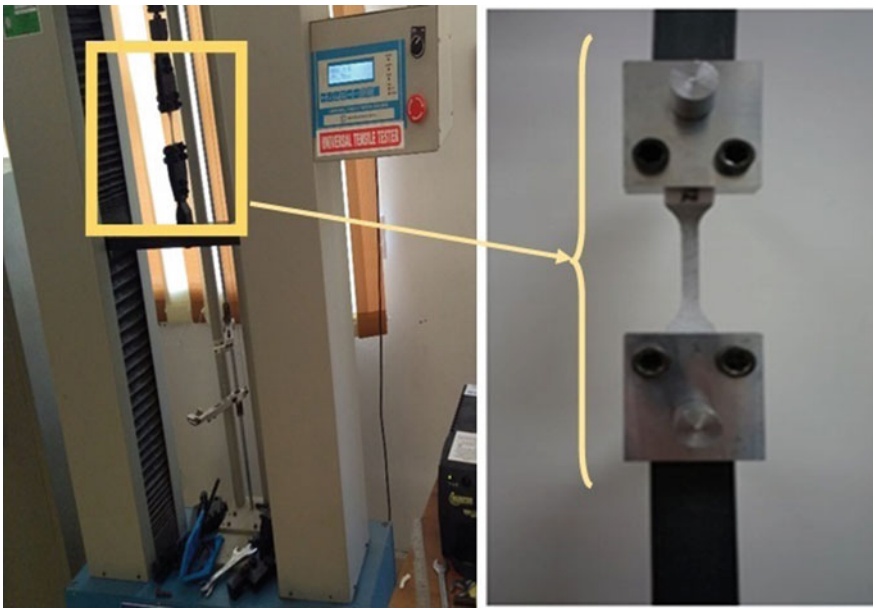

Fig. 12 Pictorial view of tensile testing of specimens

Tensile test samples were examined on Universal Tensile Testing machine (make: Zwick Roell Z010, Switzerland), refer Fig. 12. The results obtained for the tensile strength are also given in Table 1.

The obtained results were statistically analyse and signal-to-noise ratio has been studied with help of Minitab-17 software package. It has been found that the selected parameters have strong influence on the strength of the joints. Figure 13 shows S/N plot indicating the effect of parametric levels on tensile strength of the parts. From this plot, it has been found that the resulted tensile strength increased as rotational speed of the cylindrical tool increased. Maximum tensile strength is obtained with 1100 rpm, owing to more heat produced at the interface of the two mating parts of 3D printed polymer. Generally the amount of heat produced is directly proportional to the tool speed. Thus more heat was produced at high rotational speed, allowing better mixing of the polymeric material at the interface as well as better diffusion. In case of tool feed rate, it has been observed from S/N plot that higher feed rate resulted into higher tensile strength. At lower feed rate, the tool and work-material contact time was longer this excessive processing of the material resulted into peeling off the molten material from the interface, resulting into blow holes. From SEM analysis, refer Fig. 14, similar defects can be visualized.

It has been found that the excessive processing also resulted into formation of fibrous structures which has critical influence in reducing the mechanical properties of parts. Lastly, with increasing the depth of pin penetration the tensile strength of

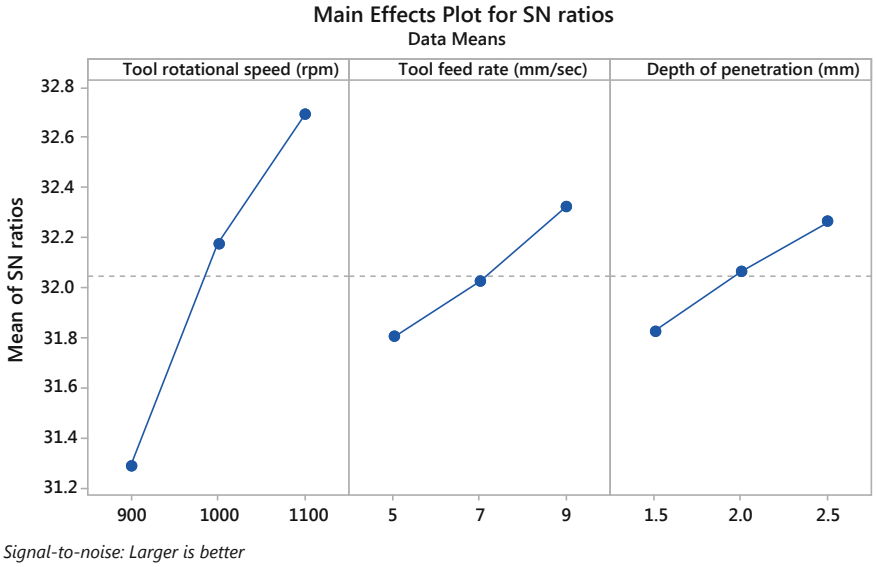

Fig. 13 S/N ratio effect plots for tensile strength versus input parameters

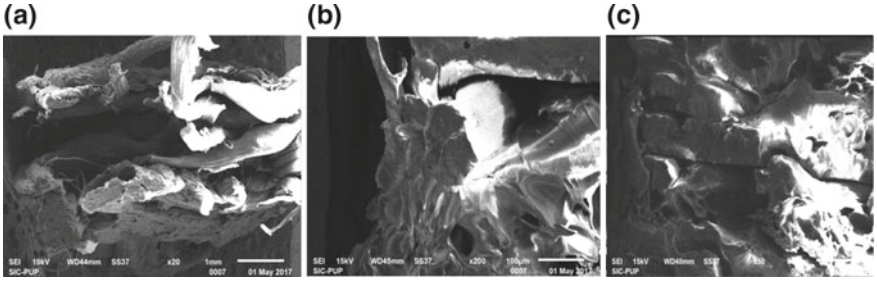

Fig. 14 Micrograph of the fractured surface indicating blow holes at several locations in sample produced with 900 rpm (**a**), 1000 rpm (**b**) and 1100 rpm (**c**)

the parts was also increased. It has been observed that better bonding of the two halves, along the interface depth, was occurred at deeper penetrations. Table 3 shows the result of Analysis of Variance (ANOVA) for S/N ratio corresponding to tensile strength data of Table 2. From ANOVA results, it has been validated that only "tool rotational speed" has statistically influenced, $P < 0.05$, the tensile strength at 95% confidence level.

Hence this parameter contributed around 80% in the obtained tensile strength. Precise control of the levels of this parameter can enhance the mechanical properties of the joints. A regression model has been developed for predicting the tensile strength, refer Eq. 1:

Table 3 Results of ANOVA for S/N ratio for tensile strength

Source	Degree of freedom	Sum of square	Variance	Fisher's value	Probability (P)	Contribution (%)
Tool rotational speed (rpm)	2	3.06222	1.53111	38.36	0.025	79.6
Tool feed rate (mm/s)	2	0.41452	0.20726	5.19	0.161	10.77
Depth of benefits (mm)	2	0.29132	0.14566	3.65	0.215	7.57
Residual Error	2	0.07983	0.03992			2.07
Total	8	3.84788				

$$\text{S/N ratio} = 23.188 + 0.007062(\text{tool rotational speed}) + 0.1310(\text{tool feed rate}) + 0.440(\text{depth of penetration}) \quad (1)$$

In order to verify the regression model, a confirmatory experiment, at suggested optimized settings, was conducted at judicially selected parametric setting, and found to be 90% accurate.

4 Conclusions

Friction stir welding is one of the latest and effective joining processes that can be used to weld metals/alloys, polymer and thereby combinations in order to satisfy wide range of industrial application, specifically including aerospace and automotive sector. From the reviewed literature it has been found that the quality of welded part is highly influenced by the process variables, which need to be optimized in précised environment. Tool geometry, depth of penetration, feed rate, etc. are reportedly most influential parameters amongst others. For this, thermal monitoring through optical and mechanical sensors can be a novel approach to monitor the temperature distributions and thereby prediction of the joint health through mathematical models.

Recently, 3D printing technology has come up to assist FSW and to produced customized parts through this hybrid manufacturing technology. A similar case study reported in this chapter outlined the FSW of 3D printed polymeric parts. It has been found that the tensile strength of the joint was significantly influenced by tool rotational speed at 95% confidence level. Formation of chips and fibrous interface are found as two major issues which are deteriorating the mechanical characteristics of the joints. In future, attempts could be made to weld dissimilar polymeric, not readily weld-able, structures made through 3D printing.

References

1. Cam G, Mistikoglu S (2014) Recent developments in friction stir welding of Al-alloys. J Mater Eng Perform 23(6):1936–1953
2. Thomas WM, Nicholas ED, Needham JC, Murch MG, Templesmith P, Dawes CJ (1991) Friction stir welding, International Patent Application No. PCT/GB92102203 and Great Britain Patent Application No. 9125978.8
3. Westermann I, Hopperstad OS, Marthinsen K, Holmedal B (2009) Ageing and work-hardening behaviour of a commercial AA7108 aluminium alloy. Mater Sci Eng, A 524(1):151–157
4. Deschamps A, Niewczas M, Bley F, Brechet Y, Embury JD, Sinq LL, Livet F, Simon JP (1999) Low-temperature dynamic precipitation in a supersaturated AI-Zn-Mg alloy and related strain hardening. Philos Mag A 79(10):2485–2504
5. Kuijpers NC, Kool WH, van der Zwaag S (2002) DSC study on Mg-Si phases in as cast AA6xxx. InMat Sci Forum 396:675–680
6. Simar A, Bréchet Y, De Meester B, Denquin A, Gallais C, Pardoen T (2012) Integrated modeling of friction stir welding of 6xxx series Al alloys: process, microstructure and properties. Progr Mat Sci 31;57(1):95–183
7. Neto DM, Neto P (2013) Numerical modeling of friction stir welding process: a literature review. Int J Adv Manuf Technol 1:1–2
8. Hamilton C, Dymek S, Sommers A (2008) A thermal model of friction stir welding in aluminum alloys. Int J Mach Tools Manuf 48(10):1120–1130
9. Gibson BT, Lammlein DH, Prater TJ, Longhurst WR, Cox CD, Ballun MC, Dharmaraj KJ, Cook GE, Strauss AM (2014) Friction stir welding: process, automation, and control. J Manuf Process 16(1):56–73
10. Feng Z, Santella ML, David SA, Steel RJ, Packer SM, Pan T, Kuo M, Bhatnagar RS (2005) Friction stir spot welding of advanced high-strength steels-a feasibility study. SAE Technical Paper
11. Nandan R, DebRoy T, Bhadeshia HK (2008) Recent advances in friction-stir welding-process, weldment structure and properties. Prog Mater Sci 53(6):980–1023
12. Figner G, Vallant R, Weinberger T, Schrottner H, Pasic H, Enzinger N (2009) Friction stir spot welds between aluminium and steel automotive sheets: influence of welding parameters on mechanical properties and microstructure. Weld World 53(1–2):R13–R23
13. Schmidt H, Hattel J, Wert J (2003) An analytical model for the heat generation in friction stir welding. Modell Simul Mater Sci Eng 12(1):143
14. Threadgill PL (2007) Terminology in friction stir welding. Sci Technol Weld Joining 12(4):357–360
15. Fazel-Najafabadi M, Kashani-Bozorg SF, Zarei-Hanzaki A (2011) Dissimilar lap joining of 304 stainless steel to CP-Ti employing friction stir welding. Mater Des 32(4):1824–1832
16. Simoncini M, Forcellese A (2012) Effect of the welding parameters and tool configuration on micro-and macro-mechanical properties of similar and dissimilar FSWed joints in AA5754 and AZ31 thin sheets. Mater Des 41:50–60
17. Bang H, Bang H, Jeon G, Oh I, Ro C (2012) Gas tungsten arc welding assisted hybrid friction stir welding of dissimilar materials Al6061-T6 aluminum alloy and STS304 stainless steel. Mater Des 37:48–55
18. Feng J, Songbai X, Wei D (2012) Reliability studies of Cu/Al joints brazed with Zn–Al–Ce filler metals. Mat Des 42:156–163
19. Honarpisheh M, Asemabadi M, Sedighi M (2012) Investigation of annealing treatment on the interfacial properties of explosive-welded Al/Cu/Al multilayer. Mater Des 37:122–127
20. Sedighi M, Honarpisheh M (2012) Experimental study of through-depth residual stress in explosive welded Al–Cu–Al multilayer. Mater Des 37:577–581
21. Tan CW, Jiang ZG, Li LQ, Chen YB, Chen XY (2013) Microstructural evolution and mechanical properties of dissimilar Al–Cu joints produced by friction stir welding. Mater Des 51:466–473
22. Liu X, Lan S, Ni J (2014) Analysis of process parameters effects on friction stir welding of dissimilar aluminum alloy to advanced high strength steel. Mater Des 59:50–62

23. Mofid MA, Abdollah-Zadeh A, Ghaini FM (2012) The effect of water cooling during dissimilar friction stir welding of Al alloy to Mg alloy. Mater Des 36:161–167
24. Sun YF, Fujii H, Takaki N, Okitsu Y (2013) Microstructure and mechanical properties of dissimilar Al alloy/steel joints prepared by a flat spot friction stir welding technique. Mater Des 47:350–357
25. Bilici MK, Yükler Aİ, Kurtulmuş M (2011) The optimization of welding parameters for friction stir spot welding of high density polyethylene sheets. Mat Des 32(7):4074–4079
26. Bilici MK, Yukler AI (2012) Effects of welding parameters on friction stir spot welding of high density polyethylene sheets. Mater Des 33:545–550
27. Bilici MK, Yükler AI (2012) Influence of tool geometry and process parameters on macrostructure and static strength in friction stir spot welded polyethylene sheets. Mat Des 33:145–152
28. Gao J, Li C, Shilpakar U, Shen Y (2015) Improvements of mechanical properties in dissimilar joints of HDPE and ABS via carbon nanotubes during friction stir welding process. Mater Des 86:289–296
29. Azarsa E, Mostafapour A (2014) Experimental investigation on flexural behavior of friction stir welded high density polyethylene sheets. J Manuf Process 16(1):149–155
30. Ratanathavorn W (2012) Hybrid joining of aluminum to thermoplastics with friction stir welding (www.diva-portal.org)
31. Mendes N, Loureiro A, Martins C, Neto P, Pires JN (2014) Morphology and strength of acrylonitrile butadiene styrene welds performed by robotic friction stir welding. Mater Des 64:81–90
32. Mendes N, Loureiro A, Martins C, Neto P, Pires JN (2014) Effect of friction stir welding parameters on morphology and strength of acrylonitrile butadiene styrene plate welds. Mater Des 58:457–464
33. Bagheri A, Azdast T, Doniavi A (2013) An experimental study on mechanical properties of friction stir welded ABS sheets. Mater Des 43:402–409
34. Paoletti A, Lambiase F, Di Ilio A (2015) Optimization of friction stir welding of thermoplastics. Procedia CIRP 33:562–567
35. Bozkurt Y (2012) The optimization of friction stir welding process parameters to achieve maximum tensile strength in polyethylene sheets. Mater Des 35:440–445
36. Wirth FX, Zaeh MF, Krutzlinger M, Silvanus J (2014) Analysis of the bonding behavior and joining mechanism during friction press joining of aluminum alloys with thermoplastics. Procedia CIRP 18:215–220
37. Liu FC, Liao J, Nakata K (2014) Joining of metal to plastic using friction lap welding. Mater Des 54:236–244
38. Khodabakhshi F, Haghshenas M, Sahraeinejad S, Chen J, Shalchi B, Li J, Gerlich AP (2014) Microstructure-property characterization of a friction-stir welded joint between AA5059 aluminum alloy and high density polyethylene. Mater Charact 98:73–82
39. Amancio-Filho ST, Bueno C, Dos Santos JF, Huber N, Hage E (2011) On the feasibility of friction spot joining in magnesium/fiber-reinforced polymer composite hybrid structures. Mater Sci Eng, A 528(10):3841–3848
40. Ratanathavorn W, Melander A (2015) Dissimilar joining between aluminium alloy (AA 6111) and thermoplastics using friction stir welding. Sci Technol Weld Joining 20(3):222–228
41. White D (2002) Object consolidation employing friction joining, US patent, Patent No.: US 6,457,629 B1
42. Lequeu PH, Muzzolini R, Ehrstrom JC, Bron F, Maziarz R (2006) Powerpoint presentation on: high performance friction stir welded structures using advanced alloys. In: Aeromat conference, Seattle, WA
43. Baumann JA (2012) Technical report on: production of energy efficient preform structures. The Boeing Company, Huntington Beach, CA
44. Sharma A, Bandari V, Ito K, Kohama K, Ramji M, BV HS (2017) A new process for design and manufacture of tailor-made functionally graded composites through friction stir additive manufacturing. J Manuf Process 26:122–130
45. Guan Q (2013) Generalized additive manufacturing based on welding/joining technologies. Автоматическая сварка 10–11:33–37

46. Palanivel S, Nelaturu P, Glass B, Mishra RS (2015) Friction stir additive manufacturing for high structural performance through microstructural control in an Mg based WE43 alloy. Mater Des 65:934–952
47. Rodrigues DM, Loureiro A, Leitao C, Leal RM, Chaparro BM, Vilaça P (2009) Influence of friction stir welding parameters on the microstructural and mechanical properties of AA 6016-T4 thin welds. Mater Des 30(6):1913–1921
48. Bilici MK (2012) Effect of tool geometry on friction stir spot welding of polypropylene sheets. Express Polymer Letters 6(10)
49. Mishra RS, Ma ZY (2005) Friction stir welding and processing. Mat Sci Eng R: Rep 50:1–78
50. Su P, Gerlich A, North TH (2005) Friction stir spot welding of aluminum and magnesium alloy sheets. SAE Technical Paper
51. Kulekci MK, Şik A, Kaluç E (2008) Effects of tool rotation and pin diameter on fatigue properties of friction stir welded lap joints. Int J Adv Manuf Technol 36(9–10):877–882
52. Hirasawa S, Badarinarayan H, Okamoto K, Tomimura T, Kawanami T (2010) Analysis of effect of tool geometry on plastic flow during friction stir spot welding using particle method. J Mater Process Technol 210(11):1455–1463
53. Chowdhury SM, Chen DL, Bhole SD, Cao X (2010) Effect of pin tool thread orientation on fatigue strength of friction stir welded AZ31B-H24 Mg butt joints. Procedia Eng 2(1):825–833
54. Tozaki Y, Uematsu Y, Tokaji K (2007) Effect of tool geometry on microstructure and static strength in friction stir spot welded aluminium alloys. Int J Mach Tools Manuf 47(15):2230–2236
55. Vijay SJ, Murugan N (2010) Influence of tool pin profile on the metallurgical and mechanical properties of friction stir welded Al–10wt.% TiB 2 metal matrix composite. Mat Des 31(7):3585–3589
56. Yang Q, Mironov S, Sato YS, Okamoto K (2010) Material flow during friction stir spot welding. Mater Sci Eng, A 527(16):4389–4398
57. Pirizadeh M, Azdast T, Ahmadi SR, Shishavan SM, Bagheri A (2014) Friction stir welding of thermoplastics using a newly designed tool. Mater Des 54:342–347
58. Eslami S, Ramos T, Tavares PJ, Moreira PM (2015) Effect of friction stir welding parameters with newly developed tool for lap joint of dissimilar polymers. Procedia Eng 114:199–207
59. Sadeghian N, Givi MK (2015) Experimental optimization of the mechanical properties of friction stir welded Acrylonitrile Butadiene Styrene sheets. Mater Des 67:145–53

4D Printing

K. Raghavendra, M. Manjaiah and N. Balashanmugam

Abstract With evolution and change in environment, Nature's structures and its material system exists with products having multiple designs and dimensions. Inspired by Nature's ability to develop structures with complexity, various research works are carried out to develop newer technology to build complex products with more design dimensions. In the process of bio mimicking nature's fabrication process 3D printing has captured the imagination of everyone from industry to research experts. However, there are various challenges need to be addressed in the process of 3D printing related to material system and product functional dynamicity. Hence, to overcome the limitations of 3D printing in flexible product development, 4D printing was generated with one or more additional design dimensions. 4D printing invented by MIT research group relies on fast growth of smart materials, 3D printers, mathematical modelling and design, and shows advantages over 3D printing. This article presents a comprehensive overview of 4D printing concept, applications and future scope for research.

Keywords 4D printing · Material · Design · Product development

1 Introduction

Ever since the industrial revolution, manufacturing sectors of all domains exhibited factories with complex mechanisms for production. 3D printing in the past thirty odd years has changed production scenario without tooling, assembly lines or supply

K. Raghavendra
Centre for Incubation Innovation Research and Consultancy, Jyothy Institute of Technology, Bengaluru, India

M. Manjaiah (✉)
Department of Mechanical and Manufacturing Engineering, Manipal Institute of Technology, Manipal Academy of Higher Education, Manipal 576104, Karnataka, India
e-mail: manjaiah.m@manipal.edu

N. Balashanmugam
Central Manufacturing Technology Institute (CMTI), Bengaluru, India

K. Gupta (ed.), *Materials Forming, Machining and Post Processing*, Materials Forming, Machining and Tribology, https://doi.org/10.1007/978-3-030-18854-2_4

chains making it a classic riotous technology. Hence, seeing the current capabilities of advanced manufacturing, it can be ensured that conventional goods, engineering components and customized medical products will be developed with aid of 3D printing factories [6, 10].

Manufacturing sectors of all engineering disciplines are under the process of technological transformation promising the establishment of customizable and sustainable manufacturing environment for the betterment of the industries.

New forms of engineering such as Additive Manufacturing are giving raise to the new industries such as 3D printing, 4D printing or direct digital manufacturing. These set of industries can be used in all industrial sectors comprising of aerospace, civil, electronics, and medical industries. Especially in medical sector, these technologies can be used in development of customized surgical tools, human implants, replacement of tissues and organs and many more [12].

Decades back with the advent of 3DP, objects developed were only tested outside human body for medications and treatments. However, with introduction of 4DP researchers are developing samples of human organs for drug and functionality testing. This can support researchers to develop human organs with desirable capabilities as compared to human body natural limits.

The right implementation of 3D and 4D printing technologies can positively transform the world in the manufacturing industries domain rapidly leading to Third Industrial Revolution through elimination of limitations encountered in the period of first and second stage industrial revolution.

1.1 3D Printing

3D printing is an additive manufacturing process, where in, the products are developed by depositing layers using different 3D techniques for designed Computer Aided Design (CAD) model or 3D scanners used to scan a model and convert it into digital data. In here, the development of objects is controlled by optimizing position and adhesion of specimen in 3D space. 3D printing is a process which turns the digital data into physical product by depositing layer by layer. 4D printing is based on the 3D printing technology, it uses a special material and refined design that is planned to prompt 3D print to change its shape.

2 Advancement in 3D Printing

Additive manufacturing also known as 3D printing has been associated with Rapid prototyping from past 30 years [5]. Research in 3D printing technology has attracted unprecedented interest since 1980s [8]. Since then, 3D printing has become a multi-billion dollar business rapidly growing in industries for development of prototypes. However, the assignment of properties of materials and distribution of the same along

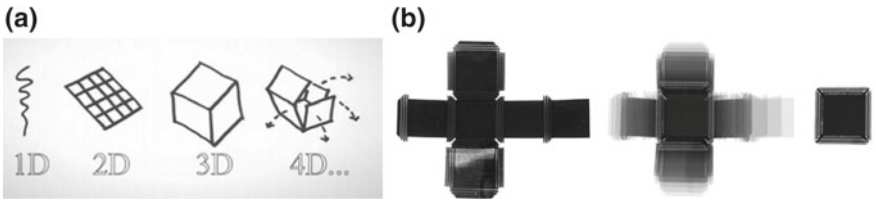

Fig. 1 **a** Simple illustration of the concept of 4D printing (P1) **b** REF T4 flat surface that self-folds into a closed cube developed using 4DP [12]

multiple dimension and direction cannot be modulated in 3D printing techniques though they develop accurate models and complex designs.

In order to overcome these limitations of 3D printing, a new technology was developed by Skylar Tibbits of **Massachusetts Institute of Technology (MIT)** in 2013 [14]. The research carried out at MIT focused on development of system smarter in solving the problems associated with reduction in wastage of energy, materials, money, time and increase in positive properties of the product. In order to achieve these, Tibbits proposed a combined concept of logic matter, materials with mathematical data programming known as **4D printing**.

Integration of mathematical models with 3DP process functionally defines the functionality of 4DP components. Figure 1a illustrates the geometrical phenomenon of 4DP. During functional products development process, the minute dimension or the micro sized part of the product is initially printed, later the structure's major dimensions are printed for enhancing the performance of the functionality of the product. Hence optimizing the process of the 4DP will lead to fast and low cost development of the component.

2.1 4D Printing: Reinventing Manufacturing

4D printing is the time targeted evolution of 3D printing. It is defined as 3D printed object where the shape, property and functional change occurs with respect to time. More comprehensively defined as per number of studies conducted on this study, it is a targeted evaluation of 3D printed object capable of performing self-assembly and multi functionality. In here, the targets are focused on development of objects having ability to memorize the structure shape, property and function before and after application of loads.

4D printing can be applied in diverse industries/fields including aerospace, automotive, electronics, medical and education. The technology can revolutionize interdisciplinary fields of industries by benefitting the process of product development at lower processing costs. In 4D printing, the time, effort and cost to create complex designs are comparatively lower in comparison to conventional manufacturing pro-

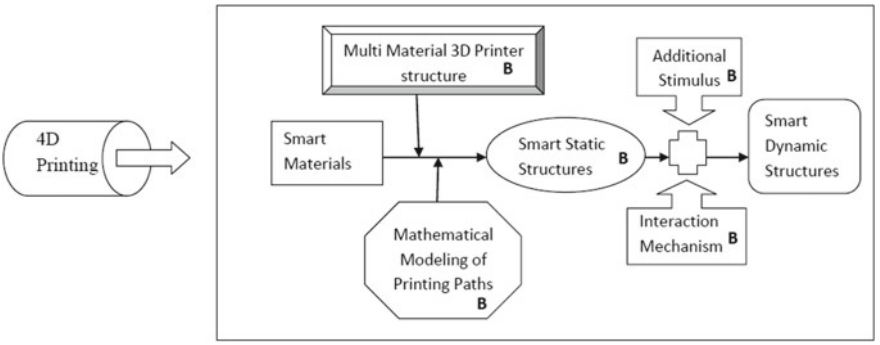

Fig. 2 4D printing with working bases

cesses. Hence 4D printing will possibly be the technology to redefine the currently existing manufacturing processes.

2.1.1 Working Principle-4D Printing

4D printing is a system having the ability of fabricating dynamic structures with adjustable shapes properties or functionality [14]. This capability can be obtained by having appropriate combination of smart materials in 3D space [13]. In order to design such complex structures mathematical modeling is desired. Hence, as shown in Fig. 2, the fundamental building blocks for effective working of a 4DP system are, 3D printing facility, stimulus, responsive material, interaction mechanism, and mathematical modeling. The optimal combination of these elements has contributed to effective evolution of 4D printed structures over time.

2.1.2 Elements for Effective Working of 4DP

I. 3D printing facility: use of 3D printing apparatus is necessary for fabrication of multi material structures with simple and complex geometry having differences in material properties such as swelling ratio, coefficient of thermal expansion etc. this will enhance the property of the structure in shape-shifting behavior.
II. Stimulus: on a need basis system, in order to trigger the change and regain of shape/property/functionality of a 4D printed structure stimulus are stipulated for a 4D printed structure. The stimulus include water, heat and light, and a combination of water and heat [12]. Stimulus are generally selected based on the specific application and the smart materials involved in the same.
III. Smart or stimulus responsive materials: is the most important component of 4D printed structure. For effective working of the 4DP structure the material should fulfill properties such as, self-sensing, decision making, responsiveness, shape

memory, self-adaptability, and multi functionality and self-repair [8]. Hence processing the same with the combination of 3DP facility and stimulus is of prior importance.

IV. Interaction mechanism: in some cases application of stimulus in a predetermined sequence defines the effectiveness of a 4D printed structure with respect to the 4th dimension time.

V. Mathematical modeling: mathematical modeling defines the design of material distribution and structure during printing by providing desired shape, property and functionality. Development of theoretical and numerical models will lead establishment of connections between 4 core elements namely; material structure, shape, material properties and stimulus properties.

4D printing is an invention made with effective combination of 3D printing and smart materials. The effectiveness can be achieved by exposing to the external stimulus through an interaction mechanism and through assistance of Mathematics.

3 Biomimetic

Biomimetic is the modern technological approach followed for replication of Nature's way of behavior in synthetic product by fabrication processes through technology surveys knowing the limitations in functionality of the materials and the processes being used.

The behavior and organization of material with time is as shown in Fig. 3. It defines the response of a system to the environmental conditions and constraints based on the material structure. Hence, seeing the materials compositions of the material system, for replication of the same in the artificial system the process involved in the development of the system should be deliberate and preconceived in design of materials, dimensions, and shape to achieve necessary functions and necessary constraints. This is considered very crucial as anisotropy in natural materials is omnipresent with most materials exhibiting anisotropic behavior in accordance to their function and behavior.

However, in technology associated with biomimetic and additive manufacturing, limitations always arise in prototyping with current methods of fabrication and materials. Hence, a new approach such as the 4D printing with use of one or more additional dimensions of materials grade, adaptation and response over time, along with control over volumetric anisotropy is being developed by research team to address such mismatch in biomimeting.

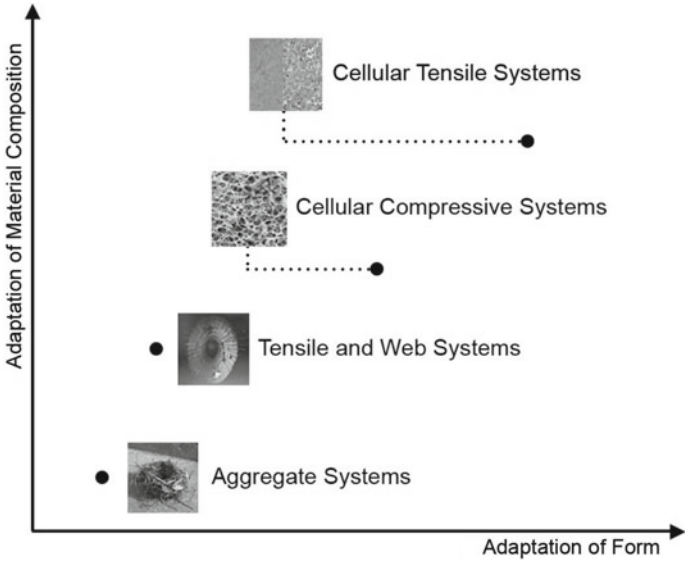

Fig. 3 Composition and form in Nature's material systems [15]

4 4D Printing Materials

Material homogeneity is omnipresent in nature and the functional material gradient determines the efficiency of a product through spatially varying compositions and properties [2]. However, industrially produced components comprise of homogeneously defined forms and materials of parts. Hence, development of such components though have manufacturing components and design tools, they may compromise with certain improvements in strength, weight, functionality and measurement. In order to overcome these limitations of material property after processing, a strategic control of material property density and directionality in the generation of complex smart structures known as digital anisotropy was introduced by researchers at **MIT** [14] to achieve controlled gradients of stiffness and elasticity. Table 1 presents some of the significant advantages of 4D printing over 3D printing.

4D printing materials are intelligent materials which do active functions from the external atmosphere and make a useful response, but this would include physical sensing materials such as piezoelectric or magnetostrictive compounds are categorize as "intelligent". The material provides an active response in a product that would otherwise be lacking and have the potential to yield a multitude of enhanced capabilities and functionalities [9]. The intelligent materials capabilities are reported in Table 2.

Table 1 4D printing over 3D printing [3]

Sl. no	Advantages over traditional manufacturing	3D Printing (3DP)	4D Printing (4DP)
1	Improvement in freedom for design	Generic conventional fabrication processes limits the product development with increase in design complexity due to machine ability constraints. Also, machining capability is reduced with the kind of material being used. However, in 3DP materials can be selected based on the design requirement and not on the machine capability	Freedom for design and development is much better in 4DP than 3DP and conventional processes. 4DP will allow development of parts with anisotropy property
2	Reduction of cost even with increase in complexity of design	Cost is high in conventional processes due to limitation in machining complex shapes and complicated materials. In 3DP additive manufacturing process since parts are printed layer by layer no additional cost is contributed	Since the process of 4DP is completely streamlined no additional cost of any matter exists in development of simple or complex structures
3	Demand based production customization	Products can be printed on a 3DP for any customized design of product requirement with no additional cost	Since 4DP is the advanced version of 3DP any complex customized product can be generated without any cost loss
4	Product customization with mass production	3DP can develop products with customizable design without changing machine and increasing the cost	4DP can further enhance the capability of personalization of products which can be universally accepted
5	Simplification of manufacturing process	Since the process of 3DP involves direct conversion of standardized digital file into physical product, human intervention with respect to operator skill is minimized	In 4DP structures can be activated through external stimulus to obtain complex functional structures and systems

(continued)

Table 1 (continued)

Sl. no	Advantages over traditional manufacturing	3D Printing (3DP)	4D Printing (4DP)
6	Single system comprising of both prototyping and production	Multiple usage of fabrication techniques is minimized in 3DP as prototypes/test parts can be made with same procedure in 3DP using a single system	In 4DP, since materials are embedded and created with dynamic functionality, higher expectation of product performance can be framed in 4DP fabrication process than any other fabrication techniques
7	Elimination of supply chains and assembly lines for complex products	3DP is a one shot fabrication process as many assembly lines and multiple fabrication units are eliminated	Since products of multiple functionality can be developed with 4DP supply chains and assembly lines are eliminated
8	Elimination of actual product transportation across the world	Since the technology is similar to most of the process able materials, products can be redeveloped with same functionality using 3DP with similar design data	Since voxels of 4DP can develop multifunctional objects game changing design to production can be gifted to the manufacturing world
9	Optimization of product properties	Since 3DP has the ability to process composites of required materials, desired properties can achieved	Use of multi materials through programmable matter (PM) in 4DP can lead to development of products with optimized customizable properties
10	Instantaneous production on a global scale	Rate of production can be increased in the global scale using 3DP as digital data of the product can be transferred to any part of the world in fraction of minutes	In 4DP, collection of voxels can enable matter formation on demand and digital data can be transferred anywhere in the world
11	Magnification of innovation ability	Very minimum limitations to product development with 3DP due to less limitations in engineering constraints	With 4DP, any material and any functionality can be developed for a product. Hence, there shall exist almost no technological limitation with 4DP

(continued)

Table 1 (continued)

Sl. no	Advantages over traditional manufacturing	3D Printing (3DP)	4D Printing (4DP)
12	Endless implementation of engineering ideas in design and development	Ease and clarity of 3DP technology can create direct relationship between the designer and the product with no space to confusion in fabrication process	4DP can create products a step ahead of 3DP due to the capability of development of multifunctional objects and material programming leading to development of dynamic and intelligent physical models

Table 2 The intelligent material capabilities

Function	Description
Shape memory	Shape changes by external stimuli
Self-assembly	Allows automated assembly
Self-actuating	Automated actuation in response
Self-sensing	Allows automated detection and sometimes quantification of external stimuli

4.1 Shape Memory Polymers (SMPs)

Shape memory polymers are the evolving active class of polymers that can be used in a wide range of application in biomedical devices and microsystems [7]. SMP have an ability to alter the shape in a predefined way to form a temporary transformation to permanent transformation when it exposed to appropriate stimuli-triggered dynamic processes. This characteristics of SMP helps in application of 4D printed materials as a shape changes with respect to time dependent. These materials have high elastic deformability, low cost, light weight and extremely biocompatible and biodegradable. These materials functions are largely depend on the glass transitions temperature (T_g). Thermoresponsive SMPs the temporary shape is presented by heating the polymer to a glass transition temperature (T_g) and then reforming into temporary shape by the physical force. Among all the SMPs thermoresponsive are the most widely applied derivatives, which demonstrates a broad tuneable range of mechanical, thermal and optical properties [1]. Also among many other applications, these polymers are used to generate medical support devices such as stents and catheters. Since such complex applications demand multiple functionality shape memory effect, polymers such as acrylates, polyurethanes and other multiple polymer blends are used. Also, in order to achieve multiple functionality within the developed device, SMP's are pre and post processed to achieve shape memory mechanisms. To achieve this, indirect heating methods using infrared light of electronic triggers is generally performed to enhance the shape recovery mechanism property. However, direct heating of SMP's is generally considered in processing SMP's.

Fig. 4 Microstereolithogrphy 3D printed thermoset polymer [11]

4.2 Thermoset Shape Memory Polymers

Thermoset SMP's are the blend of thermoset resins or polymers of similar monomers of designed composition leading to shape memory system. The monomer combinations involve polyethylene glycol or polybutadiene to form shape memory cyanate system. With aid of synthesizing/polymerizing materials such as soya oil epoxidized acrylate these polymers can be made use in fabrication of scaffolds with different printing techniques. Figure 4 represents 3D printed article developed using table top stereolithography system. Similarly UVLED digital light processing printer can also be used for such developments. Hence, with controlled UV light and LASER light projecting systems, networks can be developed via printing through high resolution projection systems.

4.3 Shape Memory Thermoplastic Polymers

Thermo plastic polymer is a polymer generally used as printing ink in 3D printers. Polyurethane elastomer was used as TPSM material by [16]. Study showed commercially available pallets of DiAPLEXMM4520 from SMP technologies having a crystallanity of 350wt% was found to be feasible for processing in 3DP. Also, shape memory filaments processable with 3DP were found in bulk. However, in order to process such materials the process parameters such as nozzle temperature, scanning speed and part cooling in 3DP initially needs to be essentially optimized in a controlled environment for establishing high quality structures. Based on optimization of process parameters of 3DP, 3D structures were fabricated with good shape memory properties.

4.4 Self-healing Hydrogel Materials

Polymeric materials are being synthesized with self-healing properties for application in 3D bio mimicking of tissue such as external skin. Hydrogel monomers/polymers are considered to be the effective raw materials due to its outstanding properties of 3D network structure and water retention capabilities fulfilling the conditions of extracellular matrix. Thus, soft hydrogels are preferred as ideal materials for preparation of scaffolds in tissue engineering applications. Applications of hydrogels vary from wound dressings, personal hygiene products and contact lenses. Currently, hydrogels are also extensively researched for biologically active compounds for use in drugs, antibodies and development of implants. Hydrogels motivate 4DP as they can be used as self-healing materials in normalizing wound tissues having the dynamic process behaviour of 4DP.

5 Applications

4D printing technology has the ability to upgrade current manufacturing business environment. Study on materials with self-changing properties will increase the application areas of 4D printed articles.

Currently researchers are exploring 4D printed structures in various fields of applications due to material's anisotropic and shape memory property. Beyond the simple regular applications, complex shelf life structures are investigated. Figure 5 shows development of prosthetic fingers for humans. Also, multicellular matrices can be made to grow into functional organs along with replacement tissues. Figure 6 shows the droplets network of tissue engineering substrate used as a support for the

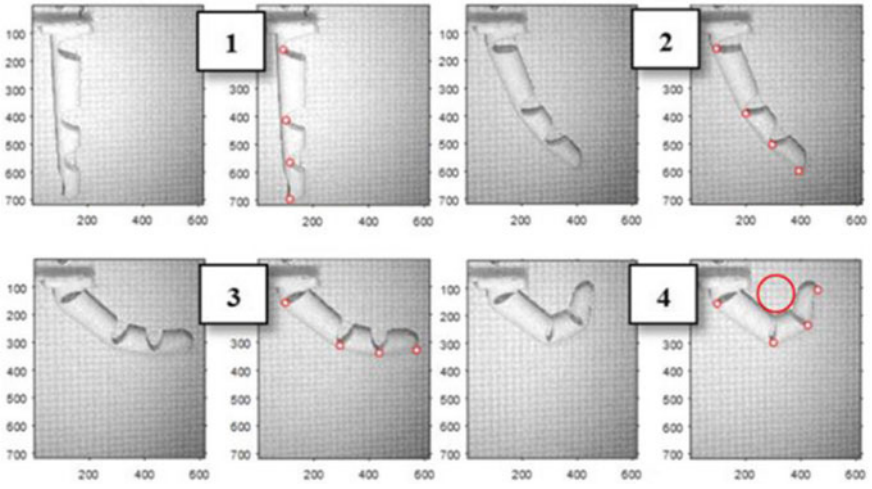

Fig. 5 Self-bending prosthetic finger [12]

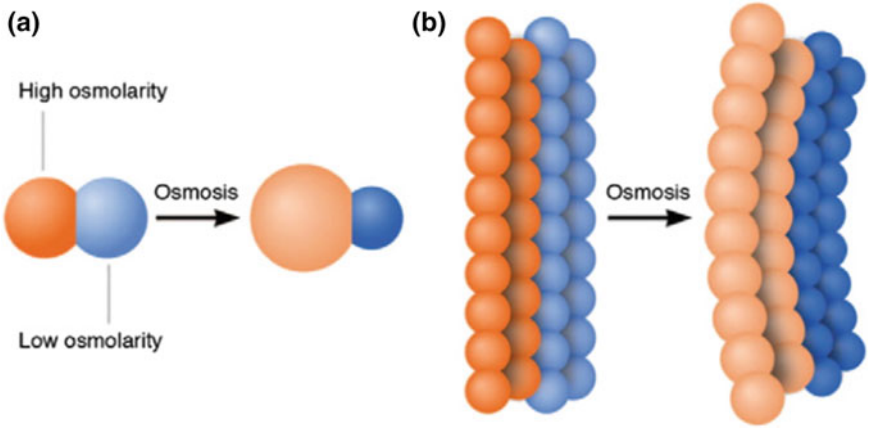

Fig. 6 **a** Osmosis effect between two droplets, **b** macroscopic deformation arising from osmosis effect [4, 12]

failing tissues functionality. Using 4DP technology dynamic reversible functional behavior with in a product can be achieved. Hence, if the shape shifting cycles of 4D printed structures can be equalized in comparison to the natural element capability, this technology can be used with multiple disciplines for various applications.

6 SWOT Analysis

SWOT is a process that shall lead to strategic planning for future of industries implementing 4DP in product development cycle. The factors of SWOT are as defined in the following:

1. Strength:

   - Raw materials and the manufacturing process programming used have high rate of efficacy due to Programmable Materials (PM).
   - Mathematical modeling has the ability to control structure functionality.
   - Materials can be programmed based on the need with multiple compositions.
   - Structure with varying functionality can processed using cuing currently available 3D printers.

2. Weakness:

   - Requires extensive domain knowledge of 3DP and Mathematical modeling as the 3DP and the material used for the 4DP system is completely mathematical program controlled.
   - Hard to define accuracy through variation in optimization of process parameters for controlling functionality of size and shape.
   - Requires experts to be processing 4DP in a controlled environment.

3. Opportunities:

   - Can be highly useful in development of artificial skin and organs especially in warzone and space.
   - Helpful in development of biocompatible medical implants of complex size and shape.
   - 4DP can be exclusive made useful in development of smart structures.

4. Threats:

   - Since new categories of raw materials are defined for process based on the functionality requirement, health effects on users and manufacturers are of major concern.
   - Ethical and technical issues relating to the application of 4D Printed products is also a major issue.

7 Conclusions

- All technologies in the modern manufacturing world are generally inspired from the nature.
- Natural systems comprising natural materials continuously adopt and evolve over a period of time leading to changes in working pattern. In order to replicate such elements processing of structures is highly dependent on materials and processing technology. One such process involved in replication of natural systems is 4DP.
- The current technology of 4DP revolutionized by Skylar Tibbits of MIT-USA is an updated version of 3DP started by Hull 30 years ago. In 4DP various technological enhancements as compared to 3DP were implemented relating to material processing and printing technology.
- 4DP is one of the technologies developed to replicate natural elements showcasing anisotropic properties. 4DP still is in superficial stage of exploration in the modern manufacturing domain. However, in order to fulfill this requirement Programmable Matter (PM) has been significantly researched in design, control and modulation of property and behavior across spatial scales for higher efficiency and effectiveness during additive manufacturing. Programmable matter and 4DP has the ability to revolutionize medical implant and other manufacturing sectors. However, the

technology needs to grow exponentially in real engineering and science research to compete with the current state of the art technology.
- With complete optimization of 4DP technology implants of medical industries will reach higher stature. Hence 4DP can be the future of manufacturing sector especially in the medical industries if proper care is taken to enhance the technological aspects of the same and there by produce cheaper products to the market.
- Hence, it can be concluded that 4DP shows a very high potential to become a new platform for bio inspired additive manufacturing technology that can perform as efficient and effective as natural systems and contribute to the welfare of human beings through evolution of stable medical implants.

8 Future Scope

In the coming years the several challenges needs to be addressed in the technological areas of 4DP, which are as following:

1. Design: suitable CAD software to support development of Programmable Materials (PM) based technological/scientific products.
2. Materials: optimization of material properties during production to create PM wit multifunctional properties.
3. Adhesion of particulates: extensive study on behavior of materials when embedded to achieve required property.
4. Energy: energy optimization to activate the PM according to the design requirement.
5. Electronics: control of electronic systems for effectiveness and efficiency.
6. Programming: digital and physical communications of voxels through programs as the defined product will be anisotropic in nature.
7. Adaptability to different environments: design and programming the product for different environmental conditions.
8. Assembly: micro and macro scale assembly during manufacturing and accidents.
9. Standardization: development of standards to incorporate 4DP in mass production.
10. Certification: certification of 4D printed products and raw materials.
11. Cost: initial cost of the 4DP system and raw materials.
12. Testing and characterization techniques for proving the effectiveness of product developed by 4DP system.
13. Technology for recycling 4DP systems and its products developed and reuse of raw materials.

References

1. Belmonte A et al (2015) Effect of the network structure and programming temperature on the shape-memory response of thiol-epoxy “click” systems. Polymers 7(10):2146–2164. https://doi.org/10.3390/polym7101505
2. Callister WD, Rethwisch DG (2009) Materials science and engineering: an introduction, 8th edn. Wiley, Hoboken
3. Campbell TA, Tibbits S, Garrett B (2014) The next wave: 4D printing programming the material world. Atlantic Council
4. Chang J et al (2018) Advanced material strategies for next-generation additive manufacturing. Materials 11(1). https://doi.org/10.3390/ma11010166
5. Gao B et al (2016) 4D bioprinting for biomedical applications. Trends Biotechnol 34(9):746–756. https://doi.org/10.1016/j.tibtech.2016.03.004 (Elsevier Ltd)
6. Ge Q et al (2014) Active origami by 4D printing. Smart Mater Struct 23(9). https://doi.org/10.1088/0964-1726/23/9/094007
7. Hassan RU, Jo S, Seok J (2018) Thermorheological characteristics and comparison of shape memory polymers fabricated by novel 3D printing technique. Funct Mater Lett 11(02):1850031. https://doi.org/10.1142/S1793604718500315
8. Khoo ZX et al (2015) 3D printing of smart materials: a review on recent progresses in 4D printing. Virtual Phys Prototyping 10(3):103–122. https://doi.org/10.1080/17452759.2015.1097054 (Taylor & Francis)
9. Li X, Shang J, Wang Z (2017) Intelligent materials: a review of applications in 4D printing. Assembly Autom 37(2):170–185. https://doi.org/10.1108/AA-11-2015-093
10. Ma J et al (2017) Spatial control of functional response in 4D-printed active metallic structures. Sci Rep 7:1–8. https://doi.org/10.1038/srep46707
11. Miao S et al (2017) 4D printing of polymeric materials for tissue and organ regeneration. Mater Today 20(10):577–591. https://doi.org/10.1016/j.mattod.2017.06.005 (Elsevier Ltd)
12. Momeni F et al (2017) A review of 4D printing. Mater Des 122:42–79. https://doi.org/10.1016/j.matdes.2017.02.068 (Elsevier Ltd)
13. Sydney Gladman A et al (2016) Biomimetic 4D printing. Nat Mater 15(4):413–418. https://doi.org/10.1038/nmat4544
14. Tibbits S (2014) 4D printing: multi-material shape change. Architectural Des 84(1):116–121. https://doi.org/10.1002/ad.1710
15. Tsai EY (2013) 4D printing : towards biomimetic additive manufacturing. Massachusetts Institute of Technology. Available at: http://dspace.mit.edu/handle/1721.1/91821
16. Yang Y et al (2016) 3D printing of shape memory polymer for functional part fabrication. Int J Adv Manuf Technol 84(9):2079–2095. https://doi.org/10.1007/s00170-015-7843-2

Non-conventional Micro-machining Processes

Lijo Paul, J. Babu and J. Paulo Davim

Abstract Nonconventional micromachining processes are developed to meet the manufacturing requirements of new materials and products where usual processes are found inadequate. Based on the type of energy used for material removal, the different micromachining processes are classified into thermal, mechanical, chemical and hybrid processes. Hybrid processes combine two or more machining processes to achieve the desired machining. Descriptions of the important micromachining processes, their material removal mechanism and salient application fields are dealt with in this chapter.

Keywords Micro machining · USM · AJM · EDM · ECM · ECDM · AWJM · LBM · ECDG

Notation

AEDMM	Abrasive electro-discharge micro-machining
AJM	Abrasive jet machining
AWJM	Abrasive water jet machining
CAD	Computer aided design
CAM	Computer aided manufacturing
CD	Chemical dissolution
CHM	Chemical milling
CMM	Coordinate measuring machine
CNC	Computer numerical control
DC	Direct current

L. Paul (✉) · J. Babu
Department of Mechanical Engineering, St. Joseph's College of Engineering & Technology, Choondacherry 686579, Kerala, India
e-mail: lijo.paul@gmail.com

J. Paulo Davim
Department of Mechanical Engineering, University of Aveiro, Campus Santiago, 3810-193 Aveiro, Portugal

K. Gupta (ed.), *Materials Forming, Machining and Post Processing*, Materials Forming, Machining and Tribology, https://doi.org/10.1007/978-3-030-18854-2_5

ECD	Electrochemical dissolution
ECDG	Electrochemical discharge grinding
ECDM	Electrochemical discharge machining
ECG	Electrochemical grinding
ECM	Electrochemical machining
EDM	Electro discharge machining
G	Grinding
HAZ	Heat-affected zone
IBMM	Ion beam micro-machining
IEG	Inter-electrode gap
LBM	Laser beam machining
MRR	Material removal rate
PMMA	Polymethyl methacrylate
PZT	Piezoelectric transducer
UHP	Ultra high power
USM	Ultrasonic machining
USMEC	Ultrasonic-assisted electrochemical machining
VAM	Vibration assisted machining
WJ	Waterjet
WJM	Water jet machining

1 Introduction

Many new high performance engineering materials are being developed to meet the stringent requirements of modern industry in terms of size and accuracy of the products. Companies worldwide are vying with each other to meet these customer requirements efficiently and effectively in the stipulated period of time. Some examples of the newer engineering materials are nitroalloy, hastalloy, nimonics, carbides, heat resistant steel, wasp-alloy, etc. These materials find wide applications in aerospace, nuclear engineering and other industries owing to their:

- high strength to weight ratio
- high hardness and
- high heat resisting quality.

However, machining of those materials is difficult and, in many cases, even impossible with conventional machining processes. The advanced machine tools such as Numerical Control/Computer Numerical Control/Direct Numerical Control/Machine Centres etc. are also found wanting in these cases as the machining processes would involve:

- thousands of slide movements
- high material removal rate and
- high speed of operations

For obtaining the 3D geometries of parts with required accuracy and precision [1]. The alternative is to develop advanced manufacturing processes in general and advanced machining processes in particular.

The non-conventional machining processes are introduced as a solution to machining complex shapes with surface integrity and miniaturization of products [2]. Taniguchi [3] mentioned in early days about the need for ultra-high precision machining for nano level accuracy tomorrow. Ultra precise holes required in miniature products are not possible with conventional machining process which leads to the need for micro level non-conventional machining process.

This chapter focusses on non-conventional micromachining processes. The contents of the chapter are: need for micro machining, non-conventional micro machining covering mechanical, thermal, chemical energy based processes and hybrid machining process. Various parameters controlling each process, mechanism of material removal and applications of the micro machining process are discussed.

2 Micro Machining Process

Micro-machining involves the removal of workpiece material in the form of chips or debris at micro/nano level having the size range 1–999 μm. The demand for products and components with dimensions in micrometer range emanated in early 1990s due to demands in electronic, medical and optical industries which needed components in micro-level with precision. The main challenge in micro-machining lies in the production of micro-tools and maintaining tool feed with respect to the workpiece. Micro parts that are produced by micro-machining are so small that they must be inspected using a microscope. Historically, the accuracy of machining improved from the normal machining to precision machining, then high precision machining and ultra-precision machining with an accuracy scale from 100 μm to a least value of 0.0003 μm [4].

2.1 Conventional Micro Machining Processes

In conventional machining processes, material from the workpiece is removed by mechanical force through plastic or brittle failure. The major drawbacks of this type of machining are the high machining force that can affect the dimensional accuracy

of the part due to micro tool and workpiece suffering consequent deformation. In traditional machining a harder tool cuts the workpiece to the desired dimensions and tolerance [5].

2.2 Need for Non-conventional Micro Machining

Micro-machining is carried out to create micro-features or surface characteristics in micro/nano level in macro or micro components. There will not be any constraint on the size of the component being machined and machining error is extremely small. The main challenge in micro-machining lies in the production of micro-tools and maintaining tool feed with respect to the workpiece. Micro parts that are produced by micro-machining are so small that they must be inspected using a microscope. Machining of these materials are time consuming and highly complex with conventional methods. The conventional machining processes with advanced machining techniques are thus unable to give economic production rate. Also attaining high aspect ratio features is still a challenging task on many occasions for producing complex features [6]. Non-conventional processes are therefore developed to overcome these difficulties in micromachining of components.

2.3 Classification of Non-conventional Micro Machining Processes

Micro-machining processes are classified based on the form of energy used in machining as mechanical, thermal and chemical methods [7]. Hybrid micromachining combines the different machining processes to achieve desired results. Various micro machining processes discussed in this chapter are:

1. Mechanical Micro machining
2. Thermal Micro Machining
3. Chemical Micro Machining
4. Hybrid Micro Machining.

Figure 1 is a schematic that shows the overall outline of non-conventional micro machining processes.

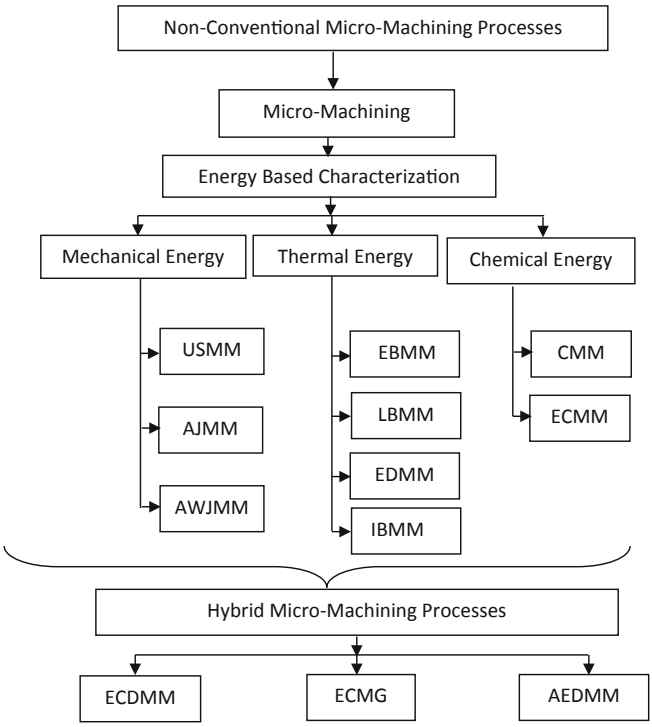

USMM	Ultra-Sonic Micro-Machining	ECMM	Electro Chemical Micro-Machining
AJMM	Abrasive Jet Micro-Machining	ECDMM	Electro Chemical Discharge Micro-Machining
AWJMM	Abrasive Water Jet Micro-Machining	ECMG	Electro Chemical Micro-Grinding
EBMM	Electron Beam Micro-Machining	AEDMM	Abrasive Electro-Discharge Micro-Machining
LBMM	Laser Beam Micro-Machining	CMM	Chemical Micro Milling
EDMM	Electro Discharge Micro-Machining	IBMM	Ion Beam Micro-Machining

Fig. 1 Classification of non-conventional machining processes

3 Mechanical Micro-machining Processes

In mechanical micro-machining processes, high velocity is imparted to a fine abrasive particle by the carrier fluid—air, water or other liquids. It hits the workpiece and removes the material in the form of micro/nano-chips. Material removal is through shear deformation in ductile workpiece and is brittle fracture in brittle workpiece.

The common mechanical micro-machining processes are:

- Ultra-Sonic Micro-Machining (USMM)
- Abrasive Jet Micro-Machining (AJMM) and
- Abrasive Water jet Micro Machining (AWJM).

3.1 Ultrasonic Micro Machining

Ultrasonic machining (USM) has been introduced as tool to machine square, irregular and complex shaped holes and surface impressions in electrically conductive and non-conductive materials [6]. Researches have reported that UMM can machine any fragile and hard materials. Machining with ultrasonic vibration in drilling and cutting is reported by R.W. Wood and A.L Loomis in 1927. The machining setup of USM was propped in 1942 by L. Balamuth. Many researchers have reported on various tool in USM and the first report on ultrasonic cutting appeared in 1953–54 [8, 9].

Ultrasonic micro machining (USMM) is used as an important process in precision engineering. High hardened materials like nickel alloys, titanium alloys and brittle materials like quartz, ceramics, and composites can be machined with micro USM process. Micro USM has found application in making micro holes in silicon of micro level hole size [10] to be used in IC boards. Micro USM has applications in electronic, mechanical and biomedical fields.

Ultrasonic vibrations are used as source for improving the micro machined surfaces in USMM. Irregular and random vibrations may result in low surface quality and accuracy. So controlled high frequency small amplitude vibrations are imparted to improve the machining processes. Such machining methods assisted by vibrations are termed as vibration assisted machining (VAM). In VAM precision machining is accompanied by small amplitude vibration between workpiece and tool which in turn will improve the machining by removing the debris faster from the machining zone. The major benefits from the VAM are improvement in machining performance in terms of better surface finishing, reduction in cutting forces, and reduction in tool wear leading to tool life extension.

Machining Method

In micro USM process high frequency vibration or linear motion are produced in ultrasonic range (above 20 kHz) with the help of piezoelectric or magnetostrictive transducer as shown in Fig. 2. The linear motion is produced from a high frequency signal which is obtained through conversion of low frequency signal. The transducer is attached to a tool holder and tool or to a sonicated chamber which in turn will vibrate in the ultrasonic range. This will provide greater accuracy to the machining process with constant waves of higher amplitude. The gap between the tool and work piece is kept to the minimum.

The gap between the tool and the workpiece is filled with abrasive slurry having loose fine particles of silicon carbide, diamond, alumina, etc. suspended in oils or

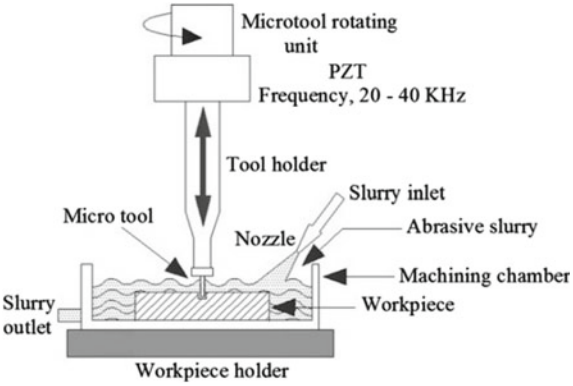

Fig. 2 Ultrasonic Micro Machining [6]

water. The micro tool is given a cyclic and ultrasonic linear vibration which in turn moves the abrasive particles towards the work piece. This abrasive action will remove the microchips from the workpiece surface. The tool moves on the work piece in a predetermined path to produce the defined features.

Applications

USM has wide application in 3 D Printing industries [11]. The micro features are produced by the micro tool which is fed to the work piece resulting in reduced machining time. Products having high aspect ratio are produced by researchers in PZT [12] the tool path being controlled with CAD/CAM [13]. Also micro tools can machine and polish steel surfaces effectively [14] including cutting micro channels for bio medical application.

3.2 Abrasive Jet Micro Machining

Abrasive Jet Machining (AJM) is an effective tool for machining hard brittle materials with high intensity flow of abrasive particles. The size of abrasives decides the accuracy of the process and fine abrasives are used for finishing operations. Effect of various abrasive hard particles on the surface of the machined work piece was studied by M. Wakuda et al. [15]. They reported that the harder particles increase the degree of fragmentation on workpiece.

AJM finish is basically carried out with a blast. The basic difference from conventional machining technique is that it features a precision jet nozzle of less than 1 mm in diameter, through which a controlled mass of fine, hard abrasive particles is continuously directed at the workpiece surface. As a consequence, AJM can meet the requirement for patterning of highly controlled micro-dimples onto the surface of difficult-to-machine materials [16].

Abrasive jet bombarding is one of the versatile materials processing techniques and is applied in abrasive jet machining, deburring, shot-peening, erosion testing, fast cleaning, surface preparation and polishing. Some special types of operations like micro-machining, polishing of micro-channels are the current issues in research and development [17].

The impact of AJM in the form of mixture of dust and smoke was reported initially in Germany in 1931 [18]. A high intense stream of gas or air with suspended abrasive particles can be taken for machining, cleaning, micromachining etc. through material erosion. The micro fracturing [19] of the workpiece occur due to high kinetic energy of abrasive particles [20] striking on surface of the workpiece.

Machining Technique

In AJM material is removed from the work piece with the kinetic energy of loose abrasives. The commonly used medium is air. Abrasive mixture is directed through a nozzle to the work piece. The tip of nozzle should be kept with a small gap from the work piece. The distance between nozzle and workpiece, diameter of nozzle, and angle of impact influence the machining process. The abrasives are propelled at high velocity, through the nozzle and strikes the work piece producing high impact forces. As the jet strikes the surface micro plastic deformation happens on the workpiece, and the material gets eroded by chipping action. The brittle broken particles getting separated on the surface of the workpiece are taken away by the carrier gas. In AJM material is removed by virtue of impact of high velocity air or gas stream of abrasive particles [21]. The AJM arrangement consists of an air compression system and machining chamber. The compressor is used to supply clean dry compressed air, with metering system to measure the air pressure. The machining chamber consists of a vibrator with a mixing chamber, nozzle and work holding devices as shown in Fig. 3. The nozzle is made from alloys of wear resistant steels. Silicon carbides, ceramic particles, diamond particles are used as abrasives.

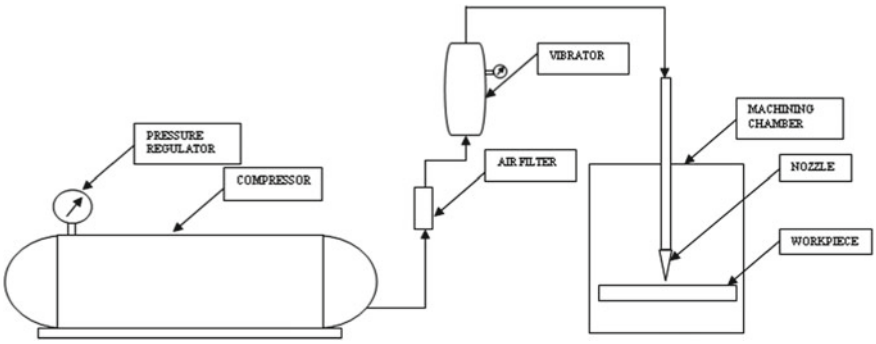

Fig. 3 Schematic layout of abrasive jet machine

Applications

The AJM finds process application in cleaning, etching, cutting, deburring and polishing of ceramic materials which are brittle in nature [22] and it is much cheaper than traditional wet etching processes. Micro fabrication of channels and holes on PMM areas are also carried out with AJM [23, 24]. AJM is an effective tool in the manufacture of microelectronic and optoelectronic devices, and 3D structures in glass [25–27].

3.3 Abrasive Water Jet Micro Machining

In abrasive water jet micro machining material removal is accomplished by eroding away the materials by either the high-speed water from a water-only-nozzle (for relatively soft materials) or the abrasives (for hard materials) that are accelerated by the high-speed waterjet (WJ) through the mixing tube. Such a mode of material removal differs from other machine tools [28]. Even for an extremely precise part, waterjet can be advantageously used as the near-net shaping tool. The net-shaped part can then be precisely trimmed with qualified tools. The operational life of these tools is greatly extended since the bulk of the material is removed by the waterjet.

AWJM process is introduced as process with no heat affected zone [29] and material independent [30]. Miller [31] has reported those abrasive particles in the range of 300 and 50 nm when passed through nozzle of 40 mm diameter, micro features of higher accuracies are obtained. Water Jet Machining (WJM) has transformed the micro machining industry to a great extent with respect to intricate features produced. Waterjet machining is comparable with most of the high end micro machining technologies like EDM, ECM and far better in terms of machining speed, low HAZ, flexibility of integrating with other processes, setup simplicity and material independence [32]. WJM has been selected as a major tool for producing net shaped products [33]. Especially for materials which are very difficult to machine with conventional machining process, WJM has proved to be an effective tool for bulk material removal. As the tool is non-contact in terms of water being used as machining source, operating life of tool is significantly high.

The AWJM process has application in machining difficult to cut materials and has shown better results with precise control. Multiple pass machining is preferred with higher scan speed. Surface finish is found to improve with multi-pass process [30]. Researchers have shown that AWJM can be an alternative tool in machining ceramics and titanium based alloys with higher surface finish in shorter time.

Mechanism of Material Removal

WJM removes material using the kinetic energy of high velocity water as shown in Fig. 4.

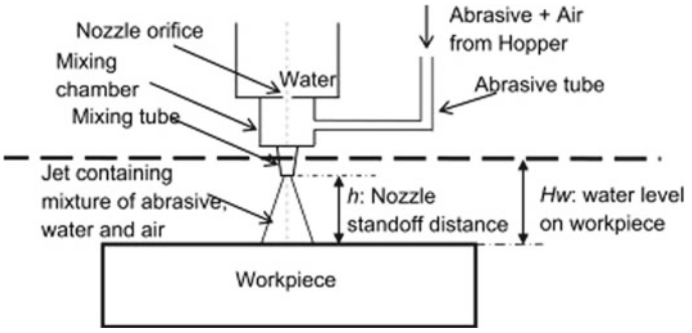

Fig. 4 Schematic sketch of AWJM process [34]

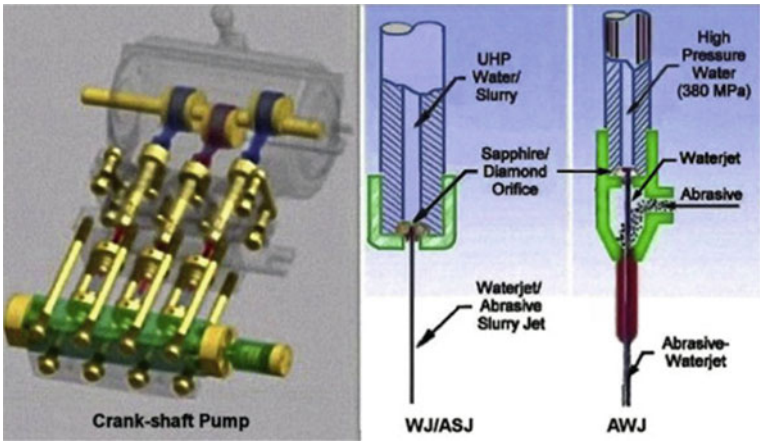

Fig. 5 Nozzle arrangement for water jet and abrasive water jet machining [30]

In this process pressure energy is generated though impact of high velocity water jet which strikes the workpiece surface. A threefold pressure increase at static pressure is obtained in water jet [30].

In AWJM process an ultra-high pressure is maintained with high pressure pump and water passes through a small orifice. In order to form abrasive waterjet, abrasives are passed into the jet of water through a feed port from the abrasive storage tank. The abrasives are uniformly . Figure 5 shows a direct-drive crankshaft pump and nozzle configurations for forming UHP WJ/ASJ and AWJ. The diameter ratio of the orifice and the mixing chamber typically ranges from 1:2 to 1:3. The Nozzle used is the same as that of waterjet machining.

Applications

Water jet Machining is highly ecofriendly and economical for machining of porous and soft materials with precise surface finish and straightness. Porous materials include woods, corrugated boards and soft materials include lead, rubber etc. Other applications of AWJM includes rock excavation [35], micro-feature cutting on sand stones, machining of fibers for automobile, chemical industries, descaling and cleaning in oil industries.

4 Thermal Micro-machining Processes

In thermal micro-machining processes, controlled localized intense heat is applied on the work piece which increases temperature in a narrow zone, equal to work piece melting/vaporization temperature. As a result, the material is removed at micro/nano level in the form of debris-irregular shaped particles or spherical globules [36]. Thermal micro-machining processes include:

- Laser Beam Micro-Machining (LBMM)
- Electro Discharge Micro-Machining (EDMM).

4.1 Laser Beam Micro Machining

LBM process has been introduced since 1970 as a tool for drilling cost effective and reliable features in difficult to machine materials at higher speeds for large scale production [37]. Multiple laser pulses has been used to produce defined holes by Tam et al. [38] and Yeo et al. [39]. Tam et al. (1990) [38] has also reported deep hole of diameter 0.25 to 1.0 mm with aspect ratio more than 10:1. A study on machining of brittle materials has been reported by Ueda et al. [40] and Spur et al. [41] with respect to temperature on workpiece surface irradiated with a CO_2 pulsed laser.

The advantages of micro laser beam machining include high flexibility, high precision and high level automation compared to conventional machining processes. Laser micro machining has become an integral part of fabrication industry especially in welding of micro components with high accuracy and finishing of micro features on various materials like ceramics, metals and polymers. Most of these products are used in medical industry, automobile sectors, nuclear industries etc. They are widely used in the fabrication of solar cells and semiconductor industries. Micro laser beam machining process uses laser beams with pulse duration in the range of femto-second to micro second for fabricating complex parts of high aspect ratio. The frequency of beams ranges from single to megahertz range which provides sufficient heat energy for melting and vaporizing the workpiece material. Micro LBM has been used as precise tool in micro manufacturing industries which includes drilling, cutting, welding

etc. The material removal involves quick heating followed by melting and evaporation. The Heat Affected Zone (HAZ) is found to be lowest as burr formation is very less in Micro LBM process.

Mechanism of Material Removal

In Micro LBM material is removed by thermal ablation [42]. CNC machine tools are used for controlling and positioning the work piece with respect to the focal point of the laser beam as shown in Fig. 6. Controller can also modulate the laser pulses during the machining. Machining is monitored through camera and focused beam power is adjusted with power monitor.

The laser beam generates heat by absorption when it falls on the work piece. The higher the penetration depth, higher the absorptivity which is dependent on the optical properties of the material. When laser falls on the metal, light excites the free electrons on workpiece depending upon photonic energy of the beam which in turn increases the electron vibration energy. The excited electron collides with nearby electrons and knocks them out. The electrons which are knocked out repeat the procedure resulting in temperature rise on the workpiece. If the workpiece absorptivity is high, extreme rise in temperature causes melting and vaporization of the workpiece resulting in thermal ablation. When absorptivity is low, temperature rise will be lower than melting point of the workpiece and there will not be any material removal.

Applications

LBM is widely used in machining and micro structuring of silcon and glass wafers [43, 44], and optical materials like Gallium and lithium-niobate. Also LBM gives accurate miniature sized features for lab on chip products, micro circuit boards with polymers, also in nano level applications with infrared sensors and detectors [45].

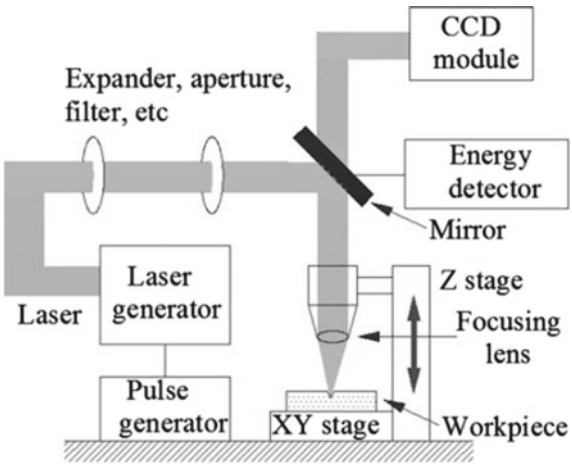

Fig. 6 Schematic sketch of LBM [6]

Micro LBM also has shown application in biomedical devices like stents fabrication, micro level holes in probes used for monitoring infected parts in the body [46] etc.

4.2 Electric Discharge Micro Machining

Kuneida and Yoshida [47] in 1997 proposed the machining with gas media (dry EDM). They have reported that molten materials were ejected from the workpiece under a gas jet under higher pressure. The benefits of EDM under jetting and intake modes of gas are considered in the study [48] and have found better result in intake modes.

The EDM process involves a controlled erosion of electrically conductive materials by the initiation of rapid and repetitive spark discharge between the electrode tool and work piece separated by a small gap of about 0.01–0.50 mm known as spark gap. The spark gap is either flooded or immersed under the dielectric fluid. The spark discharge is produced by the controlled pulsing of direct current between the workpiece and tool. Micro EDM and EDM are similar in principles, but the difference occurs in terms of the energy range and tool which is lower. In Electro discharge micromachining movements in micron are obtained through micro energy dissipation. Micro EDM is found to be an effective tool in machining extremely hard materials like hard tungsten carbide and alloys of steel. Figure 7 shows experimental setup of the EDM machining process.

Mechanism of Material Removal

Micro EDM is a thermoelectric process in which material removal takes place by melting through controlled discharge or sparks between the tool cathode and anode workpiece, which are maintained at a small gap filled with dielectric material [49]. The dielectric fluid in the spark gap is ionized under the pulsed application of the direct current, thus enabling a spark discharge to pass between the tool and the workpiece. As the tool moves towards the workpiece, the gap in which dielectric is

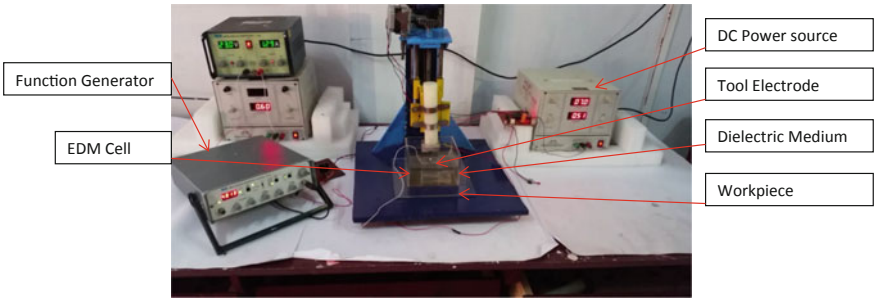

Fig. 7 Micro EDM experimental setup

kept becomes narrow and get transformed into the plasma stage. The high temperature developed by the plasma stage melts the workpiece and is flushed away from the machining zone by the continuous circulation of dielectric. The process is repeated with plasma formation and workpiece get transformed into the contour of the tool cathode.

Applications

Micro EDM has been used as an effective process in fabricating micro electrodes, gear patterns with Tungsten Carbide [50, 51], micro compressor, micro turbine impellers [52–54], high aspect ratio micro arrays, biocompatible devices from Magnesium, nano particle production etc. [55–58].

5 Chemical Micro-machining Processes

Machining by micro chemical process is adopted for different machining and finishing operations of components required by aerospace, automobile and such other industries [59]. There are two processes:

- Chemical Micro-Milling (CMM)
- Electro Chemical Micro-Machining (ECMM).

In chemical micro machining processes, chemical are used for etching away the workpiece resulting in material removal. In these processes the material removal takes place either by chemical dissolution under the presence of a strong reagent (Chemical Milling Process) or workpiece is kept as anode thereby dissolving the same under a DC power supply. (Electro Chemical Machining).

5.1 Chemical Micro Milling Process

Chemical milling (CHM) involves Chemical Dissolution (CD) in a controlled manner on a workpiece material through contact with a strong reagent. Masks are applied on areas to be protected from the chemical in the workpiece. The process is mainly used to make pockets and contours as well as removal of material having higher strength to weight ratio.

Material Removal Mechanism

The major steps in CHM consist of the following steps:

1. Pre cleaning of the workpiece surface in order to get good adhesion of the mask on workpiece surface.
2. Masks are selected so that they are chemically non-reactive and can overcome the chemical abrasion during the machining processes.
3. The mask selection is based on workpiece size, manufacturing volume and intricacies of the shape required.
4. Etching and rinsing is done to clean up. Finishing is done after removal of the mask.
5. The time of immersion in the chemical is controlled in order to avoid uneven machining.

The material removal or etch rate of the process depends on workpiece metallurgical and chemical properties and temperature of solution. Harder the materials higher the etching rate and viz verza [60]. Surface roughness get lowered with higher etch rate.

Applications

Most of the metals like zinc, copper, aluminium, steel and nickel can be machined with this process. Also it is possible to machine most of the exotic metals and non-metals with this process. CHM applications range from aeroplane wings to micro-chips. Depth of cut in the range of 2.54–12.27 mm are possible, Shallow cuts on sheet metal is a major application of CHM process for weight reduction in aircrafts.

5.2 Electro Chemical Micro Machining

The ECM principle has been discovered by Michael Faraday (1791–1867) in the nineteenth century. Faradays laws of electrolysis have been the guiding principle for electro deposition and electro dissolution techniques. A process to machine using electrolysis has been reported in 1927 by Russian researcher W. Gussef. In 1950s tremendous progress has been reported in ECM process as tool for machining high strength alloys. An anodic metal machining process has been introduced in 1959 by Anocut Engineering, Chicago. The ECM process has been widely used as effective tool to machine difficult to machine materials for gas turbine and aerospace industries in 1960s and 1970s [61].

Electrochemical Micromachining is a frontrunner in fabrication industries for producing macro and micro products with highest quality in terms of surface finish. Most of the advanced areas in automotive, aerospace, electronics, optics, medical fields find wide application of ECM in machining titanium alloys, super alloys and steel alloys which are very difficult to machine with conventional machining processes. The ECM process can produce complex geometries with no thermal damages, tool wear and burr formation regardless of the hardness and other mechanical properties

of the metals [62]. Material removal is at atomic level which makes the products to have very high surface finish.

Applications of Electro Chemical Machining (ECM) in micro fabrication and processing thin films are referred to as Electro Chemical Micro-Machining (ECMM). A variety of metals and alloys including conducting ceramics and highly corrosion-resistant alloys, can be machined using ECMM. Most of the thin films of metals and alloys that are of interest in the microelectronic industries can be anodically dissolved (machined) in neutral salt electrolytes (such as sodium nitrate, sulphate, or chloride) and ECM is commonly used for their machining.

In ECM the workpiece is made as an anode and tool is made as a cathode in an electrolytic cell. A non-toxic salt solution is used as an electrolyte and controlled metal removal from the anode takes place when the current—smooth DC or pulse DC—flows through the electrolytic cell. Pulsed DC offers many advantages as compared to smooth DC. The application of Electro Chemical Machining (ECM) in micro-fabrication and processing thin films is referred to as Electro Chemical Micro-Machining (ECMM) and is a slow micro machining process.

Mechanism of Material Removal

In Electro Chemical Micromachining (ECMM) for electrical dissolution the workpiece is the anode and micro tool the cathode, both immersed in electrolyte with a small inter-electrode gap (IEG). IEG determines the overall precision and accuracy of ECMM process as smaller the IEG better the accuracy and micro feature resolution. Two types of electrolytes are preferred in ECMM—passivating type with oxidizing anions which give better dimensional accuracy and non-passivating with aggressive anions [60]. Also various types of acid electrolyte are also preferred for special cases in ECMM process which reduces the insoluble byproducts in the process. In ECMM electrolyte is kept static during the machining to prevent any vibration of the micro tool. The schematic sketch of micro ECM setup is given in Fig. 8.

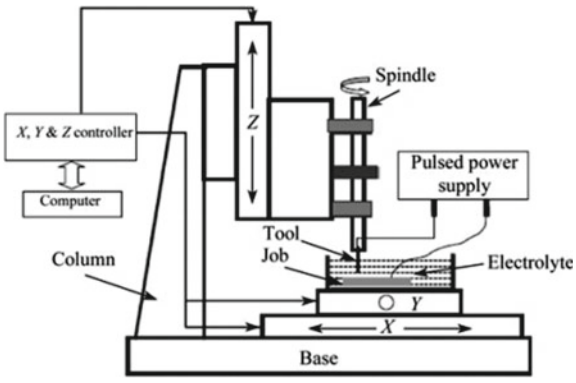

Fig. 8 Schematic sketch of micro ECM setup [62]

The CNC setup is used to control X–Y motion of the workpiece and Z axis motion of rotating tool. For getting a high current density in the order of 75–100 A/cm^2 with high mass density flow, IEG is kept in the range of 5–20 lm, and a low voltage of 1–10 V with ultra-short D.C pulse current is maintained [63]. This will effectively remove the materials from the workpiece. During the machining the micro tool is fed towards the workpiece with constant IEG. The process continues with production of mirror image of the tool on the workpiece with anodic dissolution through electro chemical dissolution.

Micro Engineering Applications

ECMM has demonstrated its effectiveness for producing micro features with excellent surface quality in various industries like optoelectronics, electronics, medical, optics, biomedical, and aerospace [64]. Examples of micro component fabrication in MEMS are: inkjet printer head parts [65], 3D micro components of intricate and complex features, micro components with silicon [66] and composite materials [67].

6 Hybrid Micro-machining Processes

Hybrid Micro-Machining Processes (HMMP) are introduced to perform ultra-precision machining in high hard materials in which machining is almost difficult [61]. Also hybrid machining provides complicated profile with high precision with improved surface quality. The productivity in hybrid machined is higher than that of the individual processes. Moreover in HMMP both mixed type and assisted type processes are commonly used.

As the applications of micro-machining of advanced engineering material expanded, HMMP came to be introduced through the combination of the above mentioned processes thereby obtaining the advantages of more than one process. Hybrid micromachining processes are developed by combining the principles of two or more processes which in turn improves the advantages of basic processes and reduces its limitations [68]. Drilling process is improved by attaching ultrasonic vibration during machining processes [69]. The hybrid machining process overcomes the limitations of individual processes from which they are developed to meet the specific demands on machining intricate and complicated parts.

Examples are Electro Chemical Discharge Micro Machining (ECDMM), Electro Discharge Micro-Grinding (EDMG) and Abrasive Electro discharge Micro-Machining (AEDMM) processes. ECDMM or Micro-ECDM is a novel hybrid machining process used for machining conducting and non-conducting engineering materials.

6.1 Electrochemical Grinding (ECG)

In ECG the process is mainly controlled by various process parameters which include voltage applied, current density, electrolyte concentration with type of delivery and type, pressure, speed and kinematic precision of the grinding wheel [70]. The ECG offers accurate machining on large surface free of residual stresses and heat affected zone (HAZ). Electrochemical grinding (ECG) is a hybrid micro machining process in which mechanical grinding is carried out in the presence of an electrolyte so that material removal take place due to combined actions of mechanical abrasive forces and electrochemical etching process. The workpiece surface obtained is reported to be good quality as it is free of burr and stresses [71, 72]. The ECG process avoids further surface finishing as no deburring is required and it overcomes the limitations caused by ECM and grinding processes.

Mechanism of Material Removal

In ECG process, the grinding wheel is kept as the cathode and workpiece is kept as the anode as shown in Fig. 9. The workpiece which is conducting is usually connected to positive DC supply and grinding wheel having carbon brush embedded with gripping action of electrolytic commutator spindle is connected to the negative DC supply. The metallic grinding wheel is filled with insulating diamond abrasive particles. During the machining process the gap between the workpiece and grinding wheel is filled with electrolyte. The grinding wheel rotation provides electrolyte at the machining area which is supplied through a nozzle [70].

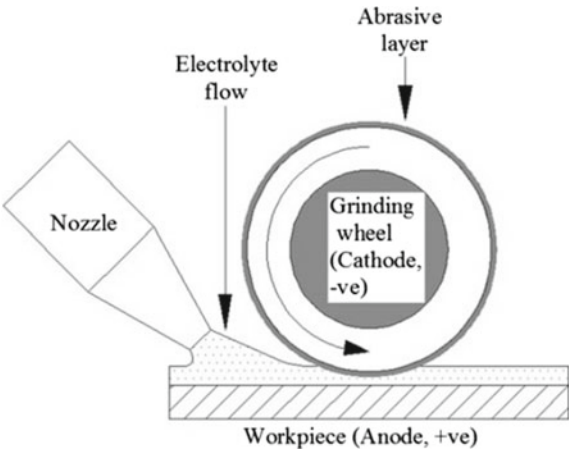

Fig. 9 Schematic setup of ECG [6] (Permission in File 1)

Applications

The ECG process is effectively applied for

1. Machining of high hardness materials, some examples being sintered carbides, creep-resisting (Inconel, Nimonic) alloys, titanium alloys, and metallic composites
2. Tool room machining requirement
3. Machining thin and fragile components.

6.2 Electrochemical Discharge Machining

Electro Chemical Discharge Machining (ECDM) is developed as a hybrid machining process to machine electrically non-conducting and conducting materials effectively and efficiently. The material removal is mainly carried out with melting and vaporisation under thermal energy of sparks generated from tool electrode and partially by chemical etching under the presence of an electrolyte. In this process basic principles of EDM and ECM are combined to overcome the limitations of each individual process. The EDM and ECM can machine only conducting materials whereas ECDM can machine both conducting and non-conducting materials effectively and efficiently. An auxiliary electrode is used in ECDM process to complete the electrical circuit while machining non-conducting materials and details are explained in coming paragraphs. Commonly machined materials in ECDM include ceramic, composites, semi conducting materials like silicon to a high level of accuracy. The electro chemical discharge occurs between the tool electrode and auxiliary electrode of grossly different dimensions when immersed in an aqueous electrolyte solution.

Basic Elements and Principles

Figure 10 shows the basic elements of ECDM cell. The cell consists of the following major components:

1. Beaker—to hold the required quantity of electrolyte
2. Electrolyte—aqueous solution of KOH or NaOH or NaCl or HCl
3. Tool Electrode—any of the conducting materials- copper, stainless steel, tungsten, tungsten-copper alloy
4. Auxiliary Electrode—Zinc (Zn), Cu, Graphite, Stainless Steel
5. Tool Feeding Mechanism
6. Work Holding Device
7. Workpiece Materials- Composites, Acrylics, glass, silicon wafer
8. DC Power Supply.

The experiment is conducted for a particular combination machining parameters such as: 30% wt NaOH electrolyte, glass workpiece, stainless steel as tool electrode (0.5 mm^2 diameter) and stainless steel cylinder (1400 mm^2 diameter) as auxiliary electrode at a temperature of 298 K.

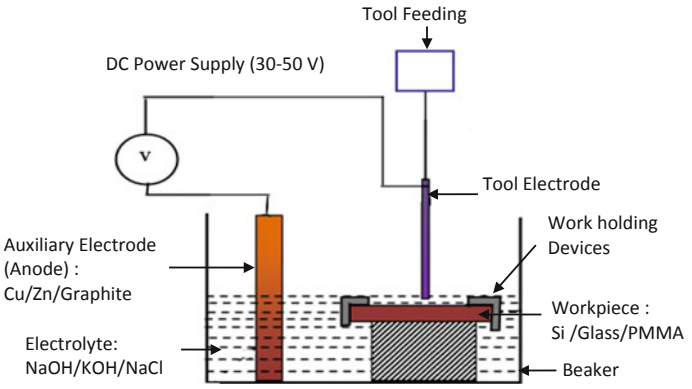

Fig. 10 Basic elements of ECDM cell [73]

When the applied voltage is below a critical voltage of about 25 V, electrolysis occurs with hydrogen bubbles forming at the tool-electrode and oxygen bubbles forming at the auxiliary electrode. As voltage is increased beyond the critical voltage, current density also increases rapidly. The density and the mean radius of the bubbles increase and bubbles finally coalesce into a gas film around the tool-electrode. Light emission is observed in the gas film where an electrical discharge occurs between the tool electrode and the surrounding electrolyte. Figure 11 shows the Voltage-Current characteristics of ECDM Process. It consists of five different regions of formation of the gas film [74].

1. Thermodynamic Region	(0–1.3 V)	O-A
2. Over Potential Region	(1.3–2 V)	
3. Ohmic Region	(2–10 V)	A-B
4. Limiting Current Region	(10–20 V)	B-C
5. Instability and the Arc Region	(Above 21 V)	C-D-E

The explanations of these regions are elaborated below. Referring to Fig. 11: the region 1 is called thermodynamic region (0–1.3 V), in which there is no current flow in the cell. In the region 2, the over potential region with voltage range 1.3–2 V, current flow increases gradually with applied potential which is mainly due to high over potential of hydrogen at the tool electrode. In the region 3, the Ohmic region having voltage range 2–10 V, current and voltage show linear relation as they increase proportionately. This is mainly due to ohmic resistance formed due to formation of hydrogen. Further increase in voltage at the electrodes in region 4, limiting current region, from 10 to 20 V, current flow stops, as bubbles formed at the cathode starts to merge to form a film. In this domain the rate of hydrogen evolution on the tool electrode is controlled by the releasing rate of hydrogen bubbles from the tool electrode towards the atmosphere. In region 5, the instability and arc region, voltage is

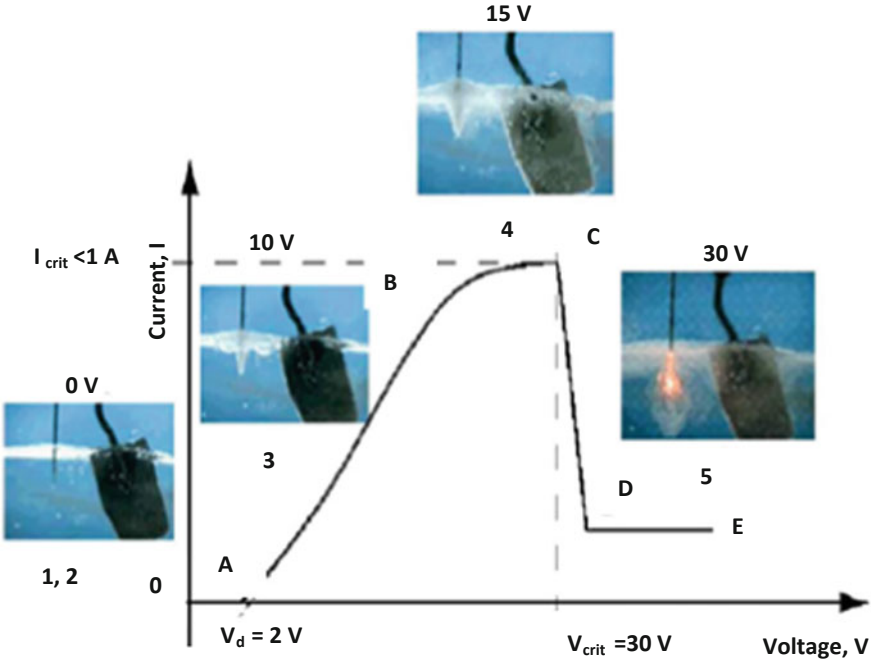

Fig. 11 Voltage-current characteristics of ECDM process [74]

kept above 21 V and current starts fluctuating. Current flow decreases due to the fluctuation due to bubble detachment at the tool electrode. It is assumed that above 21 V, due to ohmic heating temperature near the tool electrode reaches the boiling point of the electrolyte resulting in generation of water vapour bubbles. This bubble covers the entire exposed regions of the tool electrode resulting in isolation of tool from the electrolyte. Once bubbles leave the tool electrode the contact between the tool and electrolyte resumes and cycle gets repeated. This electrical switching is similar to electrical induction resulting in spark formation. Also coalescence of the water vapour with evolved hydrogen occurs in this region. The last region is termed as the working domain of the ECDM process and sparking occurs only in this region on current/voltage plots.

Mechanism of Material Removal

The mechanism of material removal in ECDM is thermal spark erosion and chemical etching. In thermal spark erosion the workpiece is heated by fraction of spark energy which raises the local spot temperature to a very high value sufficient for melting and may even vaporize the work piece material. Hence, correct estimation of energy per spark is crucial for better MRR. Several experimental evidences confirm the thermal mechanism of machining due to the thermal cracks inside the machined materials. But the experimental observations also show the MRR is due to chemical

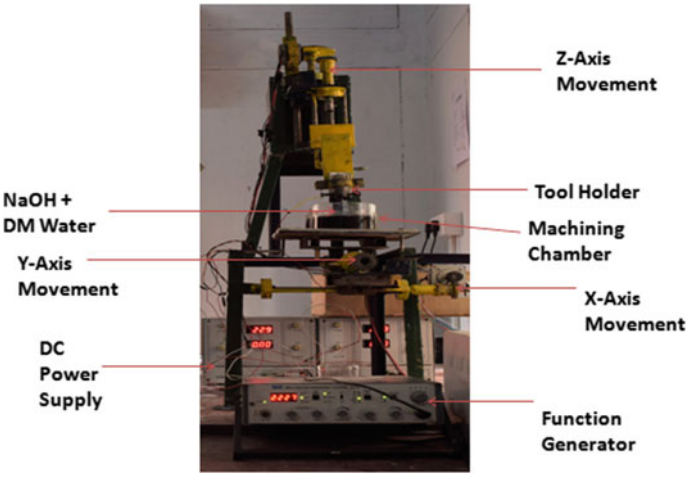

Fig. 12 ECDM experimental setup

etching. Chemical machining mechanism is supported by the fact that the machining performance depends on the type of electrolyte used. The experiments also reveal that maximum MRR takes place due to thermal erosion and very little material is etched away due to chemical etching. An experimental setup of ECDM is shown in Fig. 12.

Applications

ECDM process is found to be a good machining method for drilling of glass substrates stainless steel materials, composites and ceramics. Fabrication of intricate micro features [75], making precise dies [76] deep hole drilling [77, 78], dressing of micro tools in grinding [79, 80] etc. are done with ECDM. Also the machining performance has been shown improved the mixed electrolyte [81, 82]. The analysis of the process is carried out with finite element analysis and Response surface modeling which are in good agreement with experimental results [83, 84]. The Micro ECDM process has demonstrated application in drilling micro channels and hole which has application in fluidics [85, 86].

6.3 Abrasive Assisted Micromachining (AAMMP Process)

AAMM is a hybrid process where abrasive particles are used for assisting the micro machining process. The abrasion of small particles assist the normal machining process especially where micro channels and micro holes are produced. These micro features so produced have applications in optoelectronic devices and fluidic applications

[87–89]. One important AAMM processes is Abrasive Assisted EDM (AAEDM) machining.

Abrasive Assisted EDM (AAEDM) has been introduced as a hybrid process in which abrasive particles in dielectric are passed through the inter electrode gaps. The importance of AAEDM has been studied by Lin et al. [90] through a combination of abrasive jet machining (AJM) with EDM. They has used a hollow electrode through which abrasive particles mixed with compressed air are passed through the inter electrode gaps.

6.3.1 Powder Mixed Electro-chemical Discharge Machining Process (PM-ECDM)

In PM-ECDM the electrolyte is added with graphite powder which being conductive, reduces the micro cracks on the machined surface. Singh and Dvivedi [91] reported that conductive powder dampens the impact of spark on workpiece resulting in a smooth surface. The extend of damping is influenced by the behavior of graphite particles in the electrode workpiece gap. Han et al. [92] described two types of powder behavior (1) stable discharge due to conductive particles at the tool electrode intensifying the electric field and (2) constant transfer of charge due to dynamic movement of particles by electrostatic force. They found that when 10 μm diameter graphite powder particles are mixed with sodium hydroxide solution electrolyte, the surface finish of the borosilicate glass improved from 4.86 to 1.44 μm. Goud et al. [93] observed that improvement in surface finish with PM-ECDM was achieved by the reinforcement of surface cracks and heat erosion. They found that smaller grit size resulted in lower roughness.

Applications

The PM-ECDM finds application for machining large areas in ceramic parts. This process is advantages for finishing intricate shapes because of its ability for crack free machining.

6.4 Ultrasonic Assisted Micromachining

Ultrasonic assisted micromachining is another advanced micro machining process in which high frequency vibration in ultrasonic range is used for improving the existing machining process to obtain better quality products. They are mainly used for machining ceramic and composite that are brittle with enhanced productivity. Ultrasonic assisted EDM is an example of such processes.

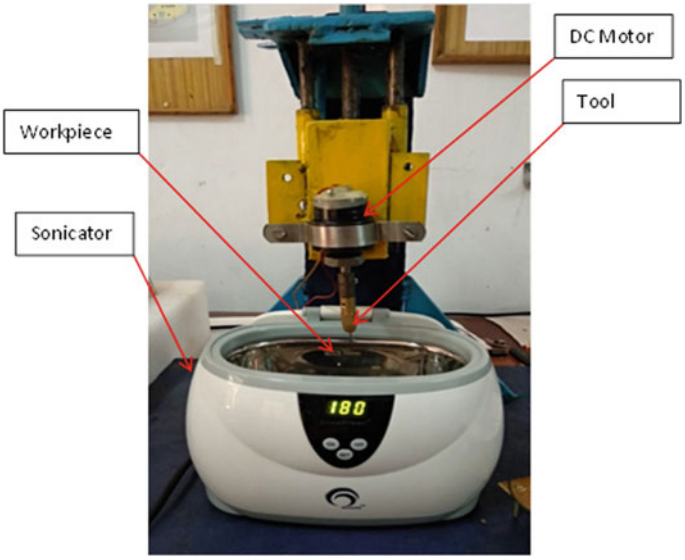

Fig. 13 EDM setup with ultrasonic vibrator

6.4.1 Ultrasonic Assisted EDM

The arrangement for vibrating the workpiece at ultrasonic frequency is shown in Fig. 13. The ultrasonic vibration is introduced in the dielectric medium with the help of a sonicator. The workpiece and the tool are kept immersed in de-ionized water. Debris removal is continuous with flow of abrasive slurry [94].

Mechanism of Material Removal

Sonication is an act of applying sound energy to agitate particles in a sample for various purposes. Ultrasonic frequencies greater than 20 kHz are used. A typical sonicator has an ultrasonic frequency of vibration at around 42 kHz. It has a digital LED display with a timer. The default timer setting is for 180 s. It has an overheat protection system embedded in it, thereby limiting the timer to 180 s in a single cycle. The operation is quiet. It has an insulating outer plastic body to prevent electric shocks. The inside of the sonicator has a stainless steel tank. The LED display has 3 control switches ON, OFF and SET buttons. High material removal rate is obtained during the machining of work piece assisted with ultrasonic vibrations. Micro holes are clearer and have better shapes because of the increase in material removal rates [95].

In ultrasonic assisted EDM, material removal rate and flushing of debris are enhanced with cavitation and acoustic waves produced, especially for micro drilling of slots and microgrooves. The craters are kept clean by slurry circulation which in turn increases the material removal rate and surface quality of the products.

Applications

The UAEDM has found to reduce the defects like burr formation, surface irregularities produced in normal EDM to a greater extent. It is used in precision machining of gears and intricate structures used in space applications.

Importance of Micromachining Processes

Miniaturization of the products and processes is no more a fashion rather it is the need of the time, because one can derive multifarious benefits from such products and processes. Micro-machining plays a major role in miniaturization of products and processes. Each of these processes has its own benefits and limitations and cannot substitute another. These processes are used to produce intricate profiles on various engineering materials with high accuracy without any subsequent processing steps, thus improving productivity. High aspect ratios of 100:1 which are not met easily in conventional processes are attained in non-conventional machining processes. All these have resulted in the steady growth in non-conventional micro machining processes with promising results. Presently the non-conventional machining processes have better capabilities over conventional processes in terms of machining harder materials, compactness, reducing cost of machining, etc.

Most of these micromachining processes are controlled automatically thereby achieving simplicity, reliability and repeatability, resulting in wider acceptance of the processes. Many of these processes are automated with vision systems, laser gauges and other inspections systems. Also these systems have the capability to adjust the various process parameters in order to improve machining quality and production rate. Due to these reasons, non-conventional machining processes are getting wider acceptance among manufacturing engineers, product designers and metallurgical engineers.

Though non-conventional machining processes are not replacing conventional machining processes, their relevance lies in the reliability of the processes and high quality of the products. The non-conventional machining processes can machine metals and alloys irrespective of their material properties. The workpiece shape and size to be produced influence the application of the machining process. Some examples of components machined by non-conventional micromachining processes are given in Table 1 to illustrate their capabilities and wide application range.

Table 1 Components manufactured with non-conventional micromachining processes

S. no.	Micromachining process	Component material	Component feature machined	Component application
1	Ultrasonic micro machining	Silicon, quartz	Micro holes, Micro channels	Fabricating micro tool, delivering liquids/gas, micro heat exchanger
2	Abrasive jet micro machining	Glass	De-burring, drilling	Cutting of optical fibers, optical lenses
3	Abrasive waterjet micro machining	Aluminum 6061-T6, 316L stainless steel	Micro channels	Lab-on-chip devices, microchip electronic cooling systems, biomedical micro-devices
4	Laser beam micro machining	Silicon wafers, thin glass sheet	Micro-texturing, machining	Microcircuit boards. Lab on chip
5	Electric discharge micro machining	Nickel-titanium alloy, WC–Co alloy (conductive materials)	Micro-slots, high aspect ratio micro-holes	Micro-forceps, gear profile
6	Chemical micro milling	Copper, aluminum and its alloys, lead, steel, titanium, nickel, ceramics, glass, plastic	Contours, pockets, depression	Minimizing thickness of walls, ribs, webs of components
7	Electro chemical micro machining	Silicon, nickel (conductive materials)	Single, arrays of micro grooves, holes and slots	Micro components for MEMS, micro nozzles, plate for ink-jet printer head
8	Electro chemical grinding	Stainless steel, aluminum, Hastelloy, Inconel	Sharp burr free edges	Burr-free sharpening of hypodermic needles, grinding of super-alloy turbine blades
9	Electro chemical discharge machining	Ceramics and glass	Drilling of micro holes and slots	Lab-on-chip devices, electronic cooling systems, 3D micro-structures

(continued)

Table 1 (continued)

S. no.	Micromachining process	Component material	Component feature machined	Component application
10	Powder mixed micro electro chemical discharge machining	Glass, silicon	Drilling of micro holes and slots	Micro device cooling application
11	Ultrasonic assisted electro discharge micro machining	Copper, stainless steel	Drilling of micro holes and slots	Mirror finishing in optical lenses

7 Conclusions

Micro-machining processes are classified based on the form of energy used in machining as mechanical, thermal and chemical methods. These processes are used to form intricate shapes and micrometer sized features on components that go into the present day electronic and electro-mechanical devices. Their capability to machine very hard and lightweight materials to high accuracy led to their wide adoption in modern industry. The limitations of many of these processes are overcome with hybrid micromachining processes in which basic principles of non-conventional machining processes are combined with micromachining processes. These form an emerging field of micromachining.

References

1. Jain VK (2009) Magnetic field assisted abrasive based micro-/nano-finishing. J Mater Process Technol 209(20):6022–6038
2. Snoeys R, Staelens F, Dekeyser W (1986) Current trends in non-conventional material removal processes. Ann CIRP 35(2)
3. Taniguchi N (1983) Current status in, and future trends of ultraprecision machining and ultrafine materials processing. Ann CIRP 32(2):573–582
4. Ashby MF (2010) Materials selection in mechanical design. Elsevier, USA
5. Hofy HE (2005) Advanced machining processes non-traditional and hybrid machining processes. McGraw-Hill, New York
6. Kibria G, Bhattacharyya B, Davim JP (2017) Non-traditional micromachining processes fundamentals and applications. Springer, pp. 63–65
7. Snoeys R, Staelens F, Dekeyser F (1986) Current trends in non-conventional material removal processes. Ann CIRP 35:467–480
8. Egashira K, Masuzawa T (1999) Microultrasonic machining by the application of workpiece vibration. CIRP Ann—Manuf Technol 48(1):131–134
9. Kremer D, Saleh SM, Ghabrial SR, Moisan A (1981) The state of the art of ultrasonic machining. CIRP Ann—Manuf Technol 30(1):107–110
10. Egashira K, Masuzawa T (1999) Micro ultrasonic machining by the application of workpiece vibration. CIRP Ann—Manuf Technol 48:131–134

11. Sun XQ, Masuzawa T, Fujino M (1996) Micro ultrasonic machining and self-aligned multilayer machining/assembly technologies for 3D micro machines. In: Proceedings of the IEEE micro electro mechanical systems (MEMS'96), pp 312–317
12. Boy JJ, Andrey E, Boulouize A, Khan-Malek C (2010) Developments in microultrasonic machining (MUSM) at FEMTO-ST. Int J Adv Manuf Technol 47:37–45
13. Yu ZY, Rajurkar KP, Tandon A (2004) Study of 3D microultrasonic machining. J Manuf Sci Eng, Trans ASME 126:727–732
14. Curodeau A, Guay J, Rodrigue D, Brault L, Gagné D, Beaudoin LP (2008) Ultrasonic abrasive l-machining with thermoplastic tooling. Int J Mach Tools Manuf 48:1553–1561
15. Wakuda M, Yamauchi Y, Kanzaki S (2003) Material response to particle impact during abrasive jet machining of alumina ceramics. J Mater Process Technol 132(1–3):177–183
16. Haldar B, Adak DK, Ghosh D, Karmakar A, Habtamu E, Ahmed M, Das S (2018) Present status and some critical issues of abrasive jet materials processing: a review. Procedia Manuf 20:523–529
17. Chastagner MW, Shih AJ, Arbor A (2007) Trans NAMRI/SME 35:359–366
18. Finnie Iain (1960) Wear 3:87–103
19. R.H. Mohammad Jafar, J.K. Spelt, M. Papini, Wear 303 (2013) 138–145
20. Mishra PK (2014) Nonconventional machining. Narosa, India
21. Nouhi A, Kowsari K, Spelt JK, Papini M (2016) Abrasive jet machining of channels on highly-curved glass and PMMA surfaces. Wear 356–357:30–39
22. El-Domiaty A, Abd El-Hafez HM, Shaker MA (2009) Drilling of glass sheets by abrasive jet machining, world academy of science, engineering and technology. Int J Mech Aerosp Ind Mechatron Manuf Eng 3:8
23. Benedict GF (1987) Non-traditional manufacturing processes. Marcel Dekker Inc., New York
24. Getu H, Ghobeity A, Spelt JK, Papini M (2007) Abrasive jet micromachining of polymethyl-methacrylate. Wear 263:1008–1015
25. Getu H, Ghobeity A, Spelt JK, Papini M (2008) Abrasive jet micromachining of acrylic and polycarbonate polymers at oblique angles of attack. Wear https://doi.org/10.1016/j.wear01.013
26. Belloy E, Thurre S, Walckiers E, Sayah A, Gijs MAM (2000) The introduction of powder blasting for sensor and microsystems applications. Sens Actuators: A: Phys 84:330–337
27. Pawlowski A, Belloy E, Sayah A, Gijs MAM (2003) Powder blasting patterning technology for microfabrication of complex suspended structures in glass. Microelectron Eng 67–68:557–565
28. Liu HT, Schubert E (2012) Micro abrasive-waterjet technology. In: Micromachining techniques for fabrication of micro and nano structured, vol 10, pp 205–234
29. Liu HT, Hovanski Y, Caldwell DD, Williford RE (2008) Low-cost manufacturing of flow channels with multi-nozzle abrasive-waterjets: a feasibility investigation. In: Proceedings of the 19th international conference on water jetting, pp 337–351
30. Liu H-T (2010) Waterjet technology for machining fine features pertaining to micromachining. J Manuf Process 12:8–18
31. Miller DS (2003) Developments in abrasive waterjets for micromachining. In: Proceedings of the 2003 WJTA American waterjet conference 2003
32. Liu HT (2016) Versatility of micro abrasive waterjet technology for machining nanomaterials. Encyclopaedia of Nanoscience and Nanotechnology, 3rd edn. CRC Press, Boca Raton
33. Liu HT, McNiel D (2010) Versatility of waterjet technology: from macro and micro machining for most materials. In: Proceedings of the 20th international conf. on water jetting, pp 419–433. BHR Group, Cranfield
34. Haghbin N, Spelt JK, Papini M (2015) Abrasive waterjet micro-machining of channels in metals: comparison between machining in air and submerged in water. Int J Mach Tools Manuf 88:108–117
35. Liu HT (2006) Collateral damage by stagnation pressure buildup during abrasive-fluid jet piercing. In: Proceedings of the 18th international conference on water jetting, pp 47–61. BHR Group, Cranfield
36. Filiz S, Conley CM, Wasserman MB, Burak Ozdoganlar N (2007) An experimental investigation of micromachinability of copper 101 using tungsten carbide micro-endmills. Int J Machine Tools Manuf 47:1088–1100

37. Snoeys R, Staelens F, Dekeyser W (1986) Current trends in non-conventional material removal processes. Ann CIRP 35(2):467–480
38. Tam SC, Williams R, Yang LJ, Jana S, Lim LE, Lau MW (1990) Laser processing of air craft components. J Mater Process Technol 32:177–194
39. Yeo C, Tam S, Jana S, Lau M (1994) A technical review of laser drilling of aerospace materials. J Mat Process Technol 42:15–49
40. Ueda T, Yamada K, Nakayama K (1997) Temperature of workpiece material irradiated with CO_2 laser. Ann CIRP 46(1):117–122
41. Spur G, Appel S, Liebelt S (1997) Non-linear modelling and simulation of laser cutting and grooving of fiber reinforced thermo plastics. In: 32nd MATADOR conference, Manchester, pp 381–386
42. Sen A, Doloi B, Bhattacharyya B (2014) Experimental studies on fibre laser micromachining of Ti-6Al-4 V. In: 5th international & 26th all India manufacturing technology, design and research conference (AIMTDR 2014)
43. Rizvi NH (2003) Femtosecond laser micromachining: current status and applications. Riken Review 50:107–112
44. Loeschner U, Mauersberger S, Ebert R (2008) Micromachining of glass with short ns-pulses and highly repetitive fs-laser pulses. In: Proceedings of the 27th international congress on applications of lasers and electro-optics (ICALEO '08), pp 193–201
45. Rizvi N (2003) Femtosecond laser micromachining: current status and applications. Riken Rev 50:77–82
46. Gower MC (2000) Industrial application of laser micromachining. Opt Express 7:56–67
47. Kunieda M, Yoshida M (1997) Electrical discharge machining in gas. Ann CIRP 46(1):143–146
48. Lin YC, Chen YF, Wang AC, Sei WL (2012) Machining performance on hybrid process of abrasive jet machining and electrical discharge machining. Trans Nonferrous Met Soc China 22:s775–s780
49. Jameson EC (2001) Description and development of electrical discharge machining (EDM). In: Electrical discharge machining, society of manufacturing engineers, Dearbern, Michigan, p 12
50. Newman ST, Ho KH (2003) The state of art—electrical discharge machining. Int J Mach Tools Manuf 43:1287–1300
51. Koch O, Ehrfeld W, Michel F, Gruber HP (2001) Recent progress in micro-electro discharge machining technology—part 1. In: Proceedings of the 13th international symposium for electromachining ISEM XIII, Bilbao, Spain
52. Jahan MP, Rahman M, Wong YS, Fuhua L (2010) On-machine fabrication of high-aspect-ratio microelectrodes and application in vibration-assisted micro- EDM drilling of tungsten carbide. Proc Inst Mech Eng Part B: J Eng Manuf 224:795–814
53. Takahata K, Shibaike N, Guckel H (2000) High-aspect-ratio WC–Co microstructure produced by the combination of LIGA and micro-EDM. Microsyst Technol 6:175–178
54. Liu K, Lauwers B, Reynaerts D (2010) Process capabilities of Micro-EDM and its applications. Int J Adv Manuf Technol 47:11–19
55. Liao YS et al (2005) Fabrication of high aspect ratio microstructure arrays by micro reverse wire-EDM. J Micromech Microeng 15:1547
56. Lin CS et al (2010) Fabrication of micro ball joint by using micro-EDM and electroforming. Microelectron Eng 87:1475–1478
57. Gao G, Zhao W, Wang Z, Gou Y (2005) Instantaneous fabrication of tungsten microelectrode based on single electrical discharge. J Mat Process Technol 168:83–88
58. Sahu RK, Hiremath Somashekhar S, Manivannan PV, Singaperumal M (2014) Generation and characterization of copper nanoparticles using micro-electrical discharge machining. Mat Manuf Process 29(4):477–486
59. HMT Production Technology (1986), 1st edn, McGraw Hill Education (India) Pvt. Ltd.
60. Han MS, Min BK, Lee SJ (2011) Micro-electrochemical discharge cutting of glass using a surface-textured tool. CIRP J Manuf Sci Technol 4(4):362–369

61. Kibria G, Bhattacharyya B, Davim JP (2017) Non-traditional micromachining processes. Springer
62. Das AK, Saha P (2013) Machining of circular micro holes by electrochemical micro-machining process. Adv Manuf 1:314–319
63. Lohrengel MM, Kluppel I, Rosenkranz C, Bettermann H, Schultze JW (2003) Microscopic investigations of electrochemical machining of Fe in $NaNO_3$. Electrochimia Acta 48:3203–3211
64. Kozak J, Rajurkar KP, Wei B (1994) Modeling and analysis of pulse electrochemical machining. Transac ASME 116:316–323
65. Landolt D, Chauvy PF, Zinger O (2003) Electrochemical micro machining, polishing and surface structuring of metals: fundamental aspects and new developments. Electrochimia Acta 48:3185–3201
66. Datta M, Landolt D (2000) Fundamental aspects and applications of electrochemical micro fabrication. Electrochimia Acta 45:2535–2558
67. Bassu M, Strambini LM, Barillaro G (2011) Advances in electrochemical micromachining of silicon: towards MEMS fabrication. Procedia Eng 25:1653–1656
68. Munda J, Malapati M, Bhattacharyya B (2007) Control of microspark and stray-current effect during EMM process. J Mat Process Technol 194:151–158
69. Karunakaran K, Pushpa V, Akula S, Suryakumar S (2008) Techno-economic analysis of hybrid layered manufacturing. Int J Intell Syst Technol Appl 4:161–176
70. Gupta K, Jain NK, Laubscher RF (2016) Hybrid machining processes: perspectives on machining and finishing. Springer
71. Heisel U, Wallaschek J, Eisseler R, Potthast C (2008) Ultrasonic deep hole drilling in electrolytic copper ECu 57. CIRP Ann-Manuf Technol 57:53–56
72. Lauwers B, Klocke F, Klink A (2014) Hybrid processes in manufacturing. CIRP Ann-Manuf Techn 63:561–583
73. Paul L (2015) Characterisation of micro features produced using micro ECDM process: experimental and theoretic investigation. A dissertation submitted for doctoral degrees, IIT Madras, India
74. Fascio V, Langen HH, Bleuler H, Comninellis C (2003) Investigations of the spark assisted chemical engraving. Electrochem Commun 5:203–207
75. Khairy ABE, Mcgeough JA (1990) Die-sinking by electro erosion-dissolution machining, CIRP Ann. Manuf Technol 39:191–195
76. Didar TF, Dolatabadi A, Wüthrich R (2008) Characterization and modeling of 2D glass micromachining by spark-assisted chemical engraving (SACE) with constant velocity. J Micromech Micro Eng 18:9
77. Jain VK, Chak SK (2000) Electrochemical spark trepanning of alumina and quartz. Mach Sci Technol 4:277–290
78. Furutani K, Maeda H (2008) Machining a glass rod with a lathe-type electro-chemical discharge machine. J Micromech Microeng 18:8
79. Schöpf M, Beltram I, Boccadoro M, Kramer D (2001) ECDM (Electrochemical discharge machining) a new method for trueing and dressing of metal bonded diamond grinding tools. CIRP Ann Manuf Technol 50:125–128
80. Peng WY, Liao YS (2004) Study of electrochemical discharge machining technology for slicing non-conductive brittle materials. J Mater Process Technol 149:363–369
81. Paul Lijo, Hiremath Somashekhar S (2016) Experimental and theoretical investigations in ECDM process—an overview. Procedia Technol 25:1242–1249
82. Paul Lijo, Hiremath Somashekhar S (2016) Improvement in machining rate with mixed electrolyte in ECDM process. Procedia Technol 25:1250–1256
83. Paul Lijo, Hiremath Somashekhar S (2013) Response surface modelling of micro holes in electrochemical discharge machining process. Procedia Eng 64:1395–1404
84. Paul Lijo, George Bibin P, Varghese Ashwin (2018) FEM of ECDM process on semi conducting materials. Appl Mech Mat 877:87–91

85. Paul Lijo, Hiremath Somashekhar S (2014) Characterisation of micro channels in electrochemical discharge machining process. Appl Mech Mat 490:238–242
86. Paul Lijo, George Bibin P, Varghese Ashwin (2018) Characterisation of Micro Channels Machined with ECDM for Fluidic Applications. Appl Mech Mat 877:82–86
87. Jain Vijay K, Gehlot Dileep (2015) Anode shape prediction in through-mask-ECMM using FEM. Mach Sci Technol 19(2):286–312
88. Solignac D, Sayah A, Constantin S, Freitag R, Gijs MA (2001) Powder blasting for realization of microchips for bio-analytic applications. Sens Actuators A 92:388–393
89. Liu C, Chen J, Engel J, Zou J, Wang X, Fan Z, Ryu K, Shaikh K, Bullen D (2003) Polymer micromachining and applications in sensors, microfluidics, and nanotechnology. In: 226th national meeting of the american chemical society (ACS), New York
90. Lin YC, Chen YF, Wang AC, Sei WL (2012) Machining performance on hybrid process of abrasive jet machining and electrical discharge machining. Trans Met Soc China 22:775–780
91. Singh T, Dvivedi A (2016) Developments in electrochemical discharge machining: a review on electrochemical discharge machining, process variants and their hybrid methods. Int J Mach Tools Manuf 105:1–13
92. Han MS, Min BK, Lee SJ (2007) Improvement of surface integrity of electro-chemical discharge machining process using powder-mixed electrolyte. J Mat Process Technol 191:224–227
93. Goud M, Sharma AK, Jawalkar C (2016) A review on material removal mechanism in electrochemical discharge machining (ECDM) and possibilities to enhance the material removal rate. Precis Eng 45:1–17
94. Thoe TB, Aspinwall DK, Wise ML (1998) Review on ultrasonic machining. Int J Mach Tools Manuf 38239–38355
95. Yu Z, Rajurkar KP, Tandon A (2004) Study of 3D micro-ultrasonic machining. J Manuf Sci Eng 126

RETRACTED CHAPTER: Investigation on Spark Erosion Machining Induced Surface Integrity of Super-Alloys

Neeraj Sharma and Kamal Kumar

Abstract Surface integrity has a significant influence on the mechanical and tribological behaviour of a material in high heat resisting applications. Non-traditional machining methods like electrical discharge machining (EDM), laser beam machining (LBM), electrochemical machining (ECM), ultrasonic machining (USM) etc. are commonly used to processes the hard materials. Wire EDM (WEDM) is most efficient spark erosion process to shape the hard materials into desired geometry and to modify their surface characteristics. In present book chapter, the experimental results pertaining to surface modification of difficult to machine materials namely WC-Co and Nimonic-90 are presented. Surface was modified through rough cut, trim cut and combination of rough and trim cuts in wire electrical discharge machining (WEDM). Surface integrity was measured in terms of surface roughness (SR), crack size and recast layer thickness. In all the cases, surface integrity was dissimilar for both the difficult to machine materials. Scanning electron microscopy (SEM) and Energy Dispersive X-ray Spectroscopy (EDS) analysis was used to evaluate the surface morphology of WEDMed surfaces.

Keywords Surface modification · Wire EDM · WC-Co · Nimonic-90 · Recast layer

The original version of this chapter was retracted: The retraction note to this chapter is available at https://doi.org/10.1007/978-3-030-18854-2_12

N. Sharma
Department of Mechanical and Industrial Engineering Technology, University of Johannesburg, Johannesburg, Republic of South Africa
e-mail: neeraj.sharma@live.com

K. Kumar (✉)
Department of Mechanical Engineering, Punjab Engineering College (Deemed to be University), Chandigarh 160012, India
e-mail: kamaljangra84@gmail.com

K. Gupta (ed.), *Materials Forming, Machining and Post Processing*, Materials Forming, Machining and Tribology, https://doi.org/10.1007/978-3-030-18854-2_6

1 Introduction

The industrial and technological growths of mechanical industry have lead to the increase in demand for hard and tough materials. The materials– cemented carbides, titanium alloys, stainless steels, ceramics and other heat resisting super alloys, etc. have attractive properties viz.: high bending stiffness, low thermal expansion, good damping capacity and better fatigue life make them potential materials for the current day manufacturing applications. They are finding in wide applications, i.e. nuclear, aerospace, and other industries due to their high strength to weight ratio, heat resistance and hardness. The improved chemical, thermal and mechanical properties of the material are imparted the high strength, heat resistance, corrosion resistance, and wear resistance to product performance and product design.

Various alloys of steel, titanium, nickel, aluminium are widely used in manufacturing of aero engine components. Metal-matrix composites, ceramic and carbon are also used. These materials give high temperature properties, low thermal diffusivity, corrosion resistance and high strength-to-weight ratio to make sure efficient fuel consumption for cost-effective operation of flight and longer functioning life. Nickel-based alloys and titanium alloys show good performance in operation as compared to steel which is very dense, and whose uses are restricted to smaller components. The most important uses of these alloys are in: (i) steam turbine power plants, e.g. blades, stack gas reheaters; (ii) aircraft gas turbines (iii) reciprocating engines (iv) metal processing (v) heat-treating equipment; (vi) medical applications (vii) space vehicles; (viii) chemical and petrochemical industries; (ix) nuclear power systems; (x) coal gasification and liquefaction systems and (xi) pollution control equipment; [1].

Nickel-based alloys play a very vital role in gas turbine compartments. An aircraft engine makes of three subassemblies, namely combustor, compressor and turbine housed in a titanium and/or aluminium casing. These materials maintain high mechanical and thermal fatigue, high mechanical and thermal shock and resistance to corrosion, creep and erosion at elevated temperature. Figure 1 shows the classification of the nickel alloys.

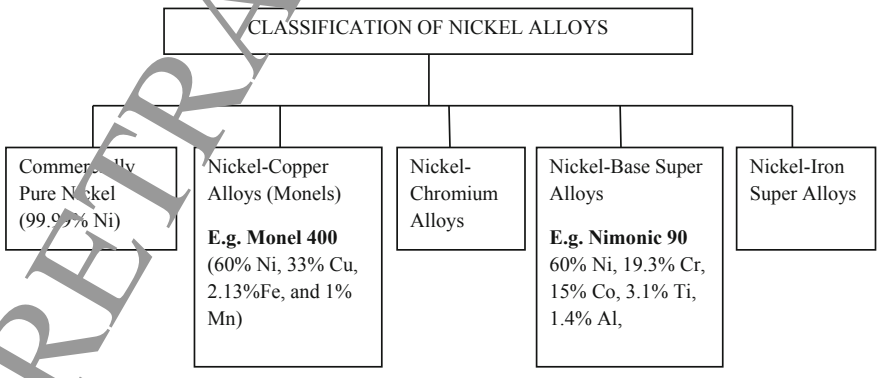

Fig. 1 Classification of nickel alloys

Nickel-based alloys are especially used for the fabricating of turbine blades, which operate at elevated temperature and pressure in aero engine. Nickel-based turbine buckets, blades can function at temperatures up to 520 °C. They are designed with series of holes arranged in order to maximise external and internal cooling of blades. Generally turbine buckets are made of RENE 77, Udimet and IN738. Advanced composite and ceramics materials have high prospective for their applications in various fields of engineering. Such superior material properties should create new challenges to manufacturing engineers to shape and size these electrically non-conductive materials efficiently and economically [2].

Tungsten-carbide is a hard to machine material and it represent high strength and high hardness at elevated temperature, which makes it suitable for dies, cutting tool and other special applications. It exhibit excellent mechanical properties, high resistance to fatigue, resistance to erosion and creep, high corrosion resistance, wear resistance and resistant to thermal shock [3].

Machining of these materials with high precision accuracy is the main challenge of manufacturing industries. But, these materials are complicated to machine with conventional machines such as turning, milling, boring and drilling, etc. If it is required to maintain high accuracy and surface quality excellence, then machining cost is increased. So that these conventional machines are unsuccessful due to excessive tool wear rate resulting poor surface finish and materials removal rate Various non-conventional machining processes have been developed for finding the efficient and better way of producing intricate geometry with high precision in high hardness and strength materials.

These processes may produce any intricate shape on any workpiece material by suitable control over the various machining parameters of the process. These processes may be classified into various groups according to the basic requirements which are as follow:

- Type of energy required
- Mechanism used in the machining processes
- Source required for material removal
- Means for transfer of energies.

The surface of material plays a vital role in its application and energy consumption. A rough surface absorbs a lot of energy as compared to smooth surface. The erosion and wear rate on rough surface is much more. This would change the suitability of the component for a particular application. The machining process opted for the processing of material plays an important on the surface quality and its morphology. During the conventional processes, material is removed in the form of chips due to shear deformation. The surface quality in conventional processes is very poor. During the non-traditional machining processes the tool is not in direct contact with the work-piece. By virtue of which, the material is removed in the form of micro-chips. Depending upon the value of input parameters the crater size increase or decrease. These crater sizes make the surface rough or fine. Also the parameters can cause micro-cracks and recast layer on the machined surface. In this chapter, an experimental study of rough and trim machining operation in WEDM of Nimonic 90 with Tungsten carbide composite has been presented.

2 Spark-Erosion Process

Spark-erosion machining is a type of non-conventional machining process, in which difficult to machine and conductive material can be processed by a soft tool without any direct contact. The gap between the tool and work-piece is maintained by some servo-mechanism. In this process, the tool is connected to the negative terminal and work-piece is connected to positive terminal. When the current flows through the circuit, a discrete spark is generated in between the tool and electrode. These sparks create a channel of plasma, which removes the material in the form of debris. Available variants of spark-erosion machining are Electric discharge machining (EDM), powder-mixed electric discharge machining (PMEDM) and Wire electric discharge machining (WEDM).

2.1 Wire Electrical Discharge Machining (Wedm)

In contrast to conventional machining process, WEDM is proven more efficient and economic for machining the high temperature resistance and super alloys. It is a specialized thermal process which is capable of truly manufacturing complex geometries in hard composite materials that are very difficult to machine by conventional machining process.

WEDM technology increases the productivity of fabricating micro tools due to more intricate tool geometries can be easily created with high quality using WEDM. It is a thermo-electrical process in which a work material is eroded by a series of discrete electrical sparks occurring between electrode (Wire) and work piece (Fig. 2). The movement of wire is controlled numerically to attain the desire accuracy of the work piece and three dimensional shapes. Dielectric fluid is continuously fed to the machining area to flush away the debris. It consumes a continuously travelling wire electrode made of thin copper, brass or coated wire of diameter 0.05–0.3 mm and is capable to attain very small corner radii and capability to machine precise, irregular shape and complex with fine surface finish and high degree of accuracy. The sparking occurs as a result of ionization of dielectric particles between the electrodes and give rise to extreme temperature rise between 8000 and 12000 °C causing fusion of the metal. WEDM uses deionised water as a dielectric fluid instead of hydrocarbon oil which is used in conventional EDM. In WEDM, quick heating and cooling causes re-deposition of melted materials and thermal stresses are generated on machined surface that results into large density of micro cracks. The surface morphology of WEDMed component is quite different from un-machined one. The surface integrity of hard to machine materials can be varied through controlling the WEDM process parameters and by adopting the multi-cut strategy. WEDM has been considering best option for making micro-scale parts with the highest degree of surface finish quality and dimensional accuracy as blade root slots in turbine discs [4].

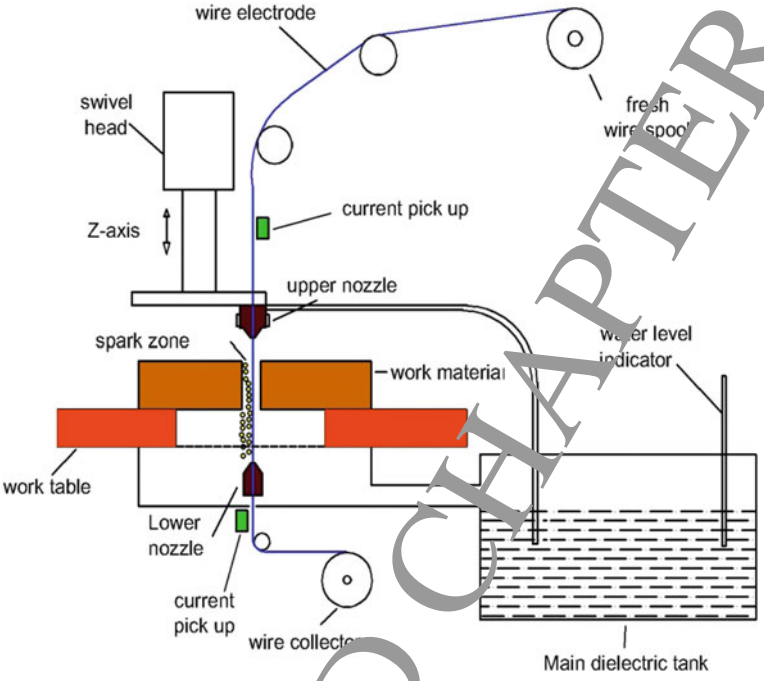

Fig. 2 Wire electrical discharge machining (WEDM) process

For aerospace applications, the surface condition of the machined work piece is of concern because of the role it plays in the useful life of the component under cyclic loading. So, an aerospace engineer/material engineer must be aware to different surface modification method to improve the reliability of aerospace components. Although it is possible to apply post-processing methods like shot peening or heat treatment to get the desirable surface that may provide consistent and required mechanical and physical properties. Hence, it is required to control the machining operation to ensure the integrity specifications. Much of the valuable data has been published mostly on processing of nickel alloys (Inconel 718, Inconel 601 etc.) by different conventional machines. However, the comprehensive study on the machinability of the Nimonic 90 in WEDM has not been reported.

High strength and toughness over an extensive temperature range increase the usage of Nimonic 90 in food processing industry, chemical industries, nuclear reactors, heat exchanger tubing, ship propellers etc. [5]. Nimonic-90 is a nickel-chromium-cobalt alloy which is most suitable for high temperature applications (600–900 °C).

2.2 Rough Cut and Trim Cutting Operation

In rough cutting operation, machined surface with meagre surface morphology is a significant problem because of re-solidification of melted debris's that do not flushed quickly out of a narrow spark gap. Trim cutting operation in WEDM could be a good choice to eliminate unwanted surface defects after rough cut in WEDM, provided proper discharge parameters and wire offset is selected [6–8]. Trim cutting is considered as a probable solution to improve the surface integrity, geometrical accuracy and fatigue life by removing the degraded materials on the machined surface. In trim cut, wire trace back the same wire route of first cut with low SF and certain values of wire offset [6, 8] as shown in Fig. 3. Wire depth (W_d) is the distance travelled perpendicular and inside the work piece during trim cutting operation. The depth of cut (W_d) is related to wire offset value. Increasing wire offset value decreases the W_d.

Despite many research works on WEDM, investigation on WEDM of Nimonic 90 is still missing. Nimonic-90 is a nickel-chromium-cobalt based alloy, most widely used in the aerospace and air craft industries in the manufacturing of turbine blades and combustion chamber, valve in turbo motors and disc in gas turbine. This material possesses excellent strength at extreme pressure and temperature.

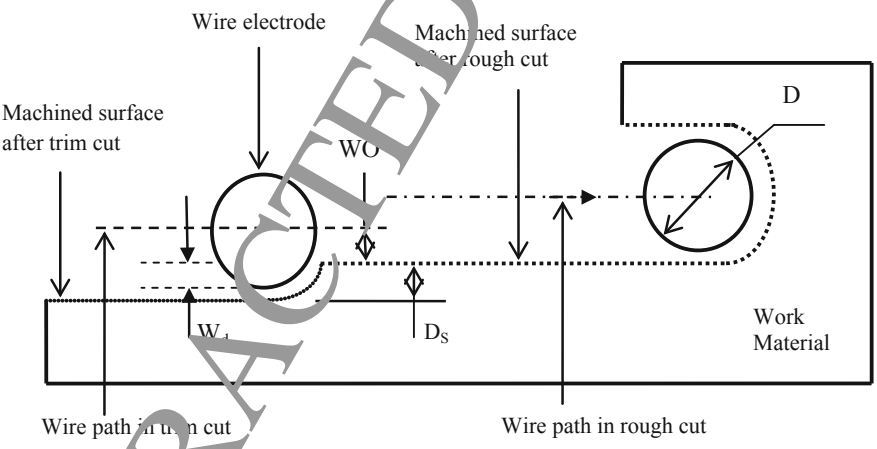

D: wire diameter; WO: wire offset; W_d: wire depth; D_S: dimensional shift

Fig. 3 Terminology used in trim cut

Table 1 Composition and properties of work materials

Materials	Composition	Density (g/cm^3)	Melting point (°C)	Hardness (HV)	Thermal conductivity	Co-efficient of thermal expansion	Young's modulus (GPa)
Nimonic 90	60% Ni, 19.3% Cr, 15% Co, 3.1% Ti, and 1.4% Al,	8.18	1370	361	11.47 W/m Ċ	12.7 µm m^{-1} Ċ	213
Tungsten carbide	WC-5.3% Co	15.63	2870	1990	84.02 W/m K	5.8 µm m^{-1} K^{-1}	550

3 Experimentations

All these materials have been machined on 5 axis sprint cut (ELPUSE-40) WEDM. WC-5.3% Co is a hard to machine material and it possess very high hardness and strength which makes it appropriate for cutting tools, die and other special components. Nimonic-90, a nickel-chromium-cobalt alloy, having creep resistance at elevated temperature (up to 950 °C) and it is mainly used to make combustion chamber and turbine blades. Table 1 shows the composition and properties of selected work materials.

Using WEDM, work materials were machined and samples were obtained in the shape of rectangle of size 8 mm × 7 mm × 12.5 mm. Firstly, consequences of discharge energy (DE) has been evaluated on cutting speed (CS) and surface roughness (SR) in rough cutting operation. Three levels of DE have been selected; low, medium and high. To vary the DE across the work surface, values of parameters namely peak current (Ip), pulse-on time (Ton), and pulse-off time (Toff) were varied. Therefore, only three parameters were the variables while the other parameters were kept constant.

Wire electrode and dielectric conditions were assigned a constant value. A zinc coated brass wire (ϕ 0.25 mm) was used as a wire electrode. Demonized water of 20 mho conductivity has been utilized as a dielectric fluid in present study. In rough cutting operation, dielectric flow rate kept at high range (12 litres per minute) due to which the debris flushing rate increases which ultimately increases the CS. The machining cost in WEDM can be reduced by keeping low wire feed rate. So, a fixed value of 5 m/min has been given to wire feed rate; 10 N of wire tension; 30 V of servo voltage and zero wire-offset value.

Table 2 shows the values of parameters for different level of DE in rough cutting operation. The experiments were conducted corresponds to three settings of DE for each work material and machining characteristics namely cutting speed and SR were observed. Some experiments were conducted to examine the effect of trim cutting

Table 2 Values of WEDM parameters in rough cutting operation

DE level	Values of variable parameters	Constant parameters
Low	Ton 106 μs, toff 40 μs, Ip 100 amp	Servo voltage (SV): 30 V; Wire diameter (WD): 250 μm; Wire tension (WT): 10 N; Wire feed rate (WF): 5 m/min.; Wire offset (WO): zero; Dielectric flow rate (DFR) 12 LM^{-1}; Servo feed (SF): 2080
Medium	Ton 112 μs, toff 40 μs, Ip 120 amp,	
High	Ton 118 μs, toff 35 μs, Ip 160 amp,	

operations on machining characteristics for each work material. Trim cutting operations were followed after a rough cutting operation corresponding to the parameters listed in Table 2. Trim cutting operations (maximum two numbers) were performed at different wire offset (WO) values of 105 and 85 μm but at constant discharge parameters. The values of discharge parameters in trim cutting operation are Ton 105 μs; Toff 35 μs; Ip 90 amp; SV 30 V; WT 8 N; WF 3 m/min; DFR: 3 LM^{-1}.

Figure 4 shows the graphic illustration of the cutting operation processed in present work. According to path programme (Fig. 4), initially a rough cut (1-2-3-4-5-2-1) was made after setting a value of offset equal. Then, trim cut (1-6-7-8-9-10-6-1) was performed as per the plan provided in Table 3.

In case of trim cutting, the prime objective is to improve SR and to reduce dimensional inaccuracy. Therefore, high DE parameters combination providing maximum cutting rate has been selected in rough cutting operation, while in trim cutting operation low DE parameters resulting, low SR, has been selected. Fixed Machining

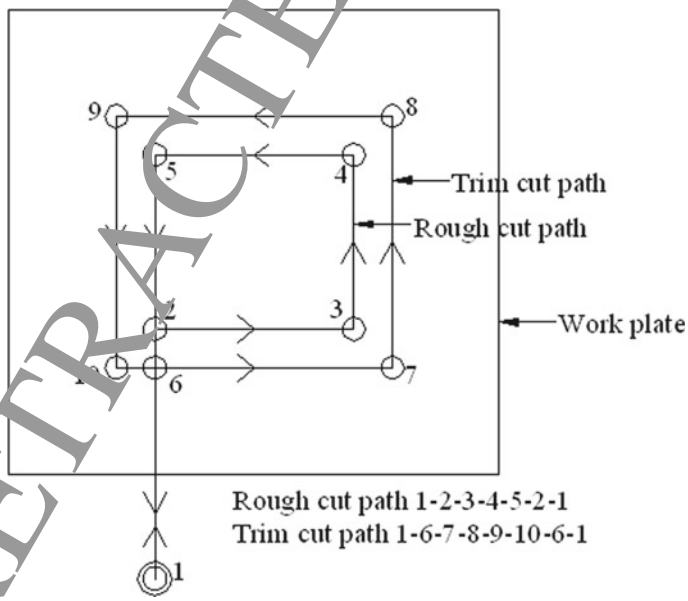

Fig. 4 Cutting operations in WEDM process

Table 3 Fixed machining parameters in rough & trim cutting operation

Rough cut parameters	Trim cut parameters
Pulse on time, ton = 118 µs	Pulse off time, toff = 30 µs
Pulse off time, toff = 35 µs	Discharge current, Ip = 11[illegible] Amp
Dielectric flow rate, FR = 12 L/min	Wire tension, W_T = 8 N
Wire feed rate, W_F = 5 mm/min	Work material thickness = 12.5 mm
Wire tension W_T = 10 N	Wire feed rate, W_F = 2 mm/min
Discharge current, Ip = 150 Amp	Servo feed, SF = 150
Servo voltage, SV = 30 V	
Servo feed, SF = 150 mm/min	

Table 4 Variable process parameters and their levels for Trim cutting conditions

Parameters	Units	Levels	
		Low (−1)	High (+1)
Pulse on time, ton	µs	104	112
Servo voltage, SV	V	20	40
Wire depth, W_d	µm	10	30
Dielectric flow rate, FR	L/min	2	6

parameters setting for rough cutting and trim cutting operation are shown in Table 3. The Ton, SV, W_d and FR have been considered as main process parameters in trim cutting operation for investigation. Dimensional shift (Ds) and SR (SR) are considered as response parameters. Table 4 shows the input parameters and their range for trim cutting operation.

4 Results Discussion

Firstly, experimentations were conducted to examine the effect of Discharge Energy (DE) and work material properties on machining performance of WEDM. CS and SR were observed for these four different work materials after rough cutting operation carried out at different levels of DE. After evaluating the effect of DE in trim and rough cut were performed and the comparative results for SR and micro-hardness has been presented.

4.1 Cutting Speed (CS)

In WEDM, CS depends on DE across the work-material and wire. Ip, Ton, Toff and SV are important discharge parameters in WEDM. Low value of Ip, Ton, SV and high value of Toff results into low DE per unit time and vice versa. High DE results in high heat generation across the spark gap and results in large melting and evaporation of work material [9, 10]. Hence, CS increases with increase in DE across the electrodes as shown in Fig. 5. It is clear from Fig. 5 that with the increase in DE, CS increases for all four work materials but in different proportions. The increase in CS is lowest in WC-Co composite while nickel alloys (Nimonic-90 and nickel-400) shows good increase in cutting speed with increasing DE. HCHCr steel shows maximum cutting speed corresponds to high level of DE. The melting temperature (nearly 2800 °C) and boiling temperature (6000 °C) for tungsten carbide is quite high as compared to other three alloys. Also, WC-Co has higher thermal conductivity which increases the fraction of heat transfer to the bulk material [11] and hence less melting and evaporation of WC-Co material takes place. As a result, rise in cutting speed for WC-5.3% Co composite is less as compared to other alloys which melts nearly at 1400 °C. At high level of DE, steel alloy completely melts and evaporates that easily flushed out of the spark gap at high dielectric flow rate.

4.2 Surface Roughness (SR)

In WEDM process, SR of machined surface is characterized by the depth and size of the craters produced. Therefore, similar to CS, SR is also function of DE across the electrodes. Figure 6 shows the effect of DE on SR in rough cutting operation.

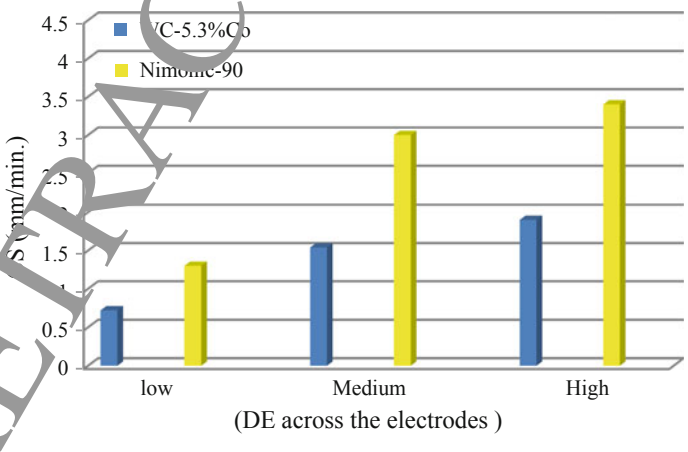

Fig. 5 Effect of DE on cutting speed

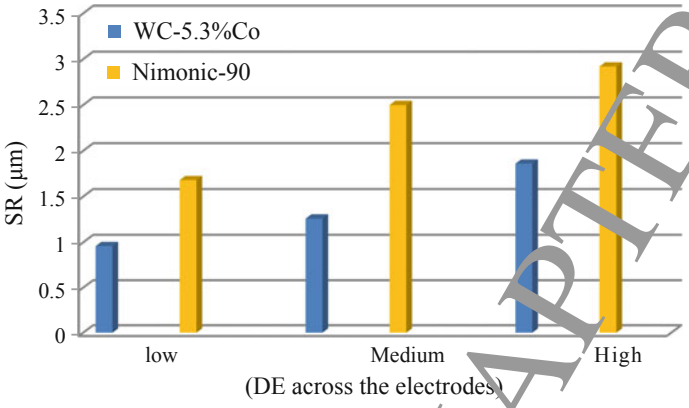

Fig. 6 Effect of DE on SR

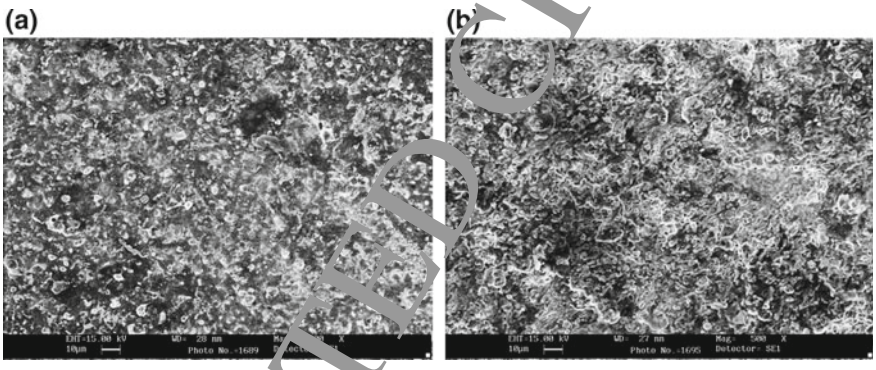

Fig. 7 Machined surface of WC-Co composite; (**a**) at Low D.E. (**b**) at High D.E

Result shows that SR increases with increasing DE for all four work materials. Figure 7 shows that SR is least for WC-Co composite as compared to Nimonic-90. These results can be confirmed by comparing the machined surface in Figs. 7 and 8. Machined surface of Nimonic-90 consists of deep and large size craters while WC-Co has small size craters. Here, thermal conductivity, melting and boiling temperature are the responsible factors. In case of work materials having low melting and evaporating temperature, high DE causes evaporation and overheating of molten metal forming gas bubbles that explode when the discharge ceases [10].

As a result of high DE, large size craters were generated on the work surface. The size and depth of crater enhances with increasing DE and hence increases the SR [12]. Figure 9 represents the effect of trim cut on SR. Trim cutting operations were conducted for two work materials under similar discharge parameters but at different values of wire off-set (WO) values of 105 and 85 μm. Trim cut was carried out after a rough cut that was performed at high level of DE. In trim cut, CS was quite high

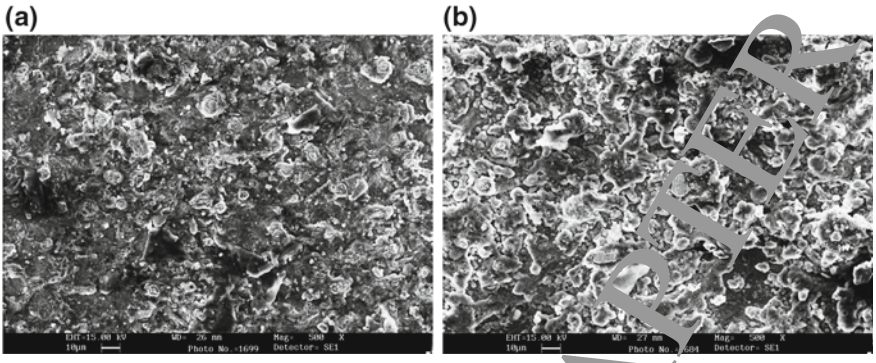

Fig. 8 Machined surface of Nimonic-90; (**a**) at Low D.E. (**b**) at High D.E

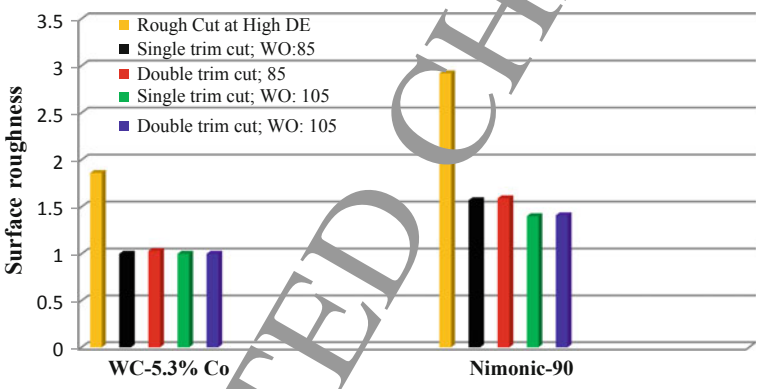

Fig. 9 Comparative effect of trim cutting operation on SR

(10–13 mm/min.) as compared to rough cut (1–2.5 mm/min) and it remains nearly same irrespective of the work material.

Result (Fig. 9) shows that surface quality is improved substantially after trim cut. Trim cutting removes a very thin layer of material from the surface and surface irregularities are reduced to improve surface quality. Here, it can be noticed that multi-trim cutting operations are not much effective. Therefore, surface finish can be improved using single trim cut at low DE with appropriate wire off-set value.

4.3 Micro Hardness

Figure 10a, b depicts the micro-hardness profile of the machined surface after rough and trim cut. Micro-hardness were evaluated at transverse segment to the surface. The value of micro-hardness decreased at the machined top surface as compared

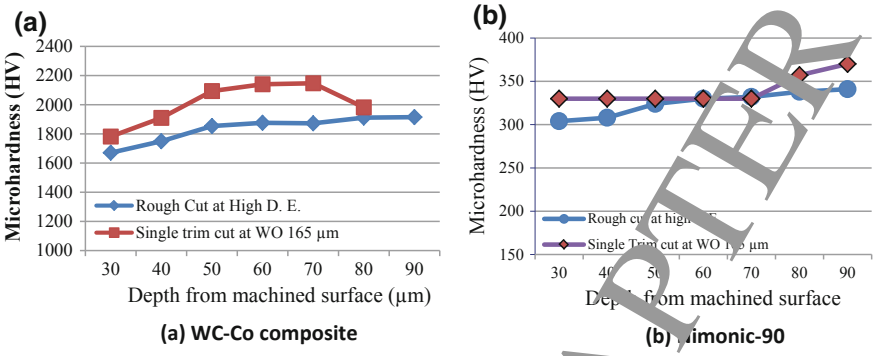

Fig. 10 **a**, **b** Micro hardness profile underneath the machined surface

to core material. The main reason of the reduction is the thermal degradation of machined surface [10]. At high DE, some part of the thermal energy is transferred to the work material that extends the heat affected zone underneath the machined surface. Figure 10b shows that for Nimonic-90, nearly closed micro hardness profiles are obtained for rough cutting and trim cutting operation underneath the machined surface except up to a depth of 40 µm. But in case of WC-Co composite, noticeable difference is obtained in micro harness profiles for rough and trim cut. In WC-Co composite, carbon percentage is more which causes quenching of machined surface due to dielectric fluid and results into micro-cracks in sub-surface [10]. Using trim cutting operation, the degraded surface is removed resulting into new surface having lesser numbers of micro-cracks and defects. Therefore, micro-hardness after trim cutting operation increases in WC-Co

5 Recast Layer

In order to examine the effect of surface damage (Recast layer) on machined surface, specimen were polished to have mirror finish to obtain the images by scanning electron microscope (SEM). Re-solidification is the main reason for recast layer (RCL), which is due to the solidification of molten material due to cool dielectric. The morphology of recast layer as observed after experiments is differs from core material and it also affects the working of the component [4] Figs. 11, 12, 13 and 14 shows the SEM micrographs of transverse section of sample correspond to sample no 3, 4, 15 and 26 respectively.

Recast layer (RCL) was observed which was discontinuous and non-uniform and the average thickness of damaged surface varies from 6 to 12 µm. At high DE, melting and evaporation of material generate gas bubbles causing high pressure energy in plasma channel [10] which plough out the material from the work surface and create large size irregularities on work surface.

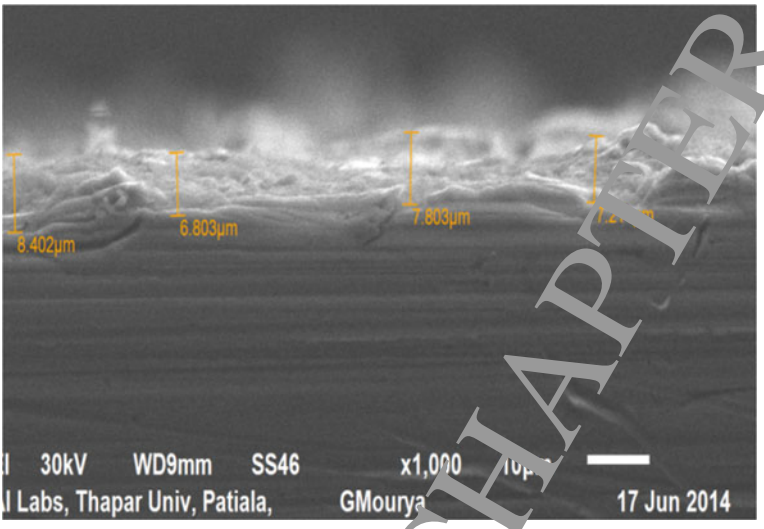

Fig. 11 SEM micrographs of transverse section o WC-Co composite (Ton 104 µs, SV 40 V, W_d 10 µm, FR 2 L/min)

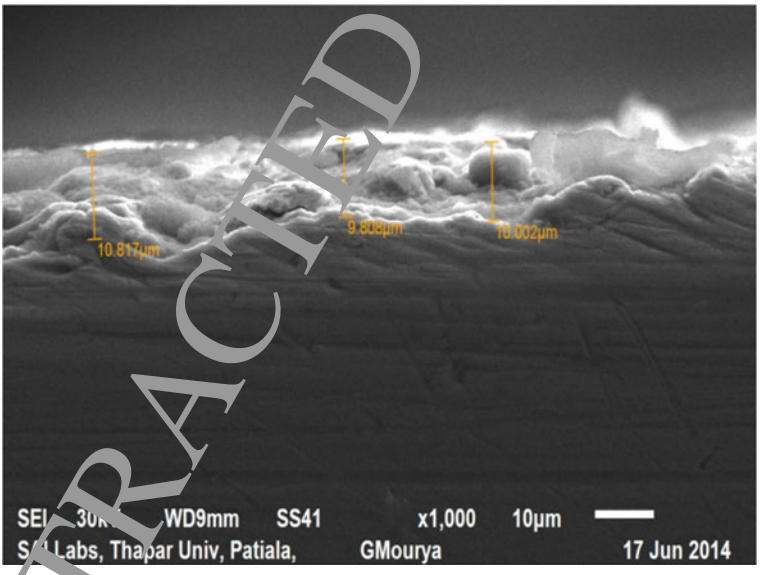

Fig. 12 SEM micrographs of transverse section of WC-Co composite (Ton 112 µs, SV 40 V, W_d 10 µm, FR 2 L/min)

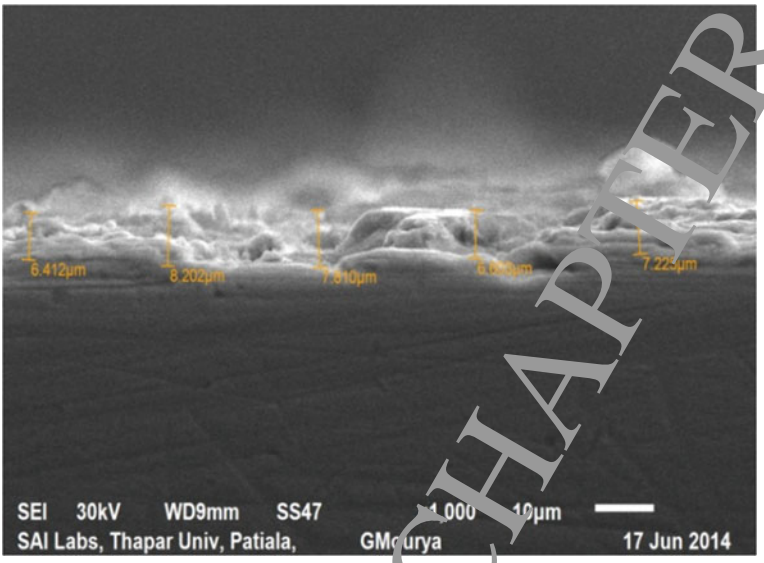

Fig. 13 SEM micrographs of transverse section of Nimonic-90 (Ton 104 µs, SV 40 V, W_d 30 µm, FR 6 L/min)

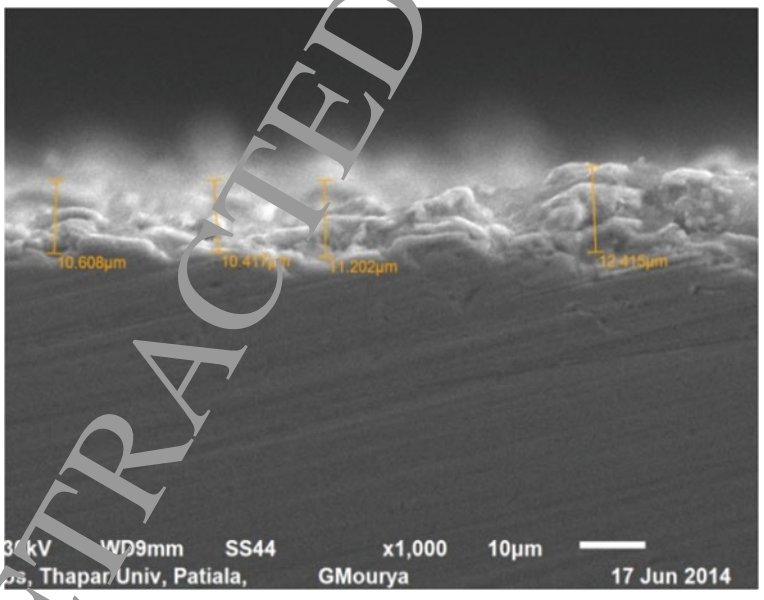

Fig. 14 SEM micrographs of transverse section of Nimonic-90 (Ton 108 µs, SV 30 V, W_d 20 µm, FR 4 L/min)

6 Conclusions

Rough and trim cutting operation in WEDM has been performed on Nimonic-90 and tungsten carbide to modify its surface characteristics. Performance characteristics namely CS, SR, micro hardness and recast layer has been considered in WEDM processing. Trim cutting operation is performed to improve the machined surface characteristics and dimensional accuracy after a rough cutting operation. Four process parameters namely Ton, SV, W_d and FR have been selected as variable parameters; while other parameters were kept fixed at their optimal setting in trim cutting operation.

Firstly, experimentations were conducted to examine the effect of DE on cutting speed and SR on work materials in rough cutting operation. Result shows that with the increase in DE, CS and SR increases which is due to the high heat generation. Comparing the SEM photographs for low and high DE, it is observed that the machined surface of Nimonic-90 consists of deep and large size craters while WC-Co has small size craters. Trim cut were performed after a rough cut (with high level of DE) under the similar discharge conditions but with different wire offset. Results show that surface quality is improved significantly after trim cut operation irrespective of rough cutting operation. It was also noticed that; multi-trim cutting operations are not much effective. Therefore, surface finish can be improved using single trim cut at small DE with appropriate wire off-set value. Micro-hardness profiles showed that at high DE, depth of thermal degradation of top surface increases and thermal degradation is affected by carbon percentage in work material. Using trim cutting operation, the degraded surface can be removed resulting into new surface having lesser numbers of micro-cracks and defects.

Using SEM micrographs effect of DE on surface morphology has been examined. Average thickness of recast layer varies from 6 to 12 μm was found on the machines surfaced after trim cutting operation. Present research approach is useful for achieving high productivity while maintain SR and geometrical accuracy within desire limits for machining complex and intricate shapes in hard and exotic materials. Machining of Nimonic-90 with WEDM at optimized setting yields better performance and more economic as compared to conventional processes that proves the potential of WEDM in aerospace industries.

References

1. Ezugwu EO, Wang ZM, Machado AR (1998) The machinability of Nickel based alloys—a review. J Mat Process Technol 86:1–16
2. Kumar V, Jangra KK, Kumar V, Sharma N (2017) WEDM of nickel based aerospace alloy: optimization of process parameters and modelling. Int J Interact Des Manuf 11:917–929
3. Kumar V, Sharma N, Kumar K, Khanna R (2018) Surface modification of WC-Co alloy using Al and Si powder through WEDM: a thermal erosion process. Part Sci Technol 36(7):878–886

4. Soo SL, Antar MT, Aspinwall DK, Sage C, Cuttell M, Perez R, Winn AJ (2012) The effect of wire electrical discharge machining on the fatigue life of Ti-6Al-2Sn-4Zr-6Mo aerospace alloy. Procedia CIRP 6:216–220
5. Lewis Shoemaker E, Gaylord Smith D (2006) A century of Monelmetal. J Miner Metal Mater Soc 78(9):22–26
6. Huang JT, Liao YS, Hsue WJ (1999) Determination of finish cutting operation and machining parameters setting in wire electrical discharge machining. J Mater Process Technol 87(1–3):69–81
7. Klink A, Guo YB, Klocke F (2011) Surface integrity evolution of powder metallurgical tool steel by main cut and finishing trim cuts in wire-EDM. Procedia Eng 19:178–183
8. Sarkar S, Sekh M, Mitra S, Bhattacharyya B (2008) Modeling and optimization of wire electrical discharge machining of γ-TiAl in trim cuttingoperation. J Mater Process Technol 205:376–387
9. Jangra K, Grover S (2012) Modeling and experimental investigation of process parameters in WEDM of WC- 5.3% Co using response surface methodology. Int J Sci 3:63–72
10. Li L, Guo YB, Wei XT, Li W (2013) Surface integrity characteristics in Wire-EDM of Inconel 718 at different discharge energy. Procedia CIRP 6:222–226
11. Jangra K (2012) Study of unmachined area in intricate machining after rough cut in WEDM. Int J Ind Eng Comput 3:887–892
12. Hewidy MS, El-Taweel TA, El-Safty MF (2005) Modelling the machining parameters of wire electrical discharge machining of Inconel 601 using RSM. J Mater Process Technol 169(2):328–336

Role of Eco-friendly Cutting Fluids and Cooling Techniques in Machining

Kishor Kumar Gajrani and Mamilla Ravi Sankar

Abstract Nowadays with growing pollution and contamination by hydrocarbon (petroleum) based cutting fluids, the scope for vegetable or synthetic biodegradable esters based eco-friendly cutting fluids is increasing. In this review work, the main focus is on sustainable machining using advanced cutting fluid application techniques with eco-friendly cutting fluids. Understanding the functions and various types of cutting fluids are critically important to maximize its performance during any machining process. Also, cutting fluid application techniques are equally important to minimize the use of cutting fluids for the desired machining processes. This review article focuses on the conventional cutting fluids, function of cutting fluids, ecological aspects of conventional cutting fluids, eco-friendly cutting fluids, cutting fluid application techniques during machining and their performances in order to establish the research field further. An overview of the role of eco-friendly cutting fluids and cooling techniques are discussed and finally concluding remarks and possible scope of future work is presented.

Keywords Cutting fluids · Cryogenic cooling · Dry machining · Eco-friendly cutting fluids · Flood cooling · Minimum quantity lubrication (MQL) · Mist cooling · Sustainable machining

1 Introduction

In today's manufacturing world, machining is the most important field due to good quality product and high productivity. For achieving high productivity, machining parameters (depth of cut, feed and cutting speed) are significantly higher that leads

K. K. Gajrani (✉)
Department of Mechanical Engineering, Indian Institute of Technology Guwahati, Guwahati, Assam 781039, India
e-mail: kishor1412@gmail.com

M. R. Sankar
Department of Mechanical Engineering, Indian Institute of Technology Tirupati, Tirupati 517506, India

K. Gupta (ed.), *Materials Forming, Machining and Post Processing*, Materials Forming, Machining and Tribology, https://doi.org/10.1007/978-3-030-18854-2_7

to a large amount of heat generation, which results in higher machining temperature. Subsequently, surface integrity, tool life and dimension accuracy of the product deteriorated. Product with better surface integrity has the capability to improve its corrosion resistance, fatigue strength and its tribological properties. Therefore, better surface quality of the product is highly desirable as well as it is also an indicator of quality of machining [1, 2]. To reduce the machining temperature as well as to improve the product surface integrity and tool life, cutting fluids are necessary during machining operations.

From the last two century, cutting fluids are widely used in machining operations. Each year, the United States alone uses around 100 million gallons of metalworking fluids [3]. In the past, generally, water was used as cutting fluids on grindstones. Then, animal product based tallow was used as wax for the lubricating purpose. Afterwards, simple oils were applied to the cutting tool surface for better lubrication. At early 20th century, soap was added in water to reduce shear strength of mating surfaces [4]. In 1936, straight oils (mineral oils) were introduced as cutting fluids for metal cutting purposes. In 1944, chemicals were added in straight oils as additives for enhancing lubricating properties of cutting fluids [5]. The complexity of cutting fluid composition is increasing day by day with the introduction of hard metals for better performance in the world. From last two to three decades, chemical additives, emulsifiers, pressure additives, biocides, rust inhibitors are added in cutting fluids to fulfil the demands of industries [6]. Figure 1 illustrated the chronological development of metalworking fluids according to [7–10].

During machining, estimated 38 metric ton lubricants were used in the year 2005. Out of all, mineral-oil based cutting fluids comprise around 85% of the global demand [12]. Mineral oil based cutting fluids are made up of petroleum-based products (hydrocarbons), which also contains various additives such as phosphorus compounds, sulfurized oils, free sulphur and fatty acids. During machining, workpiece and tool material tend to react with these additives due to high temperature at cutting zone and hamper the surface integrity as well as workpiece properties. Also, it is well known that sulphides and phosphates are hazardous to the environment as well as operators health [13]. Moreover, due to prolonged exposure of these cutting fluids, operators may have to suffer from various respiratory and skin diseases [14]. Also, the growing cost and complexity of the disposal of cutting fluids are very complex [15]. Finally, it has been realised by researchers as well as industrialist that conventional mineral oil based cutting fluids have serious health effects on operators as well as have detrimental impact on the environment [16]. Even government and environmental protection agencies made strict norms and legalised it for public welfare [17]. Also, mineral oil based cutting fluids are limited. Therefore, a sustainable solution was needed to reduce the detrimental effect on the environment and health hazards to operators.

Cutting fluids need to be highly biodegradable as well as renewable apart from being better at machining to protect the environment. Nowadays, environmental aspects of cutting fluids are measured in terms of renewability, toxicity, biodegradability, biomagnifications and bioaccountability [18, 19]. Therefore, demand for new bio-based eco-friendly cutting fluids is increasing. In general eco-friendly cutting flu-

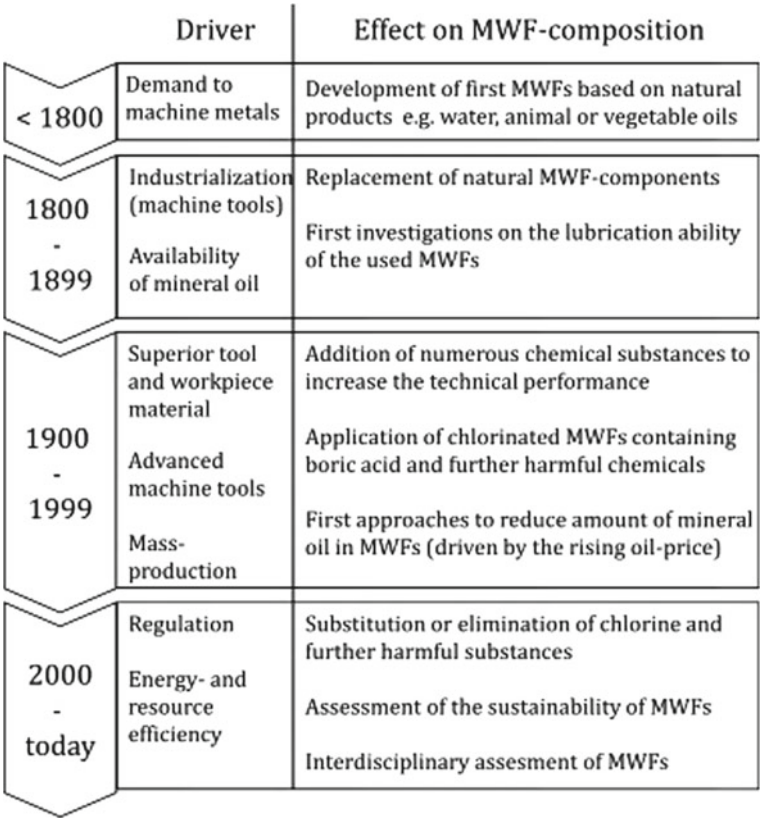

Fig. 1 Chronological development of metalworking fluids [11], with kind permission from Elsevier

ids are made up of vegetable-based oils, which are highly renewable, biodegradable, less hazardous and can be disposed of easily [20–22]. Concurrently, industries are also focusing on making machining cleaner by reducing or eliminating the amount of cutting fluids used for machining [23]. Near-dry machining (NDM) and dry machining are already known as eco-friendly machining technique and are also has been applied successfully for various machining operations [24–27]. Though, in few processes like hard turning and grinding, the use of cutting fluid is still necessary to reduce high temperature and to obtain better surface finish of workpiece [28, 29].

This study aims to find alternate answers and use protective measures against the detrimental environmental effects of conventional mineral oil based cutting fluids. Therefore, a review study is carried out to investigate the role of eco-friendly cutting fluids and cooling techniques in machining performance to find protective measures for sustainable production and a cleaner environment. This review work sums up the capability of eco-friendly cutting fluids and various cooling techniques in details.

2 Cutting Fluids

Traditionally, the cutting fluids are used to lubricate the chip-tool interface as well as the workpiece-tool interface. Also, cutting fluids other functions is to cool cutting zone and to flush away the chips from cutting area [30, 31]. Figure 2 illustrates the region of heat generation in machining.

2.1 Functions of Cutting Fluids

Cutting fluids are used in machining from more than last two centuries [20]. Cutting fluids have all four functions as mentioned above. However, its primary function is to reduce the cutting zone temperature and sliding friction [32, 33]. Nowadays, commercially available cutting fluids have wide varieties. As per the requirement of machining operations and the final output surface integrity, cutting fluids can be tuned towards more cooling or more lubrication. Cutting fluids effectiveness depends upon so many factors like its application technique, machining input parameters and type of machining operation [12].

In machining, cutting fluid lubrication property means to apply grease (in any form) to reduce abrasion and adhesion between the chip-tool interface and workpiece-tool interface [34]. Generally, lubricant reduces friction which in turns reduces the amount of heat generation. Particularly in low cutting speed, shear angle increases due to the presence of lubricant which results in thinner cut chips [35]. However, for high-speed cutting, coolants are preferred in place of lubricant due to evaporation of lubricant oil at high temperature [36].

Coolant function is to cool the chip-tool interface and workpiece-tool interface at high-speed machining operations. Coolant has ability to prolong cutting tool life by maintaining the cutting zone temperature below thermal softening. Also, coolants

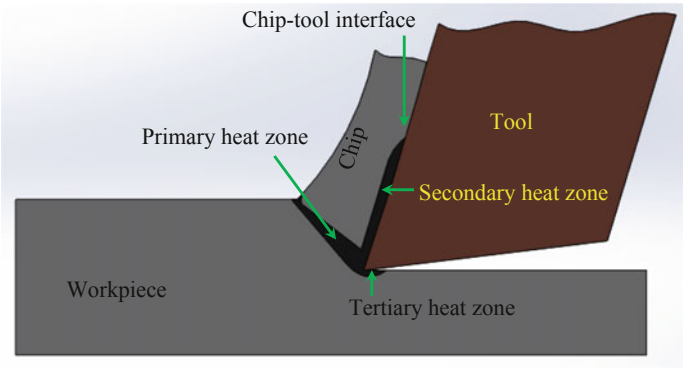

Fig. 2 Regions of heat generation in machining

are capable of reducing the tool wear (diffusion and adhesion). Water is considered as an ideal coolant for machining of non-ferrous alloys, particularly in high heat machining generation processes due to its excellent cooling capability [36].

Apart from the above two, cutting fluids also helps to flush away the generated chips and metal debris from machining zone to avoid tool clogging [37]. Chip evacuation capability of cutting fluids depends on its flow rate and viscosity. Cutting fluids having low viscosities are more capable of evacuating chips from machining zone as compared to cutting fluids having high viscosities [18]. Moreover, cutting fluids are able to reduce the required power for machining operations significantly. Therefore, cutting fluid should be chosen depending on various required properties as well as operating parameters and conditions [34].

2.2 Classification of Conventional Cutting Fluids

Initially, simple oils were considered as cutting fluids. Generally, oils were applied using brushes to cool and lubricate the machining zone. With the development of various hard materials and complex machining processes, different types of cutting fluids were required to meet individual machining demands. Cutting fluids are broadly categorized into three different classes as illustrated in Fig. 3.

2.2.1 Oil-based Cutting Fluids

Neat oils are also known as oil-based cutting fluids. They are generally derived from animal, vegetable or minerals. Among all, mineral oil based cutting fluids are most common in industries. Neat oils have good lubrication properties. Also, they have better anti-corrosion and anti-seizure characteristics, but they have poor cooling ability. Hence, they are susceptible to catch fire and results in the formation of smoke

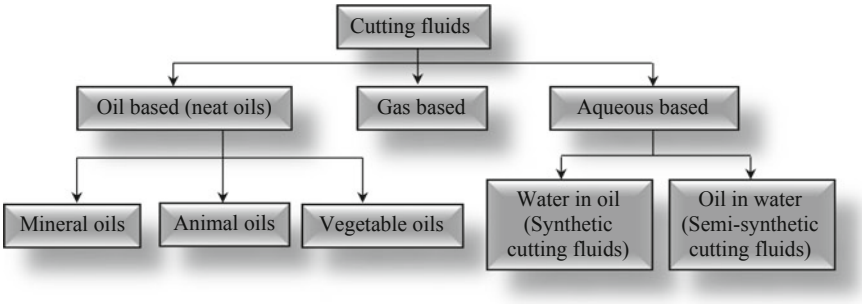

Fig. 3 Classification of conventional cutting fluids

[38]. Therefore, they are generally used for low-speed machining operations, where less heat is generated [18, 19].

2.2.2 Gas-based Coolants

Cutting fluids in the form of gases or cooled-pressurized fluids are categorized as gas-based coolants such as carbon dioxide, helium, nitrogen, argon or even air. These are generally considered as eco-friendly gas-based coolants. As these are in the gaseous state, they are highly anti-corrosive and have a high cooling ability as compared to other cutting fluids. However, they do not have any lubricating capacity. To overcome these problems, the gas-based coolant can also be applied along with a small amount of oils in the form of spray or mist. Combination of gas with small part of oil can be atomized and focused at machining zone. This application technique is known as minimum quantity lubrication (MQL) [39–42].

2.2.3 Aqueous-based Cutting Fluids

Soluble oils are also known as aqueous-based cutting fluids. Generally, these oils are mixed with water to form an emulsion with the help of emulsifiable substance before its use [33]. An emulsifier helps proper dispersion of oil in water to form a stable emulsion [18, 19]. Due to the presence of water in emulsion, it has excellent cooling properties at the same time oil present in the emulsion improves corrosion resistance. Emulsions are used for high-speed machining operations, where more heat is generated [43].

Synthetic Cutting Fluids
Synthetic cutting fluid is generally free from mineral oil and includes several performance enhancing additives. Also, it includes water in small proportion [43]. They have a transparent watery appearance with slight yellow or green in colour, which helps in good visibility during machining operations. Due to the presence of various performance-enhancing additives in synthetic cutting fluids, it has better corrosion resistance, lesser surface tension and water softening characteristics. However, it provides less lubricating effect as compared to other cutting fluids [36]. Hence, they can be used for machining operations where the main requirement it to cool machining zone.

Semi-synthetic Cutting Fluids
The main difference between synthetic and semi-synthetic cutting fluid is that later contains mineral oil. However, the former does not. Semi-synthetic cutting fluids are emulsions containing water as prime coolant and oil as secondary with various chemical additives to make it a highly effective lubricant. The concentration of water in these oils varies in the range of 50−90% [44]. Both aqueous based cutting fluids have lower bacteria growth, corrosion rate and foul odour [45]. Table 1 shows the merits and demerits of various types of cutting fluids [12, 18, 19].

Table 1 Merits and demerits of various types of cutting fluids [12, 18, 19], with kind permission from Elsevier

Cutting fluids	Merits	Demerits
Neat oils	Better corrosion resistance and good lubrication	Susceptible to fire, smoke and mist, only for low-speed machining and low cooling ability
Soluble oils (Emulsions)	Good coolant and lubrication	Susceptible to bacterial growth and workpiece corrosion
Synthetic cutting fluids	Good microbial and corrosion resistance as well as better cooling	Contamination with other machine fluids, less stable by water hardness and foaming issues
Semi-synthetic cutting fluids	Good microbial resistance and corrosion control, less foam and mist issues, no flame or smoke issues and excellent coolant	Contamination with other machine fluids and poor lubrication

2.3 Ecological Aspects of Conventional Cutting Fluids

Ecological concerns call for the reduction of cutting fluids usage in metal cutting practice. Nowadays, it has become an essential objective in industry. Efficient utilisation of cutting tools in machining is an essential focus of researchers. The performance of the cutting tool depends on the process parameters and the cutting environment. Many times, cutting fluids are used to improve the workpiece surface finish and tool life. The fluids that are used to lubricate in machining contains potentially damaging or environmentally harmful chemicals constituents. The airborne particle of cutting fluids can be inhaled by operators that cause respiratory irritation, asthma, pneumonia, dermatitis and different kinds of cancers (oesophagus, colon, skin, lung, pancreas, etc.) [46, 47].

Repeated use of cutting fluids causes changes in its chemical composition. Changes occur because of tramp oil, contamination with metal chips and environmental effects. These contaminated cutting fluids are prone to bacteria growth. As cutting fluids are applied at the high-temperature zone, they also have tendency to form mist and smoke. Also, used cutting fluids disposal causes various detrimental effects on the environment. Due to these reasons, cutting fluid focus is changed from "cooling and lubrication" to renewability, biodegradability and sustainability [48]. Some other aspects of eco-friendly cutting fluids are non-toxic nature, energy saving, life cycle assessment, biomagnifications and bioaccumulability [49, 50].

Therefore, the concept of dry machining has the merits regarding non-pollution of the atmosphere and water, reduction of the cleaning and disposal cost, and no danger to health such as allergy and skin rupture, etc. As such, dry machining has become

popular with regards to the safety of the environment as well as low production cost. However, sometimes the surface integrity of the finished product in dry turning is not superior as compared to wet turning. The concept of surface textures, minimal quantity cutting fluid, green and nano cutting fluids in turning seems to be a better alternative to conventional dry and wet machining [51–58]. Moreover, the combination of the above processes makes machining much more sustainable by reducing adverse environmental effects, associated costs and enhancing the operator's safety. Furthermore, it also improves machining performance and final workpiece surface finish.

2.4 Eco-friendly Cutting Fluids

As discussed in previous sections, conventional cutting fluids have various detrimental effects. Therefore, from the early 1990s, researchers and industrialist started focusing on the development of eco-friendly cutting fluids. Most important characteristics of eco-friendly cutting fluids are its biodegradability and sustainability.

In the presence of micro-organism (which are abundant in the atmosphere), biodegradable cutting fluids are vulnerable to break down. In its primary degradation, the recyclable substance will vanish from its original molecule and other substance such as biomass, hydrogen and CO_2 will degrade during ultimate degradation. Out of both, ultimate biodegradability is considered as a measure for biodegradability [59, 60]. Further, cutting fluids sustainability can be categorized in two different ways; (a) its source of raw materials for production such as renewable materials or fossils, and (b) related to pollution caused during its use and after use (disposal) [61]. In terms of better biodegradability, vegetable-based oils and esters are highly desirable. However, for the best environmental sustainability, gaseous based coolants are preferable like water vapour as a coolant, cryogenic nitrogen or carbon-dioxide, pressurized gas, etc.

Lubricity and biodegradability of vegetable-based cutting fluids are better due to the presence of long fatty acids chains with a number of unsaturated double and triple carbon bonds. Long fatty acids chains such as triglycerides, linolenic, linoleic and oleic acids are highly biodegradable and all are present in most of the vegetable-based cutting fluids. Gajrani et al. [29, 60] compared primary and ultimate biodegradability of petroleum-based mineral oil with commercially available ecoline bio-cutting fluid. Results show that mineral oil was ultimately 18% biodegradable. However, bio-cutting fluids was 96% biodegradable due to the presence of long fatty acids chains mostly triglycerides. Typical chemical structure of triglycerides commonly found in vegetable-based cutting fluids is illustrated in Fig. 4. Typical chemical structure of oleic, linoleic and linolenic acids are shown in Fig. 5 [12].

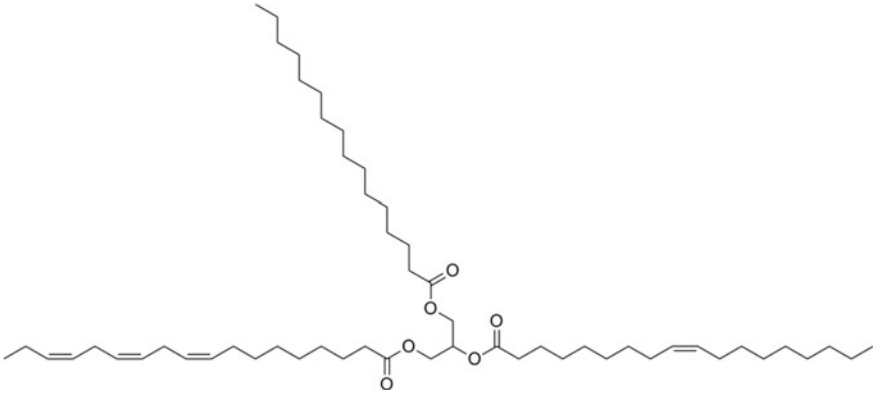

Fig. 4 Typical chemical structure of triglycerides

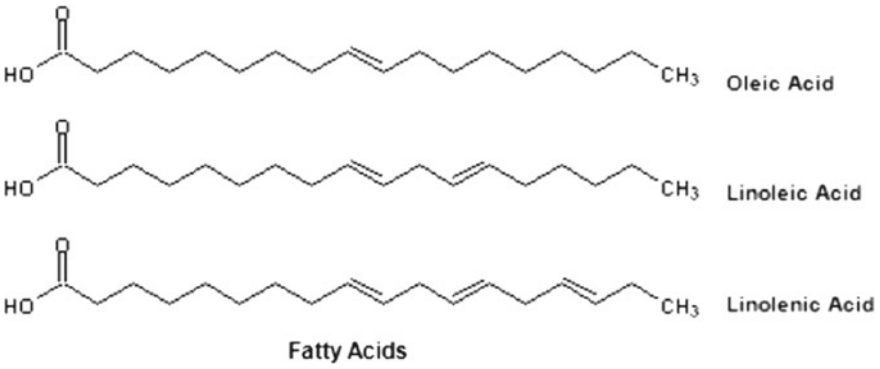

Fig. 5 Typical chemical structure of oleic, linoleic and linolenic acids [12] with kind permission from Elsevier

2.5 Cutting Fluid Application Techniques During Machining

Cutting fluid helps to reduce temperature and friction at the machining zone that leads to better workpiece surface integrity and tool life. However, workpiece surface integrity and tool life also depend upon the application techniques of the cutting fluids during machining. Further, some techniques are considerable better for few operations while other for different machining operations depending on the individual circumstances. In last two decades, new cutting fluids application technologies are also developed that aims to reduce overall consumption of cutting fluids without degrading the machining performance leading to more economical and efficient techniques as well as to improve the productivity [62]. Main conventional cutting fluids application techniques are (a) wet cooling (flood cooling), (b) high-pressure cooling, (c) cryogenic cooling and (d) mist cooling (minimum quantity lubrication)

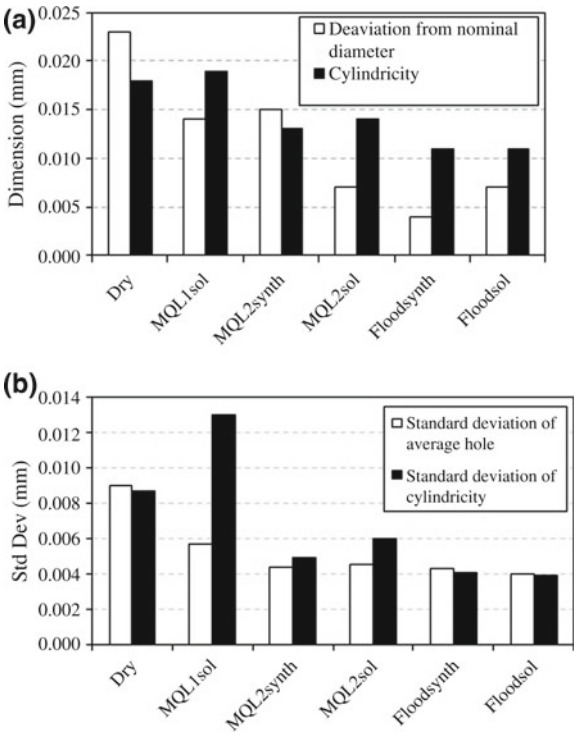

Fig. 6 Workpiece dimensional accuracy and its standard deviation with various cutting fluid application techniques [63] with kind permission from Elsevier

2.5.1 Wet Cooling (Flood Cooling)

From the last century, flooding or wet cooling is most commonly used cutting fluid application technique for coolants. In flood cooling, a continuous stream of coolant is focused at the machining zone for cooling chip-tool interface during machining [36]. Consumption of coolant is highest for flood cooling among all techniques. A typical range of coolants flow rate for single point cutting tool operation is around 10L/min and for multiple points cutting tool operation is around 225L/min/per tooth [43]. As per Schey [35], flood cooling should be applied from tool clearance face for better cooling performance. Jayal et al. [63] performed blind hole drilling operation on A390 aluminum alloy using various cutting fluid application techniques and results show that flood cooling was best among all in terms of workpiece dimensional accuracy as illustrated in Fig. 6.

In 2014, Imran et al. [64] investigated the surface integrity and wear mechanism during micro-drilling of Inconel 728 under wet cooling and compared results with dry machining. After investigation using transmission electron microscope (TEM) and scanning electron microscope (SEM), they concluded that large-scale deformations along with high discoloration density having nanocrystalline grain structures are visible under wet machining conditions as compared to dry machining. Figures 7

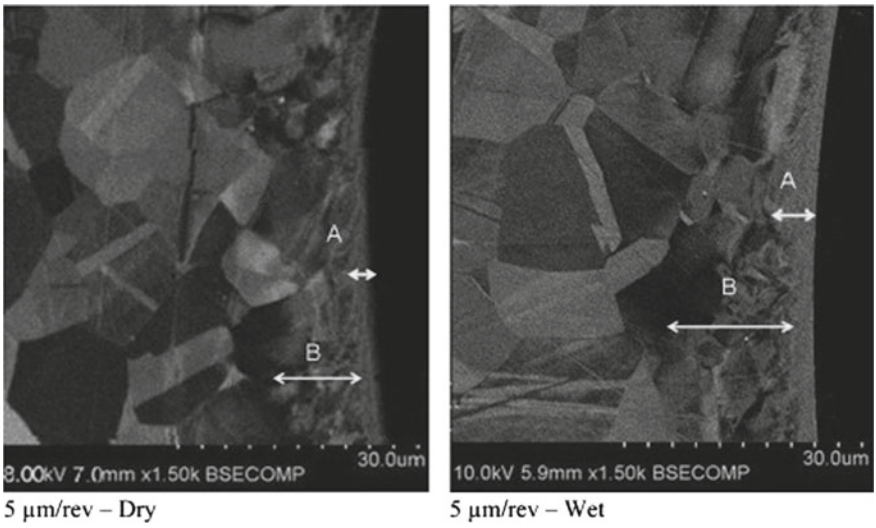

Fig. 7 Comparison of dry and wet drilling (micrograph of drill beat edge) [64] with kind permission from Elsevier

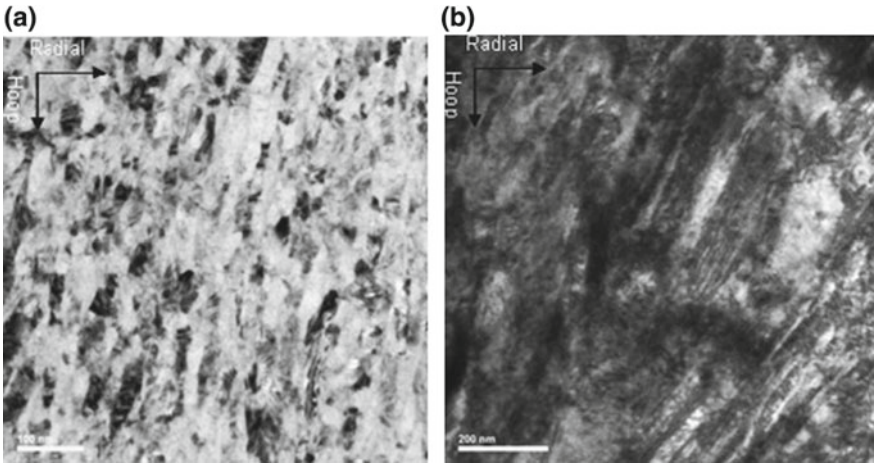

Fig. 8 Fine grain structure layer for **a** dry and **b** wet machining [64] with kind permission from Elsevier

and 8 illustrate the SEM and TEM images of dry and wet micro-drilling, respectively [64]. Figure 9 illustrates the tool wear mechanism sequence during micro-drilling under dry and wet cooling machining [64].

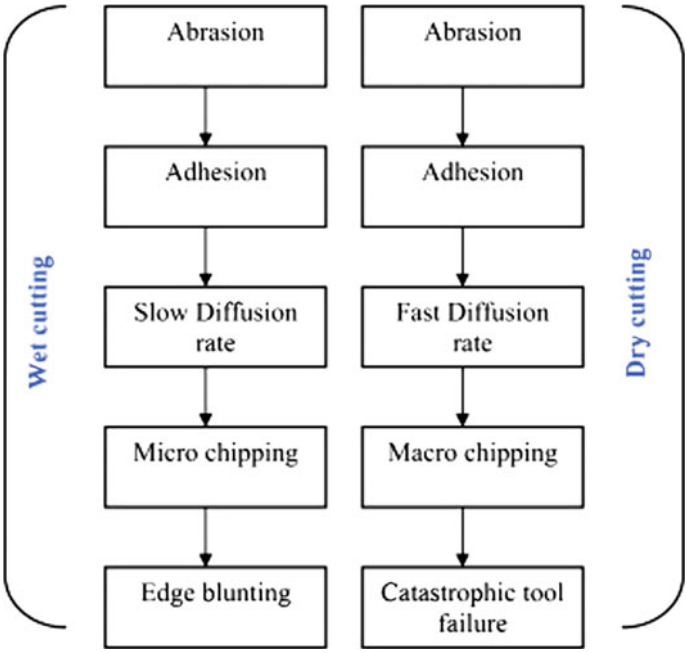

Fig. 9 Tool wear mechanisms sequence for dry and wet machining [64] with kind permission from Elsevier

2.5.2 High-pressure Cooling

Generally, this technique is used to increase the heat removal from the machining zone due to high pressure, which allows better penetration of cutting fluids at the machining zone. Specially designed nozzles are used to deliver high pressurized fluids to sustain pressure. The pressure varies in the range of 5.5–35 MPa. Apart from better cooling ability, it also improves tool life and reduces tool-chip interface contact length as high pressurized fluids forces chips away from the tool surface [62]. However, there are few limitations to this technique such as high-pressure jet may damage workpiece surface or tools, which are brittle in nature (especially ceramics) [43].

During turning of AISI 316 austenitic stainless steel, Naves et al. [65] investigated the tool wear under the influence of high pressurize fluids. The pressure of the cutting fluids was varied from 10 to 20 MPa (in the interval of 5 MPa). Machining experiments were carried out and it was observed that tool wear was least with high pressurize cooling (15 and 20 MPa) compared to dry and wet cooling techniques as illustrated in Fig. 10 [65].

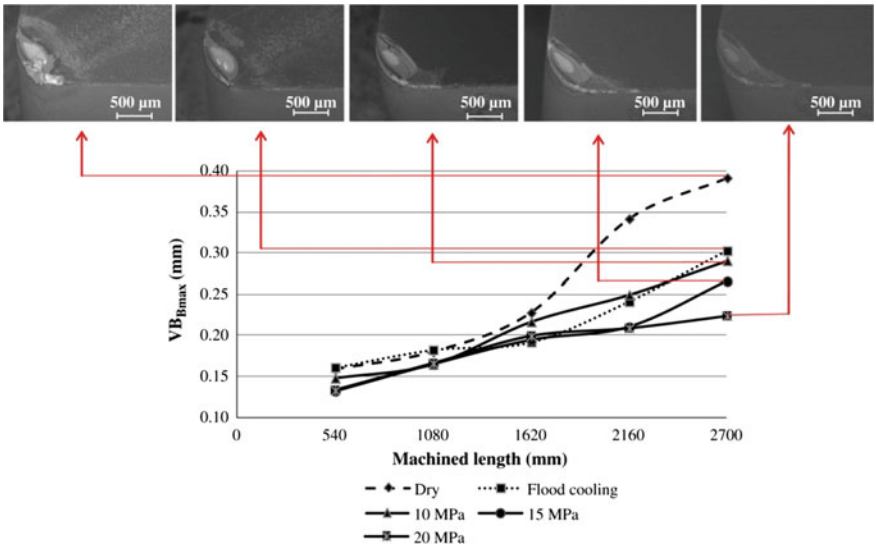

Fig. 10 Variation of tool flank wear with respect to machined length under the various cutting environment (5% concentration of cutting fluid) [65] with kind permission from Elsevier

2.5.3 Cryogenic Cooling

In this cooling technique, gases such as helium and nitrogen are used as a coolant. As both nitrogen and helium are inert gases, they are eco-friendly. Generally, these gases are injected at the chip-tool interface in liquefied form around −200 °C to cool the machining zone. These liquid gases reduce the machining zone temperature by absorbing heat and quickly evaporate in the form of gas [43]. Moreover, after machining using cryogenic cooling, chips are free from oil residue. Therefore, they can be recycled without any additional cleaning process.

In general, machining forces required with cryogenic cooling are less as compared to dry machining due to its cooling properties and ability to reduce friction at the chip-tool interface. However, the pressure and flow rate of cryogenic coolant is very crucial. If machining zone is overcooled, required cutting force will be more due to workpiece embrittlement. Cryogenic cooling is more useful at a low cutting speed. However, with the increase in cutting speed, contact of chip-tool will be plastically dominant which obstruct the passage of cryogenic fluids and reduces its efficiency.

Sharma et al. [62] have reported that under the influence of cryogenic coolant, the tool wear such as diffusion, adhesion and abrasion were reduced and tool life increased. Babic et al. [66] have mentioned that while operating with a high temperature, the operation accuracy of cryogenic cooling is inadequate. In another study, the influence of liquid nitrogen was compared with wet cooling during turning operation. Results confirmed that turning with liquid nitrogen significantly reduces flank wear, cutting force and workpiece surface roughness as compared to wet cooling

[67]. Similarly, Wang et al. [68] reported 200 and 300% improvement in workpiece surface roughness and tool life, respectively during cryogenic machining of tantalum as compared to conventional machining.

2.5.4 Mist Cooling (Minimum Quantity Lubrication)

In this technique, a combination of cutting fluids with pressurized air is applied at the machining zone in the form of mist or spray. This technique is commonly known as MQL and also known as micro-lubrication as well as minimum quantity cutting fluids (MQCF) [60]. The atomised mists with fluid droplets are effective to provide cooling effect [35]. Also, the mist is able to reach at most of the places unlike flood cooling [43]. Further, machining using the MQL technique is known as one of the cleaner production method [69]. Machining using MQL may reduce the amount of cutting fluid in the range of one-thousandth to ten-thousandth as compared to wet cooling [43]. Further, if the biodegradable cutting fluid is used as cutting fluid with MQL technique, the sustainability of overall process increases further [13]. A typical MQCF experimental setup is shown in Fig. 11 [60].

An eco-friendly cooling method known as cold water mist jet (CWMJ) was applied to reduce machining zone temperature while turning of titanium alloy [70]. Results of CWMJ were compared with flood cooling and cold air jet concerning cutting temperature and tool flank wear as illustrated in Figs. 12 and 13 [70]. It was observed that CWMJ cooling effect was much better compared among all which can be comprehended by lesser cutting temperature and tool flank wear.

In another study, only mixture of air and water were applied in the form of a mist to cool grinding zone for removal of ecological hazards (cutting oils) and to make the process more economical [66]. Authors concluded that this water and air combination has ability to cool and the maintain shape of grinding wheel as compared to conventional cutting fluids with existing application techniques. Among all, best results were obtained with two mist nozzles (each at front and back).

2.6 Role of Eco-friendly Cutting Fluids and Cooling Techniques on Machining Performance

In previous sections, various types of cutting fluids and cooling techniques are discussed. Among all MQL with a combination of biodegradable cutting fluids are generally accepted as a better eco-friendly and sustainable machining method [43]. In a study of plain turning, three different cooling techniques (MQL, dry and wet) were experimentally compared in terms of workpiece dimensional deviation and cutting temperature during machining of AISI 1040 steel. Results confirm that MQL environment was able to improve the workpiece dimensional accuracy and reduce the chip-tool interface temperature as illustrated in Fig. 14a, b [71].

Fig. 11 Minimum quantity cutting fluid experimental setup [60] with kind permission from Elsevier

In another study, machining performance of vegetable-based oils was compared with three different cutting fluids such as mineral, hydrocracked and synthetic oils using MQL technique during grinding of Al_2O_3 ceramic. Obtained results show that hydrocracked-based oil is better in terms of workpiece surface finish. However, synthetic oil uses low specific energy during rough grinding [72].

Itoigawa et al. [73] investigated the friction coefficient and chip-tool contact length during intermittent turning of aluminium alloy under dry, flood, MQL and OoW (Oil film on water with MQL) environments. The difference in MQL and OoW-MQL is that later contains a mixture of water and oil as cutting fluids. However, former only has oil. Authors claim that OoW-MQL performance is better as compared to other two due to better cooling as well as lubricating properties of OoW-MQL as compared to the only MQL with oil. Figures 15 and 16 illustrates the variation of friction coefficient and chip-tool contact length under different machining environment.

Gajrani et al. [29, 60, 74] compared the performance of mineral oil and bio-cutting fluid in terms of their biodegradation, storage stability, anti-corrosion, rheological,

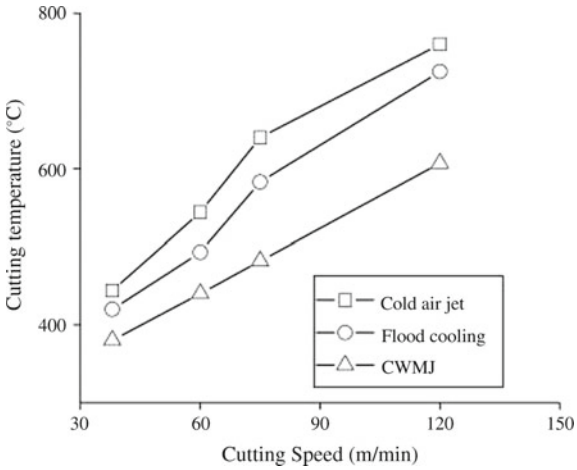

Fig. 12 Variation of cutting temperature using various cooling techniques [70] with kind permission from Elsevier

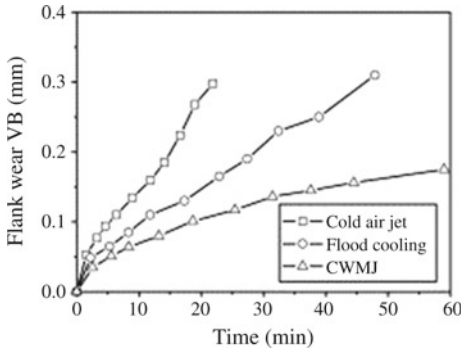

Fig. 13 Variation of tool flank wear using various cooling techniques (cutting speed = 38 m/min) [70] with kind permission from Elsevier

thermal and hard machining performance under flood and MQL environment. Results show that bio-cutting fluid is far superior to mineral oil in terms of their biodegradation, storage stability and anti-corrosion properties. Also, BCF with MQL reduces tool-chip interface length and reduces machining forces. In another study, Gajrani et al. [58] developed vegetable based green cutting fluid and conducted hard machining experiments on hardened AISI H-13 steel under dry, flood and MQL environment. Results show that GCF reduces more tool-chip interface friction coefficient and surface roughness of workpiece under MQL environment as compared to dry and flood cooling.

Further, another study compared four different cutting fluids consisting of sunflower oil-based cutting fluids with and without surfactants as well as commercial vegetable and mineral oil [75]. During turning of AISI 304 steel under MQL envi-

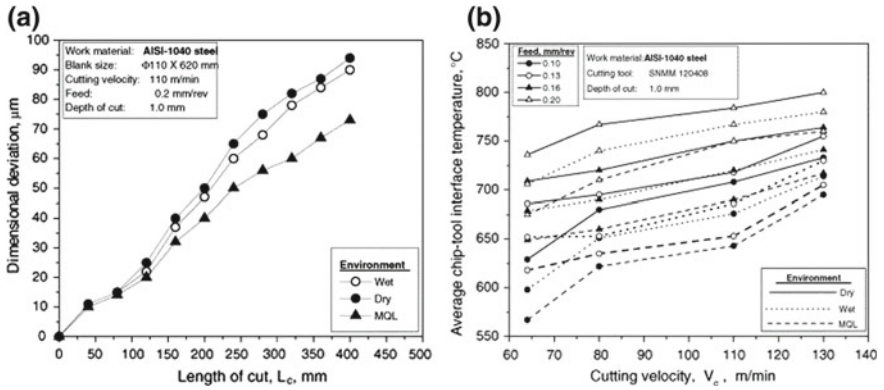

Fig. 14 Effect of MQL on **a** workpiece dimensional deviation and **b** chip-tool interface temperature [71] with kind permission from Elsevier

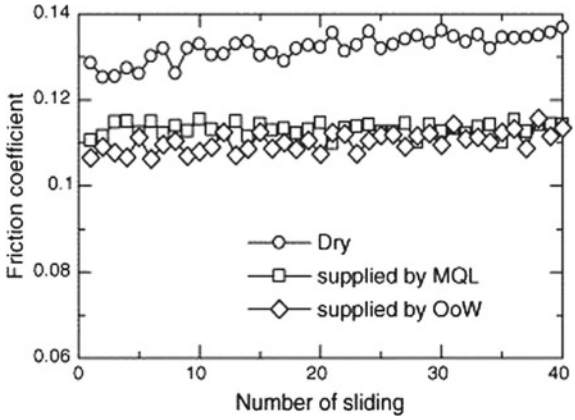

Fig. 15 Variation of friction coefficient during intermittent turning under different machining environment [73] with kind permission from Elsevier

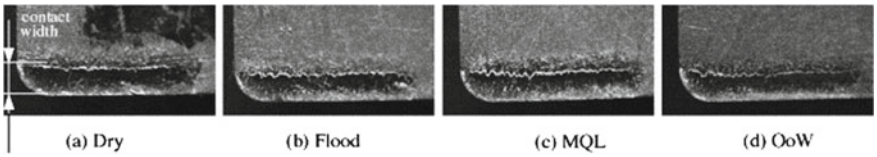

Fig. 16 Variation of chip-tool contact length after intermittent turning under different machining environment [73] with kind permission from Elsevier

ronment, sunflower oil-based cutting fluids show best workpiece surface roughness among all. Paul and Pal [76] investigated the effect of neem, kajrana and mineral oil and found that neem oil performance is better among others for reducing the cutting temperature. Gupta and Laubscher [77] presented a review on sustainable machining of titanium alloys and they also mentioned that MQL has shown promising results during machining of difficult-to-cut materials. Afterwards, few researchers have dispersed nanoparticles in the vegetable based cutting fluids to enhance its thermal conductivity. Results show that nanofluids significantly reduce cutting temperature, machining forces, tool wear, surface roughness of workpiece and also improves tool life [78–83].

3 Sustainable Machining for Future

Petroleum-based mineral oils are non-renewable and have detrimental environmental effects as well as they are harmful for operators. Therefore, the trend of cutting fluids shifted from petroleum-based cutting fluids to biodegradable and renewable vegetable-based eco-friendly cutting fluids. They are far better than mineral oils in terms of machining as well as eco-friendly nature. Also, with MQL vegetable based cutting fluids have shown a lot of potential. However, vegetable-based cutting fluids also have some limitations. They are costly and more preferred for low to medium cutting speed. Also, most of the vegetable-based cutting fluids have low oxidative and thermal stability as well as their production may raise prices of agriculture product. A number of studies have already focused and confirmed that machining performance is better with vegetable-based cutting fluids and the amount of cutting fluid required with MQL is less. Now, the researchers need to focus on further reducing the quantity of cutting fluids or to entirely eliminate the cutting fluid usage by switching to dry machining.

Dry machining with micro/nano-textured cutting tools, coated cutting tools, self-lubricating cutting tools has shown enormous potential to reduce friction coefficient and to improve machining performance. Thus, future research needs to be focused on improving dry machining and to develop new materials that can able to machine difficult to cut material without cutting fluids to make it eco-friendly process.

4 Conclusion

Initially, this study focuses on the history, functions and classifications of cutting fluids. Afterwards, ecological and environmental detrimental effects of cutting fluids are discussed. Further, eco-friendly cutting fluids merits, demerits, advantages, biodegradability, renewability, etc. are discussed in length. Moreover, the role of eco-friendly cutting fluids and various applications techniques on machining performance are deliberated.

Vegetable based eco-friendly cutting fluids are mainly preferred due to its high biodegradability and renewability in nature. Also, they provide better machining performance as compared to mineral oil-based cutting fluids in most of the cases. However, still they have few demerits such as low oxidative, low thermal stability, high freezing point as well as high cost, which needs more focus in future.

Machining with cryogenic coolants shows promising results to improve machinability of difficult-to-cut material and also to reduce workpiece surface roughness. In most cases, machining with cryogenic coolants reduces chip-tool interface coefficient of friction, machining forces and improves tool life against adhesion and abrasion wear. However, overcooling may cause embrittlement of workpiece, which may affect adversely to the product quality.

MQL is a most promising technique to reduce issues of environment and if coupled with vegetable-based cutting fluids, it shows remarkable improvement in machining performance as compared to flood cooling.

Even though cryogenic, vegetable-based cutting fluids and MQL are not the generalised solutions, but they showed tremendous improvement in making machining more sustainable. Furthermore, dry machining is becoming more popular to address environmental and operator's health issues.

References

1. Davim JP (2010) Surface integrity in machining. Springer, London. https://doi.org/10.1007/978-1-84882-874-2
2. M'Saoubi R, Outeiro JC, Chandrasekaran H, Dillon OW Jr, Jawahir IS (2008) A review of surface integrity in machining and its impact on functional performance and life of machined products. Int J Sustain Manuf 1(1–2):203–236
3. Bennett EO (1983) Water based cutting fluids and human health. Tribol Int 16(3):133–136
4. Hasib MA, Al-Faruk A, Ahmed N (2010) Mist application of cutting fluid. Int J Mech Mechatron Eng 10(1):13–18
5. Bienkowski K (1993) Coolants and lubricants: the truth. Manuf Eng (USA) 110(3):90–92
6. Sluhan CA (1986) Considerations in the selection of coolants used in flexible machining cells. Society of Manufacturing Engineers. Technical paper pp. 1–5
7. Spikes H (2004) The history and mechanisms of ZDDP. Tribol Lett 17(3):469–489
8. Taylor FW (1906) On the art of cutting metals. American Society of Mechanical Engineers
9. Wells HM, Southcombe JE (1920) The theory and practice of lubrication: The" germ" process. Central House
10. Woodbury RS (1959) History of the grinding machine: a historical study in tools and precision production. Vol. 2, The MIT Press
11. Brinksmeier E, Meyer D, Huesmann-Cordes AG, Herrmann C (2015) Metalworking fluids—mechanisms and performance. CIRP Ann 64(2):605–628
12. Debnath S, Reddy MM, Yi QS (2014) Environmental friendly cutting fluids and cooling techniques in machining: a review. J Clean Prod 83:33–47
13. Dixit US, Sarma DK, Davim JP (2012) Environmentally friendly machining. Springer Science & Business Media
14. Sankar MR, Gajrani KK (2017) Cutting fluid emissions and eco-friendly cutting fluid for sustainable machining. In: Proceedings of the national conference on sustainable mechanical engineering: today and beyond (SMETB), Tezpur University, India, pp 157–162

15. Gajrani KK, Mallick SK, Sankar MR (2017) Comparative studies on mineral oil, eco-friendly bio-cutting fluids treatment and their machining performance. In: Proceedings of the national conference on sustainable mechanical engineering: today and beyond (SMETB), Tezpur University, India, pp 111–116
16. Gajrani KK, Sankar MR (2017) Past and current status of eco-friendly vegetable oil based metal cutting fluids. Mater Today: Proc 4(2):3786–3795
17. Tschätsch H, Reichelt A (2009) Cutting fluids (coolants and lubricants). Applied machining technology. Springer, Berlin, Heidelberg, pp 349–352
18. Kuram E, Ozcelik B, Bayramoglu M, Demirbas E, Simsek BT (2013) Optimization of cutting fluids and cutting parameters during end milling by using D-optimal design of experiments. J Clean Prod 42:159–166
19. Kuram E, Ozcelik B, Demirbas E (2013) Environmentally friendly machining: vegetable based cutting fluids. In: Green manufacturing processes and systems. Springer, Berlin, Heidelberg, pp 23–47
20. Lawal SA, Choudhury IA, Nukman Y (2012) Application of vegetable oil-based metalworking fluids in machining ferrous metals—a review. Int J Mach Tools Manuf 52(1):1–12
21. Nagendramma P, Kaul S (2012) Development of ecofriendly/biodegradable lubricants: an overview. Renew Sustain Energy Rev 16(1):764–774
22. Willing A (2001) Lubricants based on renewable resources–an environmentally compatible alternative to mineral oil products. Chemosphere 43(1):89–98
23. Fratila D (2009) Evaluation of near-dry machining effects on gear milling process efficiency. J Clean Prod 17(9):839–845
24. Klocke FAEG, Eisenblätter G (1997) Dry cutting. CIRP Ann 46(2):519–526
25. Sreejith PS, Ngoi BKA (2000) Dry machining: machining of the future. J Mater Process Technol 101(1–3):287–291
26. Sharma VS, Singh G, Sørby K (2015) A review on minimum quantity lubrication for machining processes. Mater Manuf Proc 30(8):935–953
27. Sharma AK, Tiwari AK, Dixit AR (2016) Effects of minimum quantity lubrication (MQL) in machining processes using conventional and nanofluid based cutting fluids: a comprehensive review. J Clean Prod 127:1–18
28. Rao RV (2007) Cutting fluid selection for a given machining application. In: Decision making in the manufacturing environment: using graph theory and fuzzy multiple attribute decision making methods. pp 97–114
29. Gajrani KK, Sankar MR (2018) Sustainable cutting fluids: thermal, rheological, biodegradation, anti-corrosion, storage stability studies and its machining performance. Encyclopedia of Renewable and Sustainable Materials. https://doi.org/10.1016/b978-0-12-803581-8.11152-x
30. Liew PJ, Shaaroni A, Sidik NAC, Yan J (2017) An overview of current status of cutting fluids and cooling techniques of turning hard steel. Int J Heat Mass Transf 114:380–394
31. Singh R, Bajpai V (2013) Coolant and Lubrication in Machining. Handbook of Manufacturing Engineering and Technology 1–34
32. Palanisamy S, McDonald SD, Dargusch MS (2009) Effects of coolant pressure on chip formation while turning Ti6Al4V alloy. Int J Mach Tools Manuf 49(9):739–743
33. Smith GT (2008) Cutting tool technology: industrial handbook. Springer Science & Business Media
34. Soković M, Mijanović K (2001) Ecological aspects of the cutting fluids and its influence on quantifiable parameters of the cutting processes. J Mater Process Technol 109(1–2):181–189
35. Schey JA (2000) Introduction to manufacturing processes, vol 3. McGraw-Hill, New York etc
36. Groover MP (2002) Fundamentals of modern manufacturing: materials processes, and systems. John Wiley & Sons
37. Michalek DJ, Hii WWS, Sun J, Gunter KL, Sutherland JW (2003) Experimental and analytical efforts to characterize cutting fluid mist formation and behavior in machining. Appl Occup Environ Hyg 18(11):842–854
38. Shokrani A, Dhokia V, Newman ST (2012) Environmentally conscious machining of difficult-to-machine materials with regard to cutting fluids. Int J Mach Tools Manuf 57:83–101

39. Bhuyan M, Sarmah A, Gajrani KK, Pandey A, Thulkar TG, Sankar MR (2018) State of art on minimum quantity lubrication in grinding process. Mater Today: Proc 5(9):19638–19647
40. Dhar NR, Kamruzzaman M, Ahmed M (2006) Effect of minimum quantity lubrication (MQL) on tool wear and surface roughness in turning AISI-4340 steel. J Mater Process Technol 172(2):299–304
41. Dhar NR, Ahmed MT, Islam S (2007) An experimental investigation on effect of minimum quantity lubrication in machining AISI 1040 steel. Int J Mach Tools Manuf 47(5):748–753
42. Gajrani KK, Ram D, Sankar MR, Dixit US, Suvin PS, Kailas SV (2017) Machining of hardened AISI H-13 steel using minimum quantity eco-friendly cutting fluid. Int J Addit Subtractive Mater Manuf 1(3–4):240–256
43. Kalpakjian S, Schmid SR (2010) Manufacturing engineering and technology. Prentice Hall, California, United States of America
44. Foulds L (2012) Cutting fluids. In: Rustemeyer T, Elsner P, John SM, Maibach HI (eds) Kanerva's occupational dermatology. Springer, Berlin Heidelberg, pp 715–725
45. Vieira JM, Machado AR, Ezugwu EO (2001) Performance of cutting fluids during face milling of steels. J Mater Process Technol 116(2–3):244–251
46. Burge H (2006) Machining coolants. The Environmental Reporter, Technical Newsletter, EMLab P&K 4
47. Shokrani A, Dhokia V, Newman ST (2012) Environmentally conscious machining of difficult-to-machine materials with regard to cutting fluids. Int J Mach Tools Manuf 57:83–101
48. Carlsson AS (2006) Production of wax esters in crambe. Outputs from the EPOBIO Project, CPL Press, Newbury, Berks, p 60
49. Pettersson A (2007) High-performance base fluids for environmentally adapted lubricants. Tribol Int 40(4):638–645
50. Norrby T (2003) Environmentally adapted lubricants–where are the opportunities? Ind lubr Tribol 55(6):268–274
51. Gajrani KK, Sankar MR, Dixit US (2018) Tribological performance of MoS_2-filled microtextured cutting tools during dry sliding test. J Tribol 140(2):021301(1–11)
52. Gajrani KK, Reddy RPK, Sankar MR (2018) Tribomechanical, surface morphological comparison of untextured, mechanical micro-textured (MμT) and coated MμT cutting tools during machining. In: Proceedings of the institution of mechanical engineers. Part J, Journal of Engineering Tribology. https://doi.org/10.1177/1350650118764975
53. Gajrani KK, Sankar MR, Dixit US (2018) Environmentally friendly machining with MoS_2-filled mechanically microtextured cutting tools. J Mech Sci Technol 32(8):3797–3805
54. Gajrani KK, Reddy RPK, Sankar MR (2016) Experimental comparative study of conventional, micro-textured and coated micro-textured tools during machining of hardened AISI 1040 alloy steel. Int J Mach Mach Mater 18(5–6):522–539
55. Gajrani KK, Suresh S, Sankar MR (2018) Environmental friendly hard machining performance of uncoated and MoS_2 coated mechanical micro-textured tungsten carbide cutting tools. Tribol Int 125:141–155
56. Gajrani KK, Sankar MR (2018) Sustainable machining with self-lubricating coated mechanical micro-textured cutting tools. In: Reference module in materials science and materials engineering. Elsevier. https://doi.org/10.1016/b978-0-12-803581-8.11325-6
57. Gajrani KK, Sankar MR (2017) State of the art on micro to nano textured cutting tools. Mater Today: Proc 4(2):3776–3785
58. Gajrani KK, Suvin PS, Kailas SV, Sankar MR (2019) Hard machining performance of indigenously developed green cutting fluid using flood cooling and minimum quantity cutting fluid. J Clean Prod 206:108–123
59. Gannon JE, Onyekewlu IU, Bennett EO (1981) BOD, COD and TOC studies of petroleum base cutting fluids. Water Air Soil Pollut 16(1):67–71
60. Gajrani KK, Ram D, Sankar MR (2017) Biodegradation and hard machining performance comparison of eco-friendly cutting fluid and mineral oil using flood cooling and minimum quantity cutting fluid techniques. J Clean Prod 165:1420–1435

61. Alves SM, de Oliveira JFG (2008) Vegetable based cutting fluid: an environmental alternative to grinding process. In: LCE 2008: 15th CIRP international conference on life cycle engineering: conference proceedings. CIRP, p 664
62. Sharma VS, Dogra M, Suri NM (2009) Cooling techniques for improved productivity in turning. Int J Mach Tools Manuf 49(6):435–453
63. Jayal AD, Balaji AK, Sesek R, Gaul A, Lillquist DR (2007) Machining performance and health effects of cutting fluid application in drilling of A390.0 cast aluminum alloy. J Manuf Process 9(2):137–146
64. Imran M, Mativenga PT, Gholinia A, Withers PJ (2014) Comparison of tool wear mechanisms and surface integrity for dry and wet micro-drilling of nickel-base superalloys. Int J Mach Tools Manuf 76:49–60
65. Naves VTG, DaSilva MB, Da Silva FJ (2013) Evaluation of the effect of application of cutting fluid at high pressure on tool wear during turning operation of AISI 316 austenitic stainless steel. Wear 302(1–2):1201–1208
66. Babic D, Murray DB, Torrance AA (2005) Mist jet cooling of grinding processes. Int J Mach Tools Manuf 45(10):1171–1177
67. Dhananchezian M, Kumar MP (2011) Cryogenic turning of the Ti–6Al–4V alloy with modified cutting tool inserts. Cryogenics 51(1):34–40
68. Wang ZY, Rajurkar KP, Fan J, Petrescu G (2002) Cryogenic machining of tantalum. J Manuf Process 4(2):122–127
69. Zhang S, Li JF, Wang YW (2012) Tool life and cutting forces in end milling Inconel 718 under dry and minimum quantity cooling lubrication cutting conditions. J Clean Prod 32:81–87
70. An QL, Fu YC, Xu JH (2011) Experimental study on turning of TC9 titanium alloy with cold water mist jet cooling. Int J Mach Tools Manuf 51(6):549–555
71. Dhar NR, Islam MW, Islam S, Mithu MAH (2006) The influence of minimum quantity of lubrication (MQL) on cutting temperature, chip and dimensional accuracy in turning AISI-1040 steel. J Mater Process Technol 171(1):93–99
72. Emami M, Sadeghi MH, Sarhan AAD, Hasani F (2014) Investigating the minimum quantity lubrication in grinding of Al_2O_3 engineering ceramic. J Clean Prod 66:632–643
73. Itoigawa F, Childs THC, Nakamura T, Belluco W (2006) Effects and mechanisms in minimal quantity lubrication machining of an aluminum alloy. Wear 260(3):339–344
74. Gajrani KK, Suvin PS, Sankar MR, Kailas SV (2016) Comparative studies on thermal, rheological behaviour of eco-friendly cutting fluids and their machining performance. In: Proceedings of the 6th international and 27th all india manufacturing technology design and research (AIMTDR) conference. pp 674–678
75. Kuram E, Ozcelik B, Demirbas E, Sik E (2010) Effects of the cutting fluid types and cutting parameters on surface roughness and thrust force. In: Proceedings of the world congress on engineering, Vol 2, pp 978–988
76. Paul S, Pal PK (2011) Study of surface quality during high speed machining using eco-friendly cutting fluid. Mach Technol Mater 11:24–28
77. Gupta K, Laubscher RF (2017) Sustainable machining of titanium alloys: a critical review. In: Proceedings of the institution of mechanical engineers. Part B: Journal of Engineering Manufacture. Vol 231, issue 14, pp 2543–2560
78. Khandekar S, Sankar MR, Agnihotri V, Ramkumar J (2012) Nano-cutting fluid for enhancement of metal cutting performance. Mater Manuf Process 27(9):963–967
79. Boswell B, Islam MN, Davies IJ, Ginting YR, Ong AK (2017) A review identifying the effectiveness of minimum quantity lubrication (MQL) during conventional machining. Int J Adv Manuf Technol 92(1–4):321–340
80. Sharma AK, Tiwari AK, Dixit AR (2016) Effects of minimum quantity lubrication (MQL) in machining processes using conventional and nanofluid based cutting fluids: a comprehensive review. J Clean Prod 127:1–18
81. Gajrani KK, Suvin PS, Kailas SV, Sankar MR (2019) Thermal, rheological, wettability and hard machining performance of MoS_2 and CaF_2 based minimum quantity hybrid nano-green cutting fluids. J Mater Process Technol 266:125–139

82. Sidik NAC, Samion S, Ghaderian J, Yazid MNAWM (2017) Recent progress on the application of nanofluids in minimum quantity lubrication machining: a review. Int J Heat Mass Transf 108:79–89
83. Sharma AK, Tiwari AK, Dixit AR (2015) Progress of nanofluid application in machining: a review. Mater Manuf Process 30(7):813–828

Titanium Machining Using Indigenously Developed Sustainable Cryogenic Machining Facility

Navneet Khanna and Chetan Agrawal

Abstract This chapter presents details of cryogenic machining of titanium alloys. It discusses different innovative methods used in literature for cryogenic machining of titanium alloys. A detailed methodology is presented to design a sustainable cryogenic fluid delivery setup. It also covers economic aspects of cryogenic machining in comparison to dry machining. Finally, a sustainable liquid nitrogen delivery setup is designed and developed to perform cryogenic machining of Ti-6Al-4V. The design of this retrofittable cryogen delivery solution for a range of available machine tools shall provide a direct cost based impetus for improving machining of such materials, which at present does not exist for indigenous industry. For experimental analyses, three machining process parameters i.e. the cutting speed (v), feed (f) and depth of cut (d), and different machining environment i.e. dry and cryogenic are selected. Response variables selected for this study are surface roughness, resultant force and power consumption. Experiments are designed as per hybrid design of experiments (DoE) technique. Hybrid DoE is a combination of orthogonal array and full factorial methods. To investigate the results, each combination of process parameters are compared under dry and cryogenic machining. Analysis of variance technique (ANOVA) is used to reveal the effect of process parameters on response variables. The results show that better surface finish obtained under cryogenic machining in comparison to dry machining. Results of power consumption suggest suitability of cryogenic machining over dry machining at higher levels of process parameters.

Keywords Cryogenic machining · Titanium · Surface quality · Analysis of variance

N. Khanna (✉) · C. Agrawal
Department of Mechanical Engineering, Institute of Infrastructure Technology Research and Management (IITRAM), Ahmedabad 380026, India
e-mail: navneetkhanna@iitram.ac.in

K. Gupta (ed.), *Materials Forming, Machining and Post Processing*, Materials Forming, Machining and Tribology, https://doi.org/10.1007/978-3-030-18854-2_8

Nomenclature

MQL	Minimum quantity lubrication
LN_2	Liquid nitrogen
m/min	Meter per minute
v	Cutting speed in m/min
f	Feed in mm/rev
d	Depth of cut in mm
F	Resultant force
F_t	Tangential force
F_f	Feed force
S/N ratio	Signal to noise ratio
DoE	Design of experiments

1 Introduction

In today's era of manufacturing technology, the world is processing many materials, which provide flexibility in terms of weight, cost and ergonomics of final components. High precision demand, market competition and stricter environmental legislations are the driving forces for manufacturing industries to improve and optimize the performance of machining processes. Turning, milling and drilling are common machining operations to get close tolerances on the final components. Factors like cutting fluid, tool geometry and cutting process parameters affect performance characteristics and cost of components [1].

To enhance the processes of machining, cutting fluid is one of the most important factors. According to a study [2], cutting fluid constitutes almost 16% of the total machining cost which includes purchasing of cutting fluid to the disposal of chips after machining and it increases up to 20% in case of difficult to cut materials [3]. The main function of cutting fluid is to dissipate heat from cutting zone during the machining operation. Conventionally, water and oil based cutting fluids are used during machining, but due to many techno-environmental problems, industries are forced to use less harmful cutting fluids. The other way to overcome this problem is to use the concept of minimum quantity lubrication (MQL). MQL technique also yields a small increase in cutting speed and tool-life with the better surface finish. It is effective in providing lubrication to the process, however, it is not promising in extracting heat from cutting region [4]. Therefore, the next generation challenge is to replace flood cooling and MQL with cryogenic machining [5].

Cryogenic machining is one of the most sustainable machining process. Sustainability has three dimensions i.e., economic, environmental and social. Economic advantage can be achieved using better manufacturing methods and lowering energy consumption. Low energy consumption will also reduce environmental damage.

Improved product quality and worker's safety will ensure social advantage of sustainability.

Recent research in the last decade shows that cryogenic machining is superior over convention machining techniques and MQL in terms of increased tool life and improved surface integrity. To take maximum advantage of cryogenic machining, proper penetration of cooling jet is required at the tool-chip interface [6]. It also yields contamination free, undistorted surface with reduced white layer formation which significantly contributes to the fatigue life of workpiece [7].

According to the National Institute of Standards and Technology (NIST), cryogenic temperature is considered below −180 °C (−292 °F or 93.15 K) [8]. This technique is most suitable for machining of heat resistant alloy and carbon fiber reinforcement composites. This study also focuses on one of the heat resistant alloy of titanium (Ti-6Al-4V).

Titanium alloys are extensively used in aviation, automobile, chemical, marine, biomedical and aerospace industries because of their ability to retain their properties under adverse working conditions. High corrosion resistance, high specific strength, high fatigue resistance and high strength at elevated temperature make titanium alloys suitable for critical applications [9, 10].

In terms of machining of titanium alloys, it comes in the category of difficult to cut materials. This is because of poor thermal conductivity, high chemical affinity at elevated temperature and low modulus of elasticity, which results in poor surface characteristics of the machined surface, increased tool wear and low production rate [11, 12].

To address this issue cryogenic machining of Ti-6Al-4V is investigated in this study. Most of the mentioned issues are due to high-temperature generation in the cutting zone, cryogenic machining is an emerging technique which is capable of dissipating heat quickly from cutting zone due to very low boiling point of LN_2 (−196 °C). LN_2 absorbs heat from cutting zone and evaporates into atmosphere leaving no harmful gases or environmental impact. Hence, it is safe for the worker's health and environment.

This chapter is presented broadly in six sections. The second section of this chapter discusses a detailed literature review of cryogenic machining of Ti-6Al-4V. Methodology to design sustainable cryogenic machining setup and economic aspects are discussed in Sects. 3 and 4 respectively. Section 5 discusses the cryogenic machining experimentation of Ti-6Al-4V. Results and discussion are presented in Sect. 6 of this chapter. Finally, the conclusions drawn from this study are presented.

2 Literature Review

The application of liquid nitrogen (LN_2) as a cutting fluid to improve machinability of titanium alloys are widely investigated by distinguished authors. Most of the studies consider Ti-6Al-4V as a workpiece material, and coated and uncoated carbide as tool material. Researchers demonstrated performance parameters improvement by

delivering LN_2 into the cutting zone using innovative methods, thus in this section systematic review of cryogenic machining of Ti-6Al-4V is presented.

At the start of the evolution of cryogenic machining, many studies performed with focus on the innovative approach to deliver LN_2 to the cutting zone. Hong et al. [13] provide a method to inject LN_2 through micro jets to the flank face, the rake face, or both near the cutting edge. The obtained results revealed tool wear reduction even at the high-speed due to a decrease in diffusion rate at low temperature. An increase in cutting force was reported under cryogenic machining due to increase in hardness of workpiece [14, 15]. Authors also concluded that it is sufficient to apply LN_2 only to the rake face for low-speed machining.

Dandekar et al. [16] proposed a new approach to machine Ti-6Al-4V by designing a hybrid experimental setup. They simultaneously heated the workpiece and cooled the cutting tool by using laser and liquid nitrogen, respectively as shown in Fig. 1.

Dhananchezian et al. [17] presented an innovative idea of supplying LN_2 through a hole in cutting insert. The schematic of the cooling delivery setup presented in Fig. 2 used for the machining of Ti-6Al-4V. LN_2 delivered to the tool rake face through a hole of dimension (Ø 2 mm × 2.5 mm) and at main and auxiliary flank surfaces through hole of dimension (Ø 1 mm × 2 mm) made on the tool insert as shown in Fig. 3. Authors reported that there is a decrease in cutting temperature (61–66%), the surface roughness (36%), cutting force (35–42%), and flank wear (27–39%) under cryogenic machining in comparison to wet machining.

Bordin et al. [18] proposed an idea to deliver LN_2 with two channels directed onto the rake and flank faces by means of external copper nozzles of 0.9 mm internal diameter. In this setup, LN_2 supplied from Dewar (equipped with safety valve and pressure regulator) through a vacuum insulated transfer line at a pressure of 1.5 MPa,

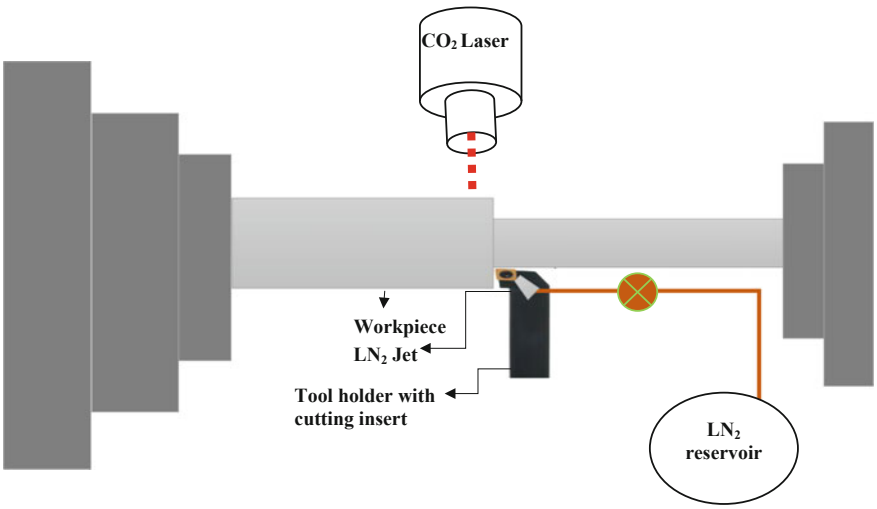

Fig. 1 Hybrid model (laser assistance + cryogenic cooling) based machining

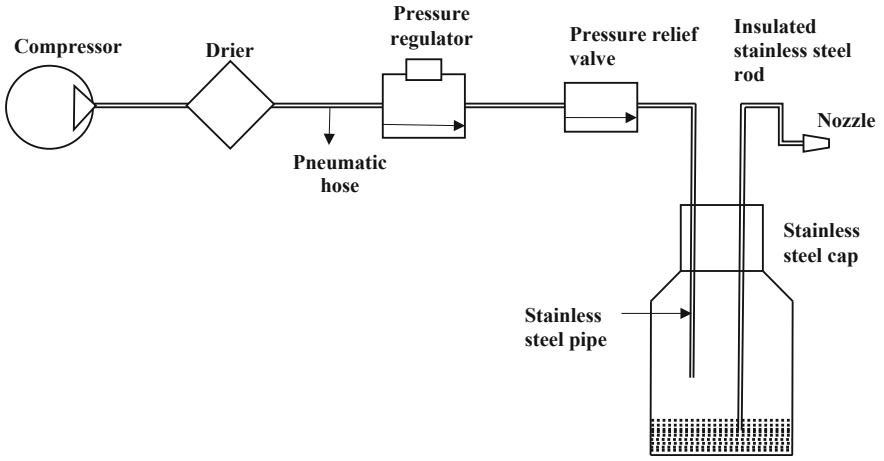

Fig. 2 LN_2 delivery system

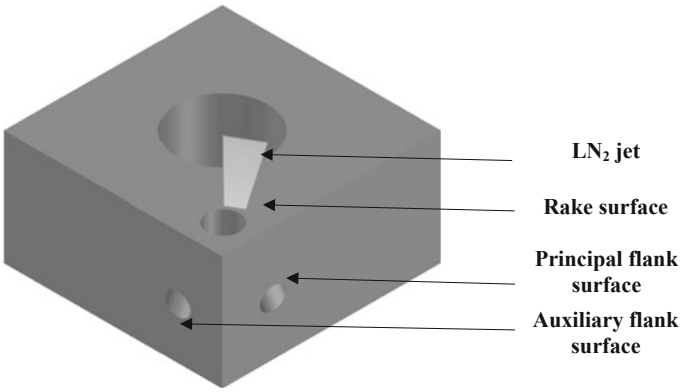

Fig. 3 Modified tool insert for effective cryogenic machining

resulting in a mass flow of 0.9 kg/min. Their experimental results show that cryogenic cooling is effective in reducing adhesive wear when machining of Ti-6Al-4V. They also investigated the feasibility of cryogenic machining of Ti-6Al-4V produced by additive manufacturing [19]. In this case, LN_2 was supplied through the nozzle of the internal diameter of 1 mm. They have reported better chip morphology and less tool wear under cryogenic machining as compared to conventional machining.

Venugopal et al. [20] used a trial and error method to set delivery parameters like pressure and flow rate to get a continuous flow of LN_2. Authors reported substantial improvement in tool life and concluded that the overcooling of workpiece can increase cutting force and may lead to embrittlement of the work material. In another study of tool wear [21], the effect of cryogenic milling of Ti-6Al-4V was compared with flood and dry cooling. In their study, nozzle position that was designed to have

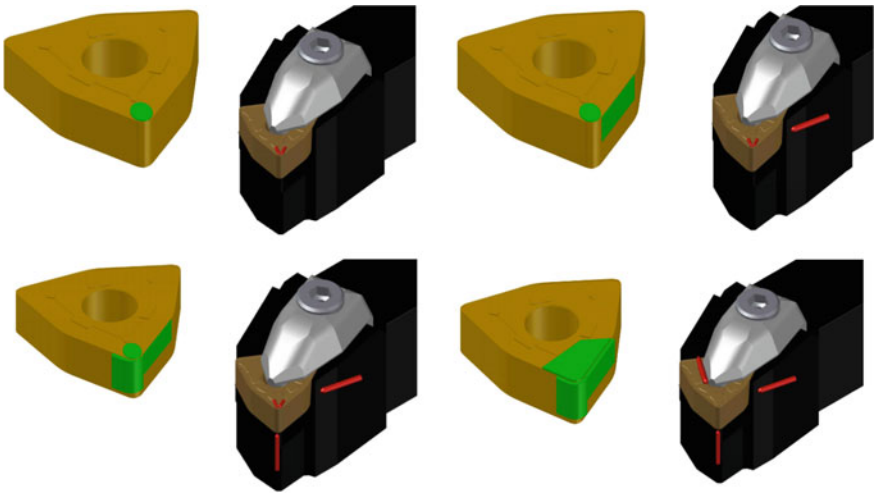

Fig. 4 Schematic of the method of cryogenic fluid delivery

a 0.5 mm clearance on each side from the cutting tool, delivery pressure and flow rate were used 0.15 MPa and 0.4 L/min respectively. They reported a significant reduction in surface roughness (30–40%) and reduced thermally induced tool wear. In another study authors developed customized insulated modular system. It can be easily attached or detached from the tool holder and delivery angle can also be controlled by a further pivot nozzle function [22]. The LN_2 was supplied at a pressure of 0.4 MPa at a flow rate of 0.35 L/min through nozzles at rake and flank face, a positive effect was reported on tool wear and chip morphology in comparison to flood cooling.

Bermingham et al. [23] supplied LN_2 through copper nozzle of 1.77 mm internal diameter at 0.8 MPa pressure. They reported a delay in the rate of abrasive wear on the flank face but wear is found to be concentrated on the nose of the tool (where the coolant was not delivered) and the result also shows that there was an increase in thrust force and a decrease in feed force. Bermingham et al. [24] presented different methods of cryogenic fluid delivery as shown in Fig. 4.

The effect of cryogenic cooling on surface integrity for Ti-6Al-4V was investigated by different authors. Rotella et al. [25] reported a significant improvement in product surface characteristics. They supplied LN_2 at a pressure of 1.2 MPa through a 2 mm nozzle. Ahmed et al. [26] also reported improvement in tool life, surface finish, and chip breakability. In this case, LN_2 was supplied at a pressure of 0.4 MPa to the tool–work interfaces. Sartori et al. [27] used LN_2 delivery pressure 1 ± 0.05 MPa and reported a lower amount of surface defects and higher values of the residual compressive stress in comparison to dry cutting, but a general worsening of the surface topography was reported in their study.

Hanenkamp et al. [28] proposed an innovative method to deliver MQL and cryogenic fluid (Liquid CO_2 in this case) through a single channel. Authors reported better surface finish in comparison to wet machining.

Sun et al. [29] investigated the effect of cryogenic machining on Ti-5553. LN_2 was supplied at a pressure of 1.5 MPa and flow rate of approximate 0.6 L/min at the tool rake face. They found a reduction in thrust force (up to 30%) and better surface finish when compared with MQL and flood cooling.

Schoopa et al. [30] performed a high-speed cryogenic finishing operation on Ti-6Al-4V with the polycrystalline diamond tool and suggested this process as an alternative to grinding. They supplied LN_2 at a pressure of 1.5 MPa and flow rate approximately 0.6 L/min with an internal nozzle diameter of 3 mm on flank side of the tool.

Mia et al. [31] performed multi-objective optimization and life cycle assessment for LN_2 assisted machining of Ti-6Al-4V and compared surface roughness, cutting force and material removal rate under dry, mono-jet and the dual-jet of LN_2. A flow rate of 2 L/min was taken for mono-jet and 3 L/min for the dual-jet. They reported better results under dual-jet LN_2 assisted cryogenic machining in comparison to mono-jet LN_2 assisted cryogenic machining and dry machining.

Recently, there has been growing interest in numerical modeling of cryogenic machining. It includes prediction of the thermo-mechanical behavior of tool holder under the cryogenic condition to reduce dimensional deviations [32]. A model to predict cutting forces, temperature, and machining-induced microstructural alterations during semi-finish turning of Ti-6Al-4V under dry and cryogenic conditions reported in the literature [33]. Umbrello et al. [34] presented a model to predict microstructure, plastic deformation and nano-hardness induced by cryogenic machining. Modeling of thermal phenomena occurring between jet and workpiece interface is also reported by researchers [35]. In their study authors concluded that the most influential parameters of the thermal distribution and heat transfer coefficient are pressure, nozzle diameter, projection angle and the distance between the nozzle and the workpiece surface. In another study, a numerical analysis based on computational fluid dynamics presented to optimize cryogenic fluid flow inside the channel [36]. In their study, best inlet pressure and liquid/gas volume fraction values reported was 0.6 MPa and 90%; respectively. This inlet pressure and liquid/gas volume fraction combination gave a minimum temperature and maximum pressure at the outlet.

On the basic of current literature review for cryogenic machining of titanium alloys, it is found that cryogenic machining significantly contributes to attain improved production rate, reduced tool wear and better surface integrity. In recent years, researchers had focused on the numerical modeling of cryogenic machining to optimize LN_2 delivery setup parameters for further improvement of this sustainable technique.

Based on the above literature review a systematic methodology to design sustainable cryogenic fluid delivery setup is presented in the next section. In literature, very few researchers have focused on the economy of cryogenic machining. Therefore a section is included in this chapter to discuss the economic advantages of cryogenic machining.

3 Methodology to Design Cryogenic Fluid Delivery Setup

Nitrogen has high liquid-to-gas expansion ratio (1:699) and extremely low boiling point (77 K). Any heat interaction of LN_2 with the environment will quickly convert it into vapor form and because of high expansion ratio, the pressure rises quickly inside closed vessels. To prevent any damage to delivery system proper safety valves and insulation must be used for each component. Extreme low temperature can also cause cool burns to human operators if handled carelessly. Cryogenic safety hand gloves, face shield, and other safety measures must be taken before conducting cryogenic machining.

Figure 5 shows major components of LN_2 delivery setup. This section provides a systematic methodology to design efficient cryogenic fluid delivery setup. The method for selection of input delivery pressure is discussed in the first subsection, the method of selecting nozzle is discussed in the second subsection and method of designing transfer line is a discussed in subsection third.

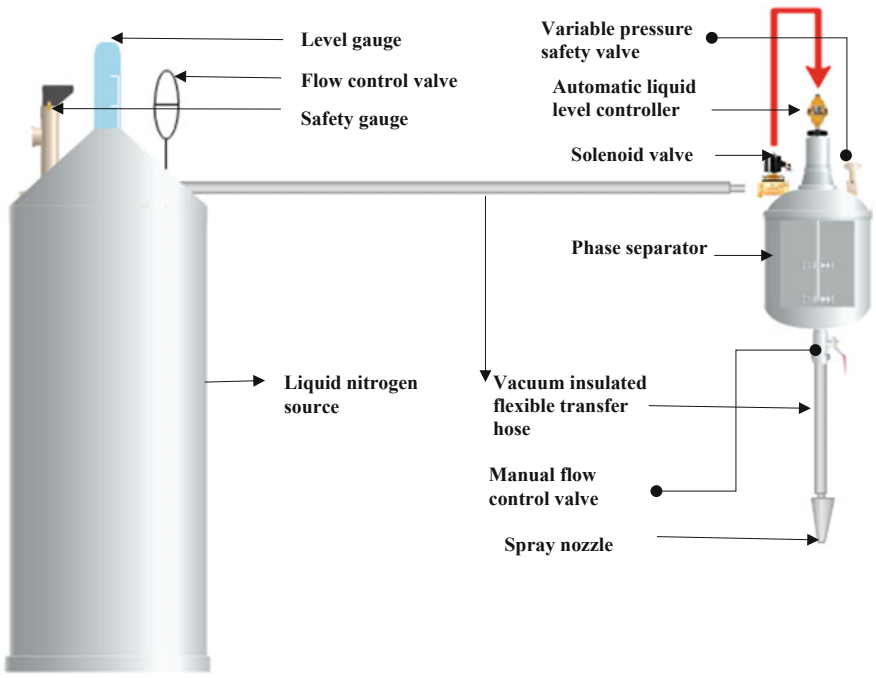

Fig. 5 Schematic of the developed LN_2 delivery setup for cryogenic machining

3.1 Selection of Delivery Pressure and Flow Rate of Cryogenic Fluid

Selection of inlet pressure is critical, as it affects outlet (cutting zone) condition of the cryogenic fluid. Optimum pressure can be selected from nitrogen phase equilibrium diagram, as the pressure increases, temperature range also increases for which nitrogen does not change from a liquid into vapor. For this reason, many authors tried to keep high pressures near 1.5 MPa, but high pressure creates a problem of turbulence and throttling of the cryogenic fluid and converts LN_2 into vapor. So to make an efficient delivery system, optimum pressure is very important to get the desired flow of cryogenic fluid in the liquid phase.

The excess flow rate of the cryogenic fluid at the cutting zone may alter properties of a workpiece and its dimensional accuracy due to overcooling of workpiece. In literature, an increase in cutting force is also reported due to overcooling of the workpiece. To prevent the adverse effect at extremely low temperature, the optimum flow rate of the cryogenic fluid must be selected. In literature, the flow rate from 0.5 to 3 L/min is used to perform cryogenic machining.

3.2 Selection of Delivery Nozzle at the Outlet

The best methods to deliver cryogenic fluid into the cutting zone can be chosen from available methods such as a channel from tool holder and tool to cool the cutting edge, cooling channel through the spindle and the spray cooling in machining zone. The appropriate method must be selected according to the machining requirement. To choose appropriate nozzle dimensions, the flow pattern and output velocity can be investigated using computational fluid dynamics for given input parameters. In literature, the nozzle of 0.9–3 mm diameter is used to perform cryogenic machining.

3.3 Designing of the Cryogenic Fluid Delivery Transfer Line

Cryogenic fluid transfer line is one of the major components used in any cryogenic fluid delivery setup. This transfer line is used to transport cryogenic fluid from source to the point of application at very low temperature. Complete insulation of the transfer line is impossible, so there is always a possibility of mixed-phase flow. To deliver the nitrogen in the pure liquid form a phase separator can be installed near the cutting zone. Designing of the transfer line can be done using the steady flow energy equation for single phase flow considering frictional, entry and exit losses in the design. The suitable factor of safety must be considered while designing the transfer line due to a high expansion ratio of LN_2.

Efficient working of cryogenic fluid delivery setup depends on factors such as flow aggressiveness, delivery phase, nozzle positioning, suitable valve selection and phase separator dimensions. To control the phase of the nitrogen a self-patented phase separator is designed and developed in the current study [37].

Cryogenic machining technique is not necessary to be a good option for machining of every material. It is mostly beneficial for heat resistant alloys. So it is necessary that the delivery system must be designed and fabricated in such a way that it is compatible and retrofittable with the existing machining facility, so that no extra machine setup cost is required.

4 Economic Aspect of Cryogenic Machining

The economic aspect of machining includes the cost of LN_2, chip management cost, cost of worker's health and safety and cost of quality.

- Cost of liquid nitrogen: If cost is compared on per liter basis, the price of one liter of LN_2 ($0.25–0.42) is approximately equal to the price of one-liter mineral water and if LN_2 is produced in-house, cost of LN_2 can be further reduced. In terms of availability of LN_2, it is readily available, as there is a lot of commercial supplier all over the world who are providing refilling of tanks at a competitive price.
- Chip management cost: Second important aspect of machining is chip disposal. Oil-based cutting fluid makes chips heavy and sticky and it is necessary to process oily chips before disposal into the environment as per government regulations. However, in the case of cryogenic machining, LN_2 quickly absorbs heat from cutting zone and evaporates into the atmosphere at normal temperature and pressure (NTP) leaving the chip absolutely dry and clean. It is easy to dispose dry chips rather than oily and heavy chips. Hence, the cost of management of chips can be reduced using the cryogenic machining technique.
- Cost of worker health and safety: Clean, healthy and safe working environment increases the productivity of the workforce and helps to keep them motivated. During machining, the high temperature is generated in the cutting zone. At this high-temperature chemical affinity between tool-workpiece-coolant increases and generates toxic fumes and mist environment. These toxic fumes and mist environment are causes of dermatitis, bronchitis and lungs problems for machine tool operators. LN_2 as a coolant provides a sustainable option due to its inert nature and ability to drastically reduce the temperature of the cutting zone. Hence cryogenic machining is greener and safer operation in comparison conventional machining techniques.
- Cost of quality: This is the cost involved to make product resourceful and to increase the reliability of specific output for the given period. The cryogenic machined components have proven improved surface characteristics and fatigue life. It also reduces cost by increasing the production rate and tool life. Hence,

cryogenic machining can reduce the cost of quality in comparison to conventional machining techniques.

For cryogenic machining, it requires an initial cost for LN_2 delivery set up as a fixed cost and cost of LN_2 as a variable cost. Improved surface characteristics, fatigue behavior, production rate and tool life are some proven aspect of cryogenic machining which can compensate its fixed and variable cost and it can be a case be most economical and sustainable option in comparison to conventional machining techniques.

5 Experimental Study on Cryogenic Machining of Ti-6Al-4V

Turning is an effective method to induce compressive nature of residual stress in the component due to high magnitude of strain and strain rates involved in machining, but temperature generation and its acceleration is a major challenge. The assistance of LN_2 as a coolant helps to dissipate heat generated during machining and it results in desirable residual stress induced in the machined components. Hence, cryogenic machining is considered as a critical factor for improving the surface properties of Ti-6Al-4V. However, the quantity of LN_2 applied in the cutting zone must be controlled otherwise it may adversely affect workpiece and results into increased cutting forces.

Performance measures such as energy consumption and surface integrity of product are useful for industries to take decisive action. Generally, machine tools are designed as per peak power required during machining. However, it also consumes power in its idle state. Idle state includes pre-machining setup and posts machining work. If process parameters of machining are optimized than machine tools can be designed to use lower power rated motors, driver and auxiliary equipment and it will reduce overall power consumption [38].

In this study, the work material is Ti-6Al-4V and tool material is coated carbide. This combination frequently used in industries. Response variables investigated are surface roughness, resultant force and power consumption. Effect of cryogenic assistance in machining compared with dry machining of Ti-6Al-4V.

5.1 Research Methodology

In order to estimate the effect of cryogenic machining in comparison to dry machining for turning of Ti-6Al-4V, hybrid DoE technique is used. Most of the data and instructions to select input process parameters for machining are available either for flood or dry machining. Since tool material behavior is temperature dependent, so to get optimum process parameters it is necessary to evaluate machining response

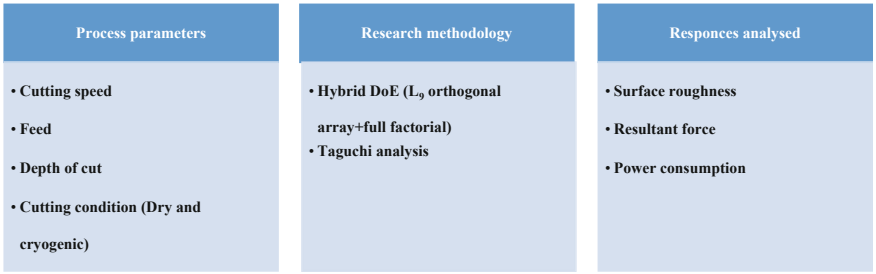

Fig. 6 Experimental design and analysis flow chart

under different machining environment. Machining under cryogenic environment may alter response behavior of the process.

Hybrid DoE is a combination of orthogonal array and full factorial methods. To get Hybrid DoE, L_9 orthogonal array was repeated for dry and cryogenic machining to effectively compare results under both environments for each process parameter combinations. Three levels of cutting speed, feed and depth of cut are taken to generate L_9 orthogonal array. Each experiment is repeated three times to minimize random error.

Three response variables namely surface roughness, resultant force and power consumption are recorded during experiments. A Taylor Hobson Sutronic S128 contact type surface roughness tester is used to check the surface finish of workpiece. Kistler dynamometer configured with DynoWare software for data acquisition is used to analyze resultant forces. Power consumption during machining is measured using Fluke 435 (series II) three phase energy and power quality analyzer (Fig. 6).

$$\text{S/N ratio} = -10\ \log\left(\sum\left(\text{Y}^2\right)/\text{n}\right) \tag{1}$$

For Taguchi analysis, the response can be classified into three ways: smaller-the-better, nominal-is-best and larger-the-better characteristics. In this study, all the responses are of the smaller-the-better characteristics type. Equation 1 is used to calculate S/N ratio of responses. Where n is number of observation and Y is the value of the observed data. The machining experiments are performed on a conventional lathe machine retrofitted with an external cryogenic delivery system. LN_2 is stored in Dewar at 1.5 MPa. A vacuum insulated transfer line is used to transfer LN_2 from Dewar to point of application. In order to apply LN_2 in the form of the jet on the rake face of cutting tool, a nozzle of 1 mm is used. Kyocera made TiAlN coated carbide turning insert (CNMG120408CQ) is selected as cutting tool. To minimize the effect of tool wear, new cutting edge is used for each experiment. Cylindrical rods of 40 mm diameter and 150 mm length of Ti-6Al-4V are taken as a workpiece (Fig. 7).

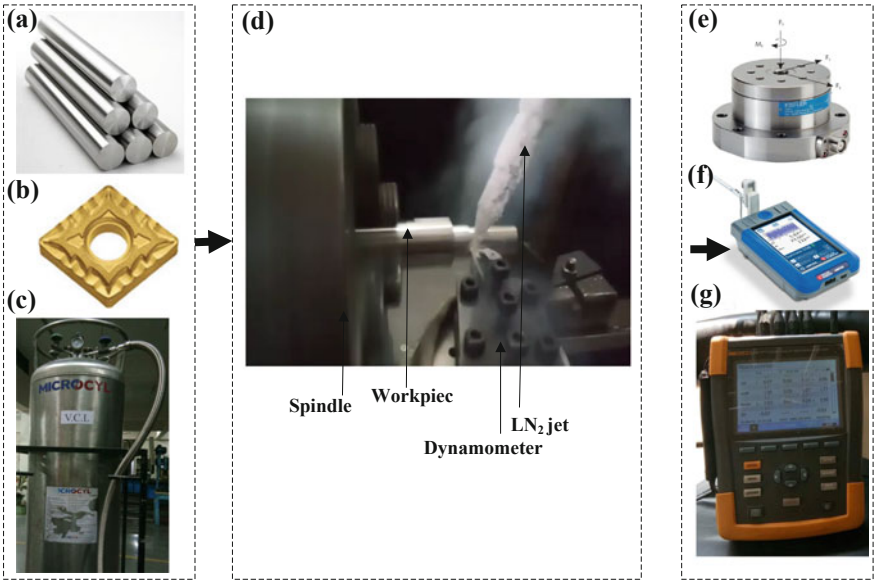

Fig. 7 Experimental setup components: **a** Ti-6Al-4V workpiece; **b** Carbide tool; **c** Liquid nitrogen source; **d** Conventional lathe machining; **e** Dynamometer; **f** Surface roughness tester; **g** Energy and power quality analyzer

6 Results and Discussion

In this section, experimental results are discussed. In first subsection surface roughness obtained during cryogenic machining and dry machining is discussed. Second and third subsections discuss the outcomes of the resultant force and power consumption respectively.

6.1 Surface Roughness

The experimental results and signal to noise (S/N) ratios for surface roughness are shown in Table 1, for the dry and the cryogenic machining. The comparative graph in Fig. 8 shows the variation of surface roughness under dry and cryogenic machining. Surface roughness is reduced at most of the combination of process parameters in case of cryogenic machining as compared to dry machining. Higher value of surface roughness is obtained under dry machining at lower cutting speed as compared to cryogenic machining.

Figure 9 shows main effects plot for S/N ratios. The effect of process parameter on surface roughness are in order of: feed > depth of cut > speed, in case of dry machining and speed > feed > depth of cut, in case of cryogenic machining. Feed

Table 1 The experimental results for surface roughness and S/N ratios

Experiment run no.	Process parameters			Average of responses		S/N ratio (dB)	
				Surface roughness (R_a)			
	v (m/min)	f (mm/rev)	d (mm)	Dry machining	Cryogenic machining	Dry machining	Cryogenic machining
Run 1	104.93	0.111	0.5	1.17	0.81	−1.36	−0.98
Run 2	104.93	0.222	1	1.25	1.04	0.35	−0.34
Run 3	104.93	0.333	1.5	1.29	1.21	−2.21	−1.66
Run 4	69.94	0.111	1	0.92	1.05	0.72	−0.42
Run 5	69.94	0.222	1.5	1.32	1.00	−2.41	0.00
Run 6	69.94	0.333	0.5	1.17	1.13	−1.36	−1.06
Run 7	46.62	0.111	1.5	1.00	0.80	0.92	1.94
Run 8	46.62	0.222	0.5	1.40	0.85	−2.92	1.41
Run 9	46.62	0.333	1	1.21	0.89	−2.01	1.01

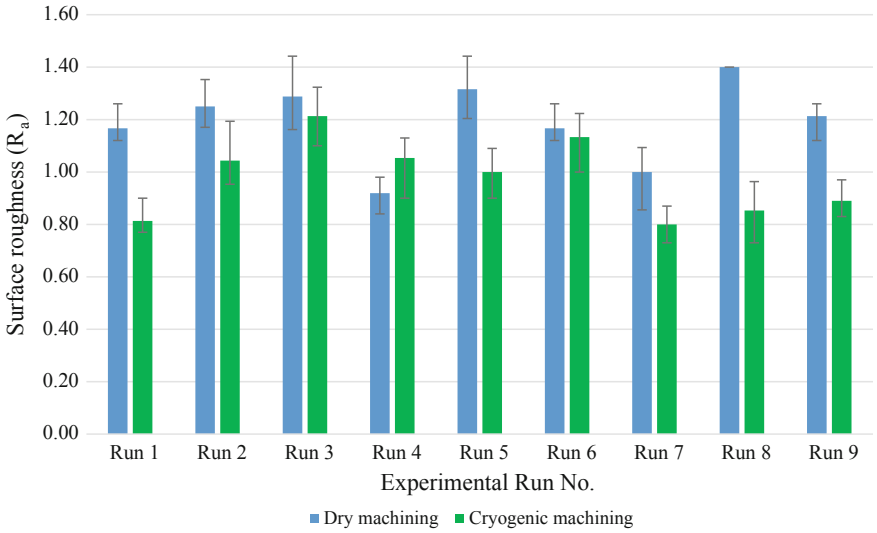

Fig. 8 Comparison of surface roughness under dry and cryogenic machining

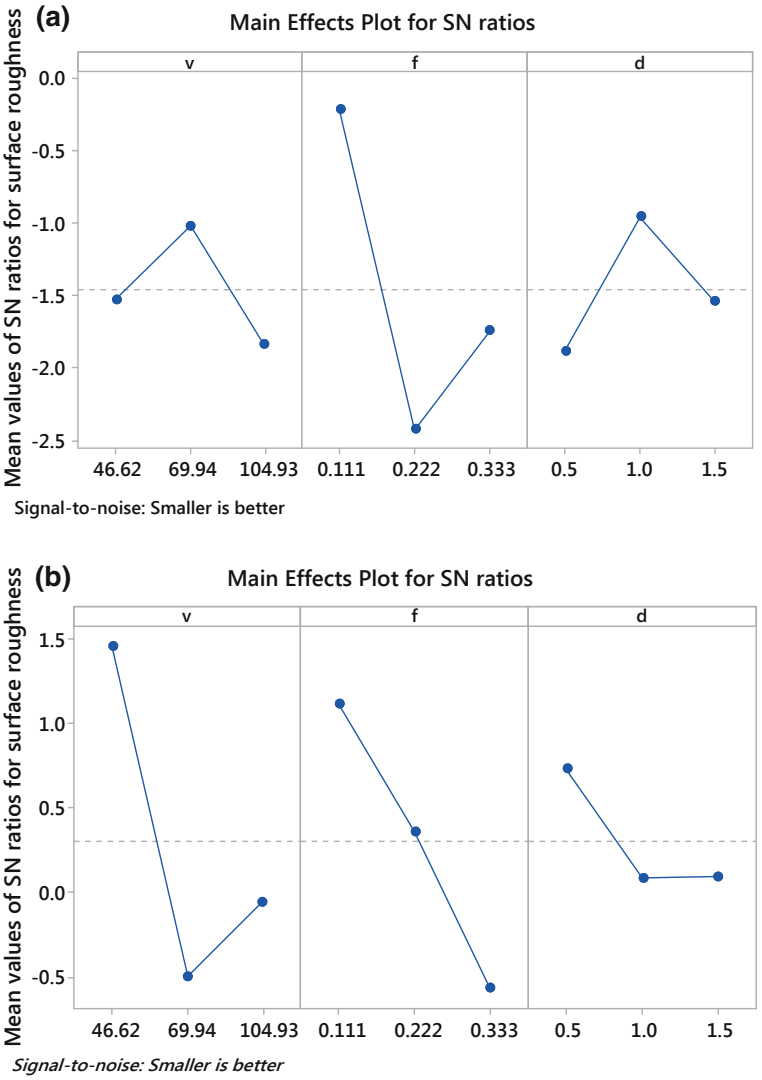

Fig. 9 Main effects plots for surface roughness **a** under dry machining; **b** under cryogenic machining

is a significant factor in dry machining as excepted but under cryogenic machining effect of speed on surface roughness is greater in comparison to feed and depth of cut.

The combined effect of proper combination of cutting speed, feed, depth of cut and the cutting environment is the possible reason for such behavior of surface roughness under cryogenic machining. At high cutting speed (104.93 m/min) up to 30%

improvement observed under cryogenic machining as compared to dry machining. At medium (69.94 m/min) and low (46.62 m/min) cutting speed, improvement up to 24% and 39% is observed respectively under cryogenic machining as compared to dry machining.

6.2 Resultant Forces

The experimental results for resultant forces and the signal to noise (S/N) ratios are shown in Table 2. Resultant forces calculated as per Eq. 2. Figure 10 shows the effect of machining process parameter on resultant forces under dry and the cryogenic cutting condition.

$$F = \sqrt{F_t^2 + F_f^2} \tag{2}$$

where F denotes the resultant force, F_t is the tangential and F_f is feed force.

Figure 11 shows the main effect plot of S/N ratio to signify the effect of process parameters on resultant forces in the order: depth of cut > feed > speed, for both dry and cryogenic machining. At a higher depth of cut, cutting area to be removed increases hence resultant forces increases. There is less significance of cutting condition as resultant forces are comparable for both dry and cryogenic machining.

Table 2 The experimental results for resultant force and S/N ratios

Experiment run no.	Process parameters			Average of responses		S/N ratio (dB)	
				Resultant force (N)			
	v (m/min)	f (mm/rev)	d (mm)	Dry machining	Cryogenic machining	Dry machining	Cryogenic machining
Run 1	104.93	0.111	0.5	94.22	109.81	−39.48	−40.81
Run 2	104.93	0.222	1	344.64	322.16	−50.75	−50.16
Run 3	104.93	0.333	1.5	602.67	716.68	−55.60	−57.11
Run 4	69.94	0.111	1	110.46	150.57	−40.86	−43.55
Run 5	69.94	0.222	1.5	503.82	464.40	−54.05	−53.34
Run 6	69.94	0.333	0.5	183.98	169.66	−45.30	−44.59
Run 7	46.62	0.111	1.5	414.13	365.81	−52.34	−51.27
Run 8	46.62	0.222	0.5	229.39	185.12	−47.21	−45.35
Run 9	46.62	0.333	1	138.34	396.47	−42.82	−51.96

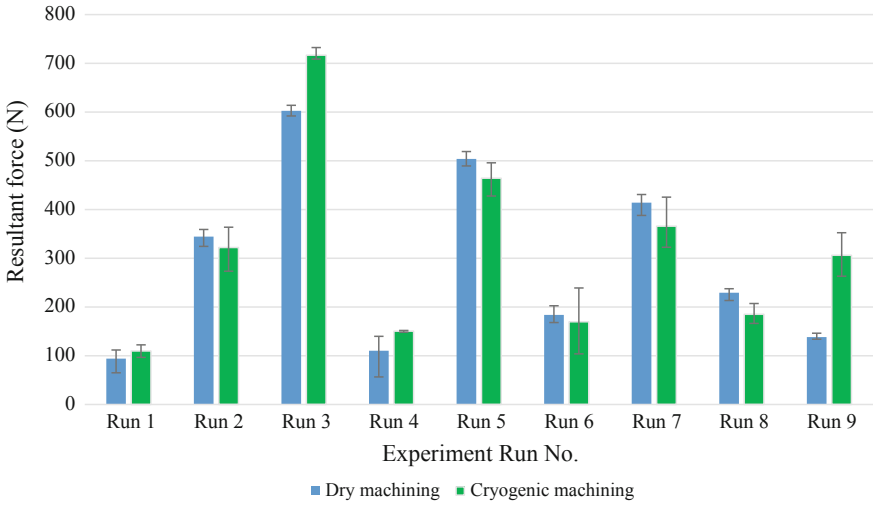

Fig. 10 Comparison of resultant force under dry and cryogenic machining

6.3 Power Consumption

The experimental results power consumption and the signal to noise (S/N) ratios are shown in Table 3 for the dry and the cryogenic machining. Figure 12 show power consumption at each combination of process parameters under dry and cryogenic machining. At lower speed power consumption for cryogenic machining increases significantly as compared to dry machining.

Figure 12 shows main effects plot of S/N ratios signify the effect of process parameter on power consumption in order: depth of cut > speed > feed, for both dry machining and cryogenic machining.

- In the first three experimental runs (1–3) cutting speed is constant and feed and depth of cut are in increasing order. It can be observed from Fig. 13 that power consumption is increasing for both dry and cryogenic machining. This is because with increment in depth of cut, cutting area increases and force required to remove bigger area also increases, which tends to consume more power.

In case of cryogenic machining, power consumption is less than dry machining at a higher depth of cut. This is due to the capability of cryogenic machining to extract a large amount of heat produced in cutting zone. Reduction in heat helps to maintain a low coefficient of friction. Hence, power consumption is less in the case of cryogenic machining.

- In the next three experimental runs (4–6) as cutting speed decreases, power consumption decreases for dry machining as expected. In case of cryogenic machining power consumption did not decrease.

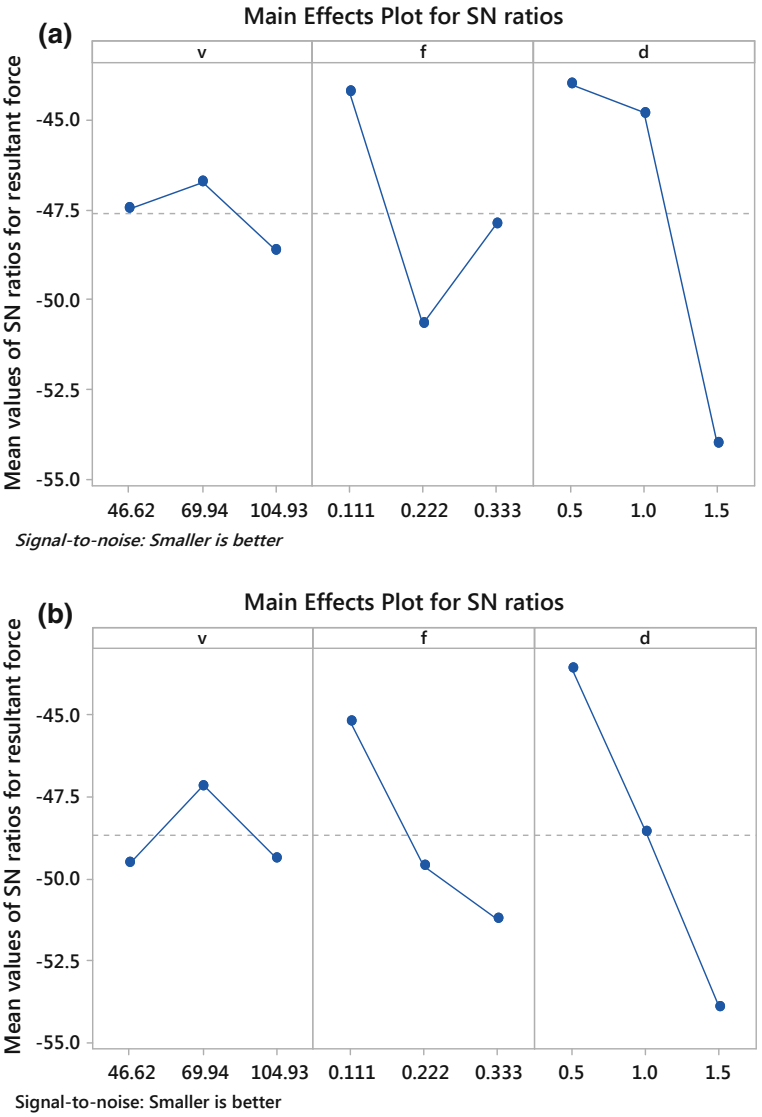

Fig. 11 Main effects plots for resultant forces **a** under dry machining; **b** under cryogenic machining

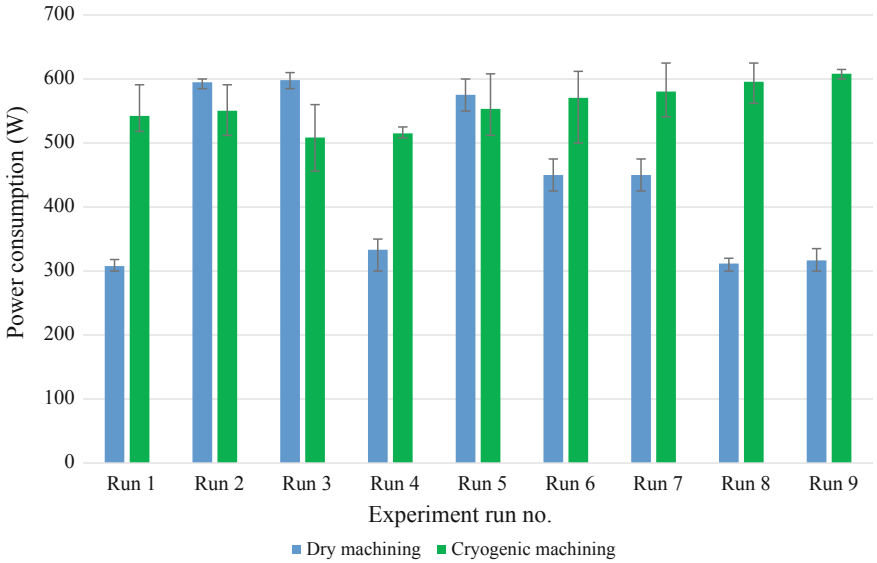

Fig. 12 Comparison of power consumption under dry and cryogenic machining

- In the last three experimental runs (7–9) as cutting speed further decreases, power consumption does not decrease for cryogenic machining. Thus, it is inferred that cryogenic machining is less suitable at low cutting speed when power consumption

Table 3 The experimental results for power consumption and S/N ratios

Experiment run no.	Process parameters			Average of responses		S/N ratio (dB)	
				Power consumption (N)			
	v (m/min)	f (mm/rev)	d (mm)	Dry machining	Cryogenic machining	Dry machining	Cryogenic machining
Run 1	104.93	0.111	0.5	307.67	542.33	−49.76	−54.69
Run 2	104.93	0.222	1	595.00	550.33	−55.49	−54.81
Run 3	104.93	0.333	1.5	598.33	508.67	−55.54	−54.13
Run 4	69.94	0.111	1	333.33	515.00	−50.46	−54.24
Run 5	69.94	0.222	1.5	575.33	553.33	−55.20	−54.86
Run 6	69.94	0.333	0.5	450.00	570.67	−53.06	−55.13
Run 7	46.62	0.111	1.5	450.00	580.33	−53.06	−55.27
Run 8	46.62	0.222	0.5	311.67	595.67	−49.87	−55.50
Run 9	46.62	0.333	1	316.67	608.33	−50.01	−55.68

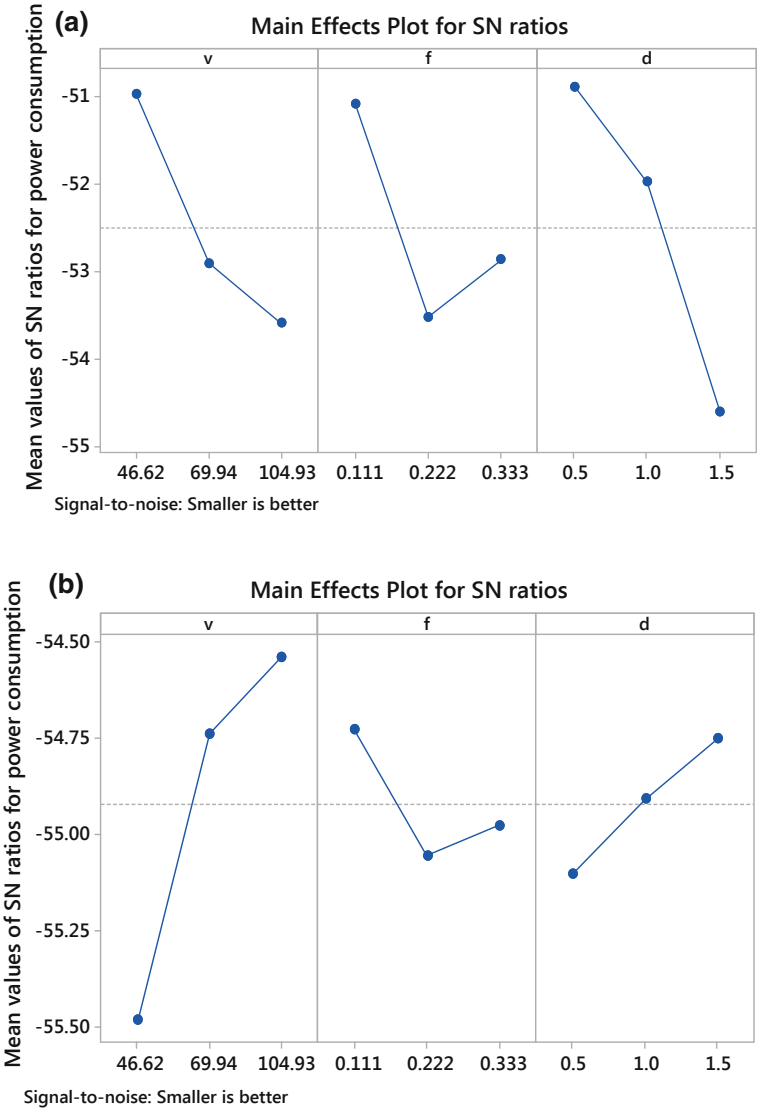

Fig. 13 Main effects plots for power consumption **a** under dry machining; **b** under cryogenic machining

is a priority. However, in the case of dry machining power consumption decreases at lower cutting speed as expected.

7 Conclusions

Experimental observations reported in this research work recommend that the use of cryogenic coolant in machining of Ti-6Al-4V titanium alloy significantly affect the surface roughness and power consumption. In particular, cryogenic cooling conditions offer better surface roughness. It is observed that at higher cutting parameters cryogenic machining leads to better results and can extend product life and performance. On the basis of the above discussions following conclusions can be drawn:

- Average surface roughness improves up to 40% at most of the combinations of process parameters under cryogenic machining as compared with dry machining. Thus it is advisable to prefer cryogenic machining for improved surface properties.
- Resultant forces are comparable for both dry and cryogenic machining. The most significant parameter which affects the resultant forces is the depth of cut. It is due to the increase in cutting area with an increment of depth of cut. Increment in cutting area requires a larger force during machining.
- From power consumption analysis, it is observed that as cutting speed decreases, power consumption in the case of cryogenic machining is significantly higher than dry machining. Thus, cryogenic machining is more suitable for high-speed machining of Ti-6Al-4V. However, surface finish under cryogenic machining significantly improves at lower speed.

The design of this retrofittable cryogen delivery solution for a range of available machine tools shall provide a direct cost based impetus for improving machining of such materials, which at present does not exist for the indigenous industry.

Acknowledgements The authors would like to thank the SERB-DST, Government of India, for the financial support given under the Project (ECR/2016/000735), titled "Design and Development of Energy Efficient Cryogenic Machining Facility for Heat Resistant Alloys and Carbon Fibre Composites".

References

1. Pusavec F, Krajnik P, Kopac J (2010) Transitioning to sustainable production—Part I: application on machining technologies. J Clean Prod 18:174–184
2. Narutaki N, Yamane Y, Tashima S, Kuroki H (1997) A new advanced ceramic for dry machining. CIRP Ann—Manuf Technol 46:43–48
3. Shokrani A, Dhokia V, Newman ST (2012) Environmentally conscious machining of difficult-to-machine materials with regards to cutting fluids. Int J Mach Tools Manuf 57:83–101

4. Boswell B, Islam MN, Davies IJ, Ginting YR, Ong AK (2017) A review identifying the effectiveness of minimum quantity lubrication (MQL) during conventional machining. Int J Adv Manuf Technol, 1–20
5. Kaynak Y, Karaca HE, Noebe RD, Jawahir IS (2013) Tool-wear analysis in cryogenic machining of NiTi shape memory alloys: a comparison of tool-wear performance with dry and MQL machining. Wear 8:51–63
6. Venugopal KA, Paul S, Chattopadhyay AB (2007) Growth of tool wear in turning of Ti-6Al-4V alloy under cryogenic cooling. Wear 262:1071–1078
7. Zurecki Z, Ghosh R, Frey JH, Products A (2003) Investigation of white layers formed in conventional and cryogenic hard turning of steels. In: Proceedings of the IMECE'03, pp 1–10
8. Gunston B (2009) The Cambridge aerospace dictionary, vol 53
9. Ezugwu EO (2005) Key improvements in the machining of difficult-to-cut aerospace superalloys. Int J Mach Tools Manuf 45:1353–1367
10. Mathonsi T, Laubscher R, Gupta K (2018) Investigation on high speed machining of titanium grade 2 under MQL conditions. Adv Manuf Technol XXXII. In: Proceedings of 16th international conference on manufacturing research ICMR. 33rd national conference on manufacturing research, 11–13 Sept 2018. IOS Press, Univ. Skövde, Sweden, vol 8, p 69
11. Khanna N, Davim JP (2015) Design-of-experiments application in machining titanium alloys for aerospace structural components. Meas J Int Meas Confed 61:280–290
12. Gupta K, Laubscher RF (2017) Sustainable machining of titanium alloys: a critical review. Proc Inst Mech Eng Part B J Eng Manuf 231:2543–2560
13. Hong SY (1999) Cryogenic machining. US PATENTS 5,901,623
14. Hong SY, Ding Y, Jeong J (2002) Experimental evaluation of friction coefficient and liquid nitrogen lubrication effect in cryogenic machining. Mach Sci Technol 6:235–250
15. Wang J, Zou H, Li C, Qiu S, Shen B (2006) The effect of microstructural evolution on hardening behavior of type 17–4PH stainless steel in long-term aging at 350 C. Mater Charact 96:274–280
16. Dandekar CR, Shin YC, Barnes J (2010) Machinability improvement of titanium alloy (Ti-6Al-4V) via LAM and hybrid machining. Int J Mach Tools Manuf 50:174–182
17. Dhananchezian M, Pradeep Kumar M (2011) Cryogenic turning of the Ti-6Al-4V alloy with modified cutting tool inserts. Cryogenics (Guildf) 51:34–40
18. Bordin A, Sartori S, Bruschi S, Ghiotti A (2017) Experimental investigation on the feasibility of dry and cryogenic machining as sustainable strategies when turning Ti6Al4V produced by additive manufacturing. J Clean Prod 142:4142–4151
19. Bordin A, Bruschi S, Ghiotti A, Bariani PF (2015) Analysis of tool wear in cryogenic machining of additive manufactured Ti6Al4V alloy. Wear 328–329:89–99
20. Venugopal KA, Paul S, Chattopadhyay AB (2007) Tool wear in cryogenic turning of Ti-6Al-4V alloy. Cryogenics (Guildf) 47:12–18
21. Ayed Y, Germain G, Melsio AP, Kowalewski P, Locufier D (2017) Impact of supply conditions of liquid nitrogen on tool wear and surface integrity when machining the Ti-6Al-4V titanium alloy. Int J Adv Manuf Technol
22. Aramcharoen A (2016) Influence of cryogenic cooling on tool wear and chip formation in turning of titanium alloy. Proc CIRP 46:83–86
23. Bermingham MJ, Kirsch J, Sun S, Palanisamy S, Dargusch MS (2011) New observations on tool life, cutting forces and chip morphology in cryogenic machining Ti-6Al-4V. Int J Mach Tools Manuf 51:500–511
24. Bermingham MJ, Palanisamy S, Kent D, Dargusch MS (2012) A comparison of cryogenic and high pressure emulsion cooling technologies on tool life and chip morphology in Ti-6Al-4V cutting. J Mater Process Technol 212:752–765
25. Rotella G, Dillon OW, Umbrello D, Settineri L, Jawahir IS (2014) The effects of cooling conditions on surface integrity in machining of Ti6Al4V alloy. Int J Adv Manuf Technol 71:47–55
26. Ahmed LS, Kumar MP (2015) Cryogenic drilling of Ti–6Al–4V alloy under liquid nitrogen cooling. Mater Manuf Process 31:951–959

27. Sartori S, Moro L, Ghiotti A, Bruschi S (2016) On the tool wear mechanisms in dry and cryogenic turning additive manufactured titanium alloys. Tribol Int 105
28. Hanenkampa N, Amon S, Gross D (2018) Hybrid supply system for conventional and CO_2/MQL-based cryogenic cooling. In: 8th CIRP conference on high perform cut (HPC 2018), pp 219–222
29. Sun Y, Huang B, Puleo DA, Jawahir IS (2015) Enhanced machinability of Ti-5553 alloy from cryogenic machining: comparison with MQL and flood-cooled machining and modeling. Proc CIRP 31:477–482
30. Schoopa J, Salesb WF, Jawahir IS (2017) High speed cryogenic finish machining of Ti-6Al4V with polycrystalline diamond tools. J Mater Process Tech 250:1–8
31. Mia M, Gupta MK, Lozano JA, Carou D, Pimenov DY, Królczyk G et al (2019) Multi-objective optimization and life cycle assessment of eco-friendly cryogenic N_2 assisted turning of Ti-6Al-4V. J Clean Prod 210:121–133
32. Novella MF, Sartori S, Bellin M, Ghiotti A, Bruschi S (2017) Modelling the thermo-mechanical behavior of a redesigned tool holder to reduce the component geometrical deviations in cryogenic machining. In: 16th CIRP conference on modelling of machining operations 58:347–352
33. Bordin A, Imbrogno S, Rotella G, Bruschi S, Ghiotti A, Umbrello D (2015) Finite element simulation of semi-finishing turning of electron beam melted Ti6Al4V under dry and cryogenic cooling. Proc CIRP 31:551–556
34. Imbrogno S, Sartori S, Bordin A, Bruschi S, Umbrello D (2017) Machining simulation of Ti6Al4V under dry and cryogenic conditions. Proc CIRP 58:475–480
35. Lequien P, Poulachon G, Outeiro JC, Rech J (2017) Hybrid experimental/modelling methodology for identifying the convective heat transfer coefficient in cryogenic assisted machining. Appl Therm Eng 128:500–507
36. Tahri C, Lequien P, Outeiro JC, Poulachon G (2017) Modelling of machining operations CFD simulation and optimize of LN_2 flow inside channels used for cryogenic machining : application to milling of titanium alloy Ti-6Al-4V. In: 16th CIRP conference on modelling of machining operations 58:584–589
37. Khanna N, Agrawal C, Joshi V (2017) Zero vapor loss integrated cryogen phase separator. Indian Patents 201721031291 A
38. Kant G, Sangwan KS (2014) Prediction and optimization of machining parameters for minimizing power consumption and surface roughness in machining. J Clean Prod 83:151–164

Advanced Laser Based Surface Treatment Techniques to Improve the Quality of the Products

S. Shiva, I. A. Palani, C. P. Paul and M. Kamaraj

Abstract Materials are subjected to surface treatments in order to alter the nature both physically and chemically. Also there are certain mending process of surface defects can be carried out using surface treatment process. The current chapter primarily focusses on exploring the impact of advanced surface processing techniques like laser glazing, laser shock peening and laser annealing. The three types of additive manufacturing are laser additive manufacturing, wire arc additive manufacturing and cold spray deposition technique. The effect of the various process parameters of the respective process are discussed in detail. The discussion is primarily focused on the development of shape memory alloy structures using the techniques mentioned and an analyses on the nature of the developed alloys. The surface morphology of the developed structures were evaluated using Scanning Electron Microscopy (SEM), The micro-hardness test reveals the mechanical properties of the samples. All the characterized results showed that SMA could be manufactured successfully using the mentioned techniques, though each system have their own pros and cons. Hence this chapter will give the researchers in beginning stage a clear idea about the evolution of near net shape manufacturing systems that can be used by their research works in developing novel research ideas.

S. Shiva (✉) · I. A. Palani
Mechatronics and Instrumentation Laboratory, Indian Institute of Technology Indore, Indore, India
e-mail: sshivabemech@gmail.com

I. A. Palani
Discipline of Metallurgy Engineering and Material Science, Indian Institute of Technology Indore, Indore, India

C. P. Paul
Laser Development Industrial Applications Division, Raja Ramanna Centre for Advanced Technology, Indore, India

BARC Training School Complex, Homi Bhabha National Institute, Anushakti Nagar, India

M. Kamaraj
Department of Metallurgical and Materials Engineering, Indian Institute of Technology Madras, Madras, India

K. Gupta (ed.), *Materials Forming, Machining and Post Processing*, Materials Forming, Machining and Tribology, https://doi.org/10.1007/978-3-030-18854-2_9

Keywords Laser processing · Laser glazing · Laser annealing · Laser shock peening

1 Introduction

The implementation of laser based surface treatment techniques are widely used in the line of micro electro mechanical systems (MEMS) and the laser based process are opted for the high efficiency of the laser to execute the work done in micro and nano-level [1–3]. In the current chapter a detail analyses about three hot options of laser based surface treatments techniques to improve the qualities of the products are discussed.

1.1 Laser Glazing

Post processing techniques play an important role in shaping the quality of the products into a much better way. Though several options of post processing techniques available, the main objective can be classified to three important tasks. First to alter the surface finish, of the formed product as per requirement. Secondly to improve the fatigue life of the product by inducing residual stress. Finally to reduce the problem of brittleness, by removing the excessive residual stress in the product. Several conventional techniques like diamond dressing, shot peening and furnace annealing were successful in producing efficient results. Though efficient results were fulfilling the requirements perfectly, the problems of high material wastage, time consumption, skilled labour for precision, non-controllable process and formation of secondary phases leading to the change in the nature of the product are in evitable. To overcome the existing issues researchers probed into several ideas by analysing the root cause of the problems and came up with even better and efficient solution of deploying surface treatment techniques with high and low power lasers.

The prevailing surface treatment techniques are mostly computerized which leads to precision in the output. Currently the three major surface treatment techniques to address the requirements mentioned above are laser glazing, laser shock peening and laser annealing. All the mentioned techniques have produced promising reliable outputs that flaunt the advantages and efficiency over the conventional process. Laser glazing is widely used to texture the hard surfaces like grinding wheel. In general the surface grains of the grinding wheel get weird out due to the constant contact between the wheel and samples. As an effect of frequent grinding the surface of the grinding wheels become very much polished and smooth in nature which sequentially affects the efficiency of the grinding wheel and also the replacement of the wheel becomes highly necessary. Laser glazing is implemented on the surface of the grinding wheel which provides a scope of re using the same wheel with better rough grinding surface [4]. The advantage of laser glazing over conventional diamond dressing is the

generation of more cutting grains and porosity pockets homogeneously in the same level throughout the sample which can be attributed to the calibre of laser, to modify the grains of the grinding wheel only on the surface level. With different operational parameters the surface wear caused in the tool of lathe machine can also be cured. Hence laser glazing has the flexibility to control the surface, smoother and rougher based on the requirements. In the process of laser glazing, pulsed lasers of higher power are generally opted to maintain the homogeneity of the output and to maintain the process effectively in surface level.

1.2 Laser Shock Peening

Development of materials for various aspects is a huge milestone achieved by metallurgists, after developing the ability to engineer the materials and change their nature based on the application to be implemented. Though the development has reached a higher level yet modern manufacturing techniques like additive manufacturing have the problems like surface cracking yet to be answered. In that accord to improve the nature of the products made of modern smart techniques the need of post processing techniques have become highly inevitable. When the reason for the crack generation is deeply analysed the researchers have reported the problem of internal stresses developed during deposition and other reasons like the fatigue load stays to be a major hindrance. The fatigue load acting on the samples gradually leads to the formation of scratch marks, surface cracks due to fatigue or thermal load etc. In general fatigue cracks generate on the surface of the samples from the point of high stress accumulations and other point of surface defects in any form. As fatigue load cyclically acts on the defect areas, leading to the formation of slip bands in the microstructure forming cracks on the surface. The repeated impact of cyclic load gradually gets distributed easily on the surface as there are not much constraints to prevent them from growing further, finally leading to the distorting of the product completely. In order to counter the rising issues surface treatment techniques are opted. The available conventional surface treatment techniques available are shot peening [5, 6], low plasticity burnishing [7, 8], roller pressing [9, 10], water jet peening [11, 12]. The primary need for the techniques shown in Fig. 1, is to impinge compressive residual stress on the surface of the samples that sequentially gives good resistance to the fatigue stress that acts on the samples.

The science behind the ability to with stand the fatigue load can be explained by comparing the strain amplitude and life of the sample. The applied alternating stress can be denoted as σ_1 and the corresponding fatigue life can be denoted as N_1. The increase in the fatigue life can be related to the reduction of alternating stress by external compressive stress σ_c, after shot peening on the surface of the samples. Hence the net stress can be denoted as $\sigma_2 = \sigma_1 - \sigma_c$. As a result the fatigue life of σ_2 is denoted by N_2 which is comparatively higher that N_1 [13, 14].

Figure 2 shows a typical distribution of stress generated by the effect of laser shot peening. The magnitude of residual stress on the surface of the compressive

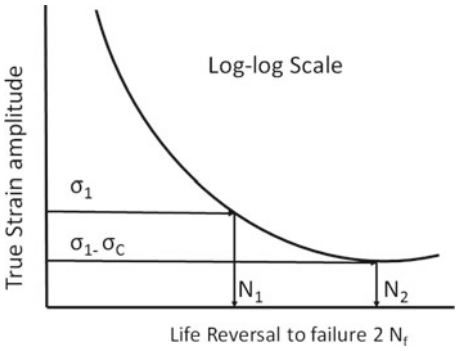

Fig. 1 Strain amplitude versus life circle

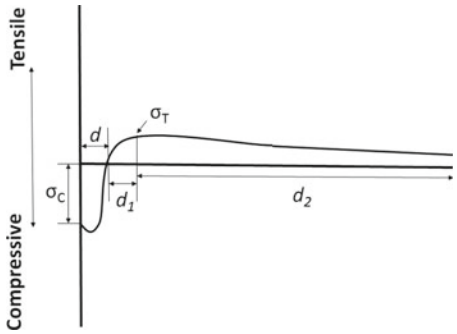

Fig. 2 The profile of stress distribution after peening process

zone depends on factors such as shot medium, intensity, size and materials nature. In order to counter the compressive stress after the shot peening process, the surface is induced with tensile stress. The depth of the compressive stress can be denoted as "d". The depth of inducing tensile stress is denoted by "d_2".

Though laser shot peening is having the efficiency of changing the materials nature based on the concepts discussed earlier. But yet there are certain problems to be addressed. The issues are as follows:

1. The peening pressure is not under control.
2. The number of shots impinged by steel balls are not in control.
3. The generation of surface roughness is not in control.
4. The peening velocity is not in control.

Due to the above mentioned factors the process was not successful for certain materials that are brittle in nature. Hence an alternate method of laser shock peening in which the efficiency equal to conventional shot peening was opted. The process of LSP has a laser pulse of high energy density which creates enough plasma by impinging on the sacrificial layer on the surface of the target. As the sacrificial layer gets ablated continuously by the effect of repeated laser pulses, the generated plasma

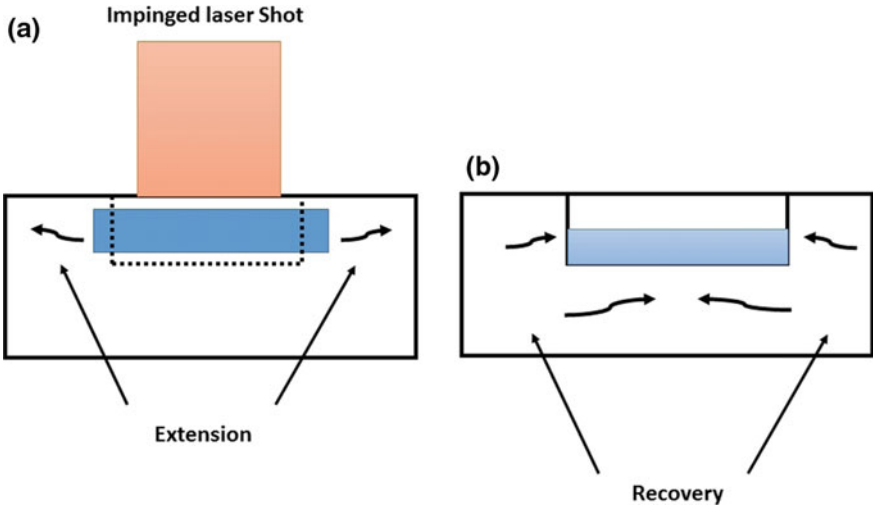

Fig. 3 The profile of stress distribution after peening process

are accumulated on the localized area leading to the injection of compressive stress on the sample. The heated plasma undergoes hydrodynamic expansion in the confined region creates a high amplitude pulse of several GPa, for a short duration. A part of the generated energy penetrates into the product in the form of shock wave. The uniaxial compression load acting on the sample as generates tensile extension in the plane parallel to the surface as shown Fig. 3.

As the pressure generated by the laser shock exceeds the dynamic yield strength of the sample, leads to plastic deformation. The microstructure of the sample faces huge variation by the effect of plastic deformation. The critical pressure is inter related with the density of the material (ρ) and sound wave velocity of the material (c) and is mathematically expressed as follows

$$P_{sw} = \rho c^2 \tag{1}$$

The process of laser shock peening is governed by the parameters like various protective coating layer, different confining medium, spot size and pulse duration, laser energy density and wavelength and laser pulse repetition.

1.2.1 Various Coating Layer

The desired property of the coating layer is to be ablative and very thin in thickness [15, 16]. Aluminium foil, black paint and adhesives or tapes are primary choice for coating layer. The coatings protect the surface layer and also enhances the intensity

of the plasma as well. Depending upon the sample's nature laser shock peening is done in the absence of coating layer as well.

1.2.2 Different Confining Medium

The confining medium plays a crucial role in proceeding the process homogeneously. In general water is used as the confining medium [17]. Other options are K9 glass, Pb glass and perplex [18]. The selection is based upon the sample to be shock peened. The primary factors governing the process are material density, acoustic velocity which decides the acoustic impedance effect in the process. The confined medium has the ability to multiple the amplitude of stress generated on the surface of the sample [19–21]. Similarly the duration of plasma is increased by the confined medium. The role of confined medium in the laser shock peening process can be divided into three different phases. Once the laser shot is impinged, the generated laser plasma is of high amplitude which is many times higher than the ablation process. Once the laser is off the adiabatic cooling of the generated pressure happens leading to prolong the generated plasma on the surface of the sample for a while. Finally the exerted pressure by the shot diminishes slowly in the aspect of amplitude and it is tough to detect plastic deformation on the surface. In case of excluding the confining medium from the entire process, the generated plasma intensity gets distributed in all directions and gets diffused very quickly.

1.2.3 Spot Size and Pulse Duration

The laser spot size plays a crucial role in the shock peening process. The laser spot size can be varied by moving the sample near or away from the focal point depending upon the energy density's availability and requirement. In general the laser energy density varies to the square of the spot size. The smaller laser spots are tend to expand the shock wave in the form of sphere, whereas the larger spot diameter produces waves in planar direction. Both sizes possess the ability to inject residual stress deeper into the sample. The magnitude of residual stress doesn't seem to be dependent on the spot size, also the magnitude of surface residual stress is higher in laser shock peening process and the magnitude gradually dips as the depth of penetration is deeply analysed. In the shock peening process the centre of the laser soot doesn't have much intensity as due the non-homogeneous on the contact surface. The laser spot has been made circular [22], square [23], elliptical and rectangular [24] for peening purposes by the researchers in the past. Also reports suggest that the short duration pulse are capable of generating high magnitude residual stress.

1.2.4 Laser Energy Density and Wavelength

The magnitude of residual stress getting impinged on the surface is directly proportional to the amount of laser energy density chosen for the shock peening process. As the laser energy density exceeds a threshold value the residual stress penetration increase in the depth and starts to decrease on the surface of the sample due to the effect of surface release waves [25]. Water is widely chosen as the confining medium for its property of dielectric breakdown threshold, which protects the sample from excessive compressive stress. In general the laser energy density is determined in GW/cm^2. The reported results prove the higher the wavelength with high frequency of laser pulse effective impact can be availed on the surface of the samples generating sufficient amount of residual stress in them. At least 1 GW/cm^2 has to be opted for effective laser shock peening, and minimum of 20% overlap is required for distributing the effect of shocks homogeneously in the sample.

1.2.5 Laser Pulse Repetition

The number of pulse repetition plays a crucial role in the amount of residual stress to be impinged in the sample [26]. The number laser shots have impact in mechanical properties of the materials like ultimate strength, young's modulus, micro-hardness etc. Hence the number of laser shots are to be chosen in such a way that there is not much effect on the surface of the samples and the properties of the samples. Also researchers have demonstrated the formation of wrinkles on the surface of the samples due to the effect of laser shock peening [27]. Hence while choosing the number of shots care must also be taken to maintain the surface morphology of the sample without any change.

1.3 Laser Annealing

The final surface treatment technique to be discussed is about laser annealing. The technique of processing the surface of delicately to bring localized effects is laser annealing. Laser annealing in general is performed using both pulsed and continuous wave laser based on the requirement and product's nature. The process is an effective surface treatment technique capable of removing the excessive stress in the product which assists the crystallization in the product. The process must be chosen to be carried out in closed or open atmosphere depending upon the product and their reacting nature with oxygen and laser.

Compilation of all surface processing techniques in TiNiCu shape memory alloy in the aspect of various property are to be focused in this chapter. Also the discussion includes the various desirable parameters and other characteristics features of the chosen three process in brief. At the end, the future prospects and recent research trends in the chosen technologies will be deliberated. This chapter will help the

researchers who are looking for ideas to perform surface treatment techniques in their research work for different products.

2 Laser Material Interaction

The laser surface processing theory initiates with the concept of laser material interaction. Hence to know the concept of laser and material interaction it is much essential to have a deeper understanding on the basic process behind the laser and material interaction. The understanding assists the users to implement the laser in altering the physical and chemical nature of certain products as per requirement by controlling certain process parameters of lasers. The main governing parameter in laser processing is the laser energy density. As the laser energy density increases a threshold value it leads to irregular material removal called ablation. Ablation distorts the material both physically and chemically. The relation between laser energy density and ablation rate is as shown in Fig. 4. The shown graph in Fig. 4 suits for all types of materials when interacting with laser. Hence based on the figure it is very important to decide the amount of laser energy density to be chosen to process the material. The important parameter to be considered for the laser processing techniques are the thermal effects getting distributed within the samples being distributed homogeneously. But the toughest challenge lies on distributing the heat uniformly throughout the sample. One more important parameter is the nature of the samples and the surface finish of the samples. Heat is dissipated into the samples by the energy possessed by photons coming in contact with the samples. The energy poses sufficient heat to alter he chemical bond in the samples. In case the energy of the photons are not sufficient enough to bring the required changes in the samples, will lead to the formation of heat affected zone, which deteriorates the mechanical properties of the sample.

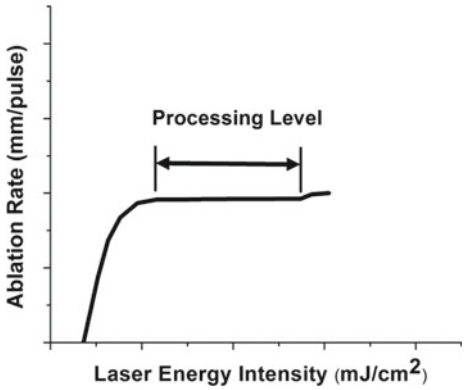

Fig. 4 Ablation rate versus Laser energy intensity

3 Numerical Modelling

Laser surface processing is primarily governed by heating rate, plasma generation and compressive stress impingement. The heating and cooling rate are predominantly governed by laser parameters and confinement properties. A finite element software was deployed to simulate the process and estimate the induced stress distribution at different processing parameters. The simulation was carried out using ANSYS 14.0 and self-developed APDL codes. The following equations and parameters were opted:

Governing Equation:

Following equation presents generalized heat equation applicable for laser shock processing process.

$$\rho C_p \left(\frac{\partial T}{\partial t}\right) - \nabla (k \nabla T) = 0 \tag{1}$$

where k (W m^{-1} K^{-1}) is the thermal conductivity, Cp (J kg^{-1} K^{-1}) is the specific heat capacity, ρ (kg m^{-3}) is the density, and t (s) is the time.

Boundary conditions and associated simplifications

The initial temperature of the process is room temperature (T_0). So the initial and final conditions are

$$T(x, z, t) = T_0, \qquad when \quad t = 0 \quad and \quad t = \infty \tag{2}$$

The effect of the various processes is modelled using Lagrangian formulation and the associated boundary condition are expressed as

$$\begin{aligned} -K(\nabla T.n)|_\Omega &= [\beta I(x, z, t) - h_c(T - T_0)]_\Omega \; if \; \Omega \in \Gamma \\ &= [-h_c(T - T_o)]_\Omega \qquad\qquad if \; \Omega \notin \Gamma \end{aligned}$$

where, n is the normal vector of the surface, β is the absorption factor, I (W m^{-2}) is the laser intensity, h_c is the heat convection coefficient (W m^{-2} K^{-1}), Ω (m^2) is the area of work piece surface, Γ (m^2) is the laser spot area, Ω and Γ are shown in Fig. 1. The value of absorption factor β is 0.3 as calculated by the similar method reported by the researchers in the past [28]. The value of heat convection coefficient [29] hc = 150 W m^{-2} K^{-1}.

The process of laser glazing is done by continuous wave laser of high energy density. The high energy density is provided by the amount of high power provided as input in the entire process. The entire power input of the continuous wave laser is as shown in in Eq. (3) [30].

$$P = \frac{2\alpha P V}{\pi \omega_\rho^2} \exp\left(\frac{-2r^2}{\omega_\rho^2}\right) \exp(-\alpha z) \tag{3}$$

As the laser pulse of high intensity is impinged on the surface of the sample, plasma is generated, and the generated plasma expands and injects shock waves on the sample. The confined medium used for the entire process enhances the intensity of pressure generated multiple times. The entire LSP process is governed by a shock pressure and plasma thickness. The relation between shock pressure and plasma thickness are being governed by the following equation [31]:

$$\frac{dL(t)}{dt} = \frac{2P(t)}{Z} \tag{4}$$

where L(t) stands for thickness of the plasma generated, P(t) stands for the pressure generated by the laser pulse impinged. The laser energy, I(t) distributed on the surface of the sample is mathematically given as follows:

$$I(t) = P(t)\frac{dL(t)}{dt} + \frac{3}{2\alpha}\frac{d}{dt}[\,\mathrm{P(t)L(t)}] \tag{5}$$

The pressure generated by the laser pulse on the surface of the sample is calculated using Fabbro's model as shown below [31]:

$$\mathrm{P} = 0.01\sqrt{\frac{\alpha}{2\alpha+3}}\sqrt{\mathrm{ZIo}} \tag{6}$$

where P (GPa) stands for peak pressure generated, α stands for absorption coefficient and for Ni–Ti, Z (g cm^{-2} s^{-1}) represents the combined shock impedance and it is obtained from the following formula $\mathrm{Z} = \frac{2}{\frac{1}{z1}+\frac{1}{z2}}$, Z1 stands for the shock impedance of Ni–Ti (3.44 × 106 g cm^{-2} s^{-1}) [32] and Z2 stands for the shock impedance of the confining medium water (1.45 × 105 g cm^{-2} s^{-1}) [33]. The residual stress generated by the shock pressure is simulated and compared with the experimental values. In the entire process the growth of plasma is considered to be only in axial direction.

Laser energy distribution for laser annealing is assumed to Gaussian [34]. It is mathematically presented as

$$I = \delta I_0 * e^{-[2r^2/r_l^2]} \tag{7}$$

where, $\mathrm{r_l}$ stands for radius of laser (m) and $r = \sqrt{x^2 + y^2}$. The MKS units were followed while determining constants in Eq. (4). The value of I_0 [35] can be derived by the formula $I_0 = \frac{2P}{\pi r^2}$, where P stands for laser beam power. The value of $\delta = 1$ when the laser is on, and $\delta = \mathrm{o}$ when the laser is off.

A mesh size independency test was performed prior to implement the proposed model, deploying a least geometric dimension ($\mathrm{D_L}$) of the model with an element size of (e). It was observed that the temperature difference in successive runs of reduced element size by a factor two becomes less than 10^{-3} for $\mathrm{D_L/e} > 30$. In present simulation study, $\mathrm{D_L/e} = 40$ is used and it corresponds to an element size of

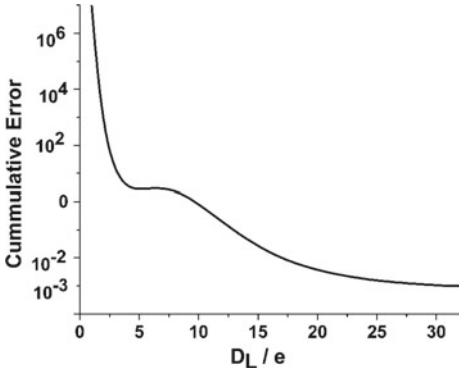

Fig. 5 Mesh independency test results

Table 1 Properties of TiNiCu

Properties	Unit	TiNiCu
Density	kg/m^3	6450
Specific heat	J/kg °C	460
Melting point	°C	1300
Poisson ratio	–	0.3
Emissivity	–	0.4
Thermal conductivity	W/m °C	0.13
Young's modulus	GPa	78
Thermal expansion coefficient		15.4×10^{-6}

~50 microns [36]. In addition, all required element quality checks of the FE model were performed as shown in Fig. 5.

The materials properties of Ni–Ti in both phases as quoted in Table 1 [37] were used for the study as the samples developed by LAM are polycrystalline in nature, i.e. presence of both phases in the samples are possible.

Thermo Mechanical Analysis

In the present work, a thermo-mechanical analysis is carried out to calculate the induced distortions and residual stresses in the samples during the laser surface treatment. The present section describes the theoretical background of mechanical analysis. It includes the mechanical boundary conditions along with material model. The nodal temperature values are estimated from the conduction heat transfer analysis are integrated as a predefined field. The material was assumed to follow an elasto-plastic law with isotropic hardening behavior (von Mises plasticity model). The detailed mathematical background of this mechanical analysis is given in the subsequent sections. Figure 6 shows the elements used in thermal and mechanical analysis in the present work.

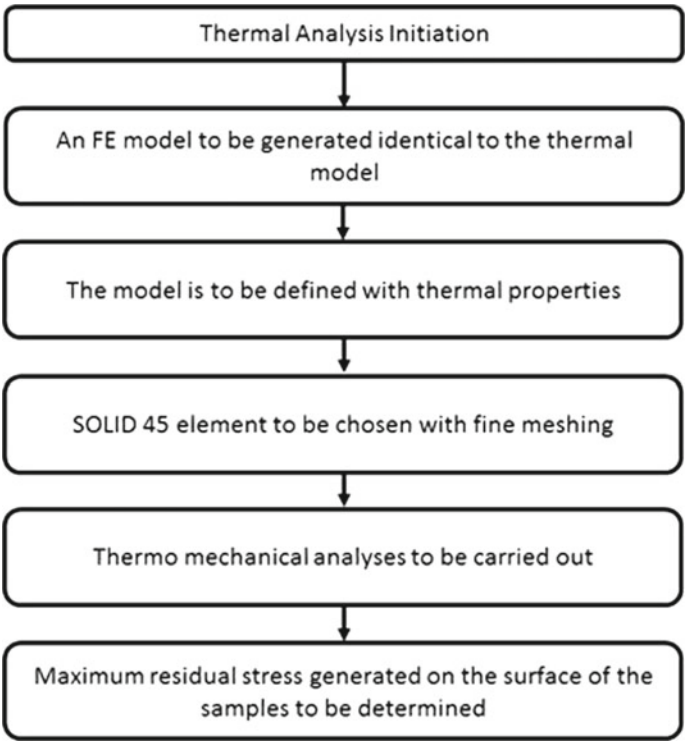

Fig. 6 Overall procedure followed in thermo-mechanical analyses

Governing Equations and Boundary Conditions

In the present work, the material response is assumed as thermo-elasto-plastic along with mechanical properties. The elasto-plastic analysis is generally performed by incremental mode of stress and strain. Rate independent plasticity is considered followed by von-Mises criterion, the associated flow rule and bilinear isotropic hardening behaviour. In Cartesian coordinate system, the strain-displacement relation can be written as [38, 39].

$$\epsilon_x = \frac{\partial u}{\partial x}; \epsilon_y = \frac{\partial v}{\partial y}; \epsilon_z = \frac{\partial w}{\partial z} \tag{8}$$

$$\gamma_{xy} = \frac{\partial u}{\partial y} + \frac{\partial v}{\partial x}; \gamma_{yz} = \frac{\partial v}{\partial z} + \frac{\partial w}{\partial y}; \gamma_{xy} = \frac{\partial w}{\partial x} + \frac{\partial u}{\partial z} \tag{9}$$

where u, v and w represents displacements in x, y, z directions respectively; εx, εy and εz refer to the normal strains in x, y and z directions respectively; and γ_{xy}, γ_{yz} and γ_{zx} represents shear strains in xy, yz and zx planes respectively. Assuming the isotropic material, the thermal strain remains same in three directions and the increment of the

total strain is sum of the incremental plastic strain, incremental thermal strain and incremental elastic strain, represented as

$$\{d\epsilon\} = \left\{d\epsilon^t\right\} + \left\{d\varepsilon^p\right\} + \left\{d\epsilon^p\right\} \tag{10}$$

Following Prandtl-Reuss flow rule and Von-Mise's yield criteria, the incremental stress can be represented as

$$\{d\sigma\} = \left[D_{ep}\right]\{d \in\} - \left[D^e\right]\{\alpha\}(\Delta T) \tag{11}$$

where

$$\left[D_{ep}\right] = \left(\left[D^e\right] - \left[D^e\right]\left\{\frac{\partial f}{\partial \sigma}\right\}\left\{\frac{\partial f}{\partial \sigma}\right\}^T\left[D^e\right]\frac{1}{3G + E_T}\right) \tag{12}$$

where [De] depict the elasticity matrix which consists of mechanical properties like Young's modulus E and Poisson's ratio μ. G is shear modulus and E_T is local slope between stress and plastic strain of specified material. The last term of Eq. (11) represents the thermal strain which may vary depending upon the temperature distribution. [Dep] is some sort of elasto-plastic matrix where the first term in Eq. (12) is due to elastic response of material or recovery of elastic response when the material is in plastic zone. The second term of the Eq. (12) is due to plastic flow of material which is zero when the material is elastic zone only. The evolution of the yield surface are governed by the hardening rule. In present case, Von-Mises yield surface is considered and bilinear isotropic hardening rule is assumed that may be appropriate for the selected material.

Material Model

In the present work, the numerical analysis is performed by considering the material properties. An elastic-plastic material model is used in the mechanical analysis module. The isotropic hardening rule is selected to consider the plasticity using the ANSYS APDL code. The elasticity is defined by Young' s modulus and Poisson' s ratio, and the plasticity is defined by yield stress and the elastic-plastic tangent modulus. Moreover, the Von Mises stress is used to predict yielding of the samples.

Computational Aspects

In the present work, the thermal and mechanical properties are used for thermo mechanical analysis. Thermal properties such as specific heat and thermal conductivity are considered. The latent heat of fusion is considered for the simulation through an artificial increase or decrease in the specific heat of the material [40]. The governing equation along with boundary conditions for heat conduction, the linear system of equations for an element is written as

$$[C(T)]\{T\} + [K(T)]\{T\} + [V(T)]\{T\} = [Q(T)] \tag{13}$$

where [K] refers to the conductivity matrix, [C] is the capacitance or specific heat matrix, {T} is nodal temperatures vector, [V] is the velocity matrix due to moving beam and {Q} is the nodal heat flow vector.

The material behavior is considered as elasto-plastic in nature. In the present work, the influence of micro-structural changes, creep and transformation induced plasticity are not considered. The plasticity is assumed as rate independent and is modelled by assuming bilinear isotropic hardening behaviour along with associated flow rule. The von-Mises yield criteria is followed as

$$\sigma_{av} = \sqrt{1/2\left[(\sigma_1 - \sigma_2)^2 + (\sigma_2 - \sigma_3)^2 + (\sigma_3 - \sigma_1)^2\right]} \tag{14}$$

where, σ_1, σ_2, σ_3 are principal stresses and σ_{av} is the average one dimensional stress.

Solution Strategy for Thermal Analysis

Figure 4.13 shows the step by step procedure (flow chart) followed in a thermo mechanical analysis based on finite element method using FE software ANSYS 14.0. Few important steps are described below.

- In mechanical analysis, the similar FE model used in thermal analysis is considered other than type of element. SOLID 45 element is used which is defined by eight nodes having three degrees of freedom at each node, translation in the nodal X, Y, and Z directions.
- Next, the material properties are defined.
- The reading of nodal temperatures is considered for overall thermal analysis at different time steps.
- Structural analysis performed and estimate the distortion and residual stresses at different sections of the samples developed by LAM.

4 Experimental Procedure

4.1 Laser Glazing

The process of laser glazing was carried out on the TiNiCu sample using 2 KW continuous wave fiber laser in a wavelength of 1054 nm. The spot diameter of 2 mm was maintained throughout the process. Immense care was taken that the chosen laser energy density does not ablate the given sample. Hence after lots of preliminary trials the laser energy density of 1100 mJ/Cm^2 was opted for the study. The sample was placed on the deposition bed and to maintain the homogeneous laser treatment the laser beam path profile as shown in Fig. 7 was carried out. After the laser glazing process the samples were carefully brought under study in various aspects.

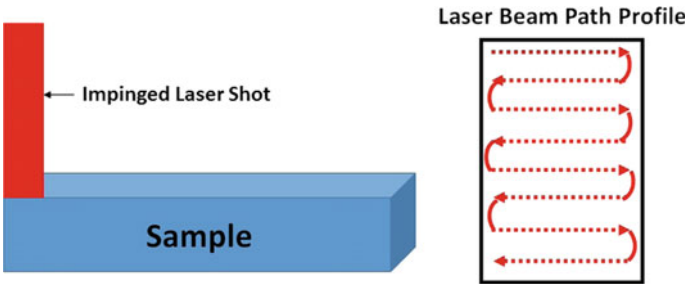

Fig. 7 Laser glazing process on the samples

4.2 Laser Shock Peening

The dimensions of TiNiCu structure fabricated using laser additive manufacturing was subjected to laser shock peening with pulsed laser. The laser shock peening experiments were carried out using the 1064 nm wavelength at Q-Switched mode of Nd:YAG laser on the Ni–Ti structure mounted on computer controlled X–Y manipulator. The schematic arrangement of laser shock peening set up is presented in Fig. 8.

The fundamental wavelength of Nd:YAG laser (1064 nm) laser was opted, expecting an improved performance in LSP. The process parameters used for laser shock peening experiments are presented in Table 2. The sample was fixed inside the LSP set up with water as the confining medium. Water was chosen as the confining medium, for its nature of breaking down the plasma after certain limit that consequently reduces the intensity of pressure acting on the sample [41]. As the sample taken for the study has very low ultimate strength, the plasma breakdown by the water prevents it from getting damaged by high pressure generated by higher laser energy

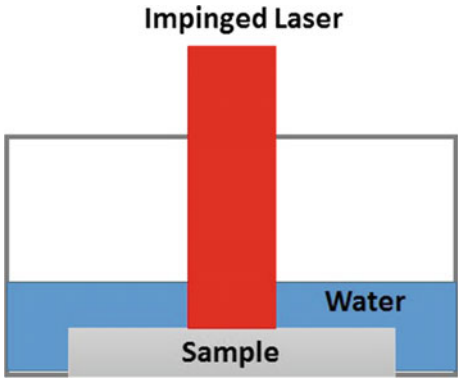

Fig. 8 Laser shock peening process

Table 2 Processing parameters used in the laser shock peening

Parameter	Unit	Value
Laser wavelength	nm	1064
Mode of operation	–	Q-switched
Laser energy per pulse	GW/cm^2	1
Laser pulse duration	ns	9
Laser pulse frequency	Hz	1
Laser spot size	mm	2
Spot overlap	%	20

density. In this study the sacrificing layer was not used in our experiments expecting to prevent excessive pressure on the sample surface, as reported by researchers in the past [42]. In general, a minimum laser energy density of 1 GW/cm^2 is a must for an effective LSP [43].

4.3 Laser Annealing

The laser annealing experiments were carried out by shining the second harmonic of Nd:YAG laser on the Ni–Ti structure mounted on X–Y manipulator. The second harmonic of Nd:YAG laser was used, as it yields improved performance due to shorter wavelength [44]. The frequency and the spot overlap are the parameters that affect the reduced cooling rate and uniform heat absorbing zone during laser annealing. They, also, result in reduced dilution and crack elimination. In general, the frequency of 1 Hz and spot overlap of 90% indicated good laser annealing [44]. The annealed samples were characterized using a number of techniques (Table 3).

Table 3 Processing parameters used in the laser annealing

Parameter	Unit	Value
Laser wavelength	nm	532
Mode of operation	–	Q-switched
Laser energy per pulse	mJ/cm^2	1100
Laser pulse duration	ns	9
Laser pulse frequency	Hz	1
Laser spot size	mm	2
Spot overlap	%	90

5 Results and Discussion

5.1 Validation of Numerical Modelling

In order to study the residual stress distribution in the samples a numerical study was carried out based on the material properties. Hence the simulation was carried out for the samples for all three laser based process as discussed earlier using the reported equations. Initially the entire sample was finely meshed and converted into small elements. The heat input was based on the laser input energy. The convective boundary conditions were chosen for the study. The residual stress distribution seems to be evenly distributed throughout the developed samples. This nature of distribution have high chances of influencing the SME properties of the developed samples.

Figure 9 shows the complete set of simulations developed for laser glazing, laser shock peening and laser annealing on the samples. The simulated models were fed with the material properties of TiNiCu. From the figure it is vividly seen that the residual stress distribution in the samples is high for laser shock peening, secondly for laser glazing and finally the minimum amount of residual stress for laser annealing. This may be attributed to the immense amount of compressive stress induced in the samples on the surface. Similarly the values of laser annealed samples are comparative less due to the nature of the process, like the utilization of the laser to remove the excessive amount of residual stress in the sample.

To validate the simulated results a real time experiment was conducted using XRD method to measure the residual stress distribution post all the laser surface treatments. A preliminary experiment of all three surface treatment process were carried out on the TiNiCu samples and the real time residual stress was compared within the residual stress values in as manufactured state of the samples. The prime factor of laser soaking on the surface of the samples due to high temperature brings change in the dimension of deposited samples, but in a very negligible amount. Also generation of micro cracks become in evitable due to greater accumulation of compressive residual stress on samples treated with laser shock peening. In case of laser glazing and laser annealing the problems don't occur as the temperature and stress gets uniformly distributed and chances of accumulation in the samples is comparatively less. Hence the risk of secondary phase formation is also very less in TiNiCu samples.

The measured and simulated values are as shown in Fig. 10. From the graph it is vivid that the simulated values are a bit higher than the real time experimentation values. The decrease in the real time experimentation values are attributed to the radiation losses. The simulation results and experimental results show the laser shock peened samples generate are of higher residual stress as expected while comparing the remaining two process. Laser annealed samples had the minimum residual stress than the laser glazed samples as well. So based on the applications and the sample's physical and chemical nature the post processing techniques can be opted to full fill the requirement and real time application.

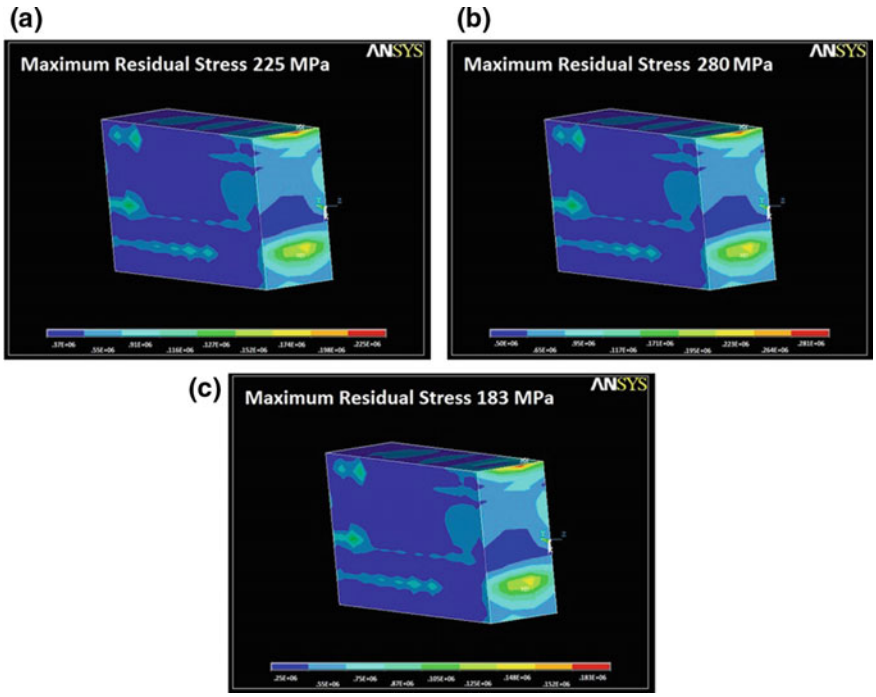

Fig. 9 Simulated residual stress distribution after (**a**) Laser glazing (**b**) Laser shock peening (**c**) Laser annealing

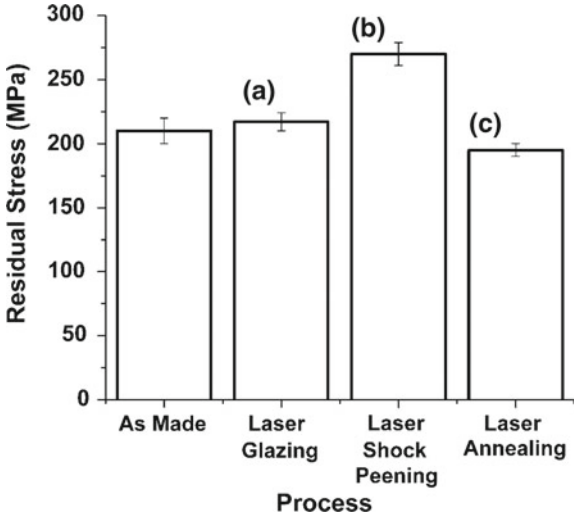

Fig. 10 Experimental residual stress distribution after (**a**) Laser glazing (**b**) Laser shock peening (**c**) Laser annealing

5.2 Surface Morphology

The surface topography of the formed samples are as shown in Fig. 11. The scanning electron microscopy images reveal homogeneous surface processing of the samples using the laser glazing, laser shock peening and laser annealing. The surface of the laser glazed sample appears to be crack and dent free as shown in Fig. 11a. The influence of continuous wave laser is visible in bringing out such homogeneous surface. Figure 11b shows the surface of the laser shock peened samples, and the impact of pulsed laser in bringing effective change on the surface of the sample is vividly visible. From the image the surface roughness of the sample is expected to be higher. Laser annealed samples are very smooth in nature unlike the other two samples. The presence of any surface flaws like cracks, craters or dents are not observed. The surface looks very smooth in nature. To further investigate the nature of grain size and surface roughness of the samples in nano-metric level atomic force microscopy was used.

The AFM results of laser glazed samples are as shown in Fig. 11d the images are of dimension $2 \times 2\ \mu m^2$. The measured grain size of the samples are 25.65 nm and the surface roughness id of 5.28 nm. The laser shock peened samples had the grain size of 22.14 nm and surface roughness of 7.89 nm. The AFM image of the laser shock peened sample is of $1 \times 1\ \mu m^2$ as shown in Fig. 11e. The results of laser annealed samples are as shown in Fig. 11f. The image dimension is of $2 \times 2\ \mu m^2$. The grain size of the sample is 32.46 nm and the surface roughness is 4.26 nm. To investigate the mechanical properties of the samples a micro-hardness test was conducted for the samples and are as discussed in the following session.

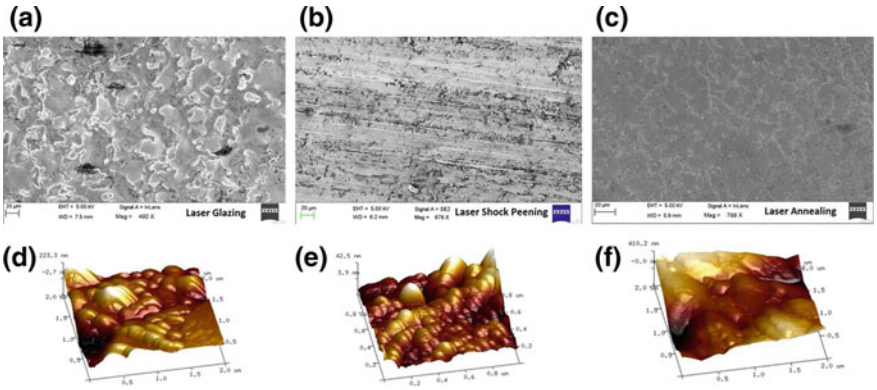

Fig. 11 Results of SEM (**a**) Laser glazing (**b**) Laser shock peening (**c**) Laser annealing and AFM results of (**d**) Laser glazing (**e**) Laser shock peening (**f**) Laser annealing

5.3 Mechanical Properties

The samples were bisected to the direction of laying and prepared using standard metallographic techniques for micro-hardness measurement. The measurement was carried out at an incremental distance of 25 mm at a load of 500 g. Figure 12, presents the micro-hardness distribution on the samples both before and after LSP. It is very clearly seen that after LSP the micro-hardness has drastically increased. The pinning effect plays a vital role in accumulating the dislocations and preventing them from proceeding further. The driving force of this pinning effect is exerted by the precipitates generally formed on the surface of the samples due to LSP. The precipitates resist the dislocations from proceeding further, leading to pin them down which sequentially leads to improved micro-hardness values. As the micro-hardness of the samples increased the ductility of the sample is expected to drastically decrease. The results of laser annealed and laser glazed samples were comparatively lower than the shock peened sample. Hence the residual stress in the sample is removed by laser glazing and laser annealing leading to low micro-hardness value of. The lower micro-hardness value is a clear indication of improved ductility in the sample.

Three different types post processing techniques are discussed in detail. The process of laser glazing can be opted for samples that have surface cracks in them. The surface cracks can spoil the physical nature of the sample very much that preventing them from real time applications. Hence laser glazing is a very good option for restricting surface cracks on the samples. Laser shock peening can be implemented on samples to improve the hardness of the sample and to get rid of certain surface flaws. The laser annealing is a localized heating process that can be used to remove the excess of residual stress in the sample. Also laser annealing is effective in crystallizing the amorphous surface of the samples. Hence based on the requirements

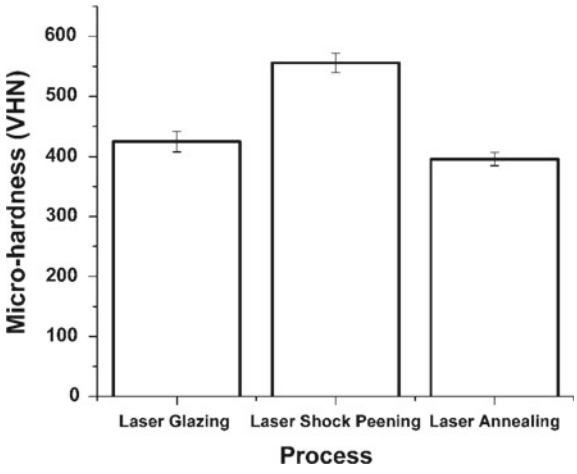

Fig. 12 Micro-hardness results of the samples

and the sample's working environment the laser based post processing techniques can be opted to improve the quality of the sample both physically and chemically.

6 Conclusion

Laser based surface processing techniques are extremely advanced techniques which can used in various applications in the aspect of repair and manufacturing component with specific application. The above discussed three laser based surface treatment techniques can be deployed to solve some minor issues that prevent the developed products fro real time applications. The scope of the laser based surface treatment techniques is deployed in areas where delicacy is given the prime priority. Availability of compact high power lasers, in continuous wave and pulsed wave form can be controlled using controllers, and efficiently get the work done based on the requirement of the users.

In this chapter the TiNiCu shape memory alloy samples were treated with three different types of laser surface treatments and the results prove the processes chosen have the ability to bring changes on the physical properties of the samples in surface level. The SEM results showed the laser shock peening process increasing the surface roughness and micro-hardness of the sample. Parallely laser annealing and laser glazing were efficient enough to bring smoother surface finish and removal of excessive residual stress. Hence the based on the requirement the available three options of laser based surface heat treatment techniques can be availed to alter the nature of the samples.

References

1. Kear BH, Breinan EM, Greenwald LE (1979) Laser glazing—a new process for production and control of rapidly chilled metallurgical microstructures. Met Technol 6(1):121–129
2. Montross CS, Wei T, Ye L, Clark G, Mai YW (2002) Laser shock processing and its effects on microstructure and properties of metal alloys: a review. Int J Fatigue 24:1021–1036
3. Liu YS, Xu D, Jiang BH et al (2005) CO_2 laser annealing of sputtering deposited N–Ti shape memory thin films. J Micromech Micro Eng 15:575
4. Lin B, Li ZC, Xu YS, Hu J (2002) Theoretical generalization and research on the mechanism of the unsteady-state grinding technique. J Mater Process Technol 129:71–75
5. Wagner L, Lutjering G (1981) Influence of shot peening on surface integrity of some machined aerospace materials. In: Proceedings of the 1st international conference on shot peening
6. Wagner L (1999) Mechanical surface treatments on titanium, aluminum and magnesium alloys. Mat Sci Eng A 263(2):210–216
7. Prevey PS, Shepard M, Smith P (2001) The effect of low plasticity burnishing (LPB) on the HCF performance and FOD resistance of Ti6Al4V. In: Proceedings of 6th national. turbine engine HCF conference, Jacksonville, Fl
8. Hornbach D, Prevey P (2007) Reducing corrosion fatigue and SCC failures in 300 M steel landing gear using low plasticity burnishing. SAE Int. Doi:10.427/2007-01-3838

9. Radzimovsky EI (1952) Stress distribution and strength condition of two rolling cylinders pressed together. University of Illinois Bull. 50 (no.44)
10. Klocke F, Liermann J (1998) Roller burnishing of hard turned surfaces. Int J Machine Tools Manf 38(5–6):419–423
11. Enomoto K, Otaka M, Kurosawa K, Saito H, Tsujimura H, Tamai Y, Uraki K, Mochizuki M (1994) Method of and apparatus for water jet peening, patent
12. Hirano K, Enomoto K, Hayashi E, Kurosawa K (1996) Effects of water jet peening on corrosion resistance and fatigue strength of type 304 stainless steel. J Soc Mat: 55–63
13. Tsuji N, Tanaka S, Takasugi T (2009) Effects of combined plasma carburizing and shot peening on fatigue and wear properties of Ti6Al4 V alloy. Surf Coat Technol 203(10–11):1400–1405
14. Atrens A, Hoffelner W, Duerig TW, Allison JE (1983) Subsurface crack initiation in high cycle fatigue in Ti6Al4V and in a typical martensitic stainless steel. Scripta Metall 17(5):601–606
15. Fabbro R, Peyre P, Berthe L, Scherpereel L (1998) Physics and applications of shock processing. Laser Appl 10:265–270
16. Zhang YK, Zhang SY (1997) Investigation of the surface qualities of laser shock processed zones and the effect on fatigue life of aluminum alloy. Surf Coat Technol 92:104–109
17. Rushau J, John R, Thompson S, Nicholas T (1999) Fatigue crack nucleation and growth rate behavior of laser shock peened titanium. Int J Fatigue 1(21):199–209
18. Hong X, Wang S, Guo D, Wu H, Wang J (1998) Confining medium and absorptive overlay: their effects on a laser induced shock ave. J Opt Lasers Eng 29:447–455
19. Bolger JA, Montross CA, Rode AV (1999) Shock waves generated in basalt rock with high powered lasers in a confined geometry. J Appl Phys. 86(10):5461–5466
20. Clauer AH, Fairand BP (1979) Applications of lasers in materials processing. In: ASM conference, Materials park OH, 44073–0002, 1–22
21. Fairand BP, Clauer AH, Jung RG, Wilcox BA (1974) Quantitative assessment of laser induced stress waves generated at confined surfces. Appl Phy Lett 25:431
22. Clauer AH, Fairand BP, Wilcox BA (1977) Pulsed laser induced deformation in an Fe-3 Wt Pct Si alloy. Met Mat Trans A 8:1871–1876
23. Cao Z, Xu H, Zou S, Che Z (2012) Investigation of surface integrity on TC17 titanium alloy treated by square spot laser shock peening. Chin J Aeronaut 25:650–656
24. Kim JH, Kim YJ, Kim JS (2012) Effects of laser source geometry on laser shock peening residual stress. Kor Soc Mech Eng 36:609–615
25. Berthe L, Fabbro R, Peyre P, Bartnicki E (1999) Wavelength dependent of laser shock wave generation in the water confinement regime. Appl Phys 85:7552–7555
26. Zhou JZ, Huang S, Sheng J, Lu JZ, Wang CD, Chen KM, Ruan HY, Chen HS (2012) Effect of repeated impacts on mechanical properties and fatigue fracture morphologies of 6061-T6 aluminium subject to laser peening. Mat. Sci. Engg. A 539:360–368
27. Brockman RA, Braisted WR, Olson SE, Tenaglia RD, Clauer AH, Langer K, Shepard MJ (2011) Prediction and characterization of residual stresses from laser shock peening. Int J Struct Integrity 2(1):34–41
28. Gedda H, Powell J, Wahlström G et al (2002) Energy redistribution during CO2 laser cladding. J Laser Appl 14(2):78–82
29. Wang X, Belloaurd Y, Vlassak JJ (2005) Laser annealing of amorphous Ni-Ti shape memory alloy thin films to locally induce shape memory properties. Acta Mater 53:4955–4961
30. Innocenzi ME, Yura HT, Fincher CL, Fields RA (1990) Thermal modeling of continuous wave end pumped solidstate lasers. Appl Phys Lett 56:1831–1833
31. Fabbro R, Fournier J, Ballard P, Devaux D, Virmont J (1990) Physical study of laser-produced plasma in confined geometry. J Appl Phys 68:775–784. https://doi.org/10.1063/1.346783
32. Millett JCF, Bourne NK, Gray GT (2002) Behavior of the shape memory alloy NiTi during one-dimensional shock loading. J Appl Phys 92:3107–3110. https://doi.org/10.1063/1.1498877
33. Wang X, Xia W, Wu X, Wei Y, Huang C (2013) Microstructure and mechanical properties of an austenite NiTi shape memory alloy treated with laser induced shock. Mat Sci Eng A 578:1–5. https://doi.org/10.1016/j.msea.2013.04.058

34. Ya Wei, Pathiraj B, Liu Shaojie (2016) 2D modelling of clad geometry and resulting thermal cycles during laser cladding. J Mater Process Technol 230:217–232
35. Toyserkani E, Khajepour A, Corbin S (2004) 3-D finite element modeling of laser cladding by powder injection: effects of pulse shaping on the process. Opt Laser Eng 41:849–867
36. Kumar A, Paul CP, Pathak AK et al (2012) A finer modelling approach for numerically predicting single track geometry in two dimensions during laser rapid manufacturing. Opt Laser Tech 44:555–565
37. Johnson Matthey Medical Components (2015) Nitinol technical properties. http://jmmedical.com/resources/221/Nitinol-Technical-Properties.html. Accessed 9 July 2015
38. Bang HS, Joo SM, Kim JM, Chang WS (2003) Mechanical Characteristics of resistance multispot welded joints. Sci Technol Weld Joining 8:369–376
39. Gupta OP (2003) Finite and boundary element methods in engineering. Oxford and IBH Publications, New Delhi
40. Trivedi A, Bag S, De A (2007) Three dimensional transient heat conduction and thermo mechanical analysis for laser spot welding using adaptive heat source. Sci Technol Weld Joining 12:24–31
41. Wu B, Shin YC (2006) Laser pulse transmission through the water break down plasma in laser shock peening. Appl Phys Lett 88(1–3):041116. https://doi.org/10.1063/1.2168022
42. Kalainathan S, Sathyajith S, Swaroop S (2012) Effect of laser shot peening without coating on the surface properties and corrosion behavior of 316L steel. Opt Laser Eng 50:1740–1745. https://doi.org/10.1016/j.optlaseng.2012.07.007
43. Morales M, Ocana JL, Molpeceres C, Porro JA, Garcia- Beltran A (2008) Model based optimization criteria for the generation of deep compressive residual stress fields in high elastic limit metallic alloys by ns-laser shock processing. Surf Coat Technol 202:2257–2262. https://doi.org/10.1016/j.surfcoat.2007.12.007
44. Palani IA, Vasa NJ, Singaperumal M (2008) Crystallization and ablation in annealing of amorphous-Si thin film on glass and crystalline-Si substrates irradiated by third harmonics of Nd3+:YAG laser. Mat Sci Semicond Process 11:107–116

LASER Cladding—A Post Processing Technique for Coating, Repair and Re-manufacturing

Catarina Valente, Teresa Morgado and Neeraj Sharma

Abstract LASER cladding technology has a strong applicability in the surface coating sector, mainly in metallic surfaces, although, it has been arousing, more and more, the interest in the components repair and rapid prototyping sector. The reason for its creation was to improve the quality of component surfaces, overcoming the already known disadvantages in traditional processes as TIG—Tungsten Inert Gas welding also known as GTAW—Gas Tungsten Arc Welding, plasma spray or HVOF—High Velocity Oxy Fuel, being these disadvantages the high dilution of the substrate material into the coating/cladding, the large increase of temperature imposed by the process resulting in distortions in the parts, the low precision in material deposition, porosities, micro-cracks, bond defects and problems in the adherence to the substrate. The application of LASER technology for material addition/deposition processes come, for example, to improve the precision of the material deposition, to reduce the dilution of the substrate and the temperature increase of the component to be coated and also, the utilization of a LASER beam, does not cause unfavourable alterations in the mechanical properties of the melt pool. LASER cladding technology can be considered interdisciplinary, in so far as it includes various technological areas, namely the LASER technology, drawing area and computer assisted production, the robotic and control area and also the area of powder metallurgy. The majority of the scientific publications about LASER cladded coatings refer mainly its use in

C. Valente
DEMI—Mechanical and Industrial Engineering Department, FCT NOVA—Faculty of Sciences and Technology, Universidade Nova de Lisboa, Lisbon, Portugal
e-mail: c.valente@campus.fct.unl.pt

T. Morgado (✉)
UNIDEMI—Research and Development Unit for Mechanical and Industrial Engineering, Universidade Nova de Lisboa, Lisbon, Portugal
e-mail: t.morgado@fct.unl.pt; tmorgado@lnec.pt; tmorgado@ipt.pt

LNEC—Laboratório de Engenharia Civil, Lisbon, Portugal

IPT—Polytechnic Institute of Tomar, Tomar, Portugal

N. Sharma
Department of Mechanical Engineering, Maharishi Markandeshwar (Deemed to be University), Mullana 133207, India
e-mail: neeraj.sharma@live.com

K. Gupta (ed.), *Materials Forming, Machining and Post Processing*, Materials Forming, Machining and Tribology, https://doi.org/10.1007/978-3-030-18854-2_10

materials from aerospace, medical and automotive industries. Therefore, this chapter will attempt to focus on the LASER Cladding growing applications of this recent technology and advantages and limitations of this process. This chapter will begin with a historic description of the LASER Cladding technology, followed by the principles of the process operation, the applicability of the process, the state of art of materials utilized in the Cladding process, and the advantages and limitations of the process. At the end of the chapter will be present the recent developments in LASER Cladding process.

Keywords LASER cladding · Powders injection · Additive manufacturing · Rapid prototyping · Coating

1 History of the Process

The LASER cladding process which emerged with the purpose of improving the surface characteristics of metallic components, mainly regarding to the corrosion and wear resistance, come to take advantage of the LASER technology invented by Maiman in the 60s and was considered at that time a great invention for science. LASER would serve as a response to a large variety of scientific questions, until then unanswered for years, as in the case of the materials processing area that has undergone a rapid development in the 70s once the power and the efficiency of the commercial LASER increased. LASER cladding technology was introduced and patented by Daniel S. Gnanamuthu in 1976, in the USA [1–3]. The reason for its creation, as previously referred, was to improve the quality of component surfaces, overcoming the already known disadvantages in traditional processes as TIG—-Tungsten Inert Gas welding also known as GTAW—Gas Tungsten Arc Welding, plasma spray or HVOF—High Velocity Oxy Fuel, being these disadvantages the high dilution of the substrate material into the coating/cladding, the large increase of temperature imposed by the process resulting in distortions in the parts, the low precision in material deposition, porosities, micro-cracks, bond defects and problems in the adherence to the substrate. The application of LASER technology for material addition/deposition processes come, for example, to improve the precision of the material deposition, to reduce the dilution of the substrate and the temperature increase of the component to be coated and also, the utilization of a LASER beam, does not cause unfavourable alterations in the mechanical properties of the melt pool [4, 5].

The pre-placed LASER cladding method, with the pre-placing of the cladding material on the substrate, was initially used by Gnanamuthu at *Rockwell International Corporation*, in California, to investigate the feasibility of the process in the application of dense ceramic cladding on metallic components. One of the research groups that had a significant impact in the development of this innovative technology, led by William M. Steen, introduced LASER cladding by powder injection. Another of the research groups, conducted by Jyoti Mazumder in the 80s, contributed to the

knowledge of possible principles of the process and also applied the technology to various metals and ceramics to have the chance to investigate their potential for cladability and also their posterior corrosion and wear resistance. Note that, one of the considered definitions for cladability, which is a term related to cladding material, includes the ability of the material to form a continuous and high density clad, with a uniform or homogeneous microstructure, having a strong metallurgical bond to the substrate, with low dilution [2].

Still in the 1980s, LASER cladding has started to arouse industry's attention, having been identified as a process that presents great advantages in improving the corrosion and wear resistance of coatings over the conventional processes. The first report of its use in industry occurred in 1981, at Rolls Royce, in the coating of turbine blades components made by Nimonic that would be used in RB-211 jet engine, having its utilization extended to the leading companies in the engine production sector at that time. In the automotive industry, LASER cladding has also started to be applied in the engine valve coating as in the case of Fiat, Toyota and Mercedes-Benz. Still in the same decade, the process was widely recognized by repair market, mainly in turbine blades repairing, both in USA and in Europe [2].

In the 90s, a large number of rapid prototyping and layered manufacturing methods of three-dimensional structures, that already used the principles of the cladding process, were introduced and patented, doing now part of the commercial available solutions [2, 3].

LASER cladding technology has become more and more recognized in the industry and by the most varied research groups. The potential of LASER cladding has been increasing as the research on this technology continues [2].

2 Principles of the Process Operation

LASER cladding is considered a surface treatment technique with LASER. It is possible to distinguish three groups of surface treatment techniques with LASER. The group of surface hardening techniques (or without surface melting techniques), the group of surface melting techniques and the group of techniques with surface melting and with addition material [6, 7]. In the case that is not possible for the base material to improve its mechanical properties on its own with melting or hardening techniques, it becomes necessary or cheaper to resort to the application of a layer of other material on the base material surface [6]. Figure 1, exemplifying the distinction considered for the surface treatment techniques with LASER, is presented below.

Within the techniques that allow the improvement of material properties by the composition alteration of the surface layer with addition of material and within the ones that have in common the formation of a melt pool in which the addition material is applied, is found LASER cladding technique that is then characterized [6]. The other techniques that belong to this group are LASER alloying and LASER dispersing that, unlike LASER cladding, are characterized by an intensive melting of the substrate where the material to be added to create the coating will be incorporated,

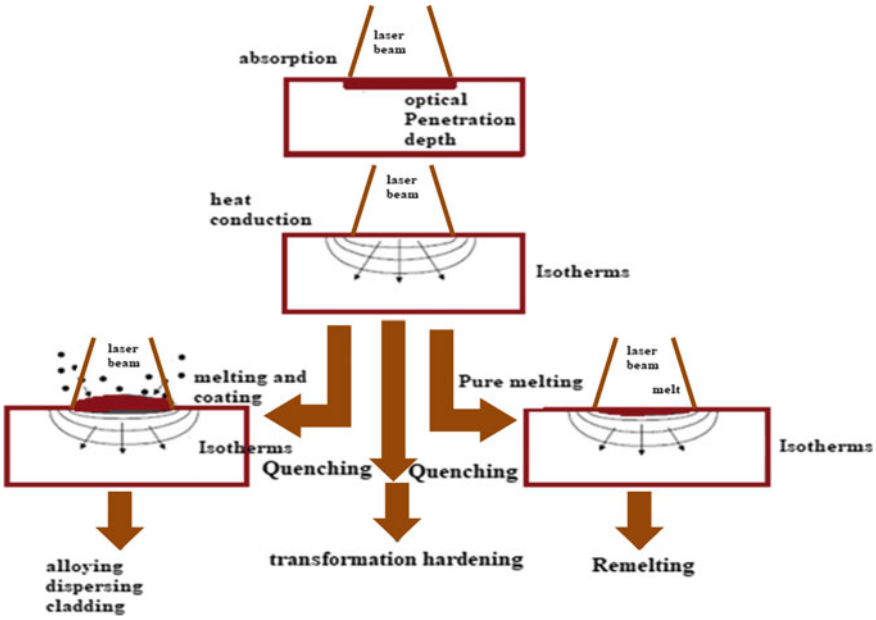

Fig. 1 Mechanisms of surface treatment techniques with LASER

interacting with the melt. On the other side, LASER cladding technique includes the melting of the addition/cladding material, minimizing the melting of the substrate material [4].

LASER cladding is a technique that has as main purpose, as already said before, to improve the mechanical properties of materials surface with the addition of thin layers of different materials [8], besides its additional application in the manufacturing of 3D components. LASER cladding uses LASER as the heat source, in the deposition of a thin layer of a certain material with desired properties on a certain substrate, that provides the melting of the cladding material surface and the substrate surface [2, 7]. The area to be cladded is heated by the absorption of energy delivered by the LASER beam. The heat input provided by a high-power LASER (in most industrial applications the most used power is above 5 kW) beam is well confined and very intense, increasing thus the heating rate of the surface layer. The heated surface layer becomes quenched, after the passing of the LASER by diffusion of heat to the coldest part of the bulk. High rates of heating/cooling in the surface layer result in grain refinement and in the formation of metastable phases and/or in the alteration of the microstructures. LASER cladding process traditionally uses CO_2 LASER and various types of Nd:YAG LASER, although, more recently, it has been betting on the use of fibre LASER [6, 9].

Cladding material can be transferred to the substrate by powder injection, wire feeding or paste feeding (methods of continuous application of the cladding material during the cladding process) and by the method of pre-placing the powders of the

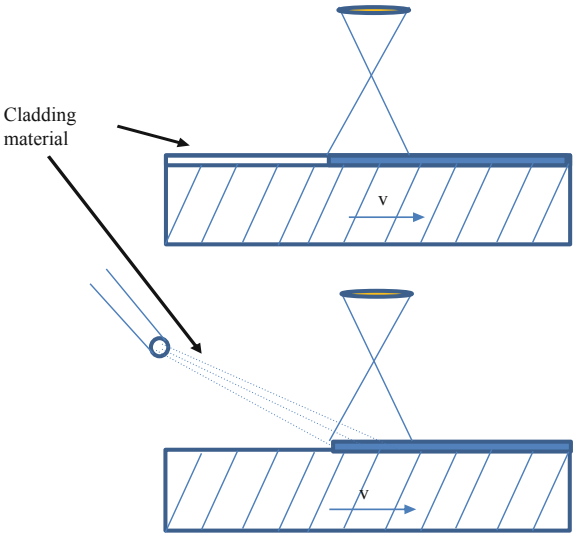

Fig. 2 Schemes of LASER cladding executed by the pre-placed powder method (top part) and by the powder injection method (bottom part) that corresponds to one of the variants of the continuous material feeding method. A LASER beam reaching the material is schematized and the dislocation direction of the substrate is represented by V

material on the substrate [2, 6]. Next, in Fig. 2, is presented a scheme of the two LASER *cladding* methods [10].

Pre-placed powder method corresponds to a two-stage method, beginning the first stage with the application of powder on the substrate. The powder should be mixed with a chemical binder, forming a distributed paste throughout the substrate, ensuring good bond between the cladding material and the substrate as the process takes place. The binder evaporates during the process, which may be the cause of some porosities in the clad layer. In the second stage, occurs the formation of a melt pool on the surface of the cladding material, being propagated subsequently to the interface with the substrate. Proceeding the heating, it is possible to cause the melt pool to be extend to the substrate, creating a strong bond between the material added and the substrate [6, 7].

Relatively to the continuous feeding method during the process by powder injection, which only presents one stage, the melt pool is formed initially on the substrate, being the cladding material injected, at the same time to that melt. In the powders interaction with the LASER beam during the feeding, powders suffer a heating before they are fed into the melt pool that is being created on the substrate. Reaching the melt pool that is created, the cladding material is going to melt, creating a strong bond between the deposited material and the substrate material. Is common the utilization of an inert gas flow as a mean of transportation of powder particles to the melt pool. In this method, instead of powder, the cladding material can come in wire form or even in the form of a paste constituted by the powders and a suitable binder

that is being supplied during the process (allowing a previous formation of alloys to be deposited), being however, this last one less common than the first two kinds of continuous material feeding (much less when compared to the powder injection—the most common) and for that less described in literature [6, 7, 11].

In relation to wire feeding, slight changes in wire position or in feeding velocity can cause significant alterations in the form and dimension of the melt pool, resulting in a hardly uniform and asymmetric clad, thus requiring greater accuracy during the process. The wire also causes a certain obstruction to the LASER, reducing the percentage of the LASER beam that reaches the surface of the base material, when compared to the powder injection form of feeding, in which the LASER passes more easily through the stream of the particles. Which also permits to enhance the advantage of adding the material in powder form is the possibility to vary the quantity of the elements present in the powder mixture, during their deposition, making possible the production of a wide variety of alloys [7]. Figure 3 presents the two methods described above and the variants of the continuous material feeding method.

Powder injection method has been shown as to be the most efficient and most used. There is already a big variety of materials that can be used as cladding material in LASER cladding by powder injection, usually forming layers with thickness ranging from 0.05 to 2 mm and widths of 0.4 mm [2, 6, 7].

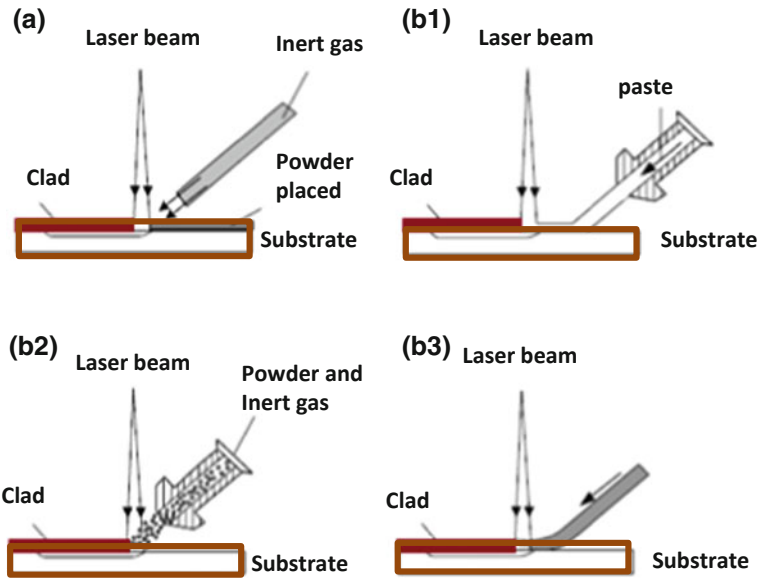

Fig. 3 Schemes of the different methods of LASER cladding and the variants **a** pre-placed powder method; **b1**–**b3** continuous material feeding method (one stage method): **b1** in paste form; **b2** in powder form; **b3** in wire form

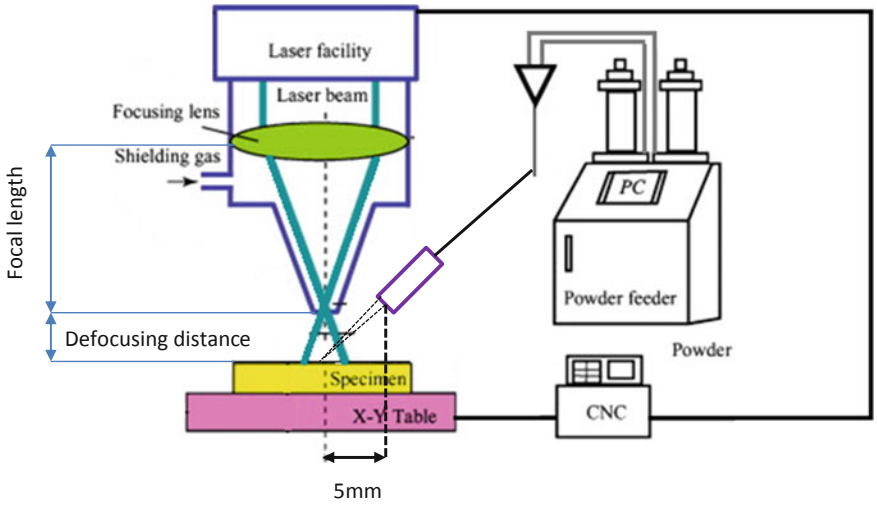

Fig. 4 Setup for a LASER cladding process [12] with kind permission from Elsevier

This LASER cladding technology can be considered interdisciplinary, in so far as it includes various technological areas, namely the LASER technology, drawing area and computer assisted production (more specifically CAD—Computer Assisted Drawing and CAM—Computer Assisted Manufacturing softwares), the robotic and control area and also the area of powder metallurgy [2]. In Fig. 4 it can be seen a setup for a LASER cladding process with powder feeding from a lateral nozzle.

To realize LASER cladding process, in case of a continuous material feeding method, is necessary a set of devices capable of bringing the powder stream, the wire or the paste that is going to correspond to the cladding material, the melt pool shielding gas and the LASER heat source [3].

The authors call to that a LASER cladding head, name used in [4], that corresponds to the set of a LASER facility, a powder/wire/paste feed nozzle(s) and a melt pool shielding gas nozzle. One example of this equipment, with no external nozzles, is demonstrated in Fig. 5.

In Fig. 6, it is possible to visualize one type of nozzle of a LASER cladding head, a coaxial nozzle with this name attributed for allowing coaxial feeding between powders and shielding gas, supplying the cladding material (powder) in its carrier gas, the LASER beam and the shielding gas (equal to the carrier) during the LASER cladding process with powder injection.

The continuous powder feeding, that is the one that is normally used, can be done by lateral/side nozzles and coaxial nozzles (Fig. 6). Argon is often used as the inert gas supplied, sharing the function of carrier of powders and shielding gas. As the name indicates, the shielding gas is utilized to shroud the melt pool region, preventing oxidation [13–15].

Fig. 5 The LASER cladding head

Although, besides the LASER cladding head that allows the reach of the LASER to the surface to be treated, the total equipment to the LASER cladding execution contains two more essential components, a positioning system XYZ (positioning table of two axis) and a powder feeder as was demonstrated in Torres et al. work [16] of development and automation of the LASER cladding equipment with powder injection from the LASER Laboratory of IST, Lisbon University, used by CeFEMA—Center of Physics and Engineering of Advanced Materials. In this work was developed a control process to the LASER cladding equipment through the utilization of a personal computer. In Fig. 6 is possible to visualize the control scheme of the equipment needed to execute the LASER cladding process (Fig. 7).

This automation, which was achieved through the development of the control process, had in mind the optimization of simultaneous utilization of the equipment components and so, allows the control of process parameters such as the overlapping of clads, number of clads, deposition rate, LASER power and powder feed rate (Fig. 8). Controlling these parameters is essential to obtain quality coatings, since these will influence their mechanical properties and durability [8, 16].

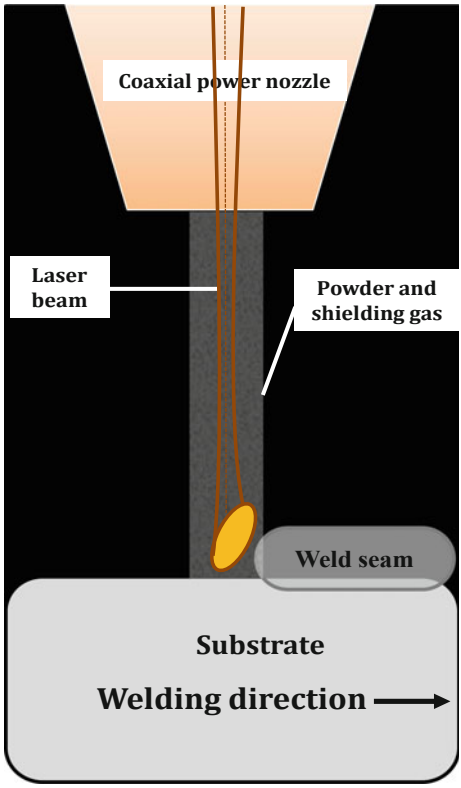

Fig. 6 LASER cladding process with the visualization of a LASER cladding coaxial nozzle

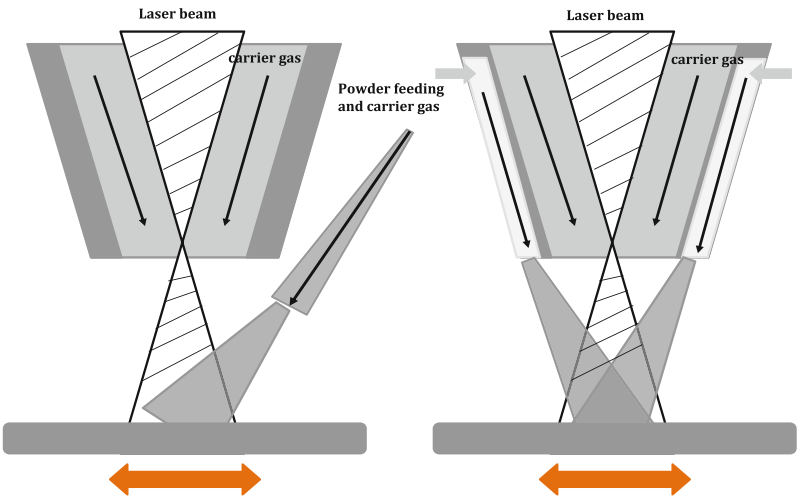

Fig. 7 Coaxial (right) and side (left) LASER cladding with powder feeding above a moving substrate [13] With Kind Permission From Elsevier

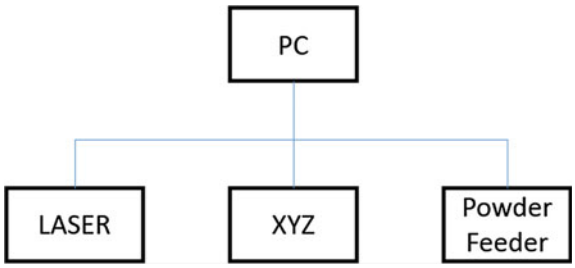

Fig. 8 Control scheme of the LASER cladding equipment

3 Applicability of the Process

LASER cladding technology has a strong applicability in the surface coating sector, mainly in metallic surfaces, although, it has been arousing, more and more, the interest in the components repair and rapid prototyping sector [2, 17].

The coating produced by LASER cladding results from the deposition of a thin layer of a material (metallic or ceramic, for example) in the surface of another material. This allows the modification of the substrate properties to properties improved by the addition material, which will hardly be achieved with only the base material. The coating is going to provide a surface layer resistant, mainly corrosion and wear resistant, and the base material is going to provide the ability to resist to the application of forces. Despite the enormous potential presented by this technology for the application in various industries that use the metallic coating, its application is a bit limited by its elevated cost and low process speed. Although, the improvement of LASER efficiency, the reduction of LASER prices, the development of new kinds of LASER and the increase of scientific publications about LASER cladding applied to a variety of materials, has reinforced that recognized potential for its application in coatings at an industrial level [2].

Most of the scientific publications about LASER cladded coatings refer mainly its use in materials from aerospace, medical and automotive industries. Some of the important materials that were study and are used as addition materials are the titanium alloys, nickel super alloys and cobalt alloys that are deposited on the substrates of materials such as unalloyed steels, alloyed steels, hardened steels, stainless steels, aluminium alloys, cast irons, nickel alloys or cobalt alloys. In certain companies, as the case of POM Inc., in Michigan, to improve the wear and high temperatures resistance, materials that offer these same characteristics were already deposited in tools that are exposed to very high temperatures, to environments with the possibility of occurring thermal shocks, thereby increasing their lifetime. More recently, since a bit more than 10 years ago, bioceramic coating in titanium alloys has been realized by LASER cladding technology, being for that utilized materials as the example of the calcium phosphate. This kind of coating has been applied, as an example, in

orthopaedic implants coated with calcium phosphate, a material that promotes the bone growth when the implant is applied [2].

With respect to the principal current market of metallic coatings applications produced by LASER cladding, we have the coating of aircraft gas turbines. Showing, once again the sense of LASER cladding application, in response to the demand for an increase in efficiency and for a reduction in costs of aircraft gas turbines, cladding materials with high mechanical resistance and resistance to elevated temperatures, as is the case of nickel-based super alloys, are being used through the application of LASER cladding to coat parts from turbines subject to the hot gas passage. Currently, is also already known the LASER cladding utilization in the deposition of this type of materials, referred in this paragraph, in spacecraft components. It is expected that with the improvements that are being operated in the new kinds of LASER, LASER cladding technology starts to represent a more important role in this gas turbine market and also in the aerospace industry in general [2].

Coating obtained by LASER cladding also has other applications in terms of the coating for industrial components (see the example in Fig. 7) with a view to the production of surfaces that are resistant to abrasive, erosive and adhesive wear, corrosion resistant in liquid medium and resistant to oxidation and corrosion at high temperatures, as well. Some examples of products that received metallic coating by LASER cladding, getting the above mentioned characteristics, were parts from drilling tools, engine valve seats, hydraulic pump components and moulds, as well as coated tools with hardfacing coatings for their surface hardening (hardfacing tools) [2].

LASER cladding technology is also used in the repair of high value components, as is the case of some tools, turbine blades and components for military industry. That repair can have the objective of re-establishing the original dimensions of the component that suffered wear and/or allowing the recovery of its mechanical properties. As an example of something repaired by LASER cladding, there is a surface made of high resistance aluminium-based alloys (7075 and 7175 alloys, not weldable). This kind of surface, also called shell by Toyserkani et al. [2], corresponds to the exterior surface of weapon components integrated in submarines that are subject to wear and damage caused by handling difficulties, by the weapon proper activity and also by the saltwater corrosive nature. Figure 9 shows repair of blade with laser cladding.

In the rapid prototyping, layered manufacturing and tooling sector, LASER cladding application allows the manufacturing of complex components and tools in a brieft time with recourse to CAD models. LASER cladding technology is already known as a technology that allows the manufacturing of components very closed to the final shape, without a great need of posterior machining, using a CAD model (sliced by a series of layers) to the construction of the product layer by layer. The little need of machining and the use of CAD models contribute for such reductions in the manufacturing time.

4 Materials Utilized in the Cladding Process

There is already a large quantity of materials that can be utilized as base material in the process, in which are included different steel grades, cast irons and non-ferrous metals such as nickel, titanium and aluminium alloys [4, 19]. Relatively to deposited materials on the base material, there is also already a large number of metals and metallic alloys (mainly hard alloys on the base of nickel, cobalt an iron) being applied, as well as a large variety of their compositions [4].

Tuominen, in his Ph.D. thesis titled *Engineering Coating by Laser Cladding—The Study of Wear and Corrosion Properties*, makes a detailed description of the groups of materials most commonly used in the LASER cladding process in the field of coating and most commonly studied when subjected to the process in this coating field, both as base and coating/cladding materials. Relatively to the base materials, the author refers as main groups the Fe-based materials group including carbon-manganese (C-Mn) steels, alloy steels, stainless steels, tool steels and cast irons, the cast and wrought aluminium alloys group, the group of Ni-based superalloys strengthened (by precipitates, for example) in the cast and wrought form, the titanium and its alloys group, the magnesium alloys group and the cooper (wrought and cast) and its alloys group. Regarding the coating/cladding materials, he refers as main groups the Co-based hardfacing alloys group, the Ni-based alloys group, the Fe-based materials group (namely, stainless steels, tool steels and Fe-based hardfacing alloys), the Cu-based alloys group, the Al-based coatings group, the Ti-based coatings group and also the group of metallic matrix composites, the group of functionally graded materials, the group of solid lubricants, the group of rare-earth element additions and the group of intermetallics [19].

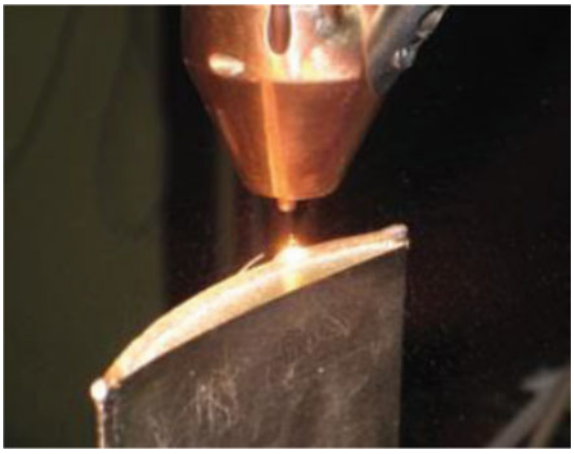

Fig. 9 A blade is being repaired with laser cladding [18]

In the case of rapid prototyping using LASER cladding technology that, among other names, is known by LASER Engineering Net Shaping or three-dimensional LASER cladding, the base material is usually metallic and serves as the construction base of the component to be built. Besides this, generally, base material corresponds to the same material that is going to be deposited (cladding material), normally by a continuous powder feeding, to produce the component, except in the cases that the use of a base material different from the cladding material is convenient to allow a better heat dissipation. Some examples of materials already tested in this rapid prototyping field of LASER cladding that allows the rapid production of components encompass aluminium, stainless steels as the 304L and the 316, tool steels as the H13 and nickel-based alloys as the Inconel 600, 625, 690 and the 718 [2, 20].

5 Advantages and Limitations

LASER cladding technology is presented as advantageous since material properties, such as wear and corrosion resistance and also hardness, can be improved with its utilization. These represent some of the properties that are advantageous when increased, for example, in mechanical components subject to aggressive environmental conditions, to high thermal cycles or in mechanical components that are exposed to corrosive environments. In addition to these properties, the components lifetime is also increased with the application of the LASER cladding. LASER cladding also presents advantages when used as a rapid prototyping technique or as a repair technique. Its utilization as a rapid prototyping technic allows the production of the components in a layer-by-layer way with a combination of characteristics that are considered unique in this process of LASER cladding as a rapid prototyping technique, both in case of the pre-placed powder method as in the continuous material feeding method in powder form. Among these characteristics are found the achievement of a homogeneous structure, good mechanical properties, as it already is a characteristic of the materials subject to LASER cladding, and the rapid production of components with complex structures that acquire a shape very close to the desired one at the end. Comparing to other existing rapid prototyping techniques, as the case of 3D printing, LASER cladding presents more quality in metallic components production. In what concerns the components repair, LASER cladding technology, mainly with powder injection, has the advantage of allowing the repair of components (mainly tools, in their critical contact surfaces), improving their life time and in some cases saving high value components that, otherwise, would have to be replaced, which would cause elevated costs. Represents an alternative to the most used welding processes that produce high temperatures in the materials to be repaired and present a destructive character [2, 8].

It should be noted that some of the competitive characteristics of LASER cladding have their origin in the use of the LASER technology. The utilization of the LASER beam as heat source introduce advantages in relation to the traditional heat sources, namely [6, 9]:

- the energy source can be well controlled due to the nature of the LASER beam, which is confined and narrow;
- allows to perform very localized surface treatments;
- the heat input is low, resulting in minimal thermal distortion;
- allows the achievement of fine microstructure due to the high heating and cooling rates;
- permits a non-contact operation, not occurring wear of tools or force application in the tolls/parts;
- the depth of penetration of the LASER is well defined.

Besides these benefits brought to LASER cladding process by the LASER utilization, the process has other unique advantages such as the minimal dilution of the substrate, a strong fusion bond created between the substrate and the cladding material, a greater ease of preventing porosities and the possibility of achieving a homogeneous distribution of the elements, mainly in the case of powder injection method [6, 9].

It is worth noting that the characteristics of the components' surface improved with the process, which are visible in the case of surfaces treated by LASER cladding in coating or repair applications (despite the also good properties obtained by components built through rapid prototyping by LASER cladding), are due to a reduced dilution that occurs between the substrate and the cladding material, which allows the preservation of the excellent mechanical properties of the coating produced. However, this improvement of surface characteristics it is not only due to the metallurgical characteristics of the coating, it also depends on the thermal cycles applied during the process. The high heating and cooling rates to what the components are subjected during the process will result in a grain refinement, which leads to an increase in mechanical resistance of the materials [2, 8].

Although, despite of the advantages presented above, the process has, at the same time, some limitations. Disturbances in the process may result in significant changes in the clad quality, even when the operational conditions are kept. This low reproducibility, observed in the significant changes, derive from the high sensibility of LASER cladding to small alterations in operational parameters such as LASER power, scanning speed and feeding rate, and it can also result from unexpected perturbations that occur during the LASER cladding as the case of variations in absorptivity. Elevated cost of investment in LASER as well as low efficiency of the LASER sources are also shown to be LASER cladding limitations, in the application of coatings, in the repair area and also in the rapid prototyping area. With continuous technological development in LASER sector and in sophisticated programs to control the process, LASER cladding reveals a great industrial potential for metallic coating (which includes the repair potential), and more recently, in rapid prototyping applications, existing already development of autonomous system of LASER cladding for rapid prototyping that dispenses an expensive formation of qualified personnel for this recent technology, making it more competitive in relation to other processes like 3D printing because of the reduction in its costs [2].

6 Recent Developments in LASER Cladding

Considering last years, LASER cladding process is being used, for example, to investigate its potential in the repair of certain materials as the case of AerMet® 100 steel as is described in Sun et al. research work [21], being this steel, a type of high resistance steel widely utilized in aerospace applications, subject to critical conditions, as in landing gears. These are steels that are expose to high stresses in service conditions, are sensitive to fracture and tend to have a limited toughness. In aircraft applications, the damages caused by impact and corrosion and the required structural integrity, make repair essential. The difficulty in repairing this kind of steels it is because it is essential that this repair allows the structure to carry high stresses, without any reduction in steels resistance to fatigue and fracture. In this research, AerMet® 100 was used as powder and as substrate. As substrate, to the execution of the repair, were utilized standard specimens obtained from bars with circular section with 13.6 mm of diameter, received in the annealed state to be then heat-threated. The utilized powders were predominantly of spherical geometry, mainly in the dimension range from 45 to 106 μm. LASER cladding was executed using the Rofin Sinar CW025 Nd:YAG LASER and a nozzle that allowed the side injection of the powders. The obtained results about the metallurgy, tension, fatigue and fracture of the AerMet® 100 in repaired condition (with the deposition of powder from the same material) and of the AerMet® 100 in substrate condition, i.e., without repair, were compared. The authors of the study reached come conclusions as the verification of the good coating/clad quality produced by LASER cladding and, as less favourable results to this kind of applications, they also verified a reduction in the yield strength, ultimate tensile strength and in the elongation and a significant reduction in the fatigue life of the material. They still identified that LASER cladding isn't the ideal option for substrates of small diameters, due to the creation of a too extended HAZ—Heat Affected Zone.

In a recent experimental study from Ansari et al. [22], coaxial LASER cladding process (with a 700 W pulsed Nd:YAG LASER) with the deposition of NiCrAlY powders, in the range of 50–100 μm, on nickel-based super alloy, more specifically on Inconel 738 super alloy with the dimensions of 100 × 100 × 5 mm, was realized and investigated with the objective of proposing an empirical-statistical model for the process that relates the geometrical characteristics of a single clad obtained by LASER cladding (width—w, height—h, penetration depth—b, wet angle—θ and dilution—D) identified in Fig. 10, with the parameters of this process. The dilution that does not appear in Fig. 10 was named geometrical dilution by the authors of the study and is given in percentage by $D = \frac{b}{h+b}$. The authors considered as principal processing parameters the powder feeding rate—F, the LASER power—P and the scanning velocity—V. The correlations between the geometry and the parameters were stablished as combinations of parameters, of the type $P^{\alpha} V^{\beta} F^{\gamma}$, to each one of the studied geometrical characteristics for a single clad. With this study, it is possible to utilize the obtained correlations to select the most suitable processing parameters of LASER cladding, reducing thus the necessity of extensive and time consumer

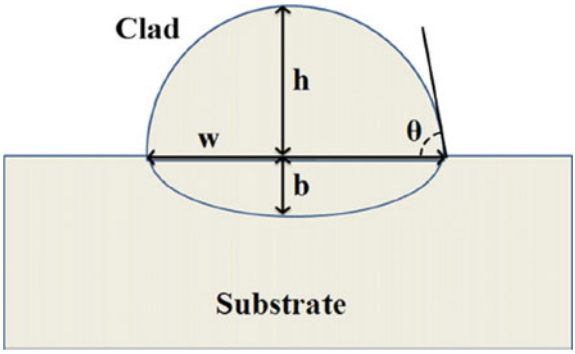

Fig. 10 Scheme of a single clad with the identification of its geometrical characteristics

experimental work. One of the main results referred in the study indicated that the height of the obtained clad statistically depended on the LASER power, having been little influenced by the powder feeding rate and by the scanning velocity, and this statistic relation was described by $P^2V^{-3/2}F^1$. Was also indicated as a result in relation to the clad height, that this has been mainly controlled by the combination of LASER power and scanning velocity, having this relation been translated by $P^{3/2}V^{-1/3}$. Relatively to penetration depth, the result obtained was that this characteristic was mainly proportional to the combination of parameters described by $P^1V^{2/3}F^{-2/3}$ and the dilution proportional to V^1F^{-1}. The authors still concluded that the wet angle have been controlled by the combination of parameters expressed by $P^1V^{-1}F^{1/2}$.

LASER cladding is also being studied as a method for improving the performance of standard grade rail, at a wear and RCF—Rolling Contact Fatigue level, as described by Lewis et al. [23]. Diverse types of metals, chosen by their elevated hardness and proven or expected high resistance to wear and RCF, were used as the cladding material for the standard R260 grade rail discs, having these been tested against discs made from standard R8 steel, in a not cladded condition, used in wheels in contact with the rails. The obtained clads, to produce the coating, had a typical width of 4 mm, making the deposition of various clads necessary to cover the entire disc width of 10 mm. This width is the dimension in contact with the standard R8 disc (standard material used in the wheels in contact with rails). The final coatings produced by LASER cladding had a nominal thickness of 1-2 mm achieved with one or two layers of clads. Among the various materials tested to coat the rails, the samples coated with martensitic stainless steel, Stellite 6 and Stellite 12 were the ones that showed reduced wear rates when compared to the standard R260 grade rail discs and produced also a reduction in the wear of the standard R8 discs. A superior initiation resistance to RCF when compared to the R260 material was also achieve for all of the samples coated with the different metals.

In a recent research work from Feng et al. [24], Inconel 625 coatings fabricated by LASER cladding and, on the other hand, by SMAW—Shielded Metal Arc Welding,

were analysed and compared, at room and elevated temperatures, in terms of their microstructure, hardness and their wear resistance. These coatings, obtained with an equipped system with a 10 kW high-power ytterbium fibre LASER denominated IPG YLS-10000, had as substrate gas turbine valves of martensitic steel COST E, with dimensions of 700 × 400 × 40 mm, that were submitted to this process to produce their surface hardening. Results indicated that the LASER cladding coating made with Inconel 625 powders (spherical particles in the range of 75–100 μm), when compared with the one obtained by SMAW, provided a finer grain, a large presence of strengthening elements as molybdenum (Mo) and niobium (Nb) remained in solid solution matrix and a lower dilution of iron that came from the base material. It was also possible to determine that, when comparing the two processes, the coating made by LASER cladding had, at room temperature, a slightly higher hardness in the coating zone being much higher in the iron dilution zone and, at elevated temperatures, had also higher hardness in all the coating. At all the different temperatures, LASER cladded coating had a lower wear rate due to the lower iron dilution and higher hardness. Therefore, the authors concluded that the coating produced by LASER cladding was preferable, since it presented a better mechanical performance at room and elevated temperatures.

About Ti–Ta alloys produced by LASER cladding, in the last 5 years of published scientific research, it was found a work from Morgado et al. [8] that approaches this theme through the presentation of an original experimental study that allows the evaluation of the wear behaviour of these alloys. To realize the wear study, Ti–Ta alloys were deposited on a commercially pure grade 2 titanium substrate by LASER cladding process. Samples of Ti-30%Ta and Ti-52%Ta were studied. As LASER cladding belongs to the group of the LASER technologies, this process allows to work with elevated temperatures that is essential to elements with high melting points as the case of the titanium and with even higher melting points in the case of tantalum. The considered importance of these innovative alloys is related with their low Young Modulus (similar to the Young Modulus of the bone) and with titanium and tantalum biocompatibility, which are ideal characteristics to their application in biomedical industry. Taking this into account, to study their wear behaviour is crucial, since it influences their structural integrity. To study the wear behaviour, as mentioned before, micro-scale wear tests were realized on the two kinds of Ti–Ta alloys and the results obtained, were very similar for both alloys, demonstrating that the alloys wear volume increases linearly with the rotation of the wear steel ball, with the sliding distance and the time test. From the analysis of the crater formed by the ball used in this test, it was possible to determine that only exists grooving abrasion and the volume of wear abrasion is higher for the alloy of lower hardness (Ti-52%Ta).

In another work from 2017 [25], was also done a mechanical characterization study in standard specimens of the Ti10Ta alloy produced by LASER cladding, with the realization of hardness, tensile and fatigue tests. From this tests was possible to determine the Vickers hardness of the Ti10Ta alloy, tensile-strain curves from which was obtain the yield strength, ultimate tensile strength and the respective strains, the Young modulus, the total strain after fracture and the medium section

reduction of the specimens, allowing to conclude about the ductility of the alloy. In Catarina work [25], was also obtained the equation that translates the uniform region of plastic deformation of the material. Additionally, fatigue behaviour of the material was studied, the *S-N* curve (or stress-number of cycles to fatigue curve) was also obtained.

References

1. Gäbler F (2016) Cladding rises to the top diode LASER cutting. Ind Laser Solu Manuf 31(2):16–18
2. Lepski D, Brückner F (2009) Laser cladding. In: Dowden J (eds) The theory of laser materials processing. Canopus Academic Publishing Limited, pp 235–279
3. Khazan P, Stroh M, Freiße H, Köhler H (2017) Manufacturing specimens made by direct powder deposition—industrial LASER solutions. [Online]. Available: http://www.industrial-lasers.com/articles/print/volume-29/issue-6/features/manufacturing-specimens-made-by-direct-powder-deposition.html. Accessed 12 Feb 2017
4. Vilar R (1999) Laser cladding. J Laser Appl 11(2):66. https://doi.org/10.2351/1.521888
5. Lambarri J, Leunda J, García Navas V, Soriano C, Sanz C (2013) Microstructural and tensile characterization of Inconel 718 LASER coatings for aeronautic components. Opt Lasers Eng 51(7):813–821
6. Goodarzi Dara Moazami, Pekkarinen Joonas, Salminen Antti (2015) Effect of process parameters in laser cladding on substrate melted areas and the substrate melted shape. J Laser Appl 27(S2):9201. https://doi.org/10.2351/1.4906376
7. Torres JMSP (2015) Improvement and automatization of a LASER cladding system. Master thesis. FCT, UNL—Universidade NOVA de Lisboa, Portugal (in Portuguese)
8. Morgado TLM, Navas H, Brites R (2016) Wear study of innovative Ti-Ta alloys. Proc Struct Integr 2:1266–1276
9. Malin V, Woods S (2017) Efficient high-power diode LASER cladding—industrial LASER solutions. [Online]. Available http://www.industrial-lasers.com/articles/print/volume-24/issue-8/features/application-report/efficient-high-power-diode-laser-cladding.html. Accessed 02 Jan 2017
10. Zanzarin S (2015) Laser cladding with metallic powders. Ph.D. thesis. University of Trento
11. Lugscheider E, Bolender H, Krappitz H (1991) LASER cladding of paste bound hardfacing alloys. Surf Eng 7(4):341–344
12. Xu G, Kutsuna M, Liu Z, Sun L (2006) Characteristic behaviours of clad layer by a multi-layer LASER cladding with powder mixture of Stellite-6 and tungsten carbide. Surf Coat Technol 201(6):3385–3392
13. de Oliveira U, Ocelík V, De Hosson JTM (2005) Analysis of coaxial LASER cladding processing conditions. Surf Coat Technol 197(2–3):127–136
14. Quintino L (2014) Overview of coating technologies. In: Surface modification by solid state processing. Elsevier, pp 1–24 (Chapter 1)
15. Borges BMFDCA (2008) LASER cladding using filler powder and wire—productivity and quality. Master thesis. IST, ULisboa—Universidade de Lisboa, Portugal (in Portuguese)
16. Torres JMSP, Morgado TLM, Navas HVG (2015) Innovative automation equipment of LASER cladding. In: Presented at the 2015 international conference on systematic innovation. Hong Kong
17. Souto HIM (2013) LASER cladding: its application to the deposition of coatings in blades of wood crushers. Master thesis. FEUP, UP—Universidade do Porto, Portugal (in Portuguese)
18. Saqib S, Urbanic RJ, Aggarwal K (2014) Analysis of laser cladding bead morphology for developing additive manufacturing travel paths. Proc CIRP 17:824–829

19. Tuominen J (2009) Engineering coatings by LASER cladding—the study of wear and corrosion properties. Ph.D. dissertation. Tampereen teknillinen yliopisto, Suomi
20. Ludovico AD, Angelastro A, Campanelli SL (2010) Experimental analysis of the direct LASER metal deposition process. In: New trends in technologies: devices, computer, communication and industrial systems. Sciyo, pp 253–272 (Chapter 14)
21. Da Sun S, Leary M, Liu Q, Brandt M (2015) Evaluation of microstructure and fatigue properties in LASER cladding repair of ultrahigh strength AerMet® 100 steel. J LASER Appl 27(S2):S29202-1–S29202-6
22. Ansari M, Shoja Razavi R, Barekat M (2016) An empirical-statistical model for coaxial LASER cladding of NiCrAlY powder on Inconel 738 superalloy. Opt. LASER Technol 86:136–144
23. Lewis SR et al (2016) Improving rail wear and RCF performance using LASER cladding. Wear 366–367:268–278
24. Feng K et al (2017) Improved high-temperature hardness and wear resistance of Inconel 625 coatings fabricated by LASER cladding. J Mater Process Technol 243:82–91
25. Valente C (2017) Study of the mechanical behaviour of a titanium-tantalum alloy, Ti10Ta, produced by LASER cladding. Master thesis. FCT, NOVA—Universidade Nova de Lisboa, Portugal (in Portuguese)

Electrochemical Behaviour and Surface Studies on Austenitic Stainless Steel and Nickel-Based Superalloy Dissimilar Weld Joints

M. Adam Khan, D. Chellaganesh, M. Uthayakumar, J. T. Winowlin Jappes and Muthukannan Duraiselvam

Abstract Development on austenitic stainless steel and nickel-based superalloys have played vital role in the field of manufacturing of engineering components. The selection of materials depends upon working environment and operating conditions. In some cases, the combination of two different materials is used to join and apply them for specific working conditions. Joining of stainless and super alloys for turbine power shaft and high temperature steam pipe lines are the two major examples of this. Challenges in current research are to join dissimilar materials without disturbing the properties of parent metals. Materials joining process either may be at fusion state or solid state. Extensive research articles are available to discuss about the joining process of similar materials. While considering the dissimilar materials, individual conditions has to be satisfied depending upon the choice of joining process. Sample thickness, weld energy required, filler material, weld speed, weld design, etc. are the pre-requisite for completion of the process. The weld zone heat transformation (thermal gradient) thickness and its metallurgical quality are the major outcome in welding process. In this chapter, the research is focused on joining of two different metals using laser and electron beam welding (EBW) process. The metallurgical changes in the weld zone are studied. Further, the electrochemical behaviour of austenitic stainless steel and nickel-based superalloy dissimilar weld has been studied using 3.5% NaCl solution. The samples exposed to corrosion medium are followed with metallurgical characterization techniques such as: Optical imaging, SEM, EDS and XRD. Results from the investigation indicate that the EBW sample is superior than laser beam welded sample. The heat convention under laser welding has induced the samples to metallurgical deficiency.

Keywords Joining · Welding · Steel · Superalloy · Laser · Corrosion

M. Adam Khan (✉) · D. Chellaganesh · M. Uthayakumar · J. T. Winowlin Jappes
School of Automotive and Mechanical Engineering and Centre for Surface Engineering, Kalasalingam Academy of Research & Education, Krishnankoil, TN 626126, India
e-mail: adamkhanm@gmail.com

M. Duraiselvam
Department of Production Engineering, National Institute of Technology, Tiruchirappalli, Tamil Nadu, India

K. Gupta (ed.), *Materials Forming, Machining and Post Processing*, Materials Forming, Machining and Tribology, https://doi.org/10.1007/978-3-030-18854-2_11

1 Introduction

Research on austenitic stainless steel and nickel based superalloy has evoked with many engineering components. The selection grade of stainless steel and superalloy are due to good mechanical properties and resistance towards corrosion [1–3]. In austenitic stainless steel major alloying element, nickel and chromium increases resistance towards pitting, galvanic and crevice corrosion [4]. At the same superalloys are extensively used in aircraft, marine, industrial and vehicular gas turbines where some of the most severe environments are encountered [5]. Distinguished grades, application and their properties of Nickel-, Iron-Nickel base, cobalt-nickel base superalloys are well explained with application and conditions by Donachie and Donachie [6] and Lai [7]. The materials manufactured as a final product are highly susceptible to corrosion. The effect of manufacturing parameters does also influence the deterioration of the material during exposure. Therefore, selection of suitable manufacturing process for the candidate material is a major concern for the proposed research.

Past two decades the advanced manufacturing processes plays a vital role in joining two materials either mechanically or by fusion [8, 9]. A variety of similar materials can be joined using standard welding parameters. Literature revealed that welding of single crystal nickel based superalloy is generally weak in fusion welding [10, 11]. However, in automotive industries, boiler power plant, turbine engine, oil refineries and for other applications joining of two different materials it is very challenging to join two different base metals [12]. During dissimilar welding, joining superalloy and stainless steel for engineering application has major issues during fusion [13, 14]. In conventional welding process improper selection of filler materials leads to weld defects such as crack formation, solidification of weldments and segregation [15]. The welding processes are selected based on to increase the mechanical strength and also to improve the metallurgical quality of the weld joints. The most common advanced welding process used to join two different materials are Laser welding, electron beam welding (EBW), ultrasonic welding, friction welding etc. [16]. These welding's are preferred to prepare seam or stitch welding which are mostly used in automotive industries [17].

The typically questions raised during welding studies are that, should the material be pre-treated before welding? It is clear that, pre-treatment or pre-heating of austenitic materials will lead to form martensitic structure and in some cases the precipitate hardenings along with carbide formation are the major issues [18]. While discussing about the crack formation, it is better to control the heat source and to provide special arrangements for proper solidification of weld pool. This can also be accomplished with the weld design, by making a narrow weld bead. Another form of defects in weld zone is called hot cracking. This is due to the (i) improper solidification of weld pool; (ii) liquation cracking in heat affected zone; and (iii) combination of above two. The major issues on welding superalloys are invariant. Especially, the nickel alloys are prone to hot cracking at elevated temperature and it is due to the solidus line between liquid-solid of weld metal [19]. In thick weld area,

the stray crystals are observed in the weld zone promoting the cracks to propagate during solidification. If the weld sample thickness is less in measurements, then the common defect arise in the centre of weld bead during solidification and it is called centreline. It is due to the addition of higher alloying elements and level of impurities formed during solidification [20]. Literatures are available to discuss more on weld defects and mechanical properties of the weld joints. However, when these weld joints are subjected to aggressive operating conditions; weld joints are susceptible towards metallurgical failure in the form of corrosions.

From the literature it is clear to confirm that the dissimilar welding and mechanical properties evaluation are the major topic covered in current scenario. However, the electrochemical behaviour of dissimilar weld joint is the major research area to be focused. Thus, the research was proposed to carry out with AISI316L and Inconel 617 candidate material. The laser beam welding (LBW) and electron beam welding (EBW) are used advanced welding processes. The weld samples are subjected to electrochemical polarisation studies and materials characterisation techniques.

2 Materials and Welding Process

2.1 Welding Materials

Stainless steel and nickel-based superalloys are widely used in different engineering applications. Aircraft engine, nuclear reactors, petrochemical industries and major defence components are made of superalloys and stainless steel materials. These materials are exposed to high temperature environment at severe operating conditions. Depending upon the alloying grade, thickness and operating conditions; suitable manufacturing processes are selected. Welding is one of the important manufacturing processes to join materials of similar and dissimilar metals. The two different candidate materials used to weld are austenitic stainless steel AISI316L and nickel-based superalloy Inconel 617. These materials are induced to face high heat energy and combustion flue gas mixture during services. The nickel-based superalloy is reputed to weldable and has good resistance to solidification cracking [21]. The chemical composition the candidate materials are listed in Table 1. The samples are sliced with abrasive water jet (AWJ) machining process. The size of the sample used to weld is—100 × 50 × 3 mm plate. Before welding the edges of the samples are prepared burr free zone and placed for welding.

Table 1 Nominal chemical composition of AISI316L and Inconel617 alloy

Materials	Ni	Cr	Co	Mo	Fe	Al	Mn	C	Traces
AISI316L	54.50	21.25	12.20	7.82	1.90	1.05	0.08	0.06	Si, Ti, Cu & B
Inconel 617	10.56	16.23	0.018	2.18	68.65	–	0.72	0.012	Si, S, P, Cu, V, Ti & Nb

These two materials are capable to join using different welding processes. Based on the thickness of the base metal, the welding processes are selected. Materials with a maximum of thickness 3 mm is possible to join using all available welding processes like laser, electron beam, resistance welding, and induction brazing etc. [12]. Most of the processes are not suitable to adopt for welding with maximum thickness. In this research, the maximum thickness of the sample is 3 mm, since electron beam welding and laser beam welding are chosen to join austenitic stainless steel and nickel based superalloy for dissimilar welding process.

2.2 Laser Beam Welding

Laser Welding is one of the best welding processes compared to conventional welding techniques for different applications including for joining the superalloy materials [22]. It is promising with high productivity, low distortion and less heat input when compared to conventional welding techniques. Two variety of laser has been used for welding process neodymium (Nd) ion and CO_2 respectively. Laser welding has the capability to weld the component without the filler material [23, 24]. Due to unique property in the LBW it has used in many engineering applications like welding, surface treatment, cutting and micro machining etc. By this method heat intensity is high deep weld penetration is possible with minimum or no heat affected zone [25]. In the HAZ intergranular liquid to temperature possible to develop on cooling tensile stress this induced to formation of crack on the grain boundaries. In the laser beam welding, the beams are directed by the flat optical element, mirrors and it focuses to small spot of the work piece to be weld (Fig. 1). To protect the material from the oxidation, it has been kept in the inert gas shielding and filler rod has used in occasionally. The intensity of the laser beam can focus from 0.1 to 1.0 mm providing a power density in watts/mm^2.

2.3 Electron Beam Welding

Electron beam welding (EBW) is fusion joining process. This technique is most popular in the aerospace and nuclear industry especially suitable for complex welding structures [26]. EBW works with the dense high electrons bombarded with work piece to fuse the material for joining of metals. Due to the energy and accelerating intensity, electrons can penetrate external layer of the material up to the depth of 10^{-2} mm [27]. The average speed of the electrons flow is between 50,000 and 200,000 km/s. Figure 2, shows the basic construction of electron beam welding process in a simple representation. This process is continuous to melt the metal and its changes into vapor state. After releasing of the vapor, the electron beams are focused and penetrate to formation of the next layer. This process is continuous to formation of the welding. There are no requirements of filler materials during joining of metals. Though the important design on welding of sample depends on the fixtures used to hold the work piece. EB welding has significant advantages over other welding processes, namely:

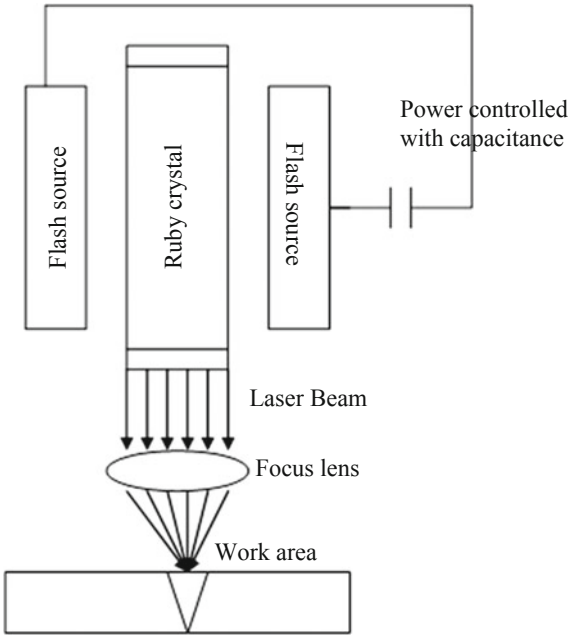

Fig. 1 Schematic view of laser beam focusing during welding process

rapid welding, controlled process, high accurate, minimum distortion, small heat affected zone, etc. The application of EBW is to weld heavy metals and ceramics such as superalloys, beryllium, columbium, tungsten, zirconium, titanium, etc.

2.4 Selection of EBW and Laser Welding Process

Based on the developments in recent generations, welding process has tremendous growth. Based on the application, appropriate welding processes are adopted. Among the fusion welding, EBW is a predominant welding process to join metals [28]. In current scenario, Laser welding and electron beam welding are the leading techniques to produce high quality weld joint. However, these welding beam intensities are variable with reference to the power consumed per unit of weld area. Figure 3, illustrates the power with reference to the weld area for different welding processes.

However, there are some constraints to be considered during selection of welding process. EBW and Laser welding are high speed welding process. In conventional joining metal process, the weld bead width remains maximum and thermal stress induced due to welding arc/heat source is more. Figure 4 represents the depth of penetration/weld bead area and power density consumed for different welding process. The maximum heat transformation zone in welding will lead to severe in crystal rearrangements. Arc welding and plasma welding is having maximum weld area

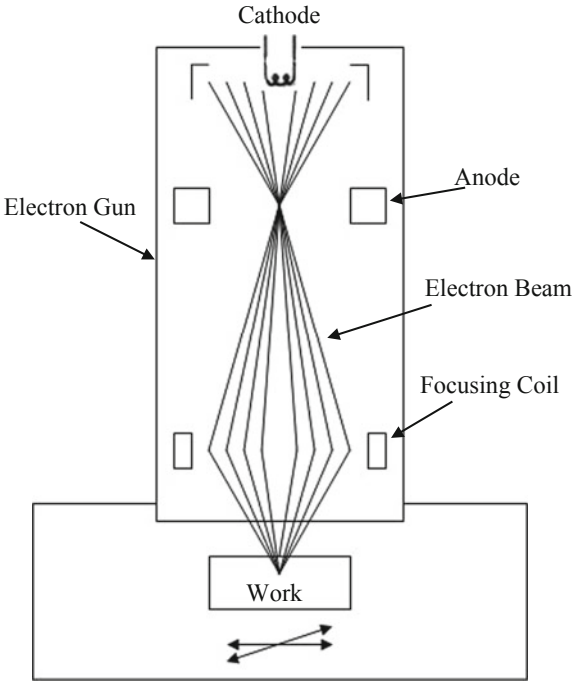

Fig. 2 Schematic illustration of electron beam welding setup

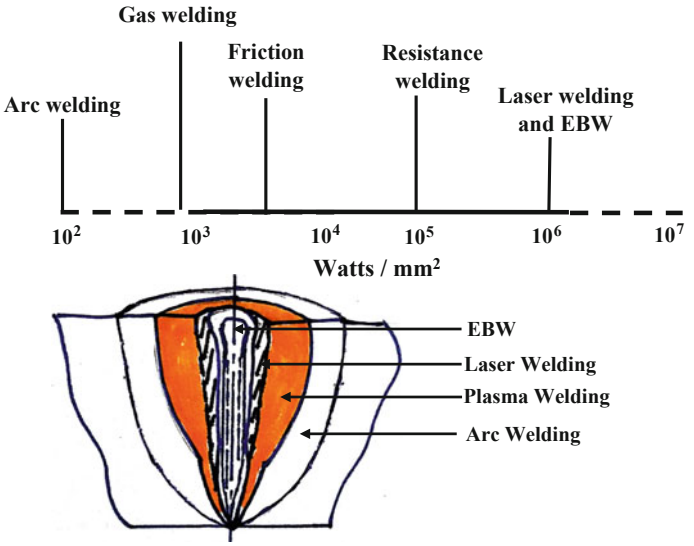

Fig. 3 Welding power and weld beam intensity for different welding processes

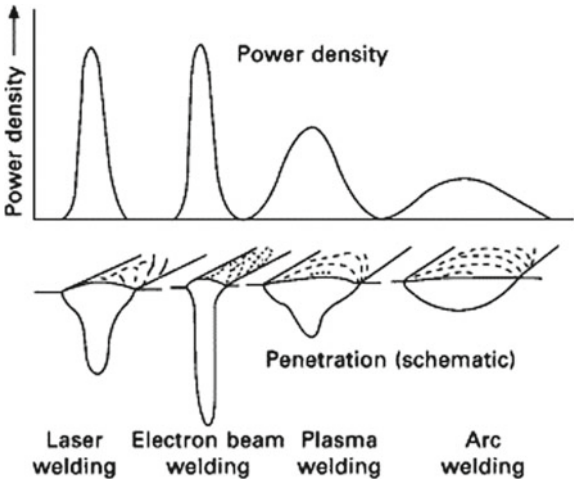

Fig. 4 Representation of penetration/weld bead and power density of different welding process

compared to EBW and laser welding (Fig. 4). However, the depth of penetration is deep and narrow for EBW compared to laser welding process. Therefore, the heat affected zones (HAZ) are reduced in EBW and Laser welding than the conventional welding processes. To control the scatter of heat, shielding gasses are used and also to protect weld area from oxidation. EBW can be done in vacuum environment to evade the x-rays generated during process and for better weldability. As the welding conditions are controlled ambient, proper cooling system should be provided for both the processes.

2.5 Welding of Dissimilar Materials

Defence industries are working to advance materials manufacturing processes for joining dissimilar materials. Joining of dissimilar materials and its validation are tough in turbine engine materials. Especially the turbine power shafts are in combination of austenitic stainless steel and nickel-based superalloys. Welding process is carried out through two different processes namely: laser beam welding and electron beam welding.

The optimum welding parameters [29, 30] used to join to two different materials are listed in Tables 2a and 2b. After welding the samples are sliced with AWJ machining process and metallurgical polishing techniques followed to prepare the samples for electrochemical investigations. The samples after mirror polish are subjected to electrochemical polarization stud ies. The sweep voltage was set between −250 and 250 mV with a sweep rate of 1 mV/s [31]. The exposed samples after obtaining volt-ampere plot are subsequently followed by material characterisation techniques. The high-resolution scanning electron microscope (Make: Zeiss–FE SEM) attached with EDS analyser (Make: Brukers EDS) are used to study the surface quality, element spec-

Table 2a Laser beam welding parameters

Parameters	Range	Unit
Power	1.25–1.4	kW
Nozzle diameter	2	mm
Nozzle-specimen distance	5	mm
Traverse speed	3	mm/s
Voltage	300	V
Lasing medium	Yittribium	

Table 2b Electron beam welding process parameter

Parameter	Range	Unit
Voltage	150	kV
Beam current	80	mA
Weld speed	5	mm/s
Gun-specimen distance	100	mm
Weld pass	Single	

troscopic analysis and image mapping of the exposed samples. The Brukers X-Ray Diffractometer Cu-Kα radiation ($\lambda = 1.541$) is used for characterisation studies.

3 Results and Discussion

The electrochemical behaviour of superalloys is better than the austenitic stainless steel. It is difficult to predict when they are fused together during welding process. The dissimilar welding of AISI316L and Inconel617 are joined through laser beam and electron beam welding process and subjected to electrochemical analysis. Figure 5 shows the volt-ampere graph of the laser beam and electron beam welded samples investigated under 3.5% NaCl solution. The activation energy for the weld samples are at different stage though their anodic reaction of the samples is significantly same at both the situation. The results from the volt-ampere TAFEL graph are listed in Table 3. Result on electrochemical voltametric analysis describes the weld quality in terms of rest potential with wide variations. That is for laser beam and electron beam welded samples the corrosion potential (E_{cor}) is −385.21 and −356.63 mV. The electrochemical behavior of electron beam welded sample leads toward positive potential volt than laser beam welded sample. At the same the current density (I_{cor}) for laser and electron beam weld is 0.000608 and 0.000566 mA/cm^2 respectively. For both the samples the corrosion rate falls at 0.00609 mm/year for electron beam and 0.00654 mm/year for laser welding. This indicates that the quality of both the welds is nearly same and the slight changes in corrosion rate and corrosion potential are due to the influence of welding processes. Thus the samples investigated under polarization studies are further subjected to metallurgical characterization techniques.

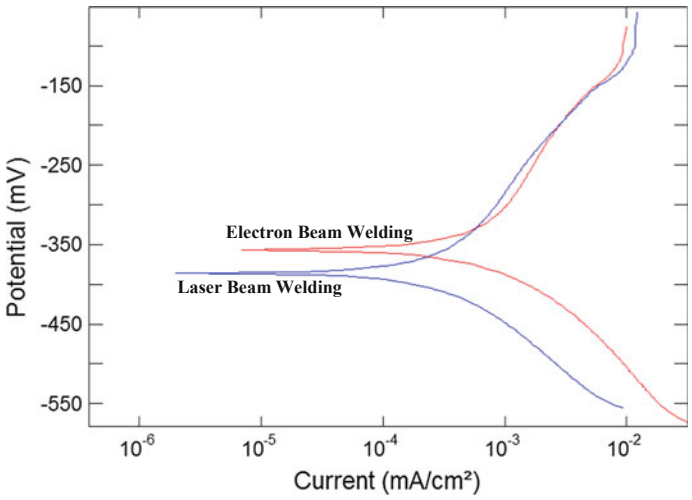

Fig. 5 volt-ampere graph of 3.5% NaCl solution samples

Table 3 Results on rest potential, corrosion potential, current density and corrosion rate for laser beam and electron beam welded samples

Sample	RP (mV)	E_{Cor} (mV)	I_{Cor} (mA/cm^2)	CR (mm/year)
Laser beam welding	−304.20	−385.21	0.000608	0.00654
Electron beam welding	−247.69	−356.63	0.000566	0.00609

Figure 5 shows the volt-ampere graph of the sample investigated under 3.5% NaCl solution.

During electrochemical analysis, materials are susceptible to corrosion based on the energy consumed, metallurgical character and influence of corrosion species. Figure 6 shows the surface morphology of the electron beam welded sample. Surface has been scanned over the weld zone as the susceptibility appears at particular region. At lower magnification the surface shows clear morphology and pitting revealed only at higher magnification. Pitted surface was observed with a salt deposit as a catalytic spot to a size of 14–16 μm. While the surface examined with energy dispersive spectroscopy influence of alloying elements with active corrosive species are studied. The EDS result with BSE image and element wt% is shown in Fig. 7. Weld zone infers that the nickel and chromium are the major alloying element found fused with cobalt, molybdenum, iron and aluminium. In addition, traces of sodium and chloride ions have been found reacted with the alloying elements. The corrosion has been initiated due to the presence of oxygen in the corrosion medium which is then reacted with the above alloying elements to form oxide compound. The major oxide compounds found through Brukers—EDS analysis are as: NiO (53.21%), Cr_2O_3 (25.05%), FeO (2.84%) and Al_2O_3 (1.70%). Thus the major oxides build passive film to protect the material from further corrosion.

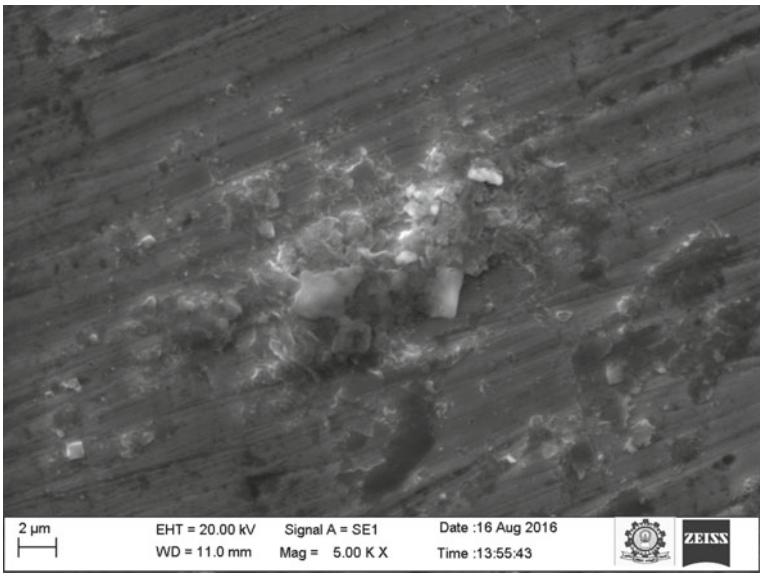

Fig. 6 SEM micrograph of electron beam welded sample after electrochemical analysis

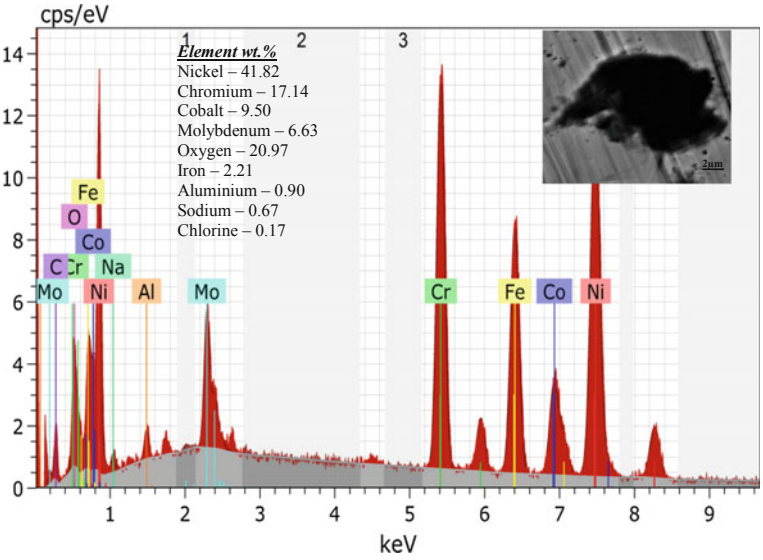

Fig. 7 EDS analysis and BSE image (as inset) of electron beam welded sample

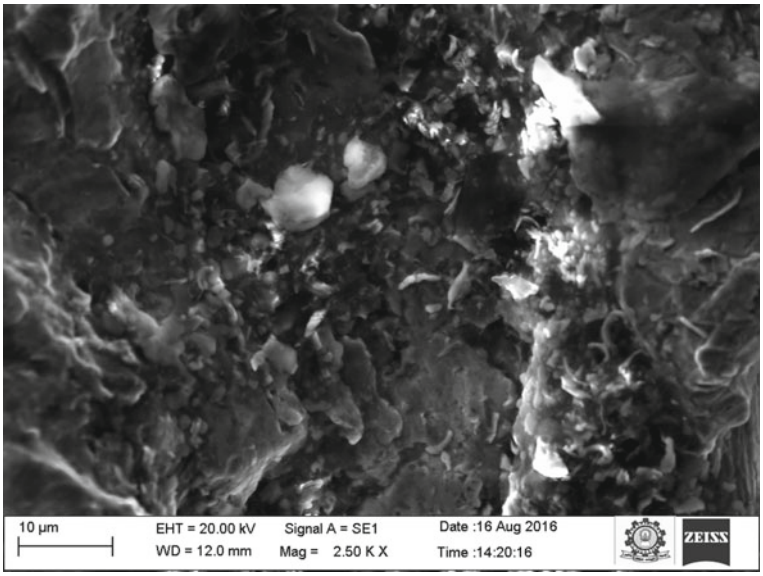

Fig. 8 Surface morphology of the laser beam welded sample exposed to 3.5% NaCl solution for polarization analysis

Superalloys are generally found inferior with laser fusion process compared to other welding techniques. While joining stainless steel and nickel based superalloy, heat developed from laser beam has influenced superalloy to undergo thermal shock. Figure 8 shows the corrosion severity in laser beam welded sample. The exposed surface has subjected to aggressive corrosion and scoring on welded zone (both in weldment and HAZ) was observed. The significant mechanism behind the corrosion was thermal shock and metallurgical effect caused due to laser source. It has led to inclined with corrosion medium for materials degradation. It is evidently proved with the help of optical image as shown in Fig. 9.

The fusion on the weld and its microstructure transformation are due to the base metal grain structure and welding conditions. Especially, the materials made of single crystals are quite different and difficult to infer. Figure 10, infers the basic transformation in grain refinement during weld pool solidification. At high intensity heat, the maximum thermal energy was produced to form coarse grain in majority at weld zone and simultaneously at heat affected zone, the grains are refined layer-to-layer based on the thermal gradient. At a stage, the refined grains are interlocked with based metal grains called fusion boundary.

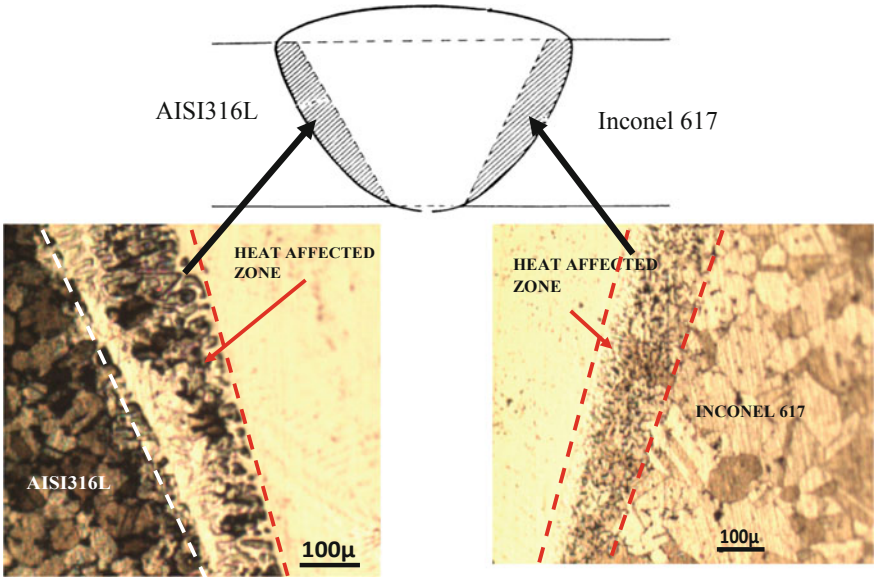

Fig. 9 Optical image of laser welded sample indicating HAZ and base metals grain structure

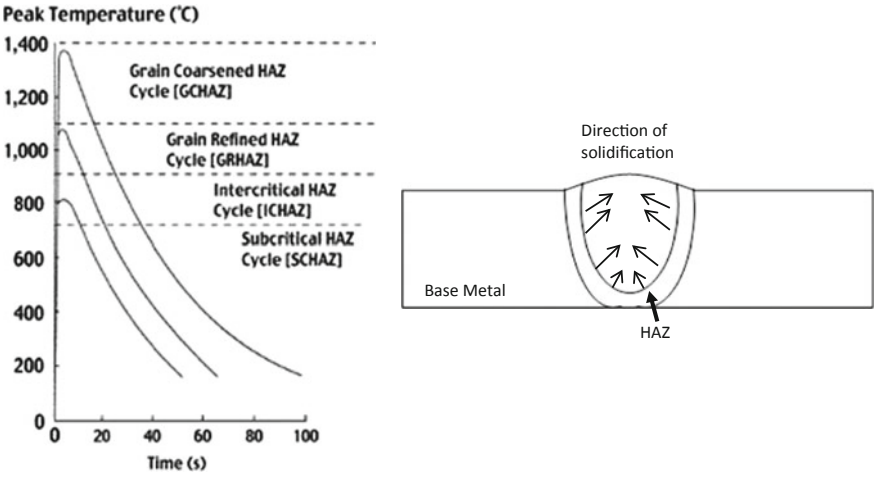

Fig. 10 Weld peak temperature and grain transformation during welding process

The base materials grain structure is clear to label the grade and subsequent zone shows heavy fusion with dendrite structure. Literature reported that HAZ and weld beads are highly susceptible to aggressive medium prone to severe corrosion. During welding the material fused together and forms metallic compounds in an undefined crystal structure. Distribution of alloying elements in weld bead and HAZ layer was observed through EDS analysis image mapping. Figure 11 shows the BSE image and spectra image mapping of the laser welded sample after corrosion investigation. This layer comprised of major alloying elements such as: Ni—25.44%, Cr—1.83%, Co—5.62%, Mo—4.00%, O—8.26%, Fe—4.72 and Cl—3.26% are listed from spectroscopic analysis. The iron and carbon from AISI316 have fused together with nickel and chromium alloy from Inconel 617 alloy. Further, the alloying compounds formed during corrosion studies are studied with the help of XRD analysis.

Figure 12 illustrates the intensity noticed from x-ray diffraction analysis. For both the welding process the elements found are same and peaks are matching with each other. As a results, the peaks of iron, nickel and formation of metallic compound (both iron and nickel) as a major element in the ratio of 5:4:1 respectively (Ref No.: Fe—98-008-8003, Ni—98-005-2851 and FeNi—98-008-8172). This shows the inferiority of the nickel ions to iron with reference to laser heat source. This may be the major reason to get the same corrosion rate for both the weld samples.

4 Conclusions

From the investigation of dissimilar welding process, the following conclusions are drawn with reference to the electrochemical polarisation analysis and material characterisation techniques.

- The welding quality of laser beam was found to be inferior compared to electron beam welding process.
- The HAZ of laser beam welding has major metallurgical deficiency in terms of thermal shock and carbon depletion.
- The Electrochemical analysis proved that EBW is superior than laser beam welding in terms of corrosion potential and corrosion rate.
- The activation of chlorine ions has indulged the laser beam welded samples to severe corrosion compared to EBW.
- The surface topography and EDS analysis supports the enhanced quality of EBW weldments.

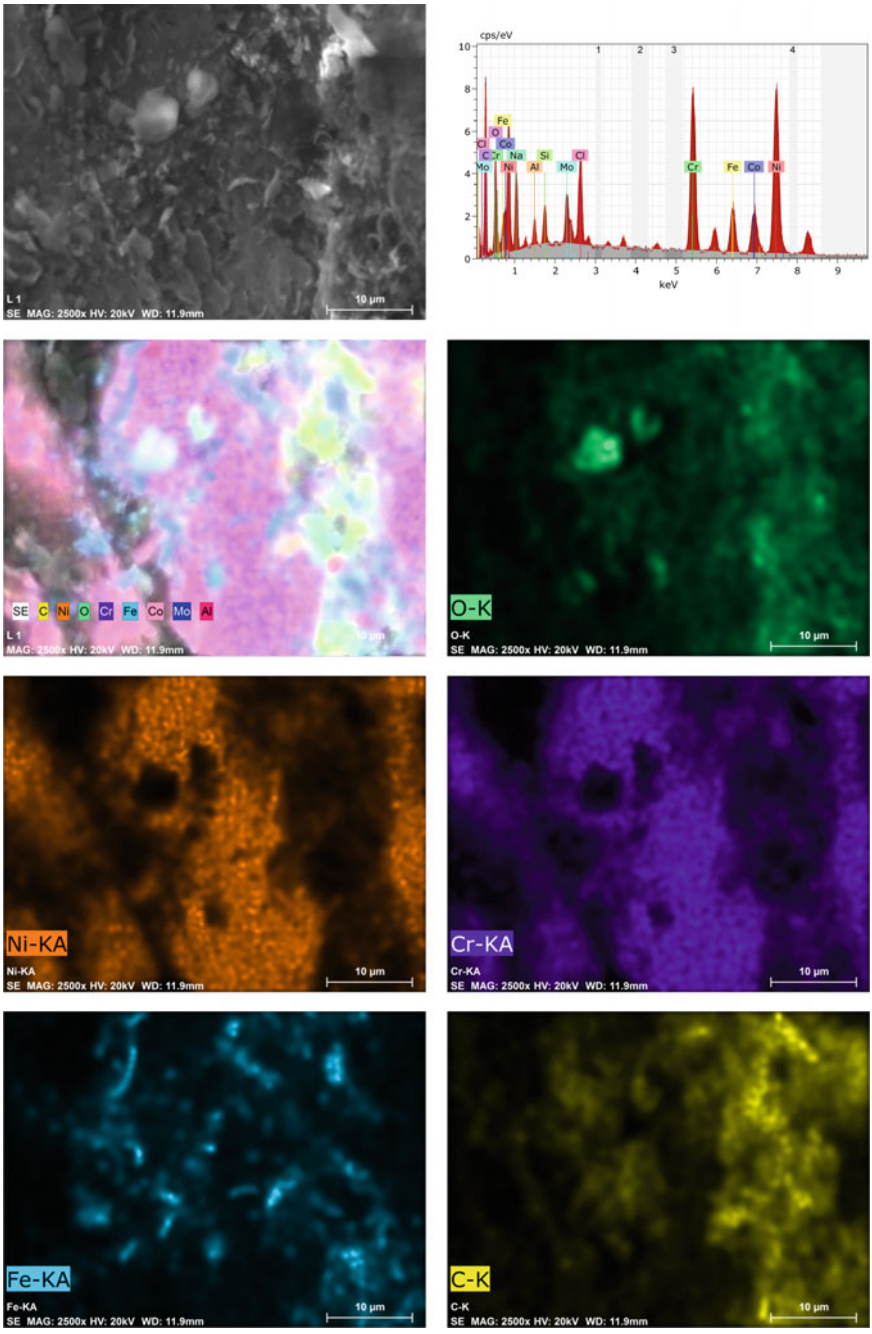

Fig. 11 SEM micrograph and EDS image mapping for the laser beam welding samples

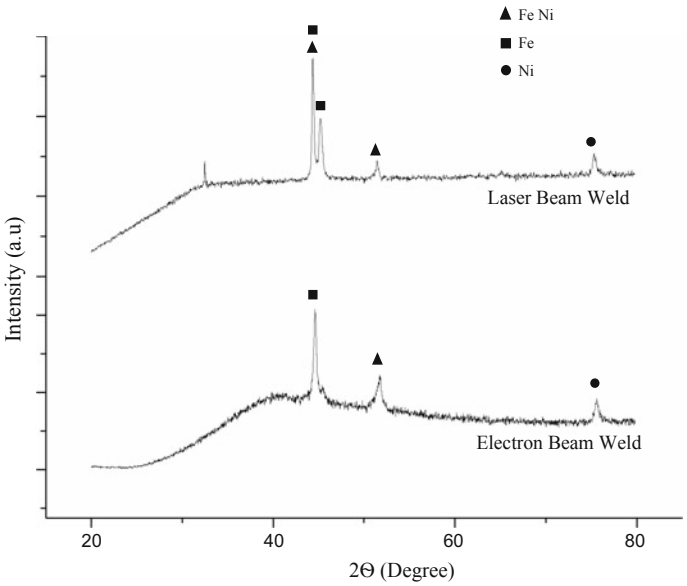

Fig. 12 XRD peaks indicating major alloying compound in laser beam and electron beam welded sample

Thus, Electron Beam welding process is significantly better than the laser welding technique.

References

1. Rapp RA (1986) Chemistry and electrochemistry of the hot corrosion of metals, corrosion. Mater Sci Eng 87:319–327
2. Liou H-Y, Hsieh R-I, Tsai W-T (2002) Microstructure and stress corrosion cracking in simulated heat-affected zones of duplex stainless steels. Corros Sci 44(12):2841–2856
3. Adam Khan M, Sundarrajan S, Natarajan S (2014) Influence of plasma coatings on Inconel 617 for gas turbine applications. Surf Eng 30:656–661
4. Sedricks AJ (1979) Corrosion of stainless steels. Wiley, New York
5. Fontana MG (1976) Corrosion engineering, 3rd edn. TATA McGraw-Hills, New York, pp 1–50
6. Donachie MJ, Donachie SJ (2002) Superallaoys, 2nd edn. ASM International, Ohia
7. Lai GY (2007) High-temperature corrosion and materials applications. ASM International, Ohia
8. Vilar R, Almeida A (2015) Repair and manufacturing of single crystal Ni-based superalloys components by laser powder deposition—a review. J Laser Appl 27 (Article in Press)
9. David SA, Siefert JA, DuPont JN, Shingledecker JP (2015) Weldability and weld performance of candidate nickel base superalloys for advanced ultrasupercritical fossil power plants part I: fundamentals. Sci Technol Weld Joining 20:532–552
10. Belloni G, Caironi G, Gariboldi A, Lo Conte A, di Milano P (2001) Effect of microstructural alteration on the creep behavior and effect of flaws in 50Cr50Ni–Nb engineering alloy. IASMiRT, Washington

11. Caironi G, Gariboldi E, Silva G, Vedani G (1993) Influence of heat treatments on the mechanical properties and microstructure of a 50Cr–50Ni niobium containing alloy. J Phys IV 03:289–295
12. Jenney CL, O'Brien A (2001) Welding handbook. American Welding Society, 9th edn, Miami
13. Naffakh H, Shamanian M, Ashrafizadeh F (2009) Dissimilar welding of AISI 310 austenitic stainless steel to nickel-based alloy Inconel 657. J Mater Process Technol 209:3628–3639
14. Prabaharan P, Devendranath Ramkumar K, Arivazhagan N (2014) Characterization of microstructure and mechanical properties of Super Ni 718 alloy and AISI 316L dissimilar weldments. J Mater Res 29:3011–3023
15. Ramkumar KD, Arivazhagan N, Narayanan S (2012) Effect of filler materials on the performance of gas tungsten arc welded AISI 304 and Monel 400. Mater Des 40:70–79
16. Rajput RK (2007) A textbook of manufacturing technology (manufacturing processes), 1st edn. India
17. Nicholas ED (2003) Friction processing technologies. Welding in the World 47:2–9
18. A Designer's Handbook Series (1988) Welding of stainless steels and other joining methods. American Iron and Steel Institute, Washington
19. David SA, Vitek JM, Babu SS, Boatner LA, Reed RW (1997) Welding of nickel base superalloy single crystals. Sci Technol Weld Joining 2(2):79–88
20. Henderson MB, Arrell D, Heobel M, Larsson R, Marchant G (2004) Nickel-based superalloy welding practices for industrial gas turbine applications. Sci Technol Weld Joining 9(1):13–21
21. Ram GDJ, Reddy AV, Rao KP, Reddy GM, Sundar JKS (2005) Microstructure and tensile properties of Inconel 718 pulsed Nd-YAG laser welds. J Mater Process Technol 167(1):73–82
22. Allen Chris, Shaw-Edwards Robert, Nijdam Thijs (2015) Nickel-containing superalloy laser weld qualities and properties. J Laser Appl 27(2):1–8
23. Sun Z, Ion JC (1995) Laser welding of dissimilar metal combinations. J Mater Sci 30(17):4205–4214
24. Sun Z, Kuo M (1999) Bridging the joint gap with wire feed laser welding. J Mater Process Technol 87(1–3):213–222
25. Chryssolouris G (1991) Laser machining: theory and practice. Springer, Berlin
26. Dong H, Li XY, Bell T (1999) Hardening response and tempering behaviour of electron beam surface melted Ti–8.5 Si alloy. J Alloy Compd 283(1–2):231–240
27. Lacki P, Adamus K (2011) Numerical simulation of the electron beam welding process. Comput Struct 89(11–12):977–985
28. Koleva EG, Mladenov GM (2011) Experience on electron beam welding. Pract Aspects Appl Electron Beam Irradiat 37:95–133
29. Yilbas M, Sami J, Nickel A, Coban SAM Said (1998) Introduction into the electron beam welding of austenitic 321-type stainless steel. J Mater Process Technol 82:13–20
30. Chen Hui-Chi, Pinkerton Andrew J, Li Lin (2011) Fibre laser welding of dissimilar alloys of Ti-6Al-4V and Inconel 718 for aerospace applications. Int J Adv Manuf Technol 52:977–987
31. Adam Khan M (2015) Electrochemical polarisation studies on plasma-sprayed nickel-based superalloy. Appl Phys A 120:801–808

Retraction Note to: Investigation on Spark Erosion Machining Induced Surface Integrity of Super-Alloys

Neeraj Sharma and Kamal Kumar

Retraction Note to: Chapter "Investigation on Spark Erosion Machining Induced Surface Integrity of Super-Alloys" in: K. Gupta (ed.), *Materials Forming, Machining and Post Processing*, Materials Forming, Machining and Tribology, https://doi.org/10.1007/978-3-030-18854-2_6

The Editor has retracted this chapter [1] because a number of the figures and tables appear to have been published previously by the authors. Figures 2, 3 and 11–14 overlap with Figures 1, 2 and 6a–d of [2]. Table 1 appears to partly overlap with Table 1 of [2]. Table 2 appears to overlap with Table 2 of [2]. Figures 5 and 6 appear to overlap partly with Figures 2 and 3 of [2]. Figures 7, 8, 10a and 10b appear to overlap with Figures 5, 6, 9a and 9c of [2]. Figure 9 appears to partly overlap with Figure 8 of [2]. Both authors agree with this retraction.

[1] Sharma N., Kumar K. (2020) Investigation on Spark Erosion Machining Induced Surface Integrity of Super-Alloys. In: Gupta K. (ed.) Materials Forming, Machining and Post Processing. Materials Forming, Machining and Tribology. Springer, Cham

[2] Kumar, V., Kumar, V & Jangra, K. (2015). An experimental investigation and statistical modelling for trim cutting operation in WEDM of Nimonic-90. International Journal of Industrial Engineering Computations, 6(3), 351-364.

[3] Kamal Kumar Jangra, Vinod Kumar, Vikas Kumar, An Experimental and Comparative Study on Rough and Trim Cutting Operation in WEDM of Hard to Machine Materials, Procedia Materials Science, Volume 5, 2014, Pages 1603-1612, https://doi.org/10.1016/j.mspro.2014.07.348.

The retracted version of this chapter can be found at https://doi.org/10.1007/978-3-030-18854-2_6

K. Gupta (ed.), *Materials Forming, Machining and Post Processing*, Materials Forming, Machining and Tribology, https://doi.org/10.1007/978-3-030-18854-2_12

Index

K. Gupta (ed.), *Materials Forming, Machining and Post Processing*, Materials Forming, Machining and Tribology, https://doi.org/10.1007/978-3-030-18854-2